Calcium Signalling & Mitochondrial Dynamics in the Exocrine Pancreas: Physiology & Pathophysiology

Thesis submitted in accordance with the requirements of the University of Liverpool for the degree of philosophiae doctor by

Matthew Charles Cane

MMXIII

For Rosie, who lovingly typed the 1st Dr. Cane's thesis and is not here to congratulate the 2nd.

Abstract

Pancreatic acinar cells release hydrolytic enzymes into the gut where they are responsible for digestion. When this process goes awry, these enzymes can be activated within the pancreas itself, characteristic of a severe and systemic inflammatory disease: acute pancreatitis. A large body of data has highlighted that the IP_3R Ca^{2+}-release channel is a central mediator of the toxic Ca^{2+} signals associated with the onset of early enzyme activation and cellular necrosis. Not only is the pancreatic acinar cell a focus of investigation into the onset of this acute disease, it is also investigated as a paradigm cell type in the fields of Ca^{2+} signalling; stimulus secretion coupling; and cellular polarity. The mitochondria, which are the ATP-producing powerhouses and Ca^{2+} signal modulators of the cell, have a well documented polarised distribution in pancreatic acinar cells.

This is a thesis of three main parts. Initial experiments aimed to determine the mechanisms of inhibition of IP_3-mediated Ca^{2+} signals by xanthines. Xanthines were shown to inhibit the IP_3R and did not inhibit Ca^{2+} influx directly. A range of methylxanthines were shown to have varied effects on Ca^{2+} oscillations, however another role of methylxanthines, PDE inhibition, is likely to be involved in this. No significant differences were seen between xanthines when inhibiting IP_3-mediated Ca^{2+} signals or necrosis, but inhibition of the Ca^{2+} signal does protect the cell against mitochondrial dysfunction. Whilst no xanthines tested offered any superior protection against pathological Ca^{2+} signals, this only goes to highlight the need for better pharmacological modulators of IP_3-mediated Ca^{2+} signals.

The development of multiplex assays to record pathological criteria such as Ca^{2+} signals and necrosis in a rapid and more user-friendly way was also undertaken. Assays for determining $\Delta\Psi_M$ and necrosis were successfully developed but throughput was limited by the primary cell isolation procedure.

Finally, the most fascinating part of this research involves the mitochondrial network in pancreatic tissue. We investigate the mechanisms and signals involved in how the mitochondrial distribution comes into being and what effect pathological signals have on this distribution. This mitochondrial belt is formed in a Ca^{2+}-dependent manner upon stimulation. Redistribution is tubulin-mediated and the maintenance of subplasmalemmal mitochondria is dependent upon Ca^{2+}-influx, highlighting a potential role for Ca^{2+} microdomains in inhibiting tubulin-mediated motility. Hyperstimulation induced actin-mediated redistribution of cellular contents, including mitochondria into the apical pole. Finally we determined the functional importance of mitochondrial redistribution away from the plasma membrane by determining the effects of redistribution on store-operated Ca^{2+} entry. This investigation strongly advocates the importance of intact tissue to bolster molecular and cellular tools in the study of organ physiology.

Acknowledgements

This thesis was funded by the Medical Research Council and superbly supervised by Dave Criddle. He should be commended not only for his essential direction and insightful advice but also for the trust and cooperation offered in the development of this project and his indefatigable perfectionism; for which I am eternally grateful and to which I must apologise.

Alexei Tepikin is munificent with his knowledge and wisdom, which has been sincerely conducive to my scientific edification. Robert Sutton has given generous access to the Pancreas Biomedical Research Unit, and, being a perspicacious individual, has greatly improved this study by suggesting all the controls which I had desperately avoided.

Svetlana Voronina has been a truly invigorating source of kindness and frankness throughout my time in Blue Block, of which all members deserve special mention – in particular Hayley Dingsdale with whom I have shared a path through science over the past four years: our trails separate, but I am sure we will call on each other often in times of scientific desperation.

Dave Booth was there to help me through the first two years of my PhD and has remained a valued font of brilliant ideas and terrible puns ever since. Mark has kept me crying with laughter on an almost daily basis and Marie has been a wonderful source of hilarious catchphrases.

Thank you to my dear Henry Ashcroft for the coffee and conversation (counselling); and to all my wonderful friends, new and old, who have supported me in their own individual ways. Nic kept me alive after turpentine poisoning; Jo gave me alcohol poisoning; Kelly handed the bugger in; and Gopika gave me somewhere to sleep on far too many occasions. I am very lucky to have so many of you to offer encouragement when helpful and distraction when necessary.

Thanks to my brother Sam and his brilliant wife Lizzie, who shared their home with me during my first few months at Imperial. And finally, I am so much more than grateful to my paradigms of parenthood, for their encouragement, emergency bank transfers, warm love and easy faith in their 4th son.

This list is painfully non-exhaustive for which I beg clemency.

Enfin! And please, *Spectemur agendo*

Table of Contents

ABBREVIATIONS

ACh	Acetylcholine
-AM	Acetoxymethyl ester
AP	Acute pancreatitis
ATP	adenosine triphosphate
BAPTA	(1,2-bis(o-aminophenoxy)ethane-N,N,N',N'-tetraacetic acid)
BSA	Bovine serum albumin
cADP ribose	cyclic Adenosine diphosphate ribose
cAMP	cyclic Adenosine monophosphate
$[Ca^{2+}]c$	cytosolic free Ca2+ concentration
CCCP	Carbonyl cyanide m-chlorophenlyhydrazone
CCK	Cholecystokinin
CICR	Ca^{2+}-induced Ca^{2+}-release
DAG	Diacylglycerol
ddH_2O	Double distilled water
DIC	Differential interference contrast
DMSO	Dimethyl sulphoxide
$\Delta\Psi_M$	Mitochondrial membrane potential
EGTA	Ethylene glycol tetra-acetic acid
ER	Endoplasmic reticulum
EtOH	Ethanol
F/F_0	Fluorescence intensity normalised to the initial intensity
F/F_μ	Fluorescence intensity normalised to the mean intensity
F/F_{min}	Fluorescence intensity normalised to the minimum intensity
F/F_{max}	Fluorescence intensity normalised to the maximum intensity
Fluo-4	Fluorescein-based Ca^{2+}-indicator
HEPES	4-(2-hydroxyethyl)-1-piperazineethanesulphonic acid
IP_3	Inositol 1,4,5 trisphosphate
IP_3R	Inositol 1,4,5 trisphosphate receptor

NA	Numerical aperture
NAADP	Nicotinic acid adenine dinucleotide phosphate
NAC	N-acetyl-L-cysteine
NADH	Nicotinamide adenine dinucleotide
NADPH	Nicotinamide adenine dinucleotide phosphate
PBS	Phosphate-buffered saline
PDE	Phosphodiesterase
PDEI	Phosphodiesterase inhibitor
PFA	Paraformaldehyde
PI	Propidium iodide
PIP_2	Phosphatidylinositol 4,5-bisphosphate
PMCA	Plasma membrane Ca^{2+} ATPase
PMT	Photomultiplier tube
ROS	Reactive oxygen species
RyR	Ryanodine receptor
SEM	Standard error of the mean
SERCA	Sarcoplasmic/endoplasmic reticulum Ca^{2+} ATPase
STIM	Stromal interaction molecule
TLCS	Taurolithocholic acid-3-sulphate
TMRM	Tetramethyl rhodamine methyl ester
TPC	Two-pore channel
TPEN	Tetrakis (2-pyridylmethyl) ethylene diamine

CHAPTER 1: INTRODUCTION

THE EXOCRINE PANCREAS

PHYSIOLOGICAL FUNCTION OF THE EXOCRINE PANCREAS

The pancreas is a gland of the digestive and endocrine systems, with both endocrine and exocrine functions. This thesis is regarding cells of the exocrine pancreas, which is responsible for the supply of digestive enzymes including trypsin, amylase, lipase and elastase. Under healthy conditions, inactive enzyme precursors are delivered to the duodenum where they are activated by enteropeptidase and responsible for the digestion of fats, carbohydrates and proteins of the chyme. The exocrine pancreas is also responsible for the secretion of bicarbonate from the ductal cells. Alkaline bile salts are released upon CCK stimulation of the gall bladder and enter the duodenum through the sphincter of Oddi via the common bile duct. The combination of bicarbonate and bile salts acts to neutralise the pH of the chyme in the duodenum, ready for further digestion by pancreatic enzymes. The pancreas is often described as having a head, body and tail. The tail is the left / lateral -most end of the pancreas, in close contact with the spleen. The body of the pancreas lies behind the stomach, and the medial / right located head is where the pancreatic duct is largest and exits into the duodenum via the sphincter of Oddi.

ACUTE PANCREATITIS

Acute pancreatitis is an inflammatory disease of the exocrine pancreas, a severely painful, debilitating and potentially fatal disease. Historically, it is described as an autodigestion of the pancreas, where enzymes are prematurely activated causing necrosis and vacuolisation. Currently, it affects over 50 in every 100,000 per annum

and is increasing in incidence year on year (Pandol et al., 2007). Whilst the most common precipitants clinically are gall stones and alcohol abuse, an array of more esoteric causes are also associated, namely viral infections; a range of drugs including steroids, chemotherapeutic agents and HIV medications; hyperlipidaemia and hypercalcaemia; ductal obstruction; autoimmunity; physical trauma including surgical interventions, namely endoscopic retrograde cholangiopancreatography (Swaroop et al., 2004, Pandol et al., 2007, Saluja et al., 2007). Approximately 1 in 5 pancreatitis sufferers will develop a severe form of the disease, often associated with massive necrosis, leading to a systemic immune response and multiple organ failure. This chain of events is highly associated with fatality. Around 1 in 20 patients will die from the disease (Banks and Freeman, 2006), but mortality amongst those patients developing severe necrosis is significantly higher, with bacterial infection worsening the outlook even more (Pandol et al., 2007). Despite a large number of clinical trials, there is no specific therapy available for use in pancreatitis. Further research into the molecular mechanisms involved in the onset of acute disease, and better screening methods for the identification and modulation of therapeutic targets is essential if progress is to be made in the treatment of this debilitating disease.

The Pancreatic Acinar Cell

The main components of the exocrine pancreas are the acinar cells, a paradigm cell type in the study of Ca^{2+} signalling and stimulus-secretion coupling for a number of decades (Petersen et al., 1999). The acinar cell is a structurally and functionally polarised cell type (Petersen, 1992, Petersen et al., 1999), groups of which form closed structures called acini, so called because of their likeness to a bunch of grapes.

Secretory granules are located on the apical side, close to the lumen of the ductal system (Fig. 1.1). The basolateral region contains a dense network of ER with strands that spread through the granular region into the apical part of the cell (Gerasimenko et al., 2002) (Fig. 1.1). The Golgi apparatus is found at the edge of the granular region (Dolman et al., 2005), close to the nucleus, which is also found in the basal region of the cell. In isolated pancreatic acinar cells, mitochondria are found in a distinct perigranular, peri-nuclear and subplasmalemmal distribution and this will be discussed in more detail later. The dense core granular vesicles containing zymogen are clearly visible in light and electron microscopy and are secreted from the cell via fusion with the apical membrane (Jamieson and Palade, 1971), releasing inactive enzyme precursors into the pancreatic duct.

Ca^{2+} Signalling in the Pancreatic Acinar Cell

Ca^{2+} as a signal

99% of the Ca^{2+} in the human body is found in the calcified matrix of bone, however the 0.9% of Ca^{2+} found inside cells acts as arguably the most diverse signalling messenger, responsible for initiating exocytosis of synaptic and secretory vesicles, contractility of muscle cells, and altered activity of thousands of enzymes and transporters (Silverthorn, 1998). Due to the low concentration of Ca^{2+} inside the cell and the high buffering capacity of Ca^{2+}-binding proteins and other chelating cytosolic components, Ca^{2+} signals are able to move in waves throughout the cell. Encoded within the frequency, amplitude and distribution of these signals, physiologically relevant information is transmitted, playing a part in almost all aspects of cellular

physiology, from fertilization, through cell function, to cell death (Berridge et al., 2000). Excitable cells are able to induce Ca^{2+} signals by depolarising the plasma membrane, inducing the activation of voltage potential-gated channels to allow influx of extracellular Ca^{2+} down an electrochemical gradient. Pancreatic acinar cells are non-excitable, and Ca^{2+} signals are formed by a release of Ca^{2+} from an internal Ca^{2+} store, predominantly the ER (Streb et al., 1984), and entry of Ca^{2+} via voltage independent routes.

Stimuli

Physiological stimulation of cells to induce a Ca^{2+} signal involves activation of receptors at the plasma membrane, the release of second messengers, and Ca^{2+}-release via channels on internal Ca^{2+} stores. Secretion of enzymes in pancreatic acinar cells is stimulated in such a way, either by the neurotransmitter acetylcholine (ACh), which activates muscarinic receptors on the basolateral membrane (Rosenzweig et al., 1983, Ashby et al., 2003), or by the circulating hormone cholecystokinin (CCK) (Murphy et al., 2008). It has also been suggested that the bile acid taurolithocholic acid 3-sulphate (TLCS) acts in a similar way and these agonists will be discussed in more detail. Receptors for these secretagogues are members of the G protein-coupled receptor super-family, which translate the binding of the agonist to the activation of cytosolic signalling cascades.

Second Messengers and Ca^{2+} Release Channels

Second messengers and Ca^{2+}-release channels relevant to this project are outlined in Fig. 1.2, and this figure may be used as a reference over the next few sections which

will discuss this machinery in more detail. Activation of PLC by G protein-coupled receptors leads to the cleavage of PIP_2 into IP_3 and DAG; both of which are important second messengers in their own right. DAG is in turn sensed by PKC and subsequently PKD; however, IP_3 acts directly on the IP_3R (Streb et al., 1983), leading to Ca^{2+} release from intracellular Ca^{2+} stores through activated IP_3R Ca^{2+}-release channels in the ER membrane. Initial Ca^{2+}-release leads to positive feedback as the IP_3R is itself sensitized biphasically to cytosolic Ca^{2+}. Further release leads to the activation of Ca^{2+}-sensitive RyRs of which type 2 is expressed in pancreatic acinar cells (Leite et al., 1999). This positive feedback of Ca^{2+} induced Ca^{2+} release (CICR) propagates a global Ca^{2+} rise (Adkins and Taylor, 1999, Straub et al., 2000). The main Ca^{2+} pool responsible for this Ca^{2+} release in pancreatic acinar cells is the ER (Streb et al., 1984). Ca^{2+} release under physiological stimulation is oscillatory in nature (Yule and Gallacher, 1988), and these oscillations originate at the apical site (Thorn et al., 1993), due to the tightly confined apical localization of the IP_3Rs (Nathanson et al., 1994). Aside from IP_3, the other two major second messengers associated with stimulation of pancreatic acinar cells are NAADP and cADP ribose, which are produced upon stimulation with CCK and discussed later. The production of cADP ribose and NAADP is performed by ADP ribosyl cyclase, CD38 or CD157 but the exact biochemical mechanisms of production are incompletely understood (Cancela et al., 1999, Lee, 2006, Churamani et al., 2007). However, recent findings using CD38 deficient mice implicate CD38 in the production of NAADP in pancreatic acinar cells (Cosker et al., 2010). cADP ribose acts primarily and directly upon RyRs, sensitizing them to channel opening by Ca^{2+} (Galione et al., 1991). There are data

which suggest that the activation is modulated by calmodulin (Lee et al., 1994), and also that cADP ribose may increase SERCA activity, which could potentially sensitize the RyR to channel opening by increasing luminal Ca^{2+} (Yamasaki-Mann et al., 2009). Conversely, the molecular targets of NAADP have been controversial for some time now (Aarhus et al., 1996). Even recently, whilst significant evidence implicates the newly discovered and characterised two-pore channels (TPC) as the Ca^{2+} release channels sensitive to NAADP (Ruas et al., 2010, Tugba Durlu-Kandilci et al., 2010), these findings have been contradicted by a study showing that TPCs are not NAADP receptors at all, but are in fact Na^{+}-selective channels sensitive to phosphoinositides (Wang et al., 2012). These discrepancies show that there is still significant controversy in this field.

Bile Acid: TLCS

In this thesis, the bile acid, TLCS is used as a stimulus for pancreatic acinar cells and tissue, to simulate a model of acute pancreatitis. A major clinical precipitant of acute pancreatitis is the presence of gall stones. One theory as to the mechanism of induction of pancreatitis by gall stones is that the sphincter of Oddi, the exit of the common bile duct into the duodenum, can be clogged by the passing of gall stones resulting in bile reflux into the pancreatic duct, leading to both the increase in ductal pressure, and direct effects of bile on the cells of the pancreatic exocrine system.

Bile salts have been proposed to act in a number of ways on the pancreatic acinar cell; for example, below critical micellar concentrations where they would induce detergent effects, bile salts have been linked to PI3K-mediated inhibition of the SERCA pump, leading to pathological Ca^{2+} overload, as the SERCA cannot clear Ca^{2+}

from the cytosol, and store-operated influx is induced by the resultant depletion of the Ca^{2+} store (Kim et al., 2002, L. Fischer, 2006, Fischer et al., 2007). Conversely, TLCS-induced Ca^{2+} signals have been shown to involve immediate and store-independent Ca^{2+} influx, induced directly by bile salts at the plasma membrane; inducing the formation of IP_3 by Ca^{2+}-induced activation of PLC near the influx site which subsequently induces Ca^{2+} release from the ER (Lau et al., 2005). Submicellar concentrations of bile acids can lead to IP_3R and RyR-mediated Ca^{2+} release from the ER and acidic stores of the pancreatic acinar cell, namely zymogen granules and endo-lysosomes (Voronina et al., 2002, Gerasimenko et al., 2006, Gerasimenko et al., 2009). In support of this, it has been shown that TLCS activates a plasma membrane G protein-coupled receptor at the luminal cell surface, Gpbar1. Mice deficient in the gene encoding this receptor displayed reduced Ca^{2+} signalling in response to TLCS stimulation, and were also protected from a model of biliary acute pancreatitis, suggesting that TLCS hyperstimulation and by extension, bile induced acute pancreatitis, may be, at least in part, receptor mediated (Perides et al., 2010).

CCK

CCK is a gastrointestinal hormone which, amongst other roles, is responsible for the release of bile from the gall bladder; cholecystokinin in Greek literally means 'bile' 'sac' 'move'. CCK-58 (the full-length human form) has been shown to produce similar responses to the small molecular weight form CCK-8 in murine pancreatic acinar cells (Criddle et al., 2009). Based on this finding, CCK-8 is used throughout this thesis to stimulate pancreatic acinar cells and pancreatic tissue. CCK has two known G protein-coupled receptors: 'type A' and 'type B'. Type A receptors have a

higher affinity for CCK than gastrin, whereas type B receptors have a similar affinity for both CCK and gastrin. Murine pancreatic acinar cells only express 'type A' receptors (Saillan-Barreau et al., 1998). CCK stimulation of pancreatic acinar cells is biphasic; the receptor has low and high affinity states. Low picomolar concentrations of CCK (associated with physiological responses) activate high-affinity receptors and higher than nanomolar concentrations of CCK (associated with hyperstimulatory Ca^{2+} overload) activate low-affinity receptors (Saillan-Barreau et al., 1998). Hyperstimulation with CCK induces the activation of PLC to generate IP_3 leading to activation of IP_3Rs and Ca^{2+} release from the ER. Low picomolar concentrations of CCK give rise to Ca^{2+} oscillations and are mediated by other second messengers, NAADP and cADP ribose (Cancela et al., 2000, Yamasaki et al., 2005). It has been shown that inhibitors of cADP ribose effectively block Ca^{2+} oscillations induced by physiological concentrations of CCK in pancreatic acinar cells (Cancela and Petersen, 1998).

Ca^{2+} Clearance

After a Ca^{2+} signal has occurred, the cell must remove Ca^{2+} from the cytosol in order to return the Ca^{2+} concentration to resting levels. Many cells employ a Na^+/Ca^{2+} exchanger to clear Ca^{2+} from the cytosol; using the high electrochemical gradient of Na^+ across the membrane to drive this process. Pancreatic acinar cells do not express the Na^+/Ca^{2+} exchanger on the plasma membrane, and so the responsibility of Ca^{2+} clearance falls to the Ca^{2+} ATPase pumps located on the plasma membrane and the sarco/endoplasmic reticulum (PMCA and SERCA respectively). PMCA and SERCA require energy in the form of ATP to extrude Ca^{2+}. This means

that not only are ATP and Ca^{2+} inherently linked through the requirements of Ca^{2+} clearance, but also that the pancreatic acinar cell is highly susceptible both to ATP depletion and Ca^{2+} overload. Whilst PMCA activity is inherently linked to ATP supply, it is also being more widely understood that control of the PMCA is more complicated than once thought, and a range of other factors including oxidative stress, phospholipid signalling and proteolytic actions are also involved in the inhibition of the PMCA under metabolic stress (Bruce, 2010).

The majority of Ca^{2+} extrusion occurs in the apical region of the pancreatic acinar cell (Belan et al., 1996, Belan et al., 1997). This is also where the majority of the PMCAs are found (Lee et al., 1997). Ca^{2+} clearance from the apical region of the pancreatic acinar cell (where Ca^{2+} signals are instigated) and continued excitation and Ca^{2+}-release from the ER, will eventually result in depletion of the Ca^{2+} store.

Store-Operated Ca^{2+} Entry

Capacitative Ca^{2+} entry, or store-operated Ca^{2+} entry, is the influx of Ca^{2+} across plasma-membrane induced by lowered ER luminal Ca^{2+} concentrations. The inward current associated with this phenomenon is known as the Ca^{2+}-release-activated Ca^{2+} current or I_{CRAC}. The essential requirement for Ca^{2+} influx in the maintenance of proper cell function in non-excitable cells has been well documented (for early review see (Putney, 1978)) but the original model for capacitative Ca^{2+} entry was not proposed until quite some time later (Putney, 1986). The first model of store-operated Ca^{2+} influx related specifically to the depletion of the Ca^{2+} store by IP_3-mediated Ca^{2+} release. It was later understood that the induction of store-operated Ca^{2+} influx was not limited to IP_3-mediated signals (Putney, 1990b, Putney,

1990a). The lack of any requirement for stimuli in the induction of I_{CRAC} was later shown by reversibly lowering the ER luminal Ca^{2+} using membrane-permeable low-affinity Ca^{2+} chelator, TPEN; essentially describing ER Ca^{2+} as the sole determinant of the Ca^{2+} influx (Hofer et al., 1998). The molecular mechanisms underlying capacitative Ca^{2+} entry remain controversial but influx is known to involve the stromal interaction molecule, or STIM. STIM is a Ca^{2+} sensor in the ER, containing an EF-hand motif on the luminal side (Liou et al., 2005). Orai1 has been shown to be a channel responsible for store operated Ca^{2+} influx (Feske et al., 2006, Prakriya et al., 2006). TRPC, and specifically TRPC3 in pancreatic acinar cells, have been shown to also act as components of the Ca^{2+} influx machinery (Kim et al., 2009, Yuan et al., 2009). STIM oligomerises upon store-depletion forming close interactions between the ER and plasma membrane (Luik et al., 2006, Wu et al., 2006, Lur et al., 2009). At low ER Ca^{2+} levels, STIM1 binds to the plasma membrane Ca^{2+} channel Orai1, activating it and leading to Ca^{2+} influx. This was most conclusively shown by the expression of a recombinant cytosolic c-terminus of STIM1, which constitutively activated I_{CRAC} (Huang et al., 2006).

It is important to note that not only is Ca^{2+} influx essential for the sustained Ca^{2+} plateau, but also for the maintenance of Ca^{2+} oscillations (Kawanishi et al., 1989, Lewis and Cahalan, 1989). More recently it has been shown that different stromal interaction molecules are responsible for induction of I_{CRAC} to differing degrees dependent upon the level of stimulation and store Ca^{2+} concentration (Kar et al., 2012).

THE IP_3R

As previously discussed, the IP_3R is a Ca^{2+} release channel found in the ER and ubiquitously expressed throughout the body (Taylor et al., 1999, Foskett et al., 2007). The channel is sensitive to both Ca^{2+} and IP_3 and opening of the receptor also requires both Ca^{2+} and IP_3 binding (Foskett et al., 2007, Taufiq Ur et al., 2009). IP_3Rs are thought to act in clusters, with individual open events occurring at very low levels under basal conditions, followed by opening of small clusters of IP_3Rs as the concentration of IP_3 increases (Taufiq Ur et al., 2009). As the Ca^{2+} concentration increases locally due to increased channel-opening, neighbouring clusters of IP_3Rs are up regulated and recruited leading to positive feedback and the development of a Ca^{2+} wave. This process will then activate RyRs in a process of CICR.

PATHOLOGICAL IP_3-MEDIATED Ca^{2+} OVERLOAD

Dysregulation of Ca^{2+} signalling involving the IP_3R has been associated with a wide range of disease states including cardiac diseases (Wehrens et al., 2005) and neurological diseases most notably Huntington's and Alzheimer's (Bezprozvanny, 2007, Foskett, 2010). Ca^{2+} overload is also associated with pathological hyperstimulation of pancreatic acinar cells by classical precipitants of acute pancreatitis. Ca^{2+} overload, and a dysregulation of normal Ca^{2+} signalling has been shown to occur in the early onset of murine models of acute pancreatitis (Ward et al., 1996), and this overload of Ca^{2+} is responsible for intracellular enzyme activation, vacuolization, mitochondrial dysfunction and necrosis which occurs in acute disease . Inhibition of Ca^{2+}-overload by protecting against down-regulation of the PMCA has been shown to be protective in pancreatic acinar cells (Mankad et al., 2012). In vitro,

cytosolic Ca^{2+}-overload is induced in pancreatic acinar cells by a range of stimuli, including CCK and bile acids such as TLCS discussed previously. Caffeine has been shown to reversibly inhibit these toxic Ca^{2+} signals in pancreatic acinar cells (Voronina et al., 2002) indicating the possible involvement of the IP_3R in these signals. The IP_3R has also been directly implicated in the deleterious effects of ethanol metabolites on pancreatic acinar cells (Criddle et al., 2006). The exact role of caffeine in ameliorating hyperstimulatory Ca^{2+} signals and the deleterious effects associated with them is unclear due to the wide range of actions of caffeine.

DIVERSITY

Three major subtypes of IP_3Rs exist as both homomeric units of the same subtype, or as heteromeric molecules, combining different subtypes into one tetramer (Monkawa et al., 1995). Generally IP_3R1 is associated with neurons and IP_3R2 with muscle but this is far from a strict rule; pancreatic acinar cells express all three subtypes of the receptor (Wojcikiewicz et al., 1999, Lur et al., 2009) and they are found in the apical region of the acini, close to the luminal membrane (Ashby and Tepikin, 2002, Lur et al., 2009). Using knock out mouse models, it has been shown that IP_3R types 2 and 3 are required for functional Ca^{2+} signalling leading to secretion in pancreatic acinar cells; CCK and ACh failed to induce Ca^{2+} signals or secretion in double knock outs for types 2 and 3 but not individual knock outs (Futatsugi et al., 2005).

INHIBITORS

Despite the diversity of subtypes and obvious tissue specificities of the IP_3R, current inhibitors lack any specificity when it comes to subtypes, and even offer little specificity to the IP_3R itself. Inhibitors commonly used in research include heparin, 2-APB, xestospongins and caffeine. Heparin is mainly used clinically is as an anticoagulant but is an effective blocker of both IP_3 binding to the IP_3R (Supattapone et al., 1988), and IP_3R Ca^{2+}-release (Ghosh et al., 1988). However, heparin is not membrane permeable and requires microinjection. 2-APB was also originally described as an inhibitor of IP_3R Ca^{2+} release (Maruyama et al., 1997), however is has since emerged that it has other roles and targets in the cell, for example inhibition of TRPV6 (Kovacs et al., 2012). 2-APB has been shown to also inhibit store-operate Ca^{2+} entry (Prakriya and Lewis, 2001). Similarly, xestospongins have been described as specific inhibitors of the IP_3R (Gafni et al., 1997) but it has since transpired that they inhibit the SERCA pump and possibly other channels (Castonguay and Robitaille, 2002). Whilst they are still used as specific IP_3R antagonists, xestospongins are also prohibitively expensive, limiting their use in superfusion and *in vivo* for example. The confidence of the pharmacological specificity of 2-APB and xestospongins did in fact contribute to the viewpoint that the IP_3R was a key component in store-operated Ca^{2+} entry due to the inhibition of Ca^{2+} influx by 2-APB and xestospongins (Ma et al., 2000). Potent and ideally subtype specific inhibitors of the IP_3R, which do not activate the RyR or inhibit SERCA or TRP channels would be extremely beneficial both in the research of live primary cells and tissue, where pharmacological modulation is essential due to the difficulties of genetic modulation, but also as potential

therapeutics in the many pathologies associated with aberrant IP_3-mediated Ca^{2+} signalling.

METHYLXANTHINES

Methylxanthines are a class of small purine-based planar molecules with a wide array of physiological actions. Found in coffee, tea and chocolate, they are widely consumed and are also used clinically. The most familiar methylxanthine, 1,3,7-trimethyxanthine or caffeine, is arguably the most popular psychoactive drug worldwide. It is degraded in the liver to form the dimethylxanthines, theophylline, paraxanthine and theobromine, as well as a plethora of other compounds including uric acid. With respects to the effect of xanthines physiologically, the mode of action in the body varies depending upon the dose and resultant serum concentration; they interact with a number of different enzymes and receptors to induce a number of physiological outcomes.

CLINICAL USE

Caffeine and theophylline are used clinically as bronchial smooth muscle relaxants and as respiratory stimulants in premature neonatal apnoea and are commonly given intravenously to premature infants to stabilize breathing (Henderson-Smart and Steer, 2010). Theophylline has also been used in the treatment of chronic obstructive pulmonary disease and asthma both as an inhaler, but more commonly orally (Barnes, 2006).

Methylxanthines and Adenosine Receptors

Adenosine receptors are G protein-coupled receptors which bind and respond to adenosine by modulating adenylate cyclase or PLC (Schulte and Fredholm, 2003). Different forms of adenosine receptors were shown to affect adenylate cyclase in either an inhibitory or a stimulatory capacity early on (Londos et al., 1980). There are four main subtypes of adenosine receptors, A_1, A_2, A_{2B} and A_3, differentially expressed in cells and tissues of the body (Schulte and Fredholm, 2003). Adenosine recpetors are expressed in the exocrine pancreas; modulation of which has been shown to ameliorate acute pancreatitis in animal models, indicating an important role in pancreatic exocrine function and pathophysiology (Celinski et al., 2006, Novak, 2008).

At concentrations achieved by dietary exposure, the main function of caffeine physiologically is as a non-specific adenosine receptor antagonist (Fredholm et al., 1999). This inhibition of adenosine receptors is attributed to the physiological effects associated with heavy coffee consumption; central nervous system and metabolic stimulation causing alertness, increased heart rate and insomnia.

Caffeine and theophylline were the first methylxanthines to be identified as adenosine receptor antagonists (Biaggioni et al., 1991). Theobromine shows relatively weak activity as an adenosine receptor antagonist to both A1 and A2a receptors (Muller et al., 1993). Paraxanthine and 1-methylxanthine are the major metabolites of caffeine (and the latter also of theophylline) in humans and are both potent adenosine receptor antagonists equitable to caffeine and theophylline, and could therefore contribute to function (Muller et al., 1993).

Methylxanthines and Phosphodiesterases

cAMP and cGMP are essential and ubiquitous second messengers involved in numerous cellular processes. Cyclic nucleotide phosphodiesterases (PDEs) are responsible for the hydrolysis of the cyclic phosphate bond in both cAMP and cGMP to produce 5′-AMP and 5′-GMP, effectively down-regulating cyclic nucleotide signalling (Francis et al., 2011). There are 11 subtypes of the PDE super-family; PDE1, 2, 3, 10 & 11 cleave both cAMP and cGMP; PDE4, 7 & 8 are specific to cAMP; and PDE5, 6 & 9 are specific to cGMP (Francis et al., 2011). The pancreas expresses an almost full complement of PDE isomers with above-average expression of PDE5, 3 and 11 (Lakics et al., 2010). Methylxanthines are non-specific inhibitors of all PDEs, raising the levels of both cAMP and cGMP in the cell. Inhibition by caffeine occurs at concentrations near the upper limit of those achieved by dietary exposure (Fredholm et al., 1999). The use of theophylline in asthma is due to its potent PDE inhibition which induces bronchiolar dilation by smooth muscle relaxation via an increase in cGMP and cAMP. Theophylline has been gradually replaced with other PDE inhibitors which offer less drug-drug interactions and less overdose-related toxicity due to a narrow therapeutic window.

Methylxanthines and Ca^{2+} Signalling

Caffeine is known to cause Ca^{2+}-release via activation of RyRs; sensitizing them to channel opening (McPherson et al., 1991). It has also been suggested that caffeine (and other methylxanthines) sensitizes the RyR to luminal Ca^{2+} rather than cytosolic Ca^{2+}, increasing channel open probability but does not, like ryanodine, maintain the channel in an open state (Kong et al., 2008). This activation of RyR

Ca^{2+}-release is thought to be the primary cause of arrhythmias associated with caffeine overdose and this attribute is common to a number of different methylxanthines (Balasubramaniam et al., 2005, Guerreiro et al., 2011). Conversely, it is also an inhibitor of IP_3-mediated Ca^{2+}-release (Parker and Ivorra, 1991, Brown et al., 1992). The inhibition is not competitive with IP_3-binding (Brown et al., 1992) suggesting that the inhibition is via modulation of the channel opening rather than primary ligand binding. The inhibition has been shown to be competitive with ATP, suggesting an interaction with the ATP-binding site (Missiaen et al., 1994).

MITOCHONDRIA

Mitochondria are paleo- endo- symbionts which have evolved with their host to become an essential compartment of all living cells. Mitochondria are often refered to as the power stations of the cell, generating ATP through oxidative phosphorylation. It is becoming ever clearer however, that mitochondria play a much more essential role in cellular physiology than simply energy providers. Mitochondria are involved in cellular Ca^{2+} signalling; shaping and defining cytosolic Ca^{2+} elevations through a balance of uptake, buffering and release, and respond to these signals by modulating metabolism.

Mitochondria are also dynamic organelles, able to change not only function, but also shape, size and distribution in response to cellular signals, and in doing so, respond to the needs of the cell with regards to ATP supply and Ca^{2+} buffering capacity (Soubannier and McBride, 2009). In this section the major roles of the mitochondria with specific regard to Ca^{2+} signalling and the pancreatic acinar cell will be introduced, and the basic machinery involved in mitochondrial motility outlined.

MITOCHONDRIA AND Ca^{2+}-SIGNALLING

Mitochondria are active members of the Ca^{2+} signalling family, and the main Ca^{2+} handling channels can be seen outlined in Fig 1.3. Mitochondria are responsible for buffering Ca^{2+} signals in the cytosol. The high Ca^{2+} loading capacity of the mitochondria gives a very high buffering capacity; the ability to maintain such Ca^{2+} concentrations in the presence of high phosphate is thought to be related to the pH of the matrix (Nicholls and Chalmers, 2004). Ca^{2+} enters the mitochondria through the voltage-dependent anion channel on the outer membrane, often called the mitochondrial porin due to a selective permeability to anions, cations, ATP, and other metabolites (Gincel et al., 2001). Mitochondria then actively uptake Ca^{2+} into the matrix, originally observed in rat kidney mitochondria using both Ca^{2+} and strontium where this process was shown to be dependent upon respiration and phosphorylation (Deluca and Engstrom, 1961, Vasington and Murphy, 1962). Despite well established observations of this kind, for many years it was largely dismissed that physiological Ca^{2+} signalling could lead to mitochondrial Ca^{2+} uptake due to the concentration of Ca^{2+} achieved during physiological Ca^{2+} signalling being below the affinity of the mitochondrial Ca^{2+} import machinery. It is now understood that mitochondria accumulate Ca^{2+} during both global Ca^{2+} waves and also during smaller physiological Ca^{2+} signals (Hajnoczky et al., 1995, Rizzuto et al., 2000) and as such, are able to contribute to the fine tuning of the Ca^{2+} signal; controlling the transmission of the Ca^{2+} signal to different regions of the cell. This role of mitochondria has since been similarly documented in pancreatic acinar cells specifically (Johnson et al., 2002).

Mitochondria import Ca^{2+} through a high capacity, low affinity, and Ru360-sensitive channel in the inner mitochondrial membrane (Kirichok et al., 2004). This has recently been identified as the mitochondrial Ca^{2+} uniporter (MCU) (Baughman et al., 2011, De Stefani et al., 2011). The MCU uses the $\Delta\Psi_M$ (~-180 mV) to drive Ca^{2+} transport into the matrix. The Ca^{2+} pore is formed from oligomerisation of the transmembrane domains which span the inner mitochondrial membrane (Baughman et al., 2011, De Stefani et al., 2011). Another essential component of the Ca^{2+} influx machinery is the Ca^{2+} binding MICU1, which contains two EF hand motifs and associates with MCU, and is essential for rapid uptake of Ca^{2+} (Perocchi et al., 2010).

Ca^{2+} is cleared from the mitochondria in a number of ways. The Na^+/Ca^{2+} exchanger and H^+/Ca^{2+} exchanger both move Ca^{2+} out of the mitochondria in exchange for Na^+ or H^+ ions respectively (Crompton et al., 1976, Puskin et al., 1976, Palty et al., 2010).

Changes in mitochondrial matrix Ca^{2+} have direct effects on enzymes found within the matrix most notably components of the TCA cycle. The TCA cycle is responsible for the generation of the reducing power to fund oxidative phosphorylation, generating the $\Delta\Psi_M$ and producing ATP. Specifically, three enzymes of the TCA cycle are upregulated by increased Ca^{2+}. Pyruvate dehydrogenase phosphate phosphatase is activated by increased Ca^{2+} which stimulates the pyruvate dehydrogenase complex activity; and isocitrate dehydrogenase and the 2-oxogluterate dehydrogenase complex are both stimulated resulting in a boost in NAD(P)H and subsequently ATP production (Denton et al., 1972, Denton et al., 1978, McCormack and Denton, 1979, Voronina and Tepikin, 2012). Direct activation of the ATP synthase itself has

also been reported (Territo et al., 2000). This increase in metabolic activity has been shown to linger after the cytosolic Ca^{2+} signal has been cleared, showing that the Ca^{2+} signal can have effects which also continue after the clearance of cytosolic Ca^{2+} (Jouaville et al., 1999).

The mitochondrial permeability transition pore can also act as a Ca^{2+} release mechanism; this is a complex responsible for permeabilising the mitochondrial membrane and allowing very fast nonspecific permeability of cellular contents smaller than 1.5 kilo-Daltons (Kroemer et al., 2007). Opening of the mitochondrial permeability transition pore is induced by pathological Ca^{2+} overload (Baumgartner et al., 2009).

Mitochondria in Disease

A range of mitochondrial related hereditary syndromes and disorders exist (Schapira, 2006). Notable examples include the syndrome combining diabetes mellitus and deafness; Leber's hereditary optic neuropathy; and Leigh syndrome. Aside from genetic disorders owing to mitochondrial dysfunction, mitochondria also play a more subtle, but often key role in a range of other more complex pathologies. For example, pathological mitochondrial Ca^{2+} can lead to opening of the mitochondrial permeability transition pore (Baumgartner et al., 2009). mPTP opening, by collapsing the proton gradient of the inner mitochondrial membrane, will necessarily have dramatic effects on ATP:ADP ratios in actively respiring cells. As ATP is well documented to be a pivotal player in the balance between apoptosis and necrosis (Leist et al., 1997), so to has opening of the mPTP been seen as a point of no return where necrosis is inevitable through the collapse of cellular ATP levels

(Berridge et al., 2000, Petersen et al., 2006, Criddle et al., 2007, Giacomello et al., 2007, Booth et al., 2011). In support of this role of ATP in determining cell fate in the pancreatic acinar cell, fatty acid ethyl esters (non-oxidative metabolites of fatty acid and ethanol) thought to be important in the development of alcohol associated pancreatitis, have also been shown to induce mitochondrial dysfunction and cell death in a process which is ameliorated by the supplementation of cellular ATP via patch pipette (Criddle et al., 2006).

In addition to the role of mitochondrial metabolism and function in pathophysiology, the control of mitochondrial motility is also the topic of intense research in a number of high profile pathologies especially neurodegenerative diseases such as Parkinson's, Huntington's and Alzheimer's diseases (Saxton and Hollenbeck, 2012).

Mitochondrial Redistribution and Motility

Mitochondrial motility has been shown to be sensitive to cytosolic and possibly also mitochondrial Ca^{2+} (Yi et al., 2004, Liu and Hajnoczky, 2009, Chang et al., 2011). The ability of the cell to control mitochondrial motility with Ca^{2+} signals seems like a likely mechanism for feedback (Yi et al., 2004). Mitochondria move into specific distributions throughout the cell using the cytoskeleton, and the motor proteins dynein and kinesin-1 are known to be responsible for motility in retrograde and anterograde directions respectively (Pilling et al., 2006). These directions correspond to inwards and outwards from the cell centre respectively, or specifically towards and away from the microtubule sorting centre. Motor proteins are employed in the microtubular motility of all sorts of cellular cargoes, and mitochondria attach to these

highways via coupling proteins on the mitochondrial membrane such as miro-1 and milton (Wang and Schwarz, 2009) (Fig. 1.4). Regulation of these proteins is thought to be the mechanism of Ca^{2+} regulation of mitochondrial motility (Liu and Hajnoczky, 2009). Whilst still a relatively new field in cellular physiology; motor-driven mitochondrial motility is known to be important in a number of cell types. Mitochondria move large distances along axons, employing the cytoskeleton, to be redistributed between the cell body and synapses of neurons (Saxton and Hollenbeck, 2012). In vascular smooth muscle, mitochondria have been shown to be highly dynamic; existing in both stationary and highly motile states. In this model, mitochondrial dynamics are essential to smooth muscle proliferation and could present a novel therapeutic target in vascular disease (Chalmers et al., 2012). Mitochondrial dynamics have also been shown to be essential for lymphocyte migration and the balance of fusion and fission is thought to be central to this regulation (Campello et al., 2006). Redistribution of mitochobndria to specific loci in order to modulate cellular function through Ca^{2+} buffering and bioenergetics is still poorly defined in complex, primary or whole tissue systems due to the novelty of the machinery involved.

Alternatively to microtubule based motility, mitochondria are also known to employ the actin network during motility in yeast (Fehrenbacher et al., 2004) but actin based mitochondrial motility is not widely seen outside of such specific examples.

Mitochondrial Distribution in the Pancreatic Acinar Cell

Mitochondria are heterogeneously distributed within pancreatic acinar cells and are at the highest density in the perigranular region (Tinel et al., 1999, Johnson et al., 2003). This population of mitochondria has been shown to buffer apically derived Ca^{2+} signals, acting as a barrier to limit the spread of the Ca^{2+} signal from the apex to the periphery of the granular region (Tinel et al., 1999, Park et al., 2001).

Another well defined distribution of mitochondria in pancreatic acinar cells is under the plasma membrane at the basal part of the cell (Tinel et al., 1999, Park et al., 2001). It is thought that these mitochondria are responsible for Ca^{2+} buffering during store-operated Ca^{2+} influx (Park et al., 2001), however, the exact role of the mitochondria at the plasma membrane is still poorly understood.

Experiments using photobleaching have indicated that these mitochondrial sub-populations are not only functionally, but also physically distinct and not connected luminally (Park et al., 2001). The specific roles of the mitochondria within these distinct populations have been observed and investigated in some detail; however, the mechanisms involved in generating and maintaining this distribution are poorly understood. For example, it is not known whether this distribution develops during polarisation, cell differentiation, or after division, or indeed whether or not this distribution could potentially be more dynamic, responding to cellular signals and generating tailored Ca^{2+} buffering for specific cellular needs.

AIMS

As described in this introduction, IP_3R-mediated Ca^{2+}-release is central in the onset of cellular damage by precipitants of acute pancreatitis, and the IP_3R inhibitor caffeine strongly ameliorates pancreatitis in vivo (Huang, 2011). Therefore, we aimed to examine the inhibitory effects of caffeine on Ca^{2+} signals in pancreatic acinar cells. Furthermore, we aimed to determine structural activity relationships of xanthines on IP_3-mediated Ca^{2+} signals, PDE inhibition and necrosis.

With the goal of developing multiplex assays for the screening of inhibitors of novel drug targets of acute pancreatitis, we also aimed to develop methods for rapid determination of $\Delta\Psi_M$ and necrosis of pancreatic acinar cells in a fluorescence microplate-reader format.

Finally, given the importance of mitochondrial distribution in the maintenance of physiological Ca^{2+} signals, and the pivotal role of mitochondrial function in pancreatic acinar cell fate, we aimed to investigate the fluidity and dynamics of the mitochondrial distribution in pancreatic tissue. This would require the development of confocal fluorescence imaging of live and fixed pancreatic tissue, enabling observations of the differences between isolated cells and undisrupted tissues. Using this model we aimed to investigate mitochondrial distributions under native and stimulated conditions; the role of the cytoskeleton in the maintenance of such distributions; and the effect of mitochondrial distribution on relevant Ca^{2+} signals.

CHAPTER 2: MATERIALS & METHODS

General Techniques

Chemicals

Unless otherwise stated all chemicals were purchased from Sigma-Aldrich and were the highest grade available. In all experiments, CCK refers to sulphated CCK-8 octapeptide (Tocris) which was stored at -80 °C at 5 µM stock solution in 140 mM NaCl, 10 mM HEPES, pH 7.3. TLCS was stored frozen at -20 °C at 50 mM in ddH_2O. A list of all pharmacological inhibitors and activators and working concentrations of specific chemicals can be seen in table 2.1. Also shown here is the applied use of these compounds within the remit of this study.

Pancreas Isolation

6 to 8 week old male CD-1 mice (Charles River Laboratories, Inc.) were killed by concussion of the brain by striking the cranium or dislocation of the neck in accordance with the Animal (Scientific Procedures) Act 1986. The carcass was immediately washed in 100% EtOH to wet the fur, and sterilise the skin. A large incision was made in the belly through the skin to reveal the abdominal wall. This incision was used to tear and skin the animal in one stroke. An incision was then made through the abdominal wall on the left flank to gain access to the peritoneal cavity. The spleen was lifted out of the abdomen with forceps and the tail of the pancreas was cut away from the spleen with dissection scissors. The tail and body of the pancreas was then gently pulled and cut away, close to the duodenum. The pancreas was then placed in ~10 ml of HEPES-buffered physiological saline (henceforth, referrals to physiological saline pertain thusly), containing (mM): NaCl 140, KCl 4.7, $MgCl_2$

1.13, HEPES 10, glucose 10, $CaCl_2$ 1, pH 7.3. The organ was then gently swilled in this solution to wash away any fluids and to highlight any attached gut adipose tissue or omentum which were separated and discarded. The pancreas was then ready for cell or tissue isolation.

Pancreatic Acinar Cell Isolation

For the isolation of primary pancreatic acinar cells, the washed and trimmed pancreas was transferred to a dry dish. 1 ml of collagenase solution (at 37 °C, ~200 units ml^{-1} (in standard physiological saline), Worthington Biochemical Corporation, Lakewood, NJ) was injected into the parenchyma of the pancreas with the aim of inflating the organ to disseminate collagenase throughout (27 G needles will do; 30 G needles are better). The collagenase-filled pancreas, and any leaked solution, was then transferred to a 2 ml Eppendorf and placed in an agitating water bath where it was incubated at 37 °C for ~15 minutes. The pancreas, along with the collagenase solution, was then transferred to a 15 ml polycarbonate tube (Sarstedt) and topped up to ~6 ml with physiological saline. The pancreas was rather vigorously sucked in and out of a 'squeezy' plastic 3 ml Pasteur pipette, with careful attention to generate as few bubbles as possible, keeping the aperture of the pipette below the surface of the solution. After this initial disruption, 1 ml pipette tips were cut diagonally to increase the bore-size of the tip and were used to further disrupt the pancreas, sucking the pancreas all the way into the tip. Decreasing bore sizes were employed as resistance diminished. The solution became progressively turbid as acini and individual cells suspended in the solution. Large chunks were allowed to settle for a few seconds before collecting the top ~5 ml of solution and transferring to a second tube. The

remaining ~1 ml containing the bulk of the pancreas was then topped up with physiological saline and the process repeated twice more, to give a final volume of 15 ml in the second tube. At this stage the remainder of the pancreas was white and fibrous. The second tube was centrifuged at 260 G for 1 minute. The pellet was resuspended in physiological saline and filtered once through a 70 µm cell strainer (BD Biosciences), spun once more and resuspended in a final solution of between 4 and 8 ml depending upon approximate turbidity.

Pancreatic Tissue Preparation

For the isolation of pancreatic tissue segments the utmost care was taken not to expose the tissue to any shear stress, crushing forces or air bubbles. The pancreas was transferred to a fresh dish containing enough physiological saline to fully and comfortably immerse the entire pancreas. Using a fresh 30 G needle syringe, the pancreas was injected with physiological saline (containing no collagenase or any enzymes) to gently separate the tissues and to display the architecture of the pancreas. The pancreas was then manually dissected using a new sterile surgical blade, following the architecture of the pancreas and avoiding cutting through the parenchyma. Individual lobes of between 1 and 4 mm were selected, removing any connective tissue, and avoiding parts of the tissue with any transparent layers of connective tissue covering the parenchyma of the organ. Tissue segments could then be transferred to a fresh container to await experimental procedures. For handling and transferring tissue, blunt forceps were used (Cupped, Plastic-Coated Forceps, World Precision Instruments, Inc., Sarasota, USA). Wherever possible, the tissue was picked up using a method of suspension; the forceps were never fully closed, allowing a bead of

physiological solution to form between the arms of the forceps, which could be used to suspend a piece of tissue. This not only protects the tissue from crushing forces and from sticking to the forceps, but it also allows for easy and rapid transfer between different solutions.

Physiological Saline for Longer Experiments

Experiments longer than 4 hours were performed in a slightly modified physiological saline solution to defend against bacterial growth; to provide a source of amino acids and phosphate; and to inhibit any trypsin which may be released through secretion, or from necrotic cells. The standard physiological saline solution was supplemented with 1X minimal essential amino acid solution, 292 µg ml^{-1} L-glutamine, 100 µg ml^{-1} penicillin and streptomycin, 1 mg ml^{-1} soybean trypsin inhibitor, 1 mM $Na_3PO_4 \cdot 12H_2O$ and 1 mM pyruvate. The solution was sterilised by passing it once through a 200 nm filter (Appleton Woods, Selly Oak, UK) and could be stored at -20 °C until required.

Human Pancreatic Tissue Sample Collection

Samples were only taken from consenting patients. Human pancreatic tissue was of high quality, which will normally only be available from surgery for left-sided pancreatectomy; resections for duodenal tumours; or non-obstructive right sided cancer resections in patients with no history of jaundice or chronic pancreatitis. Samples from patients with chronic pancreatitis or ductal obstruction are unsuitable due to the high levels of activated trypsin in this tissue. During surgery (pancreatic resection), a small piece (~1 - 3 cm^3) of pancreas was cut from the transection margin

of the remaining pancreas. This procedure was carried out using a new scalpel blade to limit gross macroscopic cell damage from diathermy burns.

The piece of pancreas was immediately washed by transfer between two 50 ml tubes of ice-cold physiological saline to remove debris and blood products. These may contain neutrophils, macrophages etc. which have the potential to induce additional oxidative stress and tissue damage. After washing, the sample was added to a third tube containing ice-cold physiological saline plus 0.01% (w/v) soybean trypsin inhibitor, 1X protease inhibitor cocktail, and 100 µM sodium pyruvate. The sample was then immediately transported in this solution on-ice to the laboratory. Crucially, the time from sampling to the start of tissue preparation should be as fast as possible (ideally less than 10 minutes) to minimise inevitable necrosis.

Human Pancreatic Tissue Slicing

Tissue with a high proportion of fat was avoided at all costs. Damage to adipocytes and release of fat into the tissue and extracellular solution directly correlated with massive necrosis of the tissue. Fatty tissue is elastic, pinkish, translucent, and buoyant. Using these identifying criteria, fatty tissue was immediately recognised and carefully removed to prevent lipid droplets from building up in the external solution. A fresh surgical blade (size 15) or sharp scissors were used to remove all unwanted sections of the tissue. Human pancreas tissue was maintained in physiological saline, on-ice, for the duration of the slicing process. Tissue was embedded in 10% gelatine and cut into ~150 µm sections using a vibratome (Leica VT1200). Tissue sections were then treated similarly to murine tissue with regards handling, loading with indicator dyes and imaging.

MICROSCOPY

MICROSCOPES AND OBJECTIVES

Microscopy was performed using a Zeiss LSM510 confocal microscope, Zeiss LSM710 confocal microscope (Carl Zeiss; Jena, Germany) or a Nikon imaging system. C-Apochromat 63X water immersion objective, NA 1.2 was used for high magnification Ca^{2+} signalling due to the combined need for high light collection, relatively long working distances and the danger of aqueous superfusion solutions interacting with oil based immersion fluids. For Ca^{2+} signalling experiments in tissue a Plan-Neofluar 10X objective, NA 0.3 was used as only low magnification was required. C-Apochromat 63X oil immersion objective, NA 1.2 was used for immunofluorescence recordings for maximum light absorption due to high confocality (see below).

SETTINGS

Pinhole settings were determined based on the requirements of the specific experiment. In the case of Ca^{2+} signalling with Fluo-4 loaded live cells, it is important to collect as much light as possible. This is predominantly due to the requirement for low irradiation. Harsh irradiation causes increased ROS generation and also damage to the signal, causing bleaching and damaging the stability of the trace. Low irradiation and higher confocality both require increased gain, which leads to increased noise. Practically, no sub-cellular architecture is under investigation and in fact, the valid signal of the Fluo-4 will be emitted from the entire cytosol, and increasing confocality effectively loses valid data. The pinhole should therefore be set to allow maximum

light collection, allowing for minimal irradiation. Immunofluorescence imaging requires no such careful treatment and these samples can withstand much greater illumination; they are not imaged over time and so there is no risk of falling baselines associated with bleaching. They are also fixed and will not respond negatively to irradiation in the same way as live cells. Finally, sub-cellular architecture is under direct investigation and this requires increased confocality and a reduced pinhole diameter.

High-magnification Ca^{2+}-signalling of isolated pancreatic acinar cells and cells of intact tissue were performed with the pinhole set to maximum, representing 8.92 Airy units and an optical slice of 7.5 µm; a significant proportion of the pancreatic acinar cell depth. Low magnification Ca^{2+}-signalling of tissue was also performed with maximum pinhole. Using the Plan-Neofluar 10X objective, this corresponded to an optical slice of 141 µm at 14 Airy units. When using TMRM to image the mitochondria, the pinhole was set at an intermediary level of ~3 Airy units, which represented an optical slice of 2.8 µm. Whilst this is slightly larger than most mitochondria, it gave the necessary allowance for inevitable movement of organelles during the course of the experiment. Immunofluorescence allowed for much greater irradiation, meaning that better signal to noise ratio was possible at even higher confocality. 1-2 Airy units were commonly used at 63X, dependent upon the brightness of the staining and the subsequent signal to noise. This corresponded to an optical slice of 0.9 to 1.7 µm.

Whilst the DIC filter was used on the condensers, true DIC was usually impossible as the condensers were not able to be lowered sufficiently to focus the

transmitted light, due to the angle of the superfusion system. Towards the end of my PhD I devised an adapter which allowed for the manifold to be further away from the condenser and at a lower angle, allowing the condenser to be lowered and the polarised light to be effectively focused. This does marginally reduce the speed of fluid change however, and should not be used when rapid change of solutions is essential. Unfortunately the great majority of the experiments performed did not employ this. All related comparative experiments were performed in the same manner. DIC was always employed for immunofluorescence. Unfortunately, the thickness of the tissue had variable effects and thicker tissue was sufficient to scatter the transmitted light to such an extent that true DIC was impossible. For this reason, transmitted light images are labelled as such, even though some display contrast which has been differentially interfered with.

Superfusion Systems and Chambers

Cells and tissues were superfused using a gravity fed system with an 8-way manifold (Warner Instruments Inc.). Thin-walled silicone tubing was used as it is more flexible than PVC and it is easier to clear any salt deposit blockages by manual massage of the tube. Exact specifications were AlteSil High Strength Tubing, 0.5 mm Bore, 0.25 mm Wall (Altec Products ltd., Bude, UK). One-way stopcocks and 8-way manifolds were purchased from World Precision Instruments, Inc, Sarasota, USA.

Superfusion chambers were made in-house by our workshop staff. These were originally designed for use with cells but were also used for tissue superfusion in this study. A range of weights, grids and tissue 'harps' were tried, all of which either disabled transmitted light, or offered too little support that the tissue, whilst unable to

be drastically moved or sucked away, was extremely active during superfusion and caused so much drift that traces were unintelligible. To combat this, I have devised the use of lens cleaning tissue (Whatman 105) to hold down the pancreatic tissue during superfusion experiments, and also for immunofluorescence. This method is described in Fig. 2.1 and involves the pancreatic tissue being gently pressed between the cover slip and the paper, with the paper held in place by it being clamped between the cover slip and the chamber. This method allowed for even and gentle distribution of pressure across the entire tissue, unlike harps, which offer heavy pressure on thin sections of tissue. The transmitted image was hardly affected due to the low optical density of the paper, even allowing clear DIC in some cases (dependent more upon the thickness of the pancreatic tissue than the paper). The paper is also, by design, extremely absorbent allowing for excellent perfusion of solutions straight to the tissue. This method of superfusion was not totally without negatives; because of the even distribution of pressure, there is excellent contact between the pancreatic tissue and the cover slip, severely impeding the spread of the solution underneath the tissue. When superfusing, it was essential that the outermost section of the tissue, which is in direct contact with the external solution, was selected for measurements.

Fluorescent Indicators

$[Ca^{2+}]_c$ was detected using Fluo-4 (Life Technologies). This was purchased in -AM form to allow for membrane permeability. After loading into the cell this -AM group is cleaved by intracellular esterases, rendering the dye membrane impermeable once more and allowing for a higher concentration than that of the extracellular loading concentration to build up inside the cell. Fluo-4 affinity to Ca^{2+} (345 nM) is in

the ideal range for measuring $[Ca^{2+}]_c$ which is between 50 nM and 5 µM (Ward et al., 1995). Fluo-4 AM was dissolved in DMSO and kept frozen in a stock solution of 2 mM. It was loaded into isolated pancreatic acinar cells and pancreatic tissue at 3 µM. The concentration of DMSO could therefore be maintained below 0.2% at all times. For isolated cells, Fluo-4 was loaded at room temperature for 30 minutes under modest agitation. Tissue required aggressive inverted agitation with a rotary mixer (Stuart tube rotator, Bibby Scientific Ltd., Staffordshire, UK). Fluo-4 was excited with a 488 nm argon laser line and emission collected between 505-530 nm. Excitation was between 0.3 and 1% laser power dependent upon zoom and objective.

Mitochondria were visualised in live cells and tissue using TMRM. This dye accumulates in the mitochondria, and fluorescence relates to the $\Delta\Psi_M$ (see Chapter 4: Introduction). TMRM was loaded at room temperature at 37.5 nM for 30 minutes. TMRM was excited with a 543 nm helium-neon laser and emission collected at 560-650 nm. Excitation was between 2-6% laser power.

NAD(P)H autofluorescence was also visualised and could be separated from the signals from Fluo-4 and TMRM simultaneously. NAD(P)H was excited using a 351 nm or 355 nm coherent laser line and emission collected between 390-450 nm. Excitation was between 1-2% laser power.

IMMUNOFLUORESCENCE

Immunofluorescence of tissue required major methodological maturation; fixing, permeabilisation and staining were all patchy (at best) from the off. Major developments of note are outlined here first, and then the overall protocol defined after. The most important development in terms of tissue preparation was the use of

aggressive agitation using a rotating mixer or something of that ilk, for almost all steps involving fixing, permeabilising, blocking and staining of tissue[1]. This meant that immunofluorescence needed to be performed in a tube or the well of a microplate, with enough solution to allow for free movement of the tissue throughout. This process obviously requires a great deal more antibody and quickly becomes prohibitively expensive. However, as the tissue segment is solid and after fixing and washing steps will not release significant debris, the antibody solutions can be reused. No apparent loss of staining or increase in non-specific staining was seen after 5 freeze / thaw cycles, and even the secondary antibodies and stains in mixed batches were reused in this way. Detergent was added to the blocking buffer and primary antibody solutions to increase the penetration of the staining, and allowed for a significantly reduced protocol; permeabilisation and blocking steps were performed simultaneously, and no wash step was required prior to the primary antibody step. Finally, because the tissue was processed in a tube or a microplate, it required mounting onto glass for imaging after the completion of the staining. This was performed in the same way as live tissue mounting, using Whatman lens cleaning papers to press the tissue down onto the cover slip (Fig. 2.1). This was performed in PBS.

Tissue was treated with relevant stimuli or inhibitors in physiological saline at 37 °C (in Eppendorf tubes or microplates if a large number of samples were being

[1] *Nota bene*: treatment of live tissue with agonists and inhibitors prior to fixation required no such agitation and, indeed, only minor stirring was necessary for agonists to have homogeneous effects.

processed). Before fixation, tissue was washed once with fresh physiological saline. This solution was then removed by an aspirator and 4% PFA in PBS was added immediately. Tissue was then fixed overnight at 4 °C on an orbital or rotating mixer. The PFA was then removed and the tissue washed once quickly in PBS and then twice more for 5 minutes, agitated. Blocking and permeabilisation buffer was then added and was of the following specifications; PBS; 10% goat serum; 1% BSA; 0.1% acetylated BSA; 1 mM $MgCl_2$; 0.3% Triton X-100; pH 7.4. Tissue was blocked and permeabilised in this buffer for at least one hour at room temperature, agitated. Primary antibodies could then be applied.

Primary antibodies were initially used at 1:100 or 1:200 to determine the quality, and then tried at lower concentrations if possible. Storage guidelines were followed strictly and antibodies stored at -20 °C were aliquoted to avoid unnecessary freeze / thaw cycles. Mitochondria were stained with a rabbit, polyclonal anti-Tom20 primary antibody (1:500, Santa Cruz Biotechnology) or a mouse, monoclonal anti-cyclophilin F antibody (1:200, Abcam, Cambridge, UK) dependent upon compatibility with other antibody species. Tubulin was stained with a mouse, monoclonal anti- α-Tubulin antibody (clone DM1A, 1:1000, Abcam). Bile salt-activated lipase was stained with a rabbit, polyclonal anti-bile salt-activated lipase antibody (catalogue number ab87431, 1:200, Abcam). Primary antibodies were diluted in the blocking and permeabilisation buffer described previously[2]. Secondary

[2] *Nota bene*: if the scientist wishes to be particularly efficient, antibodies could be added directly to the blocking and permeabilisation buffer containing the tissue, with no washing or replacement, as the buffers are

antibodies were conjugated with Alexa 488, Alexa 546 and Alexa 633 (1:1000). Nuclei were stained with Hoechst 33258 (10 µg ml^{-1} from a stock solution of 10 mg ml^{-1} in water). Actin was visualised using Alexa 546- or Alexa 633-conjugated phalloidin (1:50, Life Technologies).

Secondary antibodies were chosen dependent upon the individual experiment. Hoechst was used in almost all experiments and so no UV excitation antibodies were employed. If only one primary antibody was used, Alexa 488-conjugated secondary antibodies were employed as they have the highest quantum yield of any Alexa dyes (0.92)[3]. 488 nm is also the brightest and most stable laser line on most imaging set-ups and the quantum efficiency of the detector in this range is also much higher than further-red dyes. Alexa 546-conjugated secondary antibodies were the next most favourable, for similar reasons. Alexa 633-conjugated secondary antibodies were only used as a fourth stain as the quantum yield along with the quantum efficiency of the PMT in this range is particularly low.

Image Analysis

Software used included Zeiss LSM510 image analysis software; Zen 2009, 2010, and 2012 image analysis software (Carl Zeiss), or ImageJ. Images were only linearly adjusted (brightness and contrast), predominantly to allow for visibility of

identical. However if a large number of samples are being processed, this should be avoided; antibodies should be diluted in one large volume of fresh buffer to ensure an even concentration of antibody across samples.

[3] *Nota bene:* Quantum yield information is available from the excellent Life Technologies website - http://www.invitrogen.com/site/us/en/home/References/Molecular-Probes-The-Handbook/tables/Fluorescence-quantum-yields-and-lifetimes-for-Alexa-Fluor-dyes.html

essential features after printing but also for beautification. Any images which attempt to show quantitative information were processed identically in tandem.

Fluorescence Microplate Reader

For some applications, predominantly outlined in chapter 4 of this thesis but also used in experiments from chapter 3, a POLARstar OPTIMA fluorescence microplate reader (BMG labtech) was employed. V-bottom 96-well microplates were used (Greiner Bio-One Ltd.) as these enabled the cells to collect in the centre of the well, increasing the signal.

Measuring $\Delta\Psi_M$ with TMRM in Microplate Format

Cells were loaded with 10 µM TMRM at room temperature for 30 minutes, agitated using an orbital rotator, with the centrifuge tubes being wrapped in aluminium foil to prevent light exposure. To prevent damage to the cells from overloading, cells were resuspended in 5 ml physiological saline and a further 5ml of 20 µM TMRM solution was then added directly to give an overall TMRM concentration of 10 µM.

After loading, the cells were filtered using a 70 µm cell strainer to remove any necrotic cells (which clump together and are often seen after dequench mode loading) and centrifuged to remove any unabsorbed indicator. Cells were resuspended in 1 ml physiological saline and 150 µl of this suspension was used per well of a 96-well microplate. Injectors were used to add TLCS (from a stock of 50 mM in ddH_20) and CCCP (from a stock of 10 mM in EtOH) and the machine was set to agitate the plate after injection.

End-point Necrosis

Isolated murine pancreatic acinar cells from one pancreas were resuspended in 4 ml physiological saline. 1 ml of cells was incubated with respective test solutions and agitated by rotary inversion for 30 minutes at 37 °C. Cells were then centrifuged at 260 G for 2 minutes. 800 µl of the supernatant was removed and the pellet resuspended to increase the cell concentration 5X. Cells were then transferred to a microplate, incubated with 100 µg ml^{-1} PI and the fluorescence was measured (540 nm excitation, 590-630 nm emission). The microplate was then removed from the machine and total necrosis was induced with addition of Triton X-100 to a final concentration of 0.02%. The plate was returned to the reader and fluorescence measured again. This maximum fluorescence was used as a 100% necrosis standard for determining the percentage necrosis induced by TLCS. Exact and respective cell-free blanks were used for all compounds and combinations of compounds with Triton X-100 and / or TLCS and these values deducted from the respective test value.

Time-course Necrosis

For time course necrosis experiments, isolated cells were spun down and resuspended in 900 µl physiological saline to give a high density of cells. Cells were manually agitated to ensure homogeneity and added to wells. 75 µl of cells was added to 75 µl Caffeine at 2X or 75 µl physiological saline (for control and TLCS samples). The plate was then incubated for 20 minutes at room temperature. TLCS was then added to all wells except for the control to give a concentration of 500 µM. After 5 minutes, PI was then added to all wells at a 50 µM concentration and mixed by manual agitation.

The microplate was then placed in the reader (which was either set to room temperature or pre-heated to 37 °C), and fluorescence determined by excitation 543 nm and emission 620 nm with bottom reading. The gain was adjusted manually for each experiment to achieve a basal fluorescence intensity of between 10-15% of the maximum arbitrary unit value of 260,000 to allow for the increase associated with maximum necrosis and avoid the signal saturating, making normalisation to the maximum fluorescence impossible.

The assay was set to run with a cycle time of 600 seconds. In experiments where maximum necrosis needed to be induced, 3 µl of 1% Triton X-100 was injected to give a working concentration of 0.02%. Data were normalised to the minimum and maximum fluorescence by performing (F-Fmax) / (Fmax-Fmin) +1.

SUNDRY PROTOCOLS

PDE ASSAY

A cyclic nucleotide PDE assay kit (Enzo life sciences) was used to determine the relative PDE inhibition by methylxanthines. The assay measures the 5'-AMP produced from cleavage of 3',5-cAMP by PDE by measuring phosphate released from 5'-AMP by 5'-nucleotidase with a modified malachite green assay. Two concentrations of methylxanthines were incubated with PDE to determine the inhibition. 200 µM IBMX was supplied with the assay kit as the PDE inhibition control. The concentration of 5'-AMP produced was then determined using a standard curve of 5'-AMP for each individual experiment (R^2 >0.995).

IP_3 Uncaging

ci-IP_3/ PM (SiChem, Germany) was loaded at 2 μM simultaneously with Fluo-4. Cells were used within 2 hours of loading. IP_3 was uncaged by UV excitation of the cells with one flash of 1% power, 364 nm laser (Coherent) every 3 seconds where indicated. The entire cell region was selected for uncaging.

Area Under Curve Analysis

Area under the curve analysis was performed on hyperstimulatory Ca^{2+} plateau data using the sum of the F/F_0 values converted to percentage of the control.

ACh-Induced Ca^{2+} Spike Counting

Spike counts were performed blind by an independent scientist, directed to only count spikes which were at least 25% of the maximum peak and unambiguously distinguishable from noise. Traces where the spiking did not recover after wash-off of the test compound were discounted. All data shown are averages ± SE of at least 9 experiments from at least 3 animals. Statistical significance was determined by Student's t-test and $*,^{\dagger},^{\ddagger}$ indicates $p<0.05$.

Mitochondrial Profiling and Quantification of Distribution

Mitochondrial profiling was performed using Carl Zeiss Zen software. This software allows the user to draw a profile across a given line on the image and generate a graph of the intensity across this line. Importantly, version 2012 of this software allows the profile to be widened, averaging the profile across a set width and allowing for more than single pixel profiling. This was essential in this setting as it allowed for much greater averaging of the location of the mitochondria throughout

the relevant cytosolic region. Profile regions were chosen with the mitochondrial fluorescence channel switched off so as to blind the investigator to the location of the mitochondria. Regions of cytosol containing the nucleus were omitted, and where possible actin staining was used as a guide to avoid the lateral membranes. Fluorescence signal was normalised to the average fluorescence intensity (F/F_{μ}) in order to show relative redistribution. Other forms of normalisation were tried, but often gave very odd representations of the data, and made very diffuse distributions seem unrepresentatively high or low. Normalisation to the average intensity effectively enabled representation of where the mitochondria were moving from and to. All data shown are averages ± SEM of at least 9 regions from at least 3 individual experiments. Where required (due to differing pixel densities of images) interpolation was performed using OriginPro graphical software. Analyses of the subplasmalemmal and perigranular regions of the cells in Figs 4 and 6 were performed by measuring the average intensity of the area <5 μm from the granular region and <2 μm from the plasma membrane (also with the mitochondrial channel switched off and based solely upon the transmitted image so as to blind the investigator to the location of the mitochondria). Statistical significance was determined by Student's t-test and * indicates $p<0.05$.

CHAPTER 3: RESULTS

Xanthines and Ca^{2+} Signals

INTRODUCTION

Toxic Ca^{2+} signals are implicated in a range of diseases including acute pancreatitis, a severely debilitating and potentially fatal inflammatory disease lacking any specific therapy (Criddle et al., 2006). Disruption of normal Ca^{2+} signalling, and elevated basal $[Ca^{2+}]_c$ has been correlated with the early onset of disease in murine models of acute pancreatitis (Ward et al., 1996). Overload of Ca^{2+} is responsible for the intracellular enzyme activation, vacuolisation, and necrosis associated with the onset of acute disease. Cytosolic Ca^{2+} overload can be induced by a range of physiologically relevant stimuli, including cholecystokinin (CCK) and bile acids such as taurolithocholic acid 3-sulphate (TLCS). Caffeine has been shown to reversibly inhibit these toxic Ca^{2+} signals in pancreatic acinar cells, where it does not show any ryanodine receptor-mediated Ca^{2+} release (Voronina et al., 2002). A link between caffeine and pancreatitis has been inferred from a retrospective cohort study (Morton et al., 2004), which showed that coffee drinkers (> 4 cups per day) had a small but statistically significant reduced risk of developing alcohol-associated pancreatitis.

Experimentally, caffeine is often used to inhibit IP_3R Ca^{2+} release, a mode of action which was originally discovered in xenopus oocytes (Parker and Ivorra, 1991), and has also been shown in pancreatic acinar cells, when IP_3 was administered through a cell-attached patch pipette (Wakui et al., 1990). Other properties of caffeine have also been associated with inhibition of Ca^{2+} signalling such as PDE inhibition: The adenylyl cyclase activator forskolin, which increases the cellular concentrations of cAMP, has been shown to inhibit Ca^{2+} signals induced by non-sulphated CCK (Wakui et al., 1991) and the non-hydrolysable analogues, 8-Bromo-cAMP and 8-Bromo-GMP

have been shown to inhibit ACh-mediated Ca^{2+} signals when applied simultaneously (Camello et al., 1996). Caffeine has also been shown to inhibit the production of IP_3 in pancreatic acinar cells (Toescu et al., 1992) which could inhibit the formation of IP_3-mediated Ca^{2+} signals. This inhibition of IP_3 production could also potentially affect $[Ca^{2+}]_c$ through modulation of store-operated Ca^{2+} entry, which has been shown to be affected by levels of phosphoinositides (Walsh et al., 2010). The effect of caffeine on store-operated Ca^{2+} entry is currently poorly defined and it is possible that inhibition of this cellular mechanism could also contribute to the inhibition of Ca^{2+} signals. The role of these multiple actions of caffeine in inhibiting different types of agonist-induced Ca^{2+} signals is unclear, and it may be that a coordinated effect explains the total block of these signals in vitro.

In order to elucidate the mechanism of inhibition of Ca^{2+} overload by caffeine we investigated the effect of caffeine on CCK and TLCS hyperstimulation. Furthermore, we investigated the effect of caffeine on the store-operated Ca^{2+} plateau. The effect of cAMP on hyperstimulation was also investigated given the inhibition of oscillations by cAMP and cGMP discussed previously and as this has not been investigated. To further complement this investigation, we aimed to determine structure-activity relationships between a range of methylxanthines in terms of the inhibition of Ca^{2+} signalling in pancreatic acinar cells and the relative PDE inhibitory activity, in order to elucidate the mechanisms of inhibition of Ca^{2+} overload. We aimed to find out if any methylxanthines offer an improved inhibition of these signals, enabling the further design of targeted IP_3R inhibitors.

CAFFEINE INHIBITION OF CCK-INDUCED CA^{2+} SIGNALS

To investigate inhibition of the IP_3R in pancreatic acinar cells, and the potential effects of IP_3R inhibition on the pathophysiological processes involved in the onset of acute pancreatitis, the inhibition by caffeine of pathological Ca^{2+} signals was determined in the first instance. Pancreatic acinar cells were isolated from mice, loaded with Fluo-4, and visualised by fluorescence microscopy. An elevated Ca^{2+} plateau was formed by hyperstimulation with 10 nM CCK. Two concentrations of caffeine, 1 and 10 mM, were then superfused in addition to the CCK to determine inhibition of the Ca^{2+} plateau. 1 mM caffeine reduced the plateau by 27% ($\pm$ 2.82, n= 29), whereas 10 mM caffeine blocked the signal entirely (98.16 $\pm$ 6.56% reduction, n=11) (Fig. 3.1). In preliminary studies not shown, 10 mM caffeine had no detectable quenching of the fluo4 signal in vitro, and there was no quench to baseline fluorescence. Removal of 10 mM caffeine also caused a rebound of the Ca^{2+} signal beyond the plateau height. To complement these findings on inhibition of sustained signals, the effect of caffeine on physiological CCK-induced Ca^{2+} oscillations was investigated using 10 pM CCK (Fig. 3.2). Oscillations were induced with 10 pM CCK and after three minutes, caffeine was applied in addition to the CCK for a period of three minutes. Caffeine was subsequently removed and 10 pM CCK superfused alone for a further three minutes. 10 mM caffeine did not significantly reduce the peak height induced by 10 pM CCK (Fig. 3.2A), indicating that physiological CCK-induced Ca^{2+} oscillations are far less susceptible to inhibition by caffeine than hyperstimulatory responses, consistent with previous findings from both Balb/c mice and guinea pig pancreatic acinar cells (Sjodin and Gylfe, 2000, Lee et al., 2003). However there was

a significant inhibition of the frequency of spikes (Fig 3.2B). These experiments would be improved with longer periods of sustained oscillations as three minutes is a rather short period of time. The change in superfusion could also be partly responsible for the change in frequency and again this could be improved with longer periods of caffeine application to the oscillatory response Application of caffeine before the application of CCK was significantly less effective at inhibiting the Ca^{2+} signal induced by 10 nM CCK. Whilst post treatment lead to a drop of cytosolic Ca^{2+}, pre-treatment with caffeine converted the sustained response to an oscillatory response, but did not affect the initial peak height (Fig. 3.3).

Caffeine Inhibition of TLCS-Induced Ca^{2+} Signals

In order to investigate the effects of caffeine on bile acid induced Ca^{2+} signals, TLCS was used to induce both Ca^{2+} overload and Ca^{2+} oscillations. 500 µM TLCS induced a sustained Ca^{2+} overload in Fluo-4-loaded pancreatic acinar cells. Caffeine successfully inhibited the TLCS-induced Ca^{2+} signal in a dose-dependent manner (Fig. 3.4). No inhibition could be detected at 1 mM caffeine. At 3 mM the plateau was reduced, but $[Ca^{2+}]_c$ remained elevated (Fig. 3.4A). Upon increasing the concentration of caffeine to 5 mM, the Ca^{2+} plateau was converted to an oscillatory signal (Fig. 3.4B). 10 mM caffeine completely blocked any Ca^{2+} release induced by TLCS (Fig. 3.4C). Similarly to the effect of pre-treatment with caffeine on the CCK-induced Ca^{2+} signal, pre-treatment with caffeine offered less inhibition of the TLCS-induced Ca^{2+} signal than post-treatment. Fig. 3.5 shows this phenomenon, where pre-treatment with 10 mM caffeine prior to the TLCS-induced Ca^{2+} signal converted the

sustained response to an oscillatory response. This is in stark contrast to the complete block with 10 mM caffeine shown in Fig. 3.4.

Oscillatory Ca^{2+} signals were induced in pancreatic acinar cells by superfusion with 200 μM TLCS. TLCS-induced oscillations were relatively large and broad oscillations which were sustained for a number of minutes. 10 mM caffeine was applied to these oscillations and offered an almost complete block which was then reversed upon removal of the caffeine, when oscillations resumed (Fig. 3.6). This is unexpected given the lack of reduction of Ca^{2+} amplitude offered by caffeine during pM CCK-induced oscillations (Fig 3.2).

Effect of Caffeine on Store-Operated Ca^{2+} entry

Store-operated Ca^{2+} entry is an essential component of the sustained Ca^{2+} plateau. To investigate the role of caffeine during store-depletion, a store-operated Ca^{2+} entry plateau was induced using CCK. 10 nM CCK was applied to Fluo-4-loaded pancreatic acinar cells in zero external Ca^{2+}. Ca^{2+} was then reintroduced after the Fluo-4 signal reached baseline. Caffeine was then applied to the plateau. The CCK store-operated Ca^{2+} entry plateau was significantly inhibited by 10 mM caffeine. Furthermore, upon the removal of 10 mM caffeine, Ca^{2+} returned to the original plateau height (Fig. 3.7A).

To test the inhibition by caffeine of the Ca^{2+} influx component of the plateau, the store-operated Ca^{2+} entry plateau was induced by inhibiting SERCA refilling of the intracellular Ca^{2+} store using 2 μM thapsigargin in Ca^{2+}-free extracellular solution. The store-operated Ca^{2+} entry plateau formed upon the introduction of 5

mM Ca^{2+} to the extracellular solution was unaffected by the addition of 10 mM caffeine and remained 97% (±1.87 n=8) of the original pre-caffeine treatment height (Fig 3.7C).

The addition of 2 μM thapsigargin on top of the CCK-induced store-operated Ca^{2+} plateau was also tested. Upon the addition of thapsigargin, the plateau remained unchanged but when 10 mM caffeine was added in addition to the thapsigargin, $[Ca^{2+}]_c$ increased (Fig. 3.7B,C). The rate of store-operated Ca^{2+} entry after depletion of the Ca^{2+} store by CCK or thapsigargin was also determined. From the same protocol described previously, the store was depleted in the absence of external Ca^{2+} and the rate of entry determined after reintroduction of 5 mM Ca^{2+}. The rate of entry was significantly higher after store-depletion with CCK than with thapsigargin (Fig 3.8). Again this indicates a regulatory role of the components of the stimulus coupling pathway on Ca^{2+} influx but the exact mechanism for these differences is not understood. To complement the investigation of store-depletion induced by CCK and thapsigargin, the effects of the bile acid, TLCS were also examined. TLCS was applied at 500 μM to induce Ca^{2+} overload as seen in Fig. 3.4. Ca^{2+} signals can be seen to reduce over time during TLCS hyperstimulation in zero external Ca^{2+}, as seen in the average trace (Fig. 3.9). Subsequent addition of 5 mM external Ca^{2+} caused a rapid rise in cytosolic Ca^{2+}. Upon close investigation of the individual Ca^{2+} traces, oscillatory responses can be seen upon stimulation with 500 μM TLCS in zero Ca^{2+}, indicating that the signal is inhibited by the reduced external Ca^{2+} concentration and also that the store is not depleted. The Ca^{2+} entry segment of the traces also shows a peak plateau response, indicative more of a store Ca^{2+} release, rather than an influx

(Fig 3.9B). It is important to note that application of 5mM Ca^{2+} externally could potentially activate Ca^{2+} -sensing receptors which are known to be expressed in pancreatic acinar cells, making conclusive interpretation of these data more difficult (Bruce et al., 1999).

METHYLXANTHINES INHIBIT ACH-INDUCED CA^{2+} OSCILLATIONS

ACh was used to induce IP_3-mediated Ca^{2+} signals and the inhibition of these signals with caffeine was investigated. 50 nM ACh induced Ca^{2+} oscillations in Fluo-4 loaded pancreatic acinar cells. After three minutes caffeine was applied in combination with the ACh. 200 µM Caffeine showed no effect on ACh-induced Ca^{2+} oscillations (data not shown). 500 µM and 1 mM caffeine showed dose-dependent partial inhibition of oscillations. Strong inhibition was offered at 2 mM, and 20 mM caffeine completely blocked Ca^{2+} signals and significantly dropped the fluorescence to lower than basal levels (Fig. 3.10). This drop induced by 20 mM caffeine is likely due to quenching of the Fluo-4 at such a high concentration.

Having outlined the inhibitory effect of caffeine on CCK-induced pathological Ca^{2+} overload and ACh-induced oscillations, the relative inhibition of a range of methylxanthines on IP_3-mediated Ca^{2+} signals was investigated. The aim of this was to determine if there are any structural features which could be influential in the design of novel inhibitors and potential therapeutics. Theophylline, theobromine, paraxanthine, 1-methylxanthine and 7-methylxanthine are defined in figure 3.11 with respect to their relevant methylation. Di-methylxanthines successfully inhibited ACh-induced Ca^{2+} signals (Fig. 3.12). Theophylline and paraxanthine showed almost

complete inhibition of ACh-induced Ca^{2+} spikes at 500 µM indicating a stronger inhibition than caffeine. The di-methylxanthine theobromine offered strong inhibition at 2 mM. 1-methylxanthine showed poor inhibition of oscillations, and xanthine showed no effect (Fig.3.13). To elaborate on the relative inhibition offered by methylxanthines, the inhibition of ACh-induced Ca^{2+} oscillations was quantified by counting the number of Ca^{2+} spikes to directly compare inhibition. All methylxanthines tested were shown to significantly inhibit ACh-induced Ca^{2+} signals at 2 mM and 500 µM in a dose dependent manner. Caffeine showed a significant reduction in Ca^{2+} oscillations at 500 µM and a strong inhibition at 2 mM (Fig. 3.14). Dimethylxanthines theophylline, paraxanthine, and theobromine showed significantly more inhibition than caffeine at 500 µM, with paraxanthine showing the highest inhibition of the three dimethylxanthines. Monomethylxanthines showed the least inhibitory activity.

PDE Inhibition by Methylxanthines and the Effect on Ca^{2+} Signalling

It has been previously documented that simultaneous increases in both cAMP and cGMP (using non-hydrolysable analogues of these compounds) can offer a coordinated synergistic effect to inhibit Ca^{2+} oscillations induced by ACh (Camello et al., 1996). As discussed previously, methylxanthines are known inhibitors of phosphodiesterases, enzymes responsible for the breakdown of cAMP and cGMP. We aimed to investigate the relative phosphodiesterase inhibition, in order to compare this to the inhibition of Ca^{2+} signals and further examine the possible interrelatedness of phosphodiesterase function and Ca^{2+} release. In order to determine the relative

PDE inhibition by methylxanthines, a PDE assay kit was employed. Two concentrations of methylxanthines were incubated with the PDE enzyme and the relative inhibition was determined by measuring the amount of 5'AMP produced. With the exception of 500 μM 7-methylxanthine, all the compounds tested significantly inhibited PDE in a dose dependent manner (Fig. 3.15). Theophylline showed the greatest inhibition, statistically equivalent to the IBMX control. Methylxanthines show a similar profile of inhibition with regards to PDE and Ca^{2+} oscillations (Fig. 3.14 and Fig. 3.15). Because of the similarity between the profiles of Ca^{2+} inhibition and PDE inhibition, we aimed to further investigate the susceptibility of ACh-induced Ca^{2+} oscillations to PDEIs. Fig. 3.16 shows that the methylxanthine-based non-specific PDEIs, pentoxifylline and IBMX, significantly inhibit ACh-induced Ca^{2+} oscillations. The cAMP specific PDE4 inhibitor, rolipram, was also superfused over ACh-stimulated pancreatic acinar cells and was shown to inhibit oscillations. This inhibition of oscillations was only observed at supramaximal concentrations, where non-specific inhibition of other PDEs is more likely (Fig. 3.17A,B). However, Fig. 3.18 shows that no inhibition of the CCK-induced Ca^{2+} plateau was offered by addition of non-hydrolysable analogues of cAMP and cGMP (8-bromo-cAMP / GMP). This confirms that whilst PDE inhibition may play a role in xanthine-based inhibition of ACh-induced Ca^{2+} oscillations, PDE inhibition is not sufficient to inhibit IP_3-mediated Ca^{2+} overload during hyperstimulation.

THE MEMBRANE-PERMEABLE CAGED IP_3 ANALOGUE, CI-IP_3/PM

In order to more specifically test for the relative inhibition of the IP_3R by methylxanthines, a caged, cell permeable IP_3 analogue was used, ci-IP_3 /PM. This compound was loaded into the cell with the Ca^{2+} indicator Fluo-4 and subsequent uncaging of this IP_3 analogue with UV light (1% 351 nm every 3.9 seconds) induced a Ca^{2+} signal within the cell. Fig. 3.19 shows the effect of IP_3 uncaging on cytosolic Ca^{2+} signals. Oscillatory and sustained signals were generated and the effect was averaged to determine the relative increase in $[Ca^{2+}]c$.

Uncaging was then performed in the presence or absence of caffeine at 3 and 5 mM to determine the inhibition of the IP_3R irrespective of any inhibition of IP_3 production (Fig. 3.20). Xanthines were applied alone and IP_3 was subsequently uncaged as indicated by the dotted line in Fig. 3.20 and as described in materials and methods. After a period of 1 minute, xanthines were removed to allow for Ca^{2+} signals to occur as a control for successful IP_3-uncaging. The area under curve during the perod between 30 and 60 seconds after the application of UV was used for analysis Caffeine was shown to inhibit the IP_3 -induced Ca^{2+} signals at 3 and 5 mM in a dose dependent manner and example traces are displayed (Fig 3.20A, B). Uncaging was also performed in the presence of theophylline and paraxanthine. Fig. 3.20C shows the data after averaging of the signals and area under the curve analysis. All three methylxanthines significantly inhibited ci-IP_3 /PM –induced Ca^{2+} signals in a dose dependent manner, with almost complete inhibition seen at 5 mM and approximately half inhibition at 3 mM. Unlike the inhibition of ACh oscillations and PDE inhibition,

there were no statistically significant differences between the inhibition of ci-IP_3 /PM-induced Ca^{2+} signals by the three methylxanthines tested. Theobromine, 1-methylxanthine and 7-methylxanthine were insoluble at these concentrations and were therefore unable to be compared to caffeine, theophylline and paraxanthine.

Inhibition of Pancreatic Acinar Cell Necrosis by Methylxanthines

The effect of inhibiting TLCS-induced Ca^{2+} overload by methylxanthines on necrosis was investigated in an end point assay. Freshly isolated pancreatic acinar cells were treated for 30 minutes with TLCS alone; TLCS in the presence of caffeine, theophylline, and paraxanthine; or methylxanthines alone, in tubes rotating at 37 °C. Cells were then stained with propidium iodide (a non-membrane permeable nucleic acid dye). The fluorescence was measured in plate reader format, and maximum necrosis was then induced with 0.2% Triton X-100 and used as a reference to normalise the samples. Cells were visualised under the microscope to confirm total cell death. Caffeine, theophylline, and paraxanthine had no effect on pancreatic acinar cell necrosis per se and these samples were statistically comparable to control. Cells incubated on the rotator in TLCS at 37 °C for 30 minutes suffered ~70% necrosis. Caffeine, theophylline and paraxanthine were all shown to ameliorate necrosis at 10 mM, and theophylline and paraxanthine offered dose dependent inhibition at 5 mM, however inhibition was not significant at 3 mM (Fig. 3.21).

Protective Effect of Caffeine on Ca^{2+}-Induced Mitochondrial Dysfunction

Cytosolic Ca^{2+} overload is known to cause mitochondrial depolarisation and a drop in NAD(P)H. $\Delta\Psi_M$ was visualised in pancreatic acinar cells using TMRM and NAD(P)H auto-fluorescence recorded simultaneously. 10 nM CCK induced a fall in $\Delta\Psi_M$ (Fig. 3.22A) after only a few minutes. This drop is reversed by the addition of caffeine at 10 mM, which has been shown to completely block the Ca^{2+} signal (Fig 3.1): $\Delta\Psi_M$ returns to basal levels. This protection by caffeine is also reversed after removal of the caffeine. A similar effect was observed when looking at the NAD(P)H, where a drop was induced upon hyperstimulation and this was reversibly inhibited by 10 mM caffeine.

Discussion

In this section the effects of methylxanthines on cytosolic Ca^{2+} signalling was investigated; focusing on the involvement if PDE inhibition and IP3R inhibition. Oscillatory signals were differentially inhibited by methylxanthines, however oscillatory signals are susceptible to increases in cAMP and cGMP caused by PDE inhibition and any conclusions are therefore confounded. There was, however, no significant difference between methylxanthines upon inhibition of sustained Ca^{2+} elevations, but the concentrations required for significant inhibition were rather high. Sustained Ca^{2+} elevations were not inhibited by non-hydrolysable analogues of cAMP and cGMP. Finally, inhibition of hyperstimulatory Ca^{2+} signals by caffeine is sufficient to protect against mitochondrial dysfunction and necrosis.

Caffeine Inhibition of Ca^{2+} Overload

This study has investigated the effects of caffeine upon the sustained elevation of cytosolic Ca^{2+} in pancreatic acinar cells, which is thought to be associated with the onset of acute pancreatitis. Store-operated Ca^{2+} entry may not be directly inhibited, as suggested through the lack of inhibition offered to the thapsigargin plateau, but was indirectly inhibited through inhibition of store-depletion. This is in accordance with the current literature (Lur et al., 2011). Whilst it is not wholly conclusive that caffeine does not inhibit store-operated Ca^{2+} entry, the lack of any inhibition of the thapsigargin-induced Ca^{2+} plateau could suggest that the inhibition of CCK-induced Ca^{2+} signals is by inhibition of Ca^{2+} release from the Ca^{2+} store, and not by inhibition of Ca^{2+} entry into the cell. Indeed, the inhibition by caffeine of the Ca^{2+} signal after store-depletion is not as immediate as the inhibition of the plateau shortly after stimulation. This is possibly due to the inhibition by caffeine being solely IP_3R mediated and not by inhibition of Ca^{2+} influx; shortly after stimulation the Ca^{2+} store will not be depleted and the plateau will be immediately susceptible to inhibition of Ca^{2+} release via the IP_3R. The lack of any inhibition of the thapsigargin-induced plateau could indicate that the agonist-induced plateau reduction is by inhibition of the IP_3R, and not stimulation of Ca^{2+} clearance by upregulation of the PMCA, as Ca^{2+} clearance should not offer any selectivity to the manner of release. Finally, lack of inhibition of thapsigargin induced responses also helps to affirm that 10 mM caffeine is not quenching the Fluo-4 as may be the case at higher concentrations. It is not conclusive however, that upregulation of the SERCA is not at least in part responsible for the effect of caffeine on the plateau. Modulation of the plateau could be due to

changes in SERCA function. Inhibition of SERCA with thapsigargin would therefore mask any inhibition by caffeine and this is an important area of study which would benefit from further investigation. It should be noted however that no inhibition was offered by analogues of cAMP and cGMP, which would be the logical candidates for regulation of SERCA.

The inhibition of hyperstimulatory CCK signals by caffeine matches the concentration curve of IP_3R inhibition by caffeine in permeabilised vascular smooth muscle cells treated with 300 nM IP_3 in a $[Ca^{2+}]$ of 300 nM (Hirose et al., 1993).

Importantly, we have shown that the inhibition of Ca^{2+}-overload by caffeine is effective in ameliorating the drop in $\Delta\Psi_M$ and NAD(P)H associated with mitochondrial Ca^{2+} overload and a drop in ATP:ADP ratio.

Caffeine inhibition of the TLCS-induced Ca^{2+} plateau indicates the importance of the IP_3R in this signal, and corroborates the idea of a receptor-linked IP_3 production mechanism in TLCS stimulation of pancreatic acinar cells. However, reduction in Ca^{2+} released when external Ca^{2+} is removed argues against this theory. This is supported by the rapid release of Ca^{2+} upon addition of external Ca^{2+}. It has been shown by Aldebaran Hofer's laboratory that Ca^{2+} influx induced by the action of the bile salt deoxycholic acid at the plasma membrane activates both PKC and PLC to produce IP_3 (Lau et al., 2005). This model would rectify the discrepancies in these data, where the Ca^{2+} signal generated by TLCS is both dependent upon external Ca^{2+} and at the same time, wholly sensitive to IP_3R inhibition. The lack of inhibition of the initial spike induced by CCK could be due to activation of low affinity CCK receptors

and the production of cADP ribose and NAADP acting on Ca^{2+} release channels not sensitive to Ca^{2+}. However, as the TLCS-induced Ca^{2+} signal shows a very similar effect (in which the initial peak is not inhibited and post-treatment with caffeine actually shows a more pronounced effect), this could indicate an involvement of the concentration of Ca^{2+} inside the store. Luminal Ca^{2+} has been shown to directly sensitise the IP_3R (Nunn and Taylor, 1992) and also the RyR (Kong et al., 2008). This could offer an explanation as to the limited effect of caffeine when applied before the signal, as the store Ca^{2+} concentration is higher and so the IP_3R will be more susceptible to channel opening. When the concentration of Ca^{2+} in the store is lowered after the initial peak has dropped and a plateau ensues, the IP_3R open probability is lowered and so the effect of caffeine inhibition may be greater.

The counterintuitive caffeine-induced increase in the plateau after treatment with both thapsigargin and CCK indicated the potential complexities within the cellular Ca^{2+} homeostasis machinery. As caffeine has been shown to inhibit the production of IP_3 (Toescu et al., 1992), these data may indicate a regulatory role of PLC activity on store-operated Ca^{2+} entry, either via IP_3 itself, or via PIP_2 or DAG, and may deserve further investigation.

Methylxanthines, Ca^{2+} and PDEI

We have shown significant inhibition of ACh-induced Ca^{2+} oscillations by methylxanthines, with theophylline and paraxanthine showing the most inhibition. The inhibition of IP_3R-mediated Ca^{2+} release by theophylline is in contrast to original findings of Parker & Ivorra, in which theophylline showed little or no inhibition,

arguing for a cAMP independent mechanism offered by the PDE inhibition of theophylline (Parker and Ivorra, 1991). Here we have shown that sustained Ca^{2+} overload is not susceptible to increased cAMP, but ACh-induced Ca^{2+} oscillations are inhibited by PDE inhibition. The inhibition by methylxanthines of ACh-induced oscillations will therefore have a cAMP-dependent component. Indeed the profile of PDE inhibitory activity was similar to the profile of Ca^{2+} inhibition across the range of compounds tested.

CAGED IP_3

To our knowledge, this is the first employment of membrane permeable loadable caged IP_3 in pancreatic acinar cells. This technology is somewhat restricted however, as the amount of IP_3 able to be released upon photolysis is limited and only able to generate Ca^{2+} signals for a short period of time. Using caged IP_3 we have shown inhibition of the IP_3R by low millimolar concentrations of dimethylxanthines, theophylline and paraxanthine in intact cells for the first time, with no significant differences between these compounds. Unfortunately none of the compounds tested showed any major increased activity or suggested any structural features which could be exploited for the design of therapeutics. Indeed without good structural data, inhibitors cannot be designed and accreted to fit the respective binding site. However, this should not detract from the viability of the technology, which may be appropriate and valuable for other investigations.

End-Point Necrosis

As discussed previously, we have shown for the first time that caffeine inhibits TLCS-induced Ca^{2+} overload at low doses (3 mM). Increasing this inhibition can convert the sustained Ca^{2+} signal to an oscillatory response and importantly, it is this change from sustained to oscillatory which correlates to an amelioration of cellular necrosis. This corroborates current opinion that oscillatory Ca^{2+} signals do not give rise to the pathological events seen by sustained overload of $[Ca^{2+}]c$, as necrosis is ameliorated at concentrations where the Ca^{2+} signal is converted to oscillatory signals or abolished completely, but necrosis ensues where the $[Ca^{2+}]c$ is slightly lowered but remains sustained (Fig. 3.4 & 3.21) (Criddle et al., 2007).

Methylxanthines and Pancreatitis

Significant toxicity is associated with the use of methylxanthines clinically (Boison, 2011) and the concentrations of methylxanthines required in this study for the inhibition of Ca^{2+} overload and necrosis would be fatal in man (Zimmerman et al., 1985). Theophylline overdose has even been shown to induce acute pancreatitis (Liu et al., 2008). Whilst these data show the potential benefit of inhibiting IP_3-mediated Ca^{2+} signals in the treatment of acute pancreatitis, we were unable to identify any related compounds or structural features which would enable development of therapeutics. Specific modulators of IP_3Rs could offer therapeutic potential for a range of pathologies, specifically acute pancreatitis, and recent improved 3D modelling of the receptor (Seo et al., 2012) will hopefully allow for improved intelligent design of inhibitors.

Aside from modulation of Ca^{2+} signalling, other effects attributed to caffeine have been shown to offer protective effects to the disease state; PDE inhibition (de Campos et al., 2008, Mersin et al., 2009) and Ca^{2+} channel blockade (Hughes et al., 1996) have been shown to ameliorate pancreatitis in vivo. Both of these processes induce vasodilation and this should be considered as a putative mechanism for the significant amelioration of pancreatitis offered by caffeine in vivo.

Ca^{2+} overload has been the target of investigations into models of acute pancreatitis; inhibition of IP_3-mediated Ca^{2+} overload, by inhibition of the subsequent ryanodine receptor-mediated Ca^{2+} induced Ca^{2+} release with dantrolene, has been shown to ameliorate both caerulein (Orabi et al., 2010) and bile-induced (Husain et al., 2012) acute pancreatitis in vivo. It seems likely from the data available that caffeine amelioration of acute pancreatitis may be due to a synergistic effects on a number of different targets. Whatever the specific role, caffeine is responsible for drastic amelioration of acute pancreatitis in vivo and elucidation of the mechanisms involved could be important in the development of targeted therapeutics for the treatment of this potentially fatal disease.

CHAPTER 4: RESULTS

Multiplex Developments

INTRODUCTION

Screening of potential therapeutic compounds to inhibit identified targets requires significantly high throughput, to ensure both speed and financial viability. Moreover, because high throughput assays require less human handling, they ensure a reduction in human error associated with discontinuous experimental repeats. In this chapter, I will outline some developments made to determine the $\Delta\Psi_M$ and cellular necrosis in a multiplex format.

The change in $\Delta\Psi_M$ was chosen as a physiological measurement suitable for the development of a multiplex assay for two main reasons. Firstly, the collapse of $\Delta\Psi_M$, due to mitochondrial Ca^{2+} overload and the opening of the mPTP, has been identified as a key turning point in the development of acinar cell necrosis during pathological insult of isolated pancreatic acinar cells (Criddle et al., 2007). Inhibition of components of the mPTP has also been shown to ameliorate models of acute pancreatitis in vivo (Mukherjee R et. Al., unpublished).

Measurements of $\Delta\Psi_M$ have been accomplished in plate reader format previously, by the employment of a dequench capacity of the $\Delta\Psi_M$ dye, TMRM (Blattner et al., 2001). We aimed to employ a similar protocol for live primary murine or human pancreatic acinar cells or tissue. The ability for this protocol to be possible in plate reader format is largely due to the specific chemical characteristics of the dye TMRM. At high loading concentrations (μM range), large quantities of TMRM are recruited to the inner mitochondrial membrane and the fluorescence emission is significantly quenched. Depolarisation of the mitochondria subsequently reduces the quench of the dye and increases fluorescence. There are two major

benefits of using dequench mode in a microplate format (or indeed in any format which does not enable the selection of a mitochondrial region of interest, i.e. the entire fluorescence signal from the cell is recorded). Firstly and perhaps most obviously is brightness; despite any quench effect, more dye means more signal. Secondly, and absolutely more importantly, is the positive correlation between the change in cytosolic and mitochondrial fluorescence induced by depolarisation. In normal mode, depolarisation of the mitochondria induces an increase in cytosolic staining as the TMRM sequestration to the mitochondria drops. This negative correlation between the increase in cytosolic staining and the decrease in mitochondrial staining, effectively cancels out the overall signal. The relative brightness of dequench mode may reduce the interference by increased cytosolic staining after depolarisation in relation to normal mode TMRM. However this is totally irrelevant as any increase in the cytosolic staining only serves to reinforce the dequench effect induced by mitochondrial depolarisation and in doing so amplifies the signal. On this basis, we aimed to determine the viability of using TMRM to measure $\Delta\Psi_M$ in isolated pancreatic acinar cells in multiplex format. We also aimed to investigate the sensitivity of this assay to depolarisation induced by the bile acid TLCS and to determine if any changes could be ameliorated by cyclosporin A, an inhibitor of cyclophilin D, a modulator of the mPTP. Finally with regards to $\Delta\Psi_M$, we aimed to determine the possibility of using human pancreatic tissue. Human pancreatic acinar cells and tissue rapidly degrade during storage and often only one or two experiments can be performed before the tissue or cells die or become unresponsive. It was therefore investigated whether human tissue could be analysed in a multiplex format,

allowing for simultaneous measurements. This would allow for more experiments to be performed before the tissue degraded and standardise any effects of degradation, for example, necrosis and unresponsiveness, between simultaneous repeats.

Aside from the measurement of $\Delta\Psi_M$, cellular necrosis was also investigated as a potential multiplex assay. The necrosis assay developed here differs from that used in *Chapter 3: Inhibition of pancreatic acinar cell necrosis by methylxanthines*. Those experiments incubated the cells in Eppendorf tubes and agitated them for 30 minutes before increasing the cell density and measuring endpoint necrosis (Saxton and Hollenbeck, 2012). With the assay discussed in this chapter, we aimed to develop a more automated approach, less dependent upon error-prone human intervention, where the cells were placed in the microplate and then incubated in the presence or absence of toxin or compound of interest, and the fluorescence change measured over time.

TMRM: Dequench Mode *vs.* Normal Mode

In order to investigate the prospect of using TMRM to measure $\Delta\Psi_M$ in microplate format, experiments were performed to investigate the optimum method of loading i.e. normal vs. dequench mode. First the normal mode was tested. Isolated murine pancreatic acinar cells were loaded with 50 nM TMRM and placed in v-bottom 96-well plates. Injectors were used to automatically add agents to the cells and the fluorescence was recorded over time. As anticipated, cells loaded with 50 nM TMRM were unable to emit sufficiently to record any changes in $\Delta\Psi_M$ in plate reader format: Applications of increasing concentrations of CCCP from 50 nM to 1 µM did not induce any recordable change in $\Delta\Psi_M$ (Fig. 4.1A). A stable basal level of fluorescence

was also difficult to establish due to increased noise generated by the requirement for increased gain. Conversely, cells loaded with 10 µM TMRM gave significantly more stable recordings at basal levels (Fig. 4.1B). Application of even low concentrations of CCCP (50 nM) gave significant increases in fluorescence corresponding to depolarisation of the $\Delta\Psi_M$. Concentration dependent effects of CCCP were then seen at 500 nM and 1 µM.

PATHO-PHYSIOLOGICAL CHANGES IN $\Delta\Psi_M$

Having confirmed sufficient sensitivity of dequench mode TMRM to measure small changes in $\Delta\Psi_M$, TLCS was used to hyperstimulate the cells, inducing a Ca^{2+} overload response and a drop in $\Delta\Psi_M$. Cells were imaged over time in the plate reader and TLCS was added automatically through injectors. A significant increase in fluorescence was observed after addition of TLCS, whilst the control cells (injected with a vehicle of ddH_20) remained stable. The addition of 1 µM CCCP towards the end of the experiment induced maximal depolarisation which was then used to normalise the data (Fig 4.2). The drop in $\Delta\Psi_M$ induced by TLCS was rather rapid in onset, and then stabilised before the addition of CCCP.

Due to the good reproducibility of results from TLCS-induced depolarisation in multiplex format, the same protocol was tried using freshly collected live human tissue. Tissue was collected to exacting standards defined in the respective methods section of this thesis. Tissue was embedded in gelatine and sliced to ~150 µm. Slices were loaded with 10 µM TMRM and then placed in a flat-bottom 96-well plate and TLCS added automatically using injectors as described previously. Fig. 4.3A shows the transmitted light image from a human tissue slice to show the quality of the tissue.

TLCS induced a rise in TMRM fluorescence whilst the $\Delta\Psi_M$ in control tissue remained stable (Fig. 4.3B).

Having confirmed the suitability of multiplex format measurements of $\Delta\Psi_M$ in isolated pancreatic cells and human pancreatic tissue slices, we aimed to determine if this assay was of sufficient quality and reproducibility to detect an amelioration of the drop in $\Delta\Psi_M$ induced by TLCS with the inhibitor of CyP-D, cyclosporin A. Isolated pancreatic acinar cells in the presence of 50 μM cyclosporin A displayed less depolarisation upon TLCS hyperstimulation than control cells (Fig. 4.4A & B). After quantification by area under the curve analysis, this reduction was shown to be statistically significant (Fig. 4.4C).

TIME SERIES NECROSIS

Having outlined successful measurement of TLCS-induced changes in $\Delta\Psi_M$ we moved on to investigate and develop live necrosis assays in multiplex format. Unlike measurements of $\Delta\Psi_M$ where changes occur in minutes, time-series necrosis assays were quickly found to require hours of measurements before necrosis ensued. Because of these extended time requirements, the physiological saline was augmented with antibiotics to prevent bacterial growth and included a source of amino acids and phosphate.

Initially, the necrosis assay was performed at room temperature, using CCK. Under these conditions; CCK began to induce a distinct divergence from the control after 12.5 – 15 hours (Fig. 4.5 red); control cells showed relatively stable fluorescence for approximately 24 hours (Fig. 4.5 blue); and caffeine successfully slowed the onset of CCK-induced necrosis in a dose dependent manner (Fig. 4.5 black). The data

obtained during these experiments were rather noisy and the cells were surviving much longer than expected. To try to improve this assay further, we increased the temperature of the assay to induce further necrosis and employed the bile acid TLCS as stimulant, similar to the end point necrosis assay described previously (Chapter 3 Fig. 3.21). Fig. 4.6 shows the results of this necrosis assay, which shows very significant differences between the control and the TLCS-treated samples, and necrosis developing after a few hours. This assay also employed an internal control, by using the detergent triton X-100 to lyse the cells and induce maximum fluorescence to which the data were normalised. Whilst the control trace was very stable, there was significant error in the TLCS-treated samples. The addition of 10 mM caffeine did not significantly ameliorate the cell death induced by TLCS under these conditions. To further describe the dynamic range of this assay, the basal fluorescence was approximately 5000 a.u., increasing to a maximum of approximately 100000 a.u. after the addition of Triton X-100.

DISCUSSION

In this chapter I have outlined the development of multiplex measurements of $\Delta\Psi_M$ and necrosis using isolated pancreatic acinar cells and human pancreatic tissue.

MEASURING $\Delta\Psi_M$

Despite the stability of the control groups and the divergence of the hyperstimulated samples from the control, significant amelioration of the depolarisation by TLCS was not as distinct as hoped for. To be able to measure a large number of compounds simultaneously and with sufficient accuracy to determine the

relative strength of inhibitors, the variation would need to be much less than that shown in Fig. 4.4B, where the error bars from TLCS and TLCS & cyclosporin A are only just divergent. The assay is also significantly limited by the number of samples which could be obtained from a single mouse pancreatic acinar cell preparation (6 wells). Unfortunately, reducing this density greatly increased the variability and the assay needed modification to ensure any reproducibility. For both of these reasons, the use of cultured cells for applications involving mutiplex screening of compounds should be employed. Whilst less physiologically relevant than isolated cells, cultured cell lines would enable the sufficient number of repeats and the standardisation required for such assays. Also, if the drug target has already been chosen, for example cyclophilin D, then inhibitors can be screened in a very controlled way, and potential hits followed up using conventional techniques e.g. confocal microscopy of pancreatic cells (or ideally tissue for proper physiological relevance).

With this in mind, the testing of human tissue in multiplex format is probably the most important of these developments. Whilst the least appropriate for high throughput screening due to the scarcity and low quantity of good human samples; human tissue rapidly degrades and the more data one can extract from the tissue within a few hours of isolation the better.

Measuring Necrosis

Significant differences between the time series assay and the end point assay were observed. When the cells were agitated with TLCS in Eppendorf tubes for 30 minutes, ~70% necrosis was induced. However cells which were stimulated and recorded over time with minimal agitation took ~10 hours to reach 70% necrosis.

Whilst at first glance this suggests non-specific damage to the cells, control samples showed very low levels of necrosis in both assays (Fig 3.21 and Fig. 4.6) and so non-specific necrosis through agitation was not induced. It is therefore likely that hyperstimulation of the cells sensitises them to agitation and therefore amplifies the necrosis early on, whereas in cells allowed to rest, this sensitisation to agitation did not directly induce necrosis. It is important then to further investigate the mechanisms involved in both these cell death assays, as one or the other may be more or less useful for testing potential therapeutics. One logical candidate for hyperstimulation-induced susceptibility to agitation is hyperstimulation-induced dislocation of the cytoskeleton from the basal membrane and blebbing (discussed in depth in the following chapter). Cytoskeletal dislocation and blebbing may not cause necrosis when the cell is resting, but when the cell is agitated, the membrane may be more susceptible to rupture by shear forces; it is easy to imagine the effect that large blebs may have even in terms of drag forces to cells actively buffeted around. If this is the case then inhibitors of the mechanisms involved in cytoskeletal rearrangement may prove particularly effective in 'agitated-necrosis', but necrosis in resting conditions may involve totally different mechanisms and therefore show a different profile of amelioration by test compounds of interest. Modulators of cytoskeletal dynamics could potentially be tested for in each of these assays to further investigate this, with parallel control investigations into the lack of any effect on Ca^{2+} signalling or mitochondrial dysfunction for example.

CHAPTER 5: RESULTS

Mitochondrial Redistribution

INTRODUCTION

Mitochondria have vital roles in a range of cellular signalling cascades, detecting, modulating and integrating both Ca^{2+} signals and bioenergetics through fusion, fission and redistribution as a one coordinated network (Soubannier and McBride, 2009). However, the mitochondrial network is also capable of dramatic heterogeneity; allowing for distinct roles within sub-cellular localisations (Collins et al., 2002). Pancreatic acinar cells display a classical example of such distinct mitochondrial subpopulations which have been widely studied (Petersen, 2012) but mitochondrial fluidity and dynamics remain poorly understood in this cell type.

As discussed previously, pancreatic acinar cells are a polarised, secretory cell type, containing an ER-rich basal region, and a granular-rich apical region. Here, inactive enzymes are packed into secretory vesicles, ready for secretion through the pancreatic ductal system and into the duodenum. IP_3Rs are found in the apex of acini, and initiate the cytosolic Ca^{2+} signals necessary for enzyme secretion into the apical lumen and the duct (Lur et al., 2011). Surrounding the granular region, on the basal side, is a dense population of mitochondria. This perigranular 'belt' (which in 3-dimensions is actually more like a baseball glove) is responsible for buffering apically derived oscillatory Ca^{2+} signals (Tinel et al., 1999) which induce secretion (Maruyama et al., 1993), limiting the progression of the Ca^{2+} wave into the basal region and the nucleus. Mitochondrial Ca^{2+} uptake stimulates enzymes of the citric acid cycle (Denton et al., 1972, Denton et al., 1978, McCormack and Denton, 1979), increasing NAD(P)H levels and in turn, ATP (Voronina et al., 2010); this is essential

for both secretion and the acidification of secretory vesicles (Baker and Knight, 1978, De Lisle et al., 1988).

A sub-population of mitochondria is also located close to the basal membrane, where Ca^{2+} influx machinery is located (Lur et al., 2009); use of electron microscopy has demonstrated that mitochondria are often found very closely associated with this machinery (Lur et al., 2009). Mitochondria have been shown to be essential components of the store-operated entry machinery (Gilabert and Parekh, 2000); have been shown to uptake Ca^{2+} in response to store-operated Ca^{2+} entry (Park et al., 2001); and have been shown to form a distinct triad with the plasma membrane and ER (Alonso et al., 2009).

Mitochondrial dysfunction has been identified as a core component in the onset of acute pancreatitis, a severely debilitating disease which is potentially fatal in its systemic form and for which there is no targeted therapeutic (Criddle et al., 2007, Mukherjee et al., 2008). A large body of evidence from this group and others has shown that hyperstimulation of pancreatic acinar cells induces cytosolic (and subsequently mitochondrial) Ca^{2+} overload, which has been shown to directly lead to the loss of mitochondrial membrane potential (Baumgartner et al., 2009), collapsing ATP levels and induction of necrosis (Petersen et al., 2006, Voronina and Tepikin, 2012).

Due to the critical role of mitochondria at specific locations in the pancreatic acinar cell, disruption of mitochondrial distribution could have a major impact on pancreatic acinar cell physiology. It has not been investigated (or widely theorised) how mitochondria come to be in this distinctive network, or indeed whether the

network may be more fluidic than is commonly seen in isolated pancreatic acinar cells. Despite the large amount of evidence showing distinct mitochondrial distributions in pancreatic acinar cells, there have been reports showing a more diffuse distribution, for example in a study of mitochondrial Ca^{2+} signalling in pancreatic acinar cells (Gonzalez et al., 2000). Whilst it is rarely discussed, the variability of mitochondrial distributions in the pancreatic acinar cell is obvious to those working regularly with pancreatic acinar cells, and it may be the case that much of the work regarding the roles of distinct populations of mitochondria in the acinar cell has been performed on cells showing the 'best' distribution. For this reason we aimed to investigate the distribution of mitochondria in an unbiased and quantitative way to determine the average distribution of mitochondria under different physiological parameters. Mitochondrial motility has never been investigated in pancreatic exocrine tissue and it is unknown if changes in mitochondrial motility and distribution are associated with physiological and or pathological stimulation. Cytoskeletal degradation and redistribution upon hyperstimulation of pancreatic acinar cells has been known about for some time (Jungermann et al., 1995), but the effect these changes may have on mitochondrial motility, distribution and therefore function, remains unclear. So investigation into these processes could potentially be important to our understanding of the cellular events during the onset of acute pancreatitis, and lead to the identification of therapeutic targets for treatment of this debilitating and fatal disease.

Much of what is known regarding mitochondrial distribution and function is based on observations in isolated cells, many of which are cultured cancer cells that may not truly reflect organ physiology. In response to this, we have developed the use

of undisrupted pancreatic tissue segments. These are large (>3 mm) segments which have undergone no enzyme treatment and are handled with the utmost care to avoid shear stress, interaction with air bubbles or any physical abrasion or crushing forces. Using these techniques we aimed to assess the potential dynamicity of the mitochondrial distribution under basal and physiologically stimulated conditions; to outline the effect of hyperstimulation on the cytoskeleton of intact tissue in order to determine if any changes in mitochondrial distribution are apparent; and finally, to investigate the potential effects which any changes in organellar distribution may have on cellular Ca^{2+} signals.

Physiological Stimulation of Tissue

Outlining the Mitochondrial Distribution

To determine the mitochondrial distribution in unstimulated murine pancreatic tissue, immunofluorescence was performed using an antibody targeting the outer mitochondrial membrane translocon component, Tom20. Upon initial investigation, mitochondria were seen to be relatively evenly distributed throughout the acinar cells, with only a small increase in the perigranular, and subplasmalemmal populations, and some exclusion from the apex of the granular region, visible by the transmitted light images (Fig. 5.1A). This is in stark contrast to the well-documented distribution of mitochondria in isolated pancreatic acinar cells, which show a recognisable perigranular 'belt' region as well as subplasmalemmal mitochondria. Stimulation of the tissue with 100 pM CCK for 30 minutes resulted in a dramatic change in the localisation of mitochondria into a distribution reminiscent of that associated with

isolated pancreatic acinar cells (Fig. 5.1B). Profiling of the cytosol was then performed to objectively qualify and quantify the relative location of the mitochondria from the basal region into the apical region (Fig. 5.2A) and this was then averaged and presented as a graph of the mitochondrial profile (Fig. 5.2B). Representative of the immunofluorescence images, under control conditions the average mitochondrial profile showed mitochondria evenly decorating the cytosol but excluded from the granular region (represented by the inverse of the transmitted light corresponding to the high optical density of the secretory granules (Fig. 5.2B)). After stimulation with 100 pM CCK, no change in the subplasmalemmal region (~1 µm from the basal membrane) was observed, however there was a significant reduction in the amount of mitochondria present between 2-4 µm from the basal membrane, and an increase in the amount of mitochondria in the perigranular region (peaking at ~8 µm from the basal membrane).

Mitochondrial redistribution was further investigated in order to give clear indication of the speed and reversibility of this new phenomenon. A series of experiments was performed whereby tissue was stimulated and then washed to allow for the determination of the time dependency of both formation, and potential reversibility of mitochondrial redistribution. Specifically, tissue segments were treated with 100 pM CCK for up to 30 minutes immediately prior to fixation, or treated for 30 minutes and then washed to remove any stimulation and kept in physiological saline for up to 1 hour to determine if the mitochondrial distribution reverts to a diffuse state. The mitochondrial profile was seen to develop into a subplasmalemmal and perigranular distribution gradually over 30 to 40 minutes, and

by 1 hour after washing, the distribution had markedly reverted (Fig. 5.3A). This process was further quantified by measuring the average total fluorescence from two regions (2-4 µm and 6-11 µm from the basal membrane) and displayed as a curve to show both the drop in mitochondria between 2-4 µm and a build up of mitochondria between 6-11 µm (Fig. 5.3B). Both measurements reverted back, almost to control levels 1 hour after washing off of the stimulus.

Microtubule-Dependency of Physiological Mitochondrial Redistribution

Having outlined a phenomenon of agonist induced mitochondrial redistribution we aimed to determine whether mitochondria utilise the microtubule network during this process. Therefore, colchicine was used to depolymerise the microtubule network and inhibit motor-driven mitochondrial motility along microtubules. Immunofluorescence of tubulin showed that complete depolymerisation of tubulin was achieved after treatment with 50 µM colchicine for 1 hour, compared to tissue maintained at 1 hour under control conditions (Fig. 5.4A, B). After colchicine treatment, the mitochondrial network was diffuse throughout the cytosol and subsequent stimulation with 100 pM CCK induced no change in mitochondrial distribution. This was further confirmed by the average mitochondrial profile, indicating that mitochondrial redistribution induced by 100 pM CCK is microtubule-dependent (Fig. 5.4C, D, & E).

Ca^{2+}-Dependency of Physiological Mitochondrial Redistribution

CCK is known to induce global Ca^{2+} rises in pancreatic acinar cells via G-coupled receptor-linked production of a range of Ca^{2+}-releasing second messengers including NAADP, cADP ribose, and IP_3, which induce Ca^{2+} release from a collection of distinct internal stores. Ca^{2+} regulation of microtubule-dependent mitochondrial motility has been studied in a range of cellular systems, and was subsequently investigated here. To determine the Ca^{2+} dependency of the mitochondrial redistribution, the membrane permeable Ca^{2+} chelator, BAPTA-AM, was loaded into the tissue prior to stimulation. BAPTA-AM loading successfully blocked the Ca^{2+} response induced by 100 pM CCK (Fig. 5.5A), and was subsequently shown to also block the effects of 100 pM CCK upon mitochondrial redistribution (Fig. 5.5B and 5.5C in red, compared to 5.2B). However there was no effect on the mitochondrial distribution per se (Fig. 5.5C burgundy). To further investigate Ca^{2+} dependency, a cytosolic Ca^{2+} rise was induced in an agonist independent manner by inducing a store-operated Ca^{2+} rise. This was achieved via store-depletion by the SERCA pump inhibitor, thapsigargin (Fig. 5.6A). This protocol also induced redistribution of mitochondria into a perigranular belt and subplasmalemmal distribution, similar to that induced by 100 pM CCK (Fig. 5.6B, C, and 5.2B).

In the light of the well documented inhibitory effect of Ca^{2+} on mitochondrial motility (Yi et al., 2004), a Ca^{2+}-dependent induction of mitochondrial movement might appear counterintuitive at first glance. Indeed, mitochondrial motility in live pancreatic tissue appears to be reduced after stimulation with 100 pM CCK, with a visible stabilisation of the mitochondrial network (data not shown). Therefore, we

hypothesised that the mitochondria are in active flux during basal conditions, whereas after stimulation, mitochondrial motility is inhibited in regions of high Ca^{2+}. Over time, mitochondria would accrete to these regions and the distribution would become stable and generate the illusion of a Ca^{2+}-induced mitochondrial movement event, when in fact Ca^{2+} would be directly responsible for mitochondrial stability, resonating with current literature. To elucidate the role of Ca^{2+} in an inhibitory capacity for mitochondrial motility, we determined whether Ca^{2+} entry was responsible for the maintenance of the subplasmalemmal population of mitochondria after stimulation; inhibiting the movement of mitochondria towards the perigranular region and pinning them to the basal membrane. This was achieved by chelating external Ca^{2+} with 100 µM EGTA over a long period (90 min) and then stimulating with 100 pM CCK. Under these conditions, the amount of mitochondria remaining in the basal membrane was markedly reduced (Fig. 5.7) whereas there was no effect on the perigranular population of mitochondria.

Hyperstimulation of Tissue

Having determined the Ca^{2+} and tubulin dependency of the mitochondrial redistribution induced by physiological concentrations of CCK, we aimed to determine the effect of hyperstimulation with CCK and TLCS on the mitochondrial distribution in pancreatic tissue.

Mitochondrial Distribution after Hyperstimulation

Hyperstimulatory concentrations of CCK or bile are routinely used *in vitro* to induce pathological changes indicative of acute pancreatitis and are commonly

referred to as precipitants of the disease. Tissue was treated with 100 nM CCK, or 500 µM TLCS and the mitochondrial distribution visualised by immunofluorescence as previously described. Mitochondria were found to be severely redistributed towards the apical region of the cytosol, and in contrast to the effects of physiological stimulation, the subplasmalemmal population of mitochondria was completely dislocated from the basal plasma membrane (Fig. 5.8). This effect was highly reproducible and homogeneous. Also visible was a slight bulging of the plasma membrane in comparison to control tissue in which the basal membrane was flatter. After hyperstimulation, mitochondria were always found in the apical region of the cytosol, and the nucleus often seemed slightly apically redistributed but these observations have not been quantified in any manner in this study. In the first instance we aimed to further investigate the mitochondrial redistribution and compare this to the physiologically-induced redistribution previously described. The effect of severe apical mitochondrial redistribution was reproduced after depolymerisation of the microtubule network with colchicine, indicating that that the process was independent of the mechanism described for physiological stimulation with 100 pM CCK (comparison of Fig. 5.4 with Fig. 5.9). This conclusion was further supported by the Ca^{2+} independency of this phenomenon; BAPTA-AM was loaded into the tissue prior to either resting conditions or hyperstimulation and mitochondria were found to be diffuse and similar to control after BAPTA-AM loading, but were still severely redistributed after hyperstimulation (Fig. 5.10). These data were quantified by measuring the average density of mitochondria in the subplasmalemmal (<2 µm from the basal membrane) and peri-granular (<5 µm from the granular region) regions of

the cell. In unstimulated tissue, there was no significant difference between the mitochondria in either region of the cell. After stimulation with 100 nM CCK alone, or in presence of colchicine; after BAPTA-AM loading; and after depolarisation of the mitochondria with the protonophore CCCP, there was a large reduction in the subplasmalemmal mitochondrial population, and an increase in the perigranular region (Fig. 5.11). These data show that not only is the hyperstimulation-induced mitochondrial redistribution Ca^{2+} and microtubule independent, it is also independent of mitochondrial membrane potential and hence mitochondrial function.

As hyperstimulatory Ca^{2+} signals induced by precipitants of acute pancreatitis are known to give rise to reactive oxygen species overload (Booth et al., 2011), tissue was treated with menadione, to determine whether reactive oxygen species overload is capable of affecting the mitochondrial distribution. However there was no obvious change in distribution after treatment with 30 µM menadione. Similarly, the antioxidant NAC had no effect on the mitochondrial redistribution induced by 100 nM CCK (Fig. 5.12).

Cytoskeletal Changes after Hyperstimulation

Due to the Ca^{2+}- and microtubule-independent nature of the hyperstimulatory mitochondrial redistribution, we investigated changes in the cytoskeleton in an attempt to further elucidate the mechanism by which the mitochondria were being rearranged. Tubulin and actin were stained in unstimulated pancreatic tissue. Actin heavily decorated the lateral and apical membranes, in accordance with previous findings (Jungermann et al., 1995). However there was also some actin staining in patches on the basal membrane, visualised by a 3D projection (Fig. 5.13).

Basal membrane actin patches were also visible in the confocal slices, but to a less obvious extent (Yellow arrows, Fig. 5.14). Under control conditions the microtubules extended all the way to the basal membrane but displayed very little co-localisation with the actin patches. This cytoskeletal arrangement was seen throughout the tissue as can be seen by the lower magnification maximum intensity projection (Fig. 5.13A). Hyperstimulation subsequently induced substantial rearrangement of the cytoskeleton in acinar tissue. Lateral and apical actin remained dense, but basal patches were no longer present. Cytosolic actin cables were formed throughout the cytosol; parallel with the basal membrane and congregating in the perigranular region. This congregation of actin cables co-localised with a build up of microtubules. Mitochondria and the majority of the tubulin staining were located 'underneath' these actin cables i.e. closer to the apical region. However, the microtubules penetrated through and extended beyond this perigranular congregation of actin cables to the basal membrane, but were distinctly sparser in the basal region than under control conditions (Fig. 5.14). Actin patches did not co-localise with microtubules, but were seen in close proximity to them (Fig. 5.13B and Fig. 5.15).

To investigate the relationship between actin patches on the basal membrane and mitochondria, tissue was stimulated with 100 pM CCK, and actin, tubulin and mitochondria were stained and visualised close to the basal membrane at the lowest part of the tissue nearest the cover slip (Fig. 5.15). Actin patches did not co-localise with mitochondria; however they were seen to closely interact and were often seen to almost wrap around each other (Fig. 5.15). All images shown are after stimulation with 100 pM CCK. Control images (not shown) were similar to those stimulated with

100 pM CCK, but these were chosen due to the good clarity of the interactions. Further investigation would be required to determine the effect of physiolical stimulation on the propinquity of mitochondria with the subplasmalemmal cytoskeleton. Obviously, the removal of mitochondria and actin patches from the subplasmalemmal region after hyperstimulation precluded any investigation of these interactions under such conditions.

Because the Ca^{2+} independency of hyperstimulation-induced mitochondrial redistribution was shown with BAPTA-AM -loading, cytoskeletal redistribution upon hyperstimulation was also investigated under these conditions. BAPTA-AM -loaded pancreatic tissue was treated with 100 nM CCK and mitochondria, tubulin and actin were stained. All showed redistribution similar to hyperstimulation without Ca^{2+} chelation (Fig. 5.16). Similarly, redistribution was observed after hyperstimulation with TLCS (Fig. 5.17), again showing the formation of cytosolic actin cables. Low-magnification of the tissue under these conditions shows the wide extent of the redistribution of mitochondria, tubulin and actin. BAPTA-AM treatment alone had no affect on mitochondrial or cytoskeletal distribution per se (data not shown, however mitochondrial profiling of tissue treated with BAPTA-AM alone can be seen in Fig 5.5 where distribution resembles that of control tissue).

To confirm the Ca^{2+}-independency of mitochondrial and cytoskeletal redistribution, thapsigargin was used to deplete the Ca^{2+} store, thereby inhibiting any further release by CCK. Under these conditions, 100 nM CCK did not induce a rise in Ca^{2+} (5.18A) until external Ca^{2+} was added. Application of thapsigargin in zero Ca^{2+} did not induce mitochondrial or cytoskeletal redistribution; however, the addition of

CCK to store-depleted tissue in zero Ca^{2+} did induce severe redistribution of mitochondria and the cytoskeleton (Fig. 5.18B).

Due to the dramatic changes in actin distribution after hyperstimulation, and the location of the mitochondria distally to the actin cables (best seen in Fig. 5.14, 5.16 and 5.17), the dependency of the mitochondrial redistribution upon actin dynamics was investigated. Cytochalasin D was employed to depolymerise actin cables (Flanagan and Lin, 1980, Lin et al., 1980), and blebbistatin was used to inhibit myosin IIA to prevent actin dynamics without depolymerising actin cables (Straight et al., 2003). Treatment with cytochalasin D alone induced a change in the actin distribution to a punctuate state (Fig. 5.19). Blebbistatin did not depolymerise actin and left dense lateral and apical staining with actin patches on the basal membrane as in unstimulated tissue. Treatment with either blebbistatin or cytochalasin D alone had no effect on mitochondrial distribution (Fig. 5.20A and 5.21A). Treatment with either blebbistatin or cytochalasin D in combination with hyperstimulation inhibited the dislocation of mitochondria from the basal membrane (Fig. 5.20B and 5.21B). Inhibition of actin dynamics did not, however, inhibit the formation of a perigranular mitochondrial belt; this might be expected as cytosolic Ca^{2+} changes and microtubule polymerisation were not inhibited, and these mechanisms could be responsible for apical redistribution of mitochondria into a perigranular belt. Corroboratively, the depolymerisation of tubulin in combination with inhibition of actin dynamics and hyperstimulation led to a diffuse mitochondrial distribution (Fig. 5.20C and 5.21C) similar to control, untreated tissue (Fig. 5.1A). Colchicine alone had no effect on hyperstimulatory redistribution of mitochondria, but did prevent the mitochondrial

belt formation in the presence of cytochalasin D or Blebbistatin after hyperstimulation. This suggests that Ca^{2+} induced redistribution occurs concomitantly with actin based apical redistribution after hyperstimulation, and that these processes are distinct. These data were quantified by drawing regions of interest in the subplasmalemmal and perigranular regions and measuring the average intensity of fluorescence. Figure 5.22 demonstrates the actin dependency of pathological redistribution and shows the formation of the perigranular belt in cytochalasin D and blebbistatin-treated, hyperstimulated tissue.

In order to further investigate the mechanism of actin cable formation, the tubulin network was disrupted with colchicine. Actin cables formed upon hyperstimulation in the presence of colchicine, indicating that they are independent of microtubule dynamics (Fig 5.23). Since hyperstimulatory mitochondrial redistribution is Ca^{2+} independent, a logical upstream target was chosen to investigate the mechanism of this redistribution; depletion of PIP_2 was evaluated as a possible determinant of the dissociation of the cytoskeleton from the plasma membrane. PIP_2 levels will go down after prolonged hyperstimulation and this would be upstream of any Ca^{2+} effect. As the cytoskeleton appears to be detaching from the plasma membrane upon hyperstimulation we aimed to determine if a reduction in PIP_2 levels would be sufficient to induce a similar phenomenon. PI4K was pharmacologically inhibited and Ca^{2+} signals induced to give an indirect indication of whether or not PIP_2 was successfully depleted. However, treatment with the PI3K inhibitors wortmannin and LY294002, used at higher concentrations to inhibit PI4K, proved problematic due to the length of time required to inhibit Ca^{2+} signals (3.5 hours) even in the presence

of low concentrations of ACh (to aid depletion by generating IP_3); a significant increase in basal Ca^{2+} occurred due to this harsh treatment (Fig. 5.24), precluding an accurate assessment of PIP_2 involvement in redistribution. There were also regions of necrosis apparent, induced by this treatment (not shown). However in non-necrotic regions of tissue, there was no indication of any actin or mitochondrial dislocation from the plasma membrane (Fig. 5.25).

Mitochondrial Redistribution and Store-Operated Ca^{2+} Entry

Having outlined the hyperstimulation-induced redistribution of mitochondria towards the apical region, store-operated Ca^{2+} entry was measured using Fluo-4 under these conditions to investigate the role of the mitochondria at the basal membrane. Store-depletion was induced by inhibiting the SERCA pump with 2 µM thapsigargin for 10 minutes. Tissue was then superfused with 0.5 µM thapsigargin to ensure continued store-depletion throughout the experiment. Subsequent addition of 1 mM external Ca^{2+} induced an increase in cytosolic Ca^{2+}, which was reproducible to a comparable but slightly lesser extent after a second round of external Ca^{2+} addition at 840 seconds (Fig. 5.26A). The mitochondria were visualised simultaneously with TMRM, and showed a relatively diffuse mitochondrial distribution but a perigranular belt was visible and importantly subplasmalemmal staining was apparent throughout the experiment (Fig. 5.26A). Tissue pre-treated with 100 nM CCK was confirmed to have an apically confined perigranular mitochondrial distribution shown by TMRM staining (Fig. 5.26B) and the rate of Ca^{2+} entry appeared to be reduced in comparison to control and slower in onset. During the second re-addition of 1 mM external Ca^{2+}, the protonophore CCCP was added to depolarise the mitochondria and determine if

any further inhibition of Ca^{2+} entry could be induced. Both the reduction in mitochondrial staining and the increase in cytosolic staining of TMRM after the addition of CCCP, confirms depolarisation of the mitochondria (Fig. 5.26B). The rate of Ca^{2+} influx was inhibited by the addition of CCCP, to a much greater extent than 100 nM CCK pre-treatment alone (Fig. 5.26B). This was further quantified by averaging the store-operated Ca^{2+} entry curves, which showed a relatively small inhibition of the Ca^{2+} influx by CCK pre-treatment in comparison to the much larger inhibition induced by CCCP (Fig. 5.27A). Sigmoidal lines of best fit were calculated (average $R^2 = 0.99$) and the times at which the curves reached 20, 50, and 80% of the maximum fluorescence was determined; the average time was significantly later after pre-treatment with 100 nM CCK compared to control at each point (Fig 5.27B). The average time taken for cytosolic Ca^{2+} to increase from 20% to 80% was also augmented from 43.9±5.3 seconds in control to 61.3±4.3 seconds after 100 nM CCK pre-treatment confirming that the Ca^{2+} influx curve was slower after 100 nM CCK stimulation. These data indicate that whilst redistribution of mitochondria away from the basal membrane (induced by 100 nM CCK) is associated with a reduction in the rate of store-operated Ca^{2+} entry, depolarisation of the mitochondrial membrane potential reduces the influx rate to a much greater extent.

Nuclear Vacuolisation

Vacuolisation is a recognised feature of acute pancreatitis and has been observed in isolated pancreatic acinar cells under conditions of hyperstimulation (Sherwood et al., 2007). As may have been apparent in many of the images in this chapter; vacuolisation occurred concomitantly with cytoskeletal redistribution upon hyperstimulation with

both CCK and TLCS. The processes involved in vacuolisation were outside of the remit of this study, and these processes are being investigated in isolated cells by other members of this research group. However, one phenomenon which has been characterised over the course of these investigations in intact tissue is the presence of nuclear vacuolisation, a novel process which has not yet been reported. Nuclear vacuoles were initially noticed in TLCS-treated tissue in which the Hoechst staining often resembled a crescent moon. Vacuoles ranged in size from a couple of microns to almost the entire diameter of the nucleus. Vacuoles were also found in a stage of partial formation, with an actin coated vacuole pressing against or beginning invagination into the nucleus (Fig. 5.28). These structures were often only noticed after unrelated investigations in 'post-production' and so were not quantified and could not be said to be inhibited in any conditions as they were not actively looked for. Having said this, they were not uncommon, and indeed a number were often seen in the same field of view. One feature which was almost universally shared amongst nuclear vacuoles was a build-up of actin at the opening of the nucleus (Fig 5.28 and 5.29) which often spread into the nucleus, coating the inside of the vacuole. Vacuoles were also seen after hyperstimulation in the presence of the antioxidant NAC, showing that they are not dependent upon ROS generation (Fig. 5.29). To determine if these structures were formed by endocytosis, the membrane impermeable stain, Lucifer yellow was injected into the tissue and spread into the ductal system prior to stimulation. Vacuolisation and a swelling of the duct were seen in a 3D projection, confirming the correct distribution of the dye (Fig. 5.30). Upon further investigation, nuclear vacuoles were indeed found stained with Lucifer yellow, confirming that they

are endocytic vacuoles (Fig. 5.31). Staining with Lucifer yellow allowed for excellent visualisation of the interaction between endocytic vacuoles and the nucleus. Figure 5.31 shows a number of endocytic structures closely associated with nuclei to varying degrees. Finally, the nuclear vacuoles were seen to stain positive for a component of the secretory pathway, bile salt-activated lipase. This was visualised by immunofluorescence and confirmed that components of the secretory pathway were present within the nuclear vacuoles and seen at various stages of development (Fig. 5.32).

Discussion

Why have Mitochondrial Dynamics not been Described Previously?

Isolated cells are widely known to display a distinctive perigranular and subplasmalemmal mitochondrial distribution (Park et al., 2001, Johnson et al., 2003, Petersen, 2012), and this poses an important question as to why unstimulated tissue in this study showed a significantly more diffuse distribution. The vast majority of the work regarding this mitochondrial distribution and the implication of this distribution to the physiology of the pancreatic acinar cell has been performed on physically and / or enzymatically disrupted cells. It is likely that significant stimulation and Ca^{2+}-release occurs during enzymatic and physical separation of acinar cells as part of the isolation procedure, leading to a significantly more severe perigranular belt. Cells will be ruptured during physical dispersion processes, releasing intracellular contents, including ATP and digestive enzymes. Protease release will also cause Ca^{2+} signals via activation of PAR-2 receptors which are abundantly expressed on pancreatic acinar

cells (Kawabata et al., 2002). Cells may also be stimulated during the isolation procedure by physical shear force and even association with air bubbles, which have been shown to induce IP_3-mediated Ca^{2+} signals in epithelial cells in culture (Sobolewski et al., 2011). One study has been published which showed no significant difference between isolated cells and pancreatic cells within tissue (Johnson et al., 2003). This may be in part responsible for the lack of subsequent investigations into mitochondrial distribution in pancreatic tissue. However, the reproducibility of mitochondrial redistribution upon stimulation, along with our ability to reverse and also block it pharmacological with agents targeted to both the Ca^{2+} pathway and the cytoskeleton, raises serious questions as to the validity of previous findings.[4] It seems likely that the method of tissue maceration by cutting into 1 mm segments may have had significant stimulatory effects and again point to the importance of minimally disruptive techniques.

Therefore, when exploring the physiology of isolated pancreatic acinar cells it should be considered that the intensity and characteristics of the mitochondrial distribution is likely to echo the harshness of the stimulation imposed during the isolation procedure; mitochondrial distribution should thus not be used as a selection criterion for 'good quality' cells per se, unless of course the investigation is pertaining directly to the function of the mitochondria at distinct sites within a classical distribution.

Ca^{2+}-Induced Mitochondrial Redistribution

[4] I would also like to note that figures 3B and 5B are erroneously identical in JOHNSON, P. R., DOLMAN, N. J., POPE, M., VAILLANT, C., PETERSEN, O. H., TEPIKIN, A. V. & ERDEMLI, G. 2003. Non-uniform distribution of mitochondria in pancreatic acinar cells. *Cell Tissue Res,* 313**,** 37-45.

The control of microtubule-dependent mitochondrial motility by Ca^{2+} is well documented. It has more recently been proposed that Ca^{2+}-mediated inhibition of mitochondrial motility is dependent upon subsequent mitochondrial Ca^{2+} uptake (Chang et al., 2011). The microtubule motor proteins kinesin-1 and dynein are responsible for bidirectional motility of mitochondria. A range of adaptor proteins have been shown to regulate these motors, with significant focus in terms of Ca^{2+} regulation being directed towards the motor associating adaptor protein Milton, and the mitochondrial associate receptor protein Miro. Ca^{2+} binding to the EF-hand motif of Miro1 has been shown to be the link between Ca^{2+} increases and the inhibition of mitochondrial motility, through changes in its interaction with kinesin-1 (Wang and Schwarz, 2009). The exact mechanisms may be cell type specific, however, it is important to note that Ca^{2+}-dependent inhibition of mitochondrial motility makes physiological sense, by enabling the formation of a feedback mechanism whereby mitochondria are recruited to sites where they are needed most in a Ca^{2+} buffering capacity (Yi et al., 2004). The build up of the mitochondria in these 'buffer' regions, may also have follow on effects to increase ATP in the cell, by increasing the mitochondrial Ca^{2+} load and stimulating the electron transport chain through upregulation of the TCA cycle and increased reducing power. It could also be postulated that the location of the mitochondria in a perigranular belt could help fund the granular region with a localised supply of ATP; however there is currently no specific data showing that mitochondrial location has any effect on secretion per se, as pharmacological disruption of the microtubular network with colchicine will inhibit secretion by disabling granular exocytosis (Ueda et al., 1995).

The reduction in the subplasmalemmal population of mitochondria after chelation of external Ca^{2+} (Fig. 5.7) supports this Ca^{2+} microdomain accretion hypothesis by indicating that Ca^{2+} influx is responsible for recruitment of mitochondria to the influx site. Indeed, thapsigargin with high extracellular Ca^{2+} led to a distribution similar to that of physiological stimulation, despite the Ca^{2+} overload associated with this treatment; further indicating Ca^{2+} influx in the maintenance of the subplasmalemmal mitochondrial population (Fig. 5.6). Mitochondria which are close to the plasma membrane preferentially uptake Ca^{2+} to a greater extent during Ca^{2+} influx than during ER Ca^{2+} release (Lawrie et al., 1996); if mitochondrial Ca^{2+} increases are responsible for inhibition of motility, which has been proposed for axonal mitochondria (Chang et al., 2011), then it is plausible that the mitochondria which are close to the plasma membrane are more greatly inhibited than those in the cytosol. However it is not actually conclusive whether the Ca^{2+} dependent mitochondrial recruitment to the plasma membrane is through inhibition of motility. Another possibility is that it arises due to anchoring of the mitochondria to the plasma membrane, a process known to occur in axons, where mitochondrial associations with the subplasmalemmal cytoskeleton inhibit bidirectional motility (Chada and Hollenbeck, 2004). It is currently unknown, however, if this is a Ca^{2+}-sensitive process.

Whilst Ca^{2+} inhibition of mitochondrial motility is widely accepted, the hypothesis that mitochondria will therefore accrete at high Ca^{2+} microdomains is more divisive; mitochondria have even been shown to redistribute away from the initiation site of the Ca^{2+} signal in certain circumstances, most notably in the

immunological synapse (Schwindling et al., 2010). Here, Ca^{2+} influx was required for mitochondrial redistribution, but the direction of movement was not necessarily directed towards the source of the Ca^{2+} influx. However after depolymerisation of the actin network with cytochalasin D, mitochondria were unable to accumulate at the immunological synapse, indicating that this process is not microtubule based motor driven rearrangement, but in some way dependent upon the actin cytoskeleton (Quintana et al., 2011).

In contrast to the Ca^{2+} regulation of subplasmalemmal distribution, it is likely that the apical redistribution and formation of the mitochondrial perigranular belt (induced by physiological stimuli; Figs. 5.1-5.3) is through Ca^{2+} controlled induction of dynein activity or more likely through inhibition of kinesin activity which has been described previously (Wang and Schwarz, 2009). Microtubules in the pancreatic acinar cell are often described as 'emanating from the secretory pole', however the centrioles, which constitute a core component of the microtubule organising centre are located in the perigranular region, close to the Golgi apparatus (Motta et al., 1997). In support of this, it has been shown that inhibition of kinesin inhibits granular transport and secretion, indicating that secretion is dependent upon anterograde transport away from the cell body, towards the plus end of the microtubules (Marlowe et al., 1998). This may offer an explanation for the ability of upregulation of retrograde mitochondrial motility to induce a perigranular distribution. Furthermore, high Ca^{2+} microdomains associated with IP_3-mediated stimulation would presumably occur at the site of IP_3R Ca^{2+} release which is at the apical membrane, not the basal side of the granular region. In this study the mitochondria

found within the granular region were in fact excluded from the granular region towards the perigranular belt region after physiological stimulation with 100 pM CCK (Figs. 5.1-5.3), indicating a movement of the mitochondria away from the site of Ca^{2+} release from the IP_3R near the apex.

The mechanisms involved in Ca^{2+} dependent mitochondrial belt formation can only be speculated based upon the data offered here and such mechanistic investigations were outside the remit of the current study, predominantly due to the limitations of molecular approaches in live primary tissue which we have been unsuccessful so far in our attempts to transfect. However the ability of Ca^{2+} signals to relocate mitochondria to specific parts of the cell, fits in with literature regarding a Ca^{2+} mediated inhibition of mitochondrial movement, but further study is required in the field of Ca^{2+} regulation of mitochondrial motility before true conclusions can be made.

HYPERSTIMULATION-INDUCED REDISTRIBUTION

Mitochondria are directed towards the apex of the acini, in a Ca^{2+} dependent manner, by directed motor driven movement along microtubules. This process shows mono-phasic proportionality to the Ca^{2+} signal (unlike many effects of secretagogues on the acinar cell which offer biphasic responses) as shown by the effect of thapsigargin- induced Ca^{2+}-overload. However, hyperstimulation with compounds known to cause activation of cellular signalling pathways other than just Ca^{2+} release caused additional changes to those induced solely by Ca^{2+} signals. Pathological overload of the cells with CCK and TLCS had a dramatic effect on the mitochondrial distribution (Fig. 5.8), and this additional Ca^{2+}-independent process involved actin

and myosin. Upon hyperstimulation actin patches on the basal membrane disappeared and actin cables were formed parallel to the basal membrane, throughout the basal part of the cytosol. This actin rearrangement is directly responsible for accompanied changes in the tubulin cytoskeleton, which appears thinner in the basal region and is bundled up at the perigranular periphery (Figs 5.13-5.14). This actin dependent cytoskeletal redistribution is directly responsible for major organellar redistribution to the apical pole, even when motor driven mitochondrial motility is inhibited by depolymerisation of the microtubule network with colchicine (Fig. 5.20-5.21, 5.23). It is important to note that colchicine treatment has been shown to not inhibit the first round of secretion stimulated by secretagogues, but does inhibit subsequent rounds after readmission of stimulus; microtubules are required for transport and replenishment of secretory granules, but not for secretion of granules which are already *in situ* (Schnekenburger et al., 2009).

Cytoskeletal rearrangements after hyperstimulation have been well characterised in pancreatic acinar cells as well as in models of acute pancreatitis (Burnham and Williams, 1982, Adler et al., 1984, O'Konski and Pandol, 1990, Torgerson and McNiven, 1998). Changes have been described as a breakdown of the cytoskeleton (Jungermann et al., 1995). In isolated acini, cytoskeletal changes are accompanied with severe bulging or blebbing of the basal membrane and the formation of a ring of actin cables surrounding this bleb, close to the apex of the acinus (Torgerson and McNiven, 1998). Microtubules were seen to spread beyond the actin ring into the bleb but were much sparser than in control basal regions of the acinar cell, and showed much less association with the basal membrane of the bleb.

These observations share many similarities between those of this study, including cytoskeletal rearrangement involving subplasmalemmal dislocation of the majority of the microtubular network, and formation of cytosolic polymerised actin in some form. Indeed there is obvious bulging of the basal membrane after stimulation which can be seen most clearly in Fig. 5.14A, where after 100 nM CCK treatment, the basal membrane is bulging out in the middle of the cell, and pinched in at the junction between cells. Notice also the presence of the actin cables, between the lateral membranes at this point.

The microtubule network does also show distinct thinning at the basal membrane and a build up in the perigranular region; however it is important to note that the apparent thinning of the microtubules at the basal region is not inhibited by paclitaxel, which stabilises microtubules and had no visible effect on mitochondrial redistribution, reaffirming that this is an actin-dependent rearrangement and not simply a depolymerisation of the microtubules. On the other hand it has been well documented that hyperstimulation does indeed cause depolymerisation of tubulin most notably by investigating the size of microtubules through protein gel electrophoresis (Ueda et al., 1992, Jungermann et al., 1995), and also that taxol offers significant protection against the inhibition of secretion associated with hyperstimulation, as well as amelioration of some pancreatitis indicators (Ueda et al., 1992, Ueda et al., 1995). However the distinct facts that cytoskeletal disassembly does occur and that there is thinning of the tubulin network at the basal membrane should not be confused, as the latter is an actin dependent process. This must therefore suggest that the disassembly of the microtubules is occurring predominantly

at the granular region; where immunofluorescence techniques are distinctly limited by the high optical density of the zymogen granules. This is further supported by the notion that the inhibition of secretion is protected by taxol (Ueda et al., 1992). Interestingly, the actin dependency was originally noted in the first description of the morphological changes associated with application of hyperstimulatory secretagogues (Burnham and Williams, 1982).

Mechanistically, the Ca^{2+} independent process involved in actin rearrangement was not elucidated in this study due to time constraints. It has been shown that cortactin phosphorylation by Src kinase is responsible for cytoskeletal changes and blebbing in isolated acinar cells (Singh and McNiven, 2008). However, whilst activation of the Src kinase 'Yes' after stimulation with CCK has been shown recently, it has also been shown to activate after mobilisation of cellular Ca^{2+} through thapsigargin treatment or the Ca^{2+} ionophore A23187 (Sancho et al., 2012). This shows slight disparity with our current investigations which have found actin changes to be largely independent of cytosolic Ca^{2+} concentration (Figs. 5.16-5.18), but nevertheless it would be an important avenue of investigation for the future. We have shown that this rearrangement is not mediated by reactive oxygen species however, as it is not induced by menadione, or inhibited by NAC (Fig. 5.12). The process of PIP_2 depletion by hyperstimulation was also investigated, but these results, whilst not totally conclusive due to technical problems involving wortmannin and some induction of necrosis, did not appear to show any induction of rearrangements in the actin cytoskeleton (Figs. 5.24-5.25).

Actin based mitochondrial redistribution is known to occur in some specialised scenarios, for example and as described previously, at the immune synapse during T-cell activation (Quintana et al., 2011). In budding yeast, actin patches are found in the bud, with actin cables running between the bud and the mother cell. These cables have been implicated in motor driven mitochondrial motility in a process which is essential for correct distribution of mitochondria during the budding process (Simon et al., 1995). It has more recently been suggested that mitochondria may be rearranged directly by polymerisation of actin, driving the movement of mitochondria similarly to Lysteria monocytogenes; employing the Arp2/3 complex (Boldogh et al., 2001). There are observed differences in this scenario, where the actin cables are not directed from the basal to apical region, with mitochondria moving along motors, or being driven by polymerisation; actin cables are found parallel to the basal membrane as if dragging larger cytosolic contents like a the strings of a net. The process of cytoskeletal detachment from the basal membrane may be sufficient to stop any Ca^{2+} mediated anchoring of the mitochondria to the basal membrane. This idea would fit in with mitochondrial anchoring to the actin network (or actin patches) at the basal membrane; if the actin is redistributed apically, then the mitochondrial anchor would be affected.

It is not clear from this study as to the long term effects of these rearrangements. However, necrosis occurs in tissue many hours after hyperstimulation (unpublished data, personal communication), and so it seems unlikely that these cytoskeletal and mitochondrial changes are indicative of a terminal state. Redistirbution of mitochondria away from the plasma membrane could

theoretically affect the function of the PMCA or Na^+/K^+-ATPase. Down regulation of the Na^+/K^+-ATPase could reduce the membrane potential and contribute to necrosis. Down regulation of the PMCA could similarly lead to hightnened cytosolic Ca^{2+} levels and contribute to Ca^{2+} overload associated with deleterious hyperstimulatory signals. Further study would be required to properly investigate the effect of removing mitochondria from the plasma membrane on the function of membrane pumps.

This study in intact tissue has confirmed the relevance of previous studies with regards to cytoskeletal changes upon hyperstimulation (O'Konski and Pandol, 1990, Jungermann et al., 1995, Singh and McNiven, 2008, Schnekenburger et al., 2009, Weber et al., 2009), whilst highlighting important differences which may indicate the limitations of the isolated acini model, and has gone further to reveal the mitochondria to be majorly redistributed during this process. The intact junctions between cells; the presence of non-acinar cell types; and changes in extracellular pressure, could all offer an explanation as to the reduction in the magnitude of basal blebbing in undisrupted tissue in comparison to isolated pancreatic acini. Whatever the cause of these changes, they highlight the scientific worth of using undisrupted tissue in the investigation of such phenomena.

Nuclear Vacuolisation

The appearance of nuclear vacuoles was initially thought to have been a rare event; “probably an artefact of fixation” - Anon. However, once identified and looked for with an experienced eye, they were seen even routinely within hyperstimulated samples. The process of nuclear vacuolisation seems to be unique to intact tissue, indicating that some intrinsic property of the intact system is important for their

formation. It seems likely that this may be an issue of pressure, as vacuoles will displace cytosol and the nucleus may provide a route for the release of pressure. To our knowledge, nuclear vacuolisation has not been described in the literature with regards to pancreatitic histology. However, nuclear inclusions of varying sorts are not uncommon in pathology and these vacuoles do resemble glycogen nuclei from diabetic liver (Nagore and Scheuer, 1988). The effects of nuclear vacuoles on pancreatic pathophysiology are unclear; however, their existence is indicative of the massive effects of vacuolisation upon hyperstimulation in this cell type. The location of these vacuoles within the nucleus will undoubtedly interfere with endocytic sorting processes and the normal breakdown of the nucleus during apoptosis, which could potentiate the shift in cell death pathways, favouring necrosis. Further investigation is essential to understand the pathological implications of this phenomenon on pancreatic exocrine tissue, as well as investigating their existence clinically to determine physiological relevance.

Mitochondria and Store-operated Ca^{2+} Entry

Mitochondrial dislocation from the plasma membrane induced by 100 nM CCK was shown to significantly inhibit the rate of store-operated Ca^{2+} influx induced by thapsigargin. However, collapse of the mitochondrial membrane potential with the protonophore CCCP caused a dramatic reduction in Ca^{2+} influx, above and beyond that induced by redistribution (Fig.5.26-5.27). It has been shown that CCCP does not affect intracellular pH levels (Tinel et al., 1999), and so it is presumed that this effect is directly due to depolarisation of the mitochondrial membrane potential.

Mitochondria are known to play a role in store-operated Ca^{2+} entry; however, there are a number of theories as the exact mechanism of this modulation and the debate remains controversial (Duszynski et al., 2006). Mitochondrial Ca^{2+} uptake, respiration, and membrane potential are all required for proper functioning of store-operated Ca^{2+} channels in neurones (Ma et al., 2012). However, the localisation of mitochondria and the effect this may have on Ca^{2+} influx is much more divisive. Mitochondria are known to buffer Ca^{2+} at the plasma membrane (Malli et al., 2003) and this Ca^{2+} buffering capacity has been shown to inhibit Ca^{2+} dependent negative feedback of the influx channel components (Gilabert and Parekh, 2000). It has been suggested that Ca^{2+} buffering by ATP (through the Ca^{2+}-stimulated production of ATP) plays a major role in this process, and not just Ca^{2+} uptake (Montalvo et al., 2006). Our data indicate that whilst store-operated Ca^{2+} entry is inhibited by removal of the mitochondria from the plasma membrane, there is a major soluble component of the mitochondrial role in Ca^{2+} influx, which is able to maintain Ca^{2+} influx even when the mitochondria are not near the membrane due to the major inhibition offered by depolarisation of the mitochondria; the likely candidate being cytosolic ATP, although we did not measure this directly in pancreatic tissue.

The relatively small inhibition of store-operated Ca^{2+} entry by mitochondrial redistribution may not truly reflect the importance of the mitochondria at the plasma membrane during physiological stimulation. It has recently been shown that different stromal interaction molecules are activated by diverse stimuli due to the specific sensitivities to ER luminal Ca^{2+}; STIM2 has been shown to have a lower affinity for luminal Ca^{2+} resulting in STIM2 I_{CRAC} having a higher sensitivity to store depletion

(Kar et al., 2012). One possible theory to explain the current results is that STIM2-dependent influx may be more susceptible to redistribution of mitochondria away from the influx site than STIM1-dependent influx. It is possible that the role of mitochondria during basal Ca^{2+} influx is much more significant and the Ca^{2+} buffering capacity of the mitochondria more important; with mitochondria limiting Ca^{2+} increases locally to the influx site, providing ATP for SERCA activity, and preventing of the spread of Ca^{2+} throughout the cytosol. This may limit interference with the communication of physiological oscillatory Ca^{2+} signals and may be essential for their maintenance. These hypotheses require further attention to make firm conclusions as to the role of subplasmalemmal mitochondria during physiological stimulation, and not just inferences via the determination of effects observed during drastic and potentially deleterious store-depletion.

It is also possible that the decrease in store-operated Ca^{2+} influx by hyperstimulatory CCK-induced redistribution could be caused entirely by partial depolarisation of the mitochondria by 100 nM CCK; an effect which has been shown through mitochondrial Ca^{2+} increase in isolated pancreatic acinar cells (Voronina et al., 2004). This possibility cannot be discounted without either rescuing the inhibition of store-operated Ca^{2+} influx by mitochondrial redistribution, by preventing actin-based dislocation of the mitochondria from the plasma membrane with blebbistatin or cytochalasin D; or alternatively by inhibiting the formation of the mPTP. Indeed, inhibition of mPTP by cyclosporin A has been shown to restore the rate of store-operated Ca^{2+} influx attenuated in a cellular model of Alzheimer's disease (Ma et al., 2012) and would be in interesting aspect for further investigation within our tissue model.

General Discussion

Methylxanthines

In this study we have outlined to importance of IP_3-mediated Ca^{2+} release in pathological overload. Using a novel tool; membrane permeable caged IP_3, we have investigated inhibition of the IP_3R with methylxanthines. The inhibition of IP_3 – mediated Ca^{2+} signals was able to ameliorate TLCS-induced necrosis and hyperstimulation-induced mitochondrial dysfunction, highlighting a potential avenue for the design of targeted therapeutics to ameliorate acute pancreatitis.

The IP_3R as a Drug Target

This study has confirmed IP_3R-mediated Ca^{2+} signalling as a major component in cellular damage by precipitants of acute pancreatitis. Unfortunately in this study, we were unable to determine any increased activity of the xanthines tested over caffeine, and no structural motifs were identified which could help in the rational design of inhibitors. A number of serious problems arise when considering the prospects of the IP_3R as a therapeutic drug target. Good 3D data concerning the structure of the IP_3R has only recently been published (Seo et al., 2012), which is essential for intelligent design of inhibitors in a step-wise space-filling process. The IP_3R is also a ubiquitous and essential channel, not an ideal candidate for therapeutic inhibitors. Subtype specific inhibition may offer some glimmer of hope for the efficacy of inhibition, but this poses its own challenges with regards the practicalities of subtype specificity of inhibition. The channel is also very similar in structure to the ryanodine receptor, which caffeine is an excellent activator of in most excitable cell

types such as smooth muscle (Pessah et al., 1987). Some inhibitors of the IP_3R, originally thought of as very specific, have since been shown to modulate SERCA activity, TRP channels, store-operated Ca^{2+} influx and Ca^{2+} induced Ca^{2+} release, independently of IP_3R-inhibition (Prakriya and Lewis, 2001, Castonguay and Robitaille, 2002, Kovacs et al., 2012). All of these factors argue the difficulties associated with the IP_3R as a therapeutic drug target. However, it may be possible that subtle modulation of subtypes of the IP_3R or inhibition of modulator-binding to the channel may be more viable routes of enquiry, worthy of further investigation due to the range of severe conditions postulated to have major pathological IP_3R involvement.

The Role of Methylxanthines in Acute Pancreatitis

The amelioration achieved by caffeine in models of acute pancreatitis is dramatic (Huang, 2011). This may be due to the nature of caffeine acting on multiple drug targets simultaneously, which, as discussed (METHYLXANTHINES AND PANCREATITIS page 75), individually offer amelioration of pancreatitis in vivo. Therefore, understanding the precise activities of xanthines in the disease state could be extremely important in drug development.

Multiplex Developments

Significant benefits are achieved by employment of multiplex assays. Even though the assays developed here are far from high throughput, they are significantly faster, cheaper and more user friendly than assays involving cell counting by fluorescence microscopy. It should be noted that standard cell sorting and counting

procedures cannot be employed in this cell type due to their inherent acini conformation as large clusters.

Significant advances have been made in the development of these assays, which may prove invaluable for drug screening in future translational research. Investigations into the mechanisms of the differences between these necrosis assays may also offer important insight into the nature of pancreatic acinar cell necrosis in the onset of acute pancreatitis.

MITOCHONDRIAL AND CYTOSKELETAL DYNAMICS IN TISSUE

In this study we have shown for the first time that the mitochondria in pancreatic acinar cells are not confined to fixed subcellular locations under resting conditions as previously thought, but rather are dynamic and responsive to cellular signals. The traditional perigranular belt and subplasmalemmal distribution of mitochondria is in fact formed after stimulation in a reversible manner. This process is Ca^{2+}-dependent and involves mitochondrial motility via the microtubule network. The recruitment to the plasma membrane is directly related to Ca^{2+} influx, suggesting that regions of high Ca^{2+} slow down the mitochondria and over time these sites passively recruit the organelles. We have also outlined a second form of mitochondrial redistribution upon pathological stimulation which is mechanistically distinct to perigranular belt and subplasmalemmal redistribution. Investigations into these phenomena have enabled us to ask fundamental questions about the role of the mitochondria at the plasma membrane during store-operated Ca^{2+} entry. Current understanding of the mitochondrial distribution in the pancreatic acinar cell is greatly enhanced by these data, which also offer a novel example of organellar redistribution

upon physiological stimulation for consideration in related tissue types, especially within the field of stimulus-secretion coupling. These major, novel phenomena demand further investigation and their elucidation could lead to targeted therapy.

We have made huge steps forward in tissue imaging of live pancreatic segments including fixing, staining, loading and mounting protocols to enable the collection of high quality imaging data. These protocols will hopefully enable further research into the development of pancreatic exocrine dysfunction and damage in the onset of acute pancreatitis, and offer a new perspective on research into this debilitating disease. For example, these developments may offer a foundation for in vivo imaging, which is currently not performed in this lab and has proven extremely difficult.

This study has effectively shown the importance of the use of whole undisrupted tissue in determining physiological and pathological events, especially when developing translational approaches. Whilst isolated and cultured cell lines are invaluable for investigating molecular interactions and signalling cascades, these techniques may not be as physiologically relevant when investigating major organellar, cellular and inter-cellular processes. A combinatorial approach to investigating such complex phenomena should, therefore, accompany the drive towards translational research.

REFERENCES

AARHUS, R., DICKEY, D. M., GRAEFF, R. M., GEE, K. R., WALSETH, T. F. & LEE, H. C. 1996. Activation and inactivation of Ca2+ release by NAADP+. *J Biol Chem,* 271**,** 8513-6.

ADKINS, C. E. & TAYLOR, C. W. 1999. Lateral inhibition of inositol 1,4,5-trisphosphate receptors by cytosolic Ca(2+). *Curr Biol,* 9**,** 1115-8.

ADLER, G., KERN, H. F., PAN, G. Z. & GARDNER, J. D. 1984. Secretagogue-induced membrane alterations in dispersed acini from rat pancreas. *Eur J Cell Biol,* 33**,** 234-41.

ALONSO, M. T., MANJARRES, I. M. & GARCIA-SANCHO, J. 2009. Modulation of calcium signalling by intracellular organelles seen with targeted aequorins. *Acta Physiol (Oxf),* 195**,** 37-49.

ASHBY, M. C., CAMELLO-ALMARAZ, C., GERASIMENKO, O. V., PETERSEN, O. H. & TEPIKIN, A. V. 2003. Long distance communication between muscarinic receptors and Ca2+ release channels revealed by carbachol uncaging in cell-attached patch pipette. *J Biol Chem,* 278**,** 20860-4.

ASHBY, M. C. & TEPIKIN, A. V. 2002. Polarized calcium and calmodulin signaling in secretory epithelia. *Physiol Rev,* 82**,** 701-34.

BAKER, P. F. & KNIGHT, D. E. 1978. Calcium-dependent exocytosis in bovine adrenal medullary cells with leaky plasma membranes. *Nature,* 276**,** 620-2.

BALASUBRAMANIAM, R., CHAWLA, S., GRACE, A. A. & HUANG, C. L. 2005. Caffeine-induced arrhythmias in murine hearts parallel changes in cellular Ca(2+) homeostasis. *Am J Physiol Heart Circ Physiol,* 289**,** H1584-93.

BANKS, P. A. & FREEMAN, M. L. 2006. Practice guidelines in acute pancreatitis. *Am J Gastroenterol,* 101**,** 2379-400.

BARNES, P. J. 2006. Theophylline for COPD. *Thorax,* 61**,** 742-4.

BAUGHMAN, J. M., PEROCCHI, F., GIRGIS, H. S., PLOVANICH, M., BELCHER-TIMME, C. A., SANCAK, Y., BAO, X. R., STRITTMATTER, L., GOLDBERGER, O., BOGORAD, R. L., KOTELIANSKY, V. & MOOTHA, V. K. 2011. Integrative genomics identifies MCU as an essential component of the mitochondrial calcium uniporter. *Nature,* 476**,** 341-5.

BAUMGARTNER, H. K., GERASIMENKO, J. V., THORNE, C., FERDEK, P., POZZAN, T., TEPIKIN, A. V., PETERSEN, O. H., SUTTON, R., WATSON, A. J. & GERASIMENKO, O. V. 2009. Calcium elevation in mitochondria is the main Ca2+ requirement for mitochondrial permeability transition pore (mPTP) opening. *J Biol Chem,* 284**,** 20796-803.

BELAN, P., GERASIMENKO, O., PETERSEN, O. H. & TEPIKIN, A. V. 1997. Distribution of Ca2+ extrusion sites on the mouse pancreatic acinar cell surface. *Cell Calcium,* 22**,** 5-10.

BELAN, P. V., GERASIMENKO, O. V., TEPIKIN, A. V. & PETERSEN, O. H. 1996. Localization of Ca2+ extrusion sites in pancreatic acinar cells. *J Biol Chem,* 271**,** 7615-9.

BERRIDGE, M. J., LIPP, P. & BOOTMAN, M. D. 2000. The versatility and universality of calcium signalling. *Nat Rev Mol Cell Biol,* 1**,** 11-21.

BEZPROZVANNY, I. 2007. Inositol 1,4,5-tripshosphate receptor, calcium signalling and Huntington's disease. *Subcell Biochem,* 45**,** 323-35.

BIAGGIONI, I., PAUL, S., PUCKETT, A. & ARZUBIAGA, C. 1991. Caffeine and theophylline as adenosine receptor antagonists in humans. *J Pharmacol Exp Ther,* 258**,** 588-93.

BLATTNER, J. R., HE, L. & LEMASTERS, J. J. 2001. Screening assays for the mitochondrial permeability transition using a fluorescence multiwell plate reader. *Anal Biochem,* 295**,** 220-6.

BOISON, D. 2011. Methylxanthines, seizures, and excitotoxicity. *Handb Exp Pharmacol***,** 251-66.

BOLDOGH, I. R., YANG, H. C., NOWAKOWSKI, W. D., KARMON, S. L., HAYS, L. G., YATES, J. R., 3RD & PON, L. A. 2001. Arp2/3 complex and actin dynamics are required for actin-based mitochondrial motility in yeast. *Proc Natl Acad Sci U S A,* 98**,** 3162-7.

BOOTH, D. M., MURPHY, J. A., MUKHERJEE, R., AWAIS, M., NEOPTOLEMOS, J. P., GERASIMENKO, O. V., TEPIKIN, A. V., PETERSEN, O. H., SUTTON, R. & CRIDDLE, D. N. 2011. Reactive oxygen species induced by bile acid induce apoptosis and protect against necrosis in pancreatic acinar cells. *Gastroenterology,* 140**,** 2116-25.

BROWN, G. R., SAYERS, L. G., KIRK, C. J., MICHELL, R. H. & MICHELANGELI, F. 1992. The opening of the inositol 1,4,5-trisphosphate-sensitive Ca2+ channel in rat cerebellum is inhibited by caffeine. *Biochem J,* 282 (Pt 2)**,** 309-12.

BRUCE, J. 2010. Plasma membrane calcium pump regulation by metabolic stress. *World J Biol Chem,* 1**,** 221-8.

BRUCE, J. I., YANG, X., FERGUSON, C. J., ELLIOTT, A. C., STEWARD, M. C., CASE, R. M. & RICCARDI, D. 1999. Molecular and functional identification of a Ca2+ (polyvalent cation)-sensing receptor in rat pancreas. *J Biol Chem,* 274**,** 20561-8.

BURNHAM, D. B. & WILLIAMS, J. A. 1982. Effects of high concentrations of secretagogues on the morphology and secretory activity of the pancreas: a role for microfilaments. *Cell Tissue Res,* 222**,** 201-12.

CAMELLO, P. J., PETERSEN, O. H. & TOESCU, E. C. 1996. Simultaneous presence of cAMP and cGMP exert a co-ordinated inhibitory effect on the agonist-evoked Ca2+ signal in pancreatic acinar cells. *Pflugers Arch,* 432**,** 775-81.

CAMPELLO, S., LACALLE, R. A., BETTELLA, M., MANES, S., SCORRANO, L. & VIOLA, A. 2006. Orchestration of lymphocyte chemotaxis by mitochondrial dynamics. *J Exp Med,* 203**,** 2879-86.

CANCELA, J. M., CHURCHILL, G. C. & GALIONE, A. 1999. Coordination of agonist-induced Ca2+-signalling patterns by NAADP in pancreatic acinar cells. *Nature,* 398**,** 74-6.

CANCELA, J. M., GERASIMENKO, O. V., GERASIMENKO, J. V., TEPIKIN, A. V. & PETERSEN, O. H. 2000. Two different but converging messenger pathways to intracellular Ca(2+) release: the roles of nicotinic acid adenine dinucleotide phosphate, cyclic ADP-ribose and inositol trisphosphate. *EMBO J,* 19**,** 2549-57.

CANCELA, J. M. & PETERSEN, O. H. 1998. The cyclic ADP ribose antagonist 8-NH2-cADP-ribose blocks cholecystokinin-evoked cytosolic Ca2+ spiking in pancreatic acinar cells. *Pflugers Arch,* 435**,** 746-8.

CASTONGUAY, A. & ROBITAILLE, R. 2002. Xestospongin C is a potent inhibitor of SERCA at a vertebrate synapse. *Cell Calcium,* 32**,** 39-47.

CELINSKI, K., PROZOROW-KROL, B., KOROLCZUK, A., SLOMKA, M., KOROBOWICZ, E., BISKUP, W., MADRO, A., CICHOZ-LACH, H. & CZECHOWSKA, G. 2006. The role of adenosine A2a receptors in experimental acute pancreatitis. *Adv Med Sci,* 51**,** 105-10.

CHADA, S. R. & HOLLENBECK, P. J. 2004. Nerve growth factor signaling regulates motility and docking of axonal mitochondria. *Curr Biol,* 14**,** 1272-6.

CHALMERS, S., SAUNTER, C., WILSON, C., COATS, P., GIRKIN, J. M. & MCCARRON, J. G. 2012. Mitochondrial motility and vascular smooth muscle proliferation. *Arterioscler Thromb Vasc Biol,* 32**,** 3000-11.

CHANG, K. T., NIESCIER, R. F. & MIN, K. T. 2011. Mitochondrial matrix Ca2+ as an intrinsic signal regulating mitochondrial motility in axons. *Proc Natl Acad Sci U S A,* 108**,** 15456-61.

CHURAMANI, D., BOULWARE, M. J., GEACH, T. J., MARTIN, A. C., MOY, G. W., SU, Y. H., VACQUIER, V. D., MARCHANT, J. S., DALE, L. & PATEL, S. 2007. Molecular characterization of a novel intracellular ADP-ribosyl cyclase. *PLoS One,* 2**,** e797.

COLLINS, T. J., BERRIDGE, M. J., LIPP, P. & BOOTMAN, M. D. 2002. Mitochondria are morphologically and functionally heterogeneous within cells. *EMBO J,* 21**,** 1616-27.

COSKER, F., CHEVIRON, N., YAMASAKI, M., MENTEYNE, A., LUND, F. E., MOUTIN, M. J., GALIONE, A. & CANCELA, J. M. 2010. The ecto-enzyme CD38 is a NAADP synthase which couples receptor activation to Ca2+ mobilization from lysosomes in pancreatic acinar cells. *J Biol Chem*.

CRIDDLE, D. N., BOOTH, D. M., MUKHERJEE, R., MCLAUGHLIN, E., GREEN, G. M., SUTTON, R., PETERSEN, O. H. & REEVE, J. R., JR. 2009. Cholecystokinin-58 and cholecystokinin-8 exhibit similar actions on

calcium signaling, zymogen secretion, and cell fate in murine pancreatic acinar cells. *Am J Physiol Gastrointest Liver Physiol,* 297**,** G1085-92.

CRIDDLE, D. N., GERASIMENKO, J. V., BAUMGARTNER, H. K., JAFFAR, M., VORONINA, S., SUTTON, R., PETERSEN, O. H. & GERASIMENKO, O. V. 2007. Calcium signalling and pancreatic cell death: apoptosis or necrosis? *Cell Death Differ,* 14**,** 1285-94.

CRIDDLE, D. N., MURPHY, J., FISTETTO, G., BARROW, S., TEPIKIN, A. V., NEOPTOLEMOS, J. P., SUTTON, R. & PETERSEN, O. H. 2006. Fatty acid ethyl esters cause pancreatic calcium toxicity via inositol trisphosphate receptors and loss of ATP synthesis. *Gastroenterology,* 130**,** 781-93.

CROMPTON, M., CAPANO, M. & CARAFOLI, E. 1976. The Sodium-Induced Efflux of Calcium from Heart Mitochondria. *European Journal of Biochemistry,* 69**,** 453-462.

DE CAMPOS, T., DEREE, J., MARTINS, J. O., LOOMIS, W. H., SHENVI, E., PUTNAM, J. G. & COIMBRA, R. 2008. Pentoxifylline attenuates pulmonary inflammation and neutrophil activation in experimental acute pancreatitis. *Pancreas,* 37**,** 42-9.

DE LISLE, R. C., STEINBERG, R. & WILLIAMS, J. A. 1988. Zymogen granules of mouse parotid acinar cells are acidified in situ in an ATP-dependent manner. *Cell Tissue Res,* 253**,** 267-9.

DE STEFANI, D., RAFFAELLO, A., TEARDO, E., SZABO, I. & RIZZUTO, R. 2011. A forty-kilodalton protein of the inner membrane is the mitochondrial calcium uniporter. *Nature,* 476**,** 336-40.

DELUCA, H. F. & ENGSTROM, G. W. 1961. Calcium uptake by rat kidney mitochondria. *Proc Natl Acad Sci U S A,* 47**,** 1744-50.

DENTON, R. M., RANDLE, P. J. & MARTIN, B. R. 1972. Stimulation by calcium ions of pyruvate dehydrogenase phosphate phosphatase. *Biochem J,* 128**,** 161-3.

DENTON, R. M., RICHARDS, D. A. & CHIN, J. G. 1978. Calcium ions and the regulation of NAD+-linked isocitrate dehydrogenase from the mitochondria of rat heart and other tissues. *Biochem J,* 176**,** 899-906.

DOLMAN, N. J., GERASIMENKO, J. V., GERASIMENKO, O. V., VORONINA, S. G., PETERSEN, O. H. & TEPIKIN, A. V. 2005. Stable Golgi-mitochondria complexes and formation of Golgi Ca(2+) gradients in pancreatic acinar cells. *J Biol Chem,* 280**,** 15794-9.

DUSZYNSKI, J., KOZIEL, R., BRUTKOWSKI, W., SZCZEPANOWSKA, J. & ZABLOCKI, K. 2006. The regulatory role of mitochondria in capacitative calcium entry. *Biochim Biophys Acta,* 1757**,** 380-7.

FEHRENBACHER, K. L., YANG, H. C., GAY, A. C., HUCKABA, T. M. & PON, L. A. 2004. Live cell imaging of mitochondrial movement along actin cables in budding yeast. *Curr Biol,* 14**,** 1996-2004.

FESKE, S., GWACK, Y., PRAKRIYA, M., SRIKANTH, S., PUPPEL, S. H., TANASA, B., HOGAN, P. G., LEWIS, R. S., DALY, M. & RAO, A. 2006. A mutation in Orai1 causes immune deficiency by abrogating CRAC channel function. *Nature,* 441**,** 179-85.

FISCHER, L., GUKOVSKAYA, A. S., PENNINGER, J. M., MARENINOVA, O. A., FRIESS, H., GUKOVSKY, I. & PANDOL, S. J. 2007. Phosphatidylinositol 3-kinase facilitates bile acid-induced Ca(2+) responses in pancreatic acinar cells. *Am J Physiol Gastrointest Liver Physiol,* 292**,** G875-86.

FLANAGAN, M. D. & LIN, S. 1980. Cytochalasins block actin filament elongation by binding to high affinity sites associated with F-actin. *J Biol Chem,* 255**,** 835-8.

FOSKETT, J. K. 2010. Inositol trisphosphate receptor Ca2+ release channels in neurological diseases. *Pflugers Arch,* 460**,** 481-94.

FOSKETT, J. K., WHITE, C., CHEUNG, K. H. & MAK, D. O. 2007. Inositol trisphosphate receptor Ca2+ release channels. *Physiol Rev,* 87**,** 593-658.

FRANCIS, S. H., BLOUNT, M. A. & CORBIN, J. D. 2011. Mammalian cyclic nucleotide phosphodiesterases: molecular mechanisms and physiological functions. *Physiol Rev,* 91**,** 651-90.

FREDHOLM, B. B., BATTIG, K., HOLMEN, J., NEHLIG, A. & ZVARTAU, E. E. 1999. Actions of caffeine in the brain with special reference to factors that contribute to its widespread use. *Pharmacol Rev,* 51**,** 83-133.

FUTATSUGI, A., NAKAMURA, T., YAMADA, M. K., EBISUI, E., NAKAMURA, K., UCHIDA, K., KITAGUCHI, T., TAKAHASHI-IWANAGA, H., NODA, T., ARUGA, J. & MIKOSHIBA, K. 2005. IP3 receptor types 2 and 3 mediate exocrine secretion underlying energy metabolism. *Science,* 309**,** 2232-4.

GAFNI, J., MUNSCH, J. A., LAM, T. H., CATLIN, M. C., COSTA, L. G., MOLINSKI, T. F. & PESSAH, I. N. 1997. Xestospongins: potent membrane permeable blockers of the inositol 1,4,5-trisphosphate receptor. *Neuron,* 19**,** 723-33.

GALIONE, A., LEE, H. C. & BUSA, W. B. 1991. Ca(2+)-induced Ca2+ release in sea urchin egg homogenates: modulation by cyclic ADP-ribose. *Science,* 253**,** 1143-6.

GERASIMENKO, J. V., FLOWERDEW, S. E., VORONINA, S. G., SUKHOMLIN, T. K., TEPIKIN, A. V., PETERSEN, O. H. & GERASIMENKO, O. V. 2006. Bile acids induce Ca2+ release from both the endoplasmic reticulum and acidic intracellular calcium stores through activation of inositol trisphosphate receptors and ryanodine receptors. *J Biol Chem,* 281**,** 40154-63.

GERASIMENKO, J. V., LUR, G., SHERWOOD, M. W., EBISUI, E., TEPIKIN, A. V., MIKOSHIBA, K., GERASIMENKO, O. V. & PETERSEN, O. H. 2009. Pancreatic protease activation by alcohol metabolite depends on Ca2+ release via acid store IP3 receptors. *Proc Natl Acad Sci U S A,* 106**,** 10758-63.

GERASIMENKO, O. V., GERASIMENKO, J. V., RIZZUTO, R. R., TREIMAN, M., TEPIKIN, A. V. & PETERSEN, O. H. 2002. The distribution of the endoplasmic reticulum in living pancreatic acinar cells. *Cell Calcium,* 32**,** 261-8.

GHOSH, T. K., EIS, P. S., MULLANEY, J. M., EBERT, C. L. & GILL, D. L. 1988. Competitive, reversible, and potent antagonism of inositol 1,4,5-trisphosphate-activated calcium release by heparin. *J Biol Chem,* 263**,** 11075-9.

GIACOMELLO, M., DRAGO, I., PIZZO, P. & POZZAN, T. 2007. Mitochondrial Ca2+ as a key regulator of cell life and death. *Cell Death Differ,* 14**,** 1267-74.

GILABERT, J. A. & PAREKH, A. B. 2000. Respiring mitochondria determine the pattern of activation and inactivation of the store-operated Ca(2+) current I(CRAC). *EMBO J,* 19**,** 6401-7.

GINCEL, D., ZAID, H. & SHOSHAN-BARMATZ, V. 2001. Calcium binding and translocation by the voltage-dependent anion channel: a possible regulatory mechanism in mitochondrial function. *Biochem J,* 358**,** 147-55.

GONZALEZ, A., SCHULZ, I. & SCHMID, A. 2000. Agonist-evoked mitochondrial Ca2+ signals in mouse pancreatic acinar cells. *J Biol Chem,* 275**,** 38680-6.

GUERREIRO, S., MARIEN, M. & MICHEL, P. P. 2011. Methylxanthines and ryanodine receptor channels. *Handb Exp Pharmacol***,** 135-50.

HAJNOCZKY, G., ROBB-GASPERS, L. D., SEITZ, M. B. & THOMAS, A. P. 1995. Decoding of cytosolic calcium oscillations in the mitochondria. *Cell,* 82**,** 415-24.

HENDERSON-SMART, D. J. & STEER, P. A. 2010. Caffeine versus theophylline for apnea in preterm infants. *Cochrane Database Syst Rev***,** CD000273.

HIROSE, K., IINO, M. & ENDO, M. 1993. Caffeine inhibits Ca(2+)-mediated potentiation of inositol 1,4,5-trisphosphate-induced Ca2+ release in permeabilized vascular smooth muscle cells. *Biochem Biophys Res Commun,* 194**,** 726-32.

HOFER, A. M., FASOLATO, C. & POZZAN, T. 1998. Capacitative Ca2+ entry is closely linked to the filling state of internal Ca2+ stores: a study using simultaneous measurements of ICRAC and intraluminal [Ca2+]. *J Cell Biol,* 140**,** 325-34.

HUANG, G. N., ZENG, W., KIM, J. Y., YUAN, J. P., HAN, L., MUALLEM, S. & WORLEY, P. F. 2006. STIM1 carboxyl-terminus activates native SOC, I(crac) and TRPC1 channels. *Nat Cell Biol,* 8**,** 1003-10.

HUANG, W., MUKHERJEE, R., CANE, M.C., ELLIOTT, V., BOOTH, D.M., MCLAUGHLIN, E., PETERSEN, O.H., TEPIKIN, A.V., CRIDDLE, D.N., & SUTTON, R. 2011. Protective Effect of Caffeine in Murine Acute Pancreatitis. *Pancreatology,* 11 (supplement 1)**,** 1-80.

HUGHES, C. B., EL-DIN, A. B., KOTB, M., GABER, L. W. & GABER, A. O. 1996. Calcium channel blockade inhibits release of TNF alpha and improves survival in a rat model of acute pancreatitis. *Pancreas,* 13**,** 22-8.

HUSAIN, S. Z., ORABI, A. I., MUILI, K. A., LUO, Y., SARWAR, S., MAHMOOD, S. M., WANG, D., CHOO-WING, R., SINGH, V. P., PARNESS, J., ANANTHANARAVANAN, M., BHANDARI, V. & PERIDES, G. 2012. Ryanodine receptors contribute to bile acid-induced pathological calcium signaling and pancreatitis in mice. *Am J Physiol Gastrointest Liver Physiol*.

JAMIESON, J. D. & PALADE, G. E. 1971. Synthesis, intracellular transport, and discharge of secretory proteins in stimulated pancreatic exocrine cells. *J Cell Biol,* 50**,** 135-58.

JOHNSON, P. R., DOLMAN, N. J., POPE, M., VAILLANT, C., PETERSEN, O. H., TEPIKIN, A. V. & ERDEMLI, G. 2003. Non-uniform distribution of mitochondria in pancreatic acinar cells. *Cell Tissue Res,* 313**,** 37-45.

JOHNSON, P. R., TEPIKIN, A. V. & ERDEMLI, G. 2002. Role of mitochondria in Ca(2+) homeostasis of mouse pancreatic acinar cells. *Cell Calcium,* 32**,** 59-69.

JOUAVILLE, L. S., PINTON, P., BASTIANUTTO, C., RUTTER, G. A. & RIZZUTO, R. 1999. Regulation of mitochondrial ATP synthesis by calcium: evidence for a long-term metabolic priming. *Proc Natl Acad Sci U S A,* 96**,** 13807-12.

JUNGERMANN, J., LERCH, M. M., WEIDENBACH, H., LUTZ, M. P., KRUGER, B. & ADLER, G. 1995. Disassembly of rat pancreatic acinar cell cytoskeleton during supramaximal secretagogue stimulation. *Am J Physiol,* 268**,** G328-38.

KAR, P., BAKOWSKI, D., DI CAPITE, J., NELSON, C. & PAREKH, A. B. 2012. Different agonists recruit different stromal interaction molecule proteins to support cytoplasmic Ca2+ oscillations and gene expression. *Proc Natl Acad Sci U S A,* 109**,** 6969-74.

KAWABATA, A., KURODA, R., NISHIDA, M., NAGATA, N., SAKAGUCHI, Y., KAWAO, N., NISHIKAWA, H., ARIZONO, N. & KAWAI, K. 2002. Protease-activated receptor-2 (PAR-2) in the pancreas and parotid gland: Immunolocalization and involvement of nitric oxide in the evoked amylase secretion. *Life Sci,* 71**,** 2435-46.

KAWANISHI, T., BLANK, L. M., HAROOTUNIAN, A. T., SMITH, M. T. & TSIEN, R. Y. 1989. Ca2+ oscillations induced by hormonal stimulation of individual fura-2-loaded hepatocytes. *J Biol Chem,* 264**,** 12859-66.

KIM, J. Y., KIM, K. H., LEE, J. A., NAMKUNG, W., SUN, A. Q., ANANTHANARAYANAN, M., SUCHY, F. J., SHIN, D. M., MUALLEM, S. & LEE, M. G. 2002. Transporter-mediated bile acid uptake causes Ca2+-dependent cell death in rat pancreatic acinar cells. *Gastroenterology,* 122**,** 1941-53.

KIM, M. S., HONG, J. H., LI, Q., SHIN, D. M., ABRAMOWITZ, J., BIRNBAUMER, L. & MUALLEM, S. 2009. Deletion of TRPC3 in mice reduces store-operated Ca2+ influx and the severity of acute pancreatitis. *Gastroenterology,* 137**,** 1509-17.

KIRICHOK, Y., KRAPIVINSKY, G. & CLAPHAM, D. E. 2004. The mitochondrial calcium uniporter is a highly selective ion channel. *Nature,* 427**,** 360-4.

KONG, H., JONES, P. P., KOOP, A., ZHANG, L., DUFF, H. J. & CHEN, S. R. 2008. Caffeine induces Ca2+ release by reducing the threshold for luminal Ca2+ activation of the ryanodine receptor. *Biochem J,* 414**,** 441-52.

KOVACS, G., MONTALBETTI, N., SIMONIN, A., DANKO, T., BALAZS, B., ZSEMBERY, A. & HEDIGER, M. A. 2012. Inhibition of the human epithelial calcium channel TRPV6 by 2-aminoethoxydiphenyl borate (2-APB). *Cell Calcium*.

KROEMER, G., GALLUZZI, L. & BRENNER, C. 2007. Mitochondrial membrane permeabilization in cell death. *Physiol Rev,* 87**,** 99-163.

L. FISCHER, A. S. G. A. J. M. P. E. A. 2006. Phosphatidylinositol 3 kinase facilitates bile acid-induced Ca2+ responses in pancreatic acinar cells. *Am J Physiol Gastrointest Liver Physiol,* 292**,** pp. G875–G886.

LAKICS, V., KARRAN, E. H. & BOESS, F. G. 2010. Quantitative comparison of phosphodiesterase mRNA distribution in human brain and peripheral tissues. *Neuropharmacology,* 59**,** 367-74.

LAU, B. W., COLELLA, M., RUDER, W. C., RANIERI, M., CURCI, S. & HOFER, A. M. 2005. Deoxycholic acid activates protein kinase C and phospholipase C via increased Ca2+ entry at plasma membrane. *Gastroenterology,* 128**,** 695-707.

LAWRIE, A. M., RIZZUTO, R., POZZAN, T. & SIMPSON, A. W. 1996. A role for calcium influx in the regulation of mitochondrial calcium in endothelial cells. *J Biol Chem,* 271**,** 10753-9.

LEE, H. C. 2006. Structure and enzymatic functions of human CD38. *Mol Med,* 12**,** 317-23.

LEE, H. C., AARHUS, R., GRAEFF, R., GURNACK, M. E. & WALSETH, T. F. 1994. Cyclic ADP ribose activation of the ryanodine receptor is mediated by calmodulin. *Nature,* 370**,** 307-9.

LEE, K. K., UHM, D. Y. & PARK, M. K. 2003. Low affinity cholecystokinin receptor inhibits cholecystokinin- and bombesin-induced oscillations of cytosolic Ca2+ concentration. *FEBS Lett,* 538**,** 134-8.

LEE, M. G., XU, X., ZENG, W., DIAZ, J., KUO, T. H., WUYTACK, F., RACYMAEKERS, L. & MUALLEM, S. 1997. Polarized expression of Ca2+ pumps in pancreatic and salivary gland cells. Role in initiation and propagation of [Ca2+]i waves. *J Biol Chem,* 272**,** 15771-6.

LEIST, M., SINGLE, B., CASTOLDI, A. F., KUHNLE, S. & NICOTERA, P. 1997. Intracellular adenosine triphosphate (ATP) concentration: a switch in the decision between apoptosis and necrosis. *J Exp Med,* 185**,** 1481-6.

LEITE, M. F., DRANOFF, J. A., GAO, L. & NATHANSON, M. H. 1999. Expression and subcellular localization of the ryanodine receptor in rat pancreatic acinar cells. *Biochem J,* 337 (Pt 2)**,** 305-9.

LEWIS, R. S. & CAHALAN, M. D. 1989. Mitogen-induced oscillations of cytosolic Ca2+ and transmembrane Ca2+ current in human leukemic T cells. *Cell Regul,* 1**,** 99-112.

LIN, D. C., TOBIN, K. D., GRUMET, M. & LIN, S. 1980. Cytochalasins inhibit nuclei-induced actin polymerization by blocking filament elongation. *J Cell Biol,* 84**,** 455-60.

LIOU, J., KIM, M. L., HEO, W. D., JONES, J. T., MYERS, J. W., FERRELL, J. E., JR. & MEYER, T. 2005. STIM is a Ca2+ sensor essential for Ca2+-store-depletion-triggered Ca2+ influx. *Curr Biol,* 15**,** 1235-41.

LIU, P. H., LEE, B. J., WANG, C. Y. & HUNG, D. Z. 2008. Acute pancreatitis after severe theophylline overdose. *Clin Toxicol (Phila),* 46**,** 1103.

LIU, X. & HAJNOCZKY, G. 2009. Ca2+-dependent regulation of mitochondrial dynamics by the Miro-Milton complex. *Int J Biochem Cell Biol,* 41**,** 1972-6.

LONDOS, C., COOPER, D. M. & WOLFF, J. 1980. Subclasses of external adenosine receptors. *Proc Natl Acad Sci U S A,* 77**,** 2551-4.

LUIK, R. M., WU, M. M., BUCHANAN, J. & LEWIS, R. S. 2006. The elementary unit of store-operated Ca2+ entry: local activation of CRAC channels by STIM1 at ER-plasma membrane junctions. *J Cell Biol,* 174**,** 815-25.

LUR, G., HAYNES, L. P., PRIOR, I. A., GERASIMENKO, O. V., FESKE, S., PETERSEN, O. H., BURGOYNE, R. D. & TEPIKIN, A. V. 2009. Ribosome-free terminals of rough ER allow formation of STIM1 puncta and segregation of STIM1 from IP(3) receptors. *Curr Biol,* 19**,** 1648-53.

LUR, G., SHERWOOD, M. W., EBISUI, E., HAYNES, L. P., FESKE, S., SUTTON, R., BURGOYNE, R., MIKOSHIBA, K., PETERSEN, O. H. & TEPIKIN, A. V. 2011. IP3 receptors and Orai channels in pancreatic acinar cells: co-localisation and its consequences. *Biochem J*.

MA, H. T., PATTERSON, R. L., VAN ROSSUM, D. B., BIRNBAUMER, L., MIKOSHIBA, K. & GILL, D. L. 2000. Requirement of the inositol trisphosphate receptor for activation of store-operated Ca2+ channels. *Science,* 287**,** 1647-51.

MA, T., GONG, K., YAN, Y., SONG, B., ZHANG, X. & GONG, Y. 2012. Mitochondrial modulation of store-operated Ca(2+) entry in model cells of Alzheimer's disease. *Biochem Biophys Res Commun,* 426**,** 196-202.

MALLI, R., FRIEDEN, M., OSIBOW, K. & GRAIER, W. F. 2003. Mitochondria efficiently buffer subplasmalemmal Ca2+ elevation during agonist stimulation. *J Biol Chem,* 278**,** 10807-15.

MANKAD, P., JAMES, A., SIRIWARDENA, A. K., ELLIOTT, A. C. & BRUCE, J. I. 2012. Insulin protects pancreatic acinar cells from cytosolic calcium overload and inhibition of plasma membrane calcium pump. *J Biol Chem,* 287**,** 1823-36.

MARLOWE, K. J., FARSHORI, P., TORGERSON, R. R., ANDERSON, K. L., MILLER, L. J. & MCNIVEN, M. A. 1998. Changes in kinesin distribution and phosphorylation occur during regulated secretion in pancreatic acinar cells. *Eur J Cell Biol,* 75**,** 140-52.

MARUYAMA, T., KANAJI, T., NAKADE, S., KANNO, T. & MIKOSHIBA, K. 1997. 2APB, 2-aminoethoxydiphenyl borate, a membrane-penetrable modulator of Ins(1,4,5)P3-induced Ca2+ release. *J Biochem,* 122**,** 498-505.

MARUYAMA, Y., INOOKA, G., LI, Y. X., MIYASHITA, Y. & KASAI, H. 1993. Agonist-induced localized Ca2+ spikes directly triggering exocytotic secretion in exocrine pancreas. *EMBO J,* 12**,** 3017-22.

MCCORMACK, J. G. & DENTON, R. M. 1979. The effects of calcium ions and adenine nucleotides on the activity of pig heart 2-oxoglutarate dehydrogenase complex. *Biochem J,* 180**,** 533-44.

MCPHERSON, P. S., KIM, Y. K., VALDIVIA, H., KNUDSON, C. M., TAKEKURA, H., FRANZINI-ARMSTRONG, C., CORONADO, R. & CAMPBELL, K. P. 1991. The brain ryanodine receptor: a caffeine-sensitive calcium release channel. *Neuron,* 7**,** 17-25.

MERSIN, H., IRKIN, F., BERBEROGLU, U., GULBEN, K., OZDEMIR, H. & ONGURU, O. 2009. The selective inhibition of type IV phosphodiesterase attenuates the severity of the acute pancreatitis in rats. *Dig Dis Sci,* 54**,** 2577-82.

MISSIAEN, L., PARYS, J. B., DE SMEDT, H., HIMPENS, B. & CASTEELS, R. 1994. Inhibition of inositol trisphosphate-induced calcium release by caffeine is prevented by ATP. *Biochem J,* 300 (Pt 1)**,** 81-4.

MONKAWA, T., MIYAWAKI, A., SUGIYAMA, T., YONESHIMA, H., YAMAMOTO-HINO, M., FURUICHI, T., SARUTA, T., HASEGAWA, M. & MIKOSHIBA, K. 1995. Heterotetrameric complex formation of inositol 1,4,5-trisphosphate receptor subunits. *J Biol Chem,* 270**,** 14700-4.

MONTALVO, G. B., ARTALEJO, A. R. & GILABERT, J. A. 2006. ATP from subplasmalemmal mitochondria controls Ca2+-dependent inactivation of CRAC channels. *J Biol Chem,* 281**,** 35616-23.

MORTON, C., KLATSKY, A. L. & UDALTSOVA, N. 2004. Smoking, coffee, and pancreatitis. *Am J Gastroenterol,* 99**,** 731-8.

MOTTA, P. M., MACCHIARELLI, G., NOTTOLA, S. A. & CORRER, S. 1997. Histology of the exocrine pancreas. *Microsc Res Tech,* 37**,** 384-98.

MUKHERJEE, R., CRIDDLE, D. N., GUKOVSKAYA, A., PANDOL, S., PETERSEN, O. H. & SUTTON, R. 2008. Mitochondrial injury in pancreatitis. *Cell Calcium,* 44**,** 14-23.

MULLER, C. E., SHI, D., MANNING, M., JR. & DALY, J. W. 1993. Synthesis of paraxanthine analogs (1,7-disubstituted xanthines) and other xanthines unsubstituted at the 3-position: structure-activity relationships at adenosine receptors. *J Med Chem,* 36**,** 3341-9.

MURPHY, J. A., CRIDDLE, D. N., SHERWOOD, M., CHVANOV, M., MUKHERJEE, R., MCLAUGHLIN, E., BOOTH, D., GERASIMENKO, J. V., RARATY, M. G., GHANEH, P., NEOPTOLEMOS, J. P., GERASIMENKO, O. V., TEPIKIN, A. V., GREEN, G. M., REEVE, J. R., JR., PETERSEN, O. H. & SUTTON, R. 2008. Direct activation of cytosolic Ca2+ signaling and enzyme secretion by cholecystokinin in human pancreatic acinar cells. *Gastroenterology,* 135**,** 632-41.

NAGORE, N. & SCHEUER, P. J. 1988. The pathology of diabetic hepatitis. *J Pathol,* 156**,** 155-60.

NATHANSON, M. H., FALLON, M. B., PADFIELD, P. J. & MARANTO, A. R. 1994. Localization of the type 3 inositol 1,4,5-trisphosphate receptor in the Ca2+ wave trigger zone of pancreatic acinar cells. *J Biol Chem,* 269**,** 4693-6.

NICHOLLS, D. G. & CHALMERS, S. 2004. The integration of mitochondrial calcium transport and storage. *J Bioenerg Biomembr,* 36**,** 277-81.

NOVAK, I. 2008. Purinergic receptors in the endocrine and exocrine pancreas. *Purinergic Signal,* 4**,** 237-53.

NUNN, D. L. & TAYLOR, C. W. 1992. Luminal Ca2+ increases the sensitivity of Ca2+ stores to inositol 1,4,5-trisphosphate. *Mol Pharmacol,* 41**,** 115-9.

O'KONSKI, M. S. & PANDOL, S. J. 1990. Effects of caerulein on the apical cytoskeleton of the pancreatic acinar cell. *J Clin Invest,* 86**,** 1649-57.

ORABI, A. I., SHAH, A. U., AHMAD, M. U., CHOO-WING, R., PARNESS, J., JAIN, D., BHANDARI, V. & HUSAIN, S. Z. 2010. Dantrolene mitigates caerulein-induced pancreatitis in vivo in mice. *Am J Physiol Gastrointest Liver Physiol,* 299**,** G196-204.

PALTY, R., SILVERMAN, W. F., HERSHFINKEL, M., CAPORALE, T., SENSI, S. L., PARNIS, J., NOLTE, C., FISHMAN, D., SHOSHAN-BARMATZ, V., HERRMANN, S., KHANANSHVILI, D. & SEKLER, I. 2010. NCLX is an essential component of mitochondrial Na+/Ca2+ exchange. *Proc Natl Acad Sci U S A,* 107**,** 436-41.

PANDOL, S. J., SALUJA, A. K., IMRIE, C. W. & BANKS, P. A. 2007. Acute pancreatitis: bench to the bedside. *Gastroenterology,* 133**,** 1056 e1-1056 e25.

PARK, M. K., ASHBY, M. C., ERDEMLI, G., PETERSEN, O. H. & TEPIKIN, A. V. 2001. Perinuclear, perigranular and sub-plasmalemmal mitochondria have distinct functions in the regulation of cellular calcium transport. *EMBO J,* 20**,** 1863-74.

PARKER, I. & IVORRA, I. 1991. Caffeine inhibits inositol trisphosphate-mediated liberation of intracellular calcium in Xenopus oocytes. *J Physiol,* 433**,** 229-40.

PERIDES, G., LAUKKARINEN, J. M., VASSILEVA, G. & STEER, M. L. 2010. Biliary acute pancreatitis in mice is mediated by the G-protein-coupled cell surface bile acid receptor Gpbar1. *Gastroenterology,* 138**,** 715-25.

PEROCCHI, F., GOHIL, V. M., GIRGIS, H. S., BAO, X. R., MCCOMBS, J. E., PALMER, A. E. & MOOTHA, V. K. 2010. MICU1 encodes a mitochondrial EF hand protein required for Ca(2+) uptake. *Nature,* 467**,** 291-6.

PESSAH, I. N., STAMBUK, R. A. & CASIDA, J. E. 1987. Ca2+-activated ryanodine binding: mechanisms of sensitivity and intensity modulation by Mg2+, caffeine, and adenine nucleotides. *Mol Pharmacol,* 31**,** 232-8.

PETERSEN, O. H. 1992. Stimulus-secretion coupling: cytoplasmic calcium signals and the control of ion channels in exocrine acinar cells. *J Physiol,* 448**,** 1-51.

PETERSEN, O. H. 2012. Specific mitochondrial functions in separate sub-cellular domains of pancreatic acinar cells. *Pflugers Arch,* 464**,** 77-87.

PETERSEN, O. H., BURDAKOV, D. & TEPIKIN, A. V. 1999. Polarity in intracellular calcium signaling. *Bioessays,* 21**,** 851-60.

PETERSEN, O. H., SUTTON, R. & CRIDDLE, D. N. 2006. Failure of calcium microdomain generation and pathological consequences. *Cell Calcium,* 40**,** 593-600.

PILLING, A. D., HORIUCHI, D., LIVELY, C. M. & SAXTON, W. M. 2006. Kinesin-1 and Dynein are the primary motors for fast transport of mitochondria in Drosophila motor axons. *Mol Biol Cell,* 17**,** 2057-68.

PRAKRIYA, M., FESKE, S., GWACK, Y., SRIKANTH, S., RAO, A. & HOGAN, P. G. 2006. Orai1 is an essential pore subunit of the CRAC channel. *Nature,* 443**,** 230-3.

PRAKRIYA, M. & LEWIS, R. S. 2001. Potentiation and inhibition of Ca(2+) release-activated Ca(2+) channels by 2-aminoethyldiphenyl borate (2-APB) occurs independently of IP(3) receptors. *J Physiol,* 536**,** 3-19.

PUSKIN, J. S., GUNTER, T. E., GUNTER, K. K. & RUSSELL, P. R. 1976. Evidence for more than one Ca2+ transport mechanism in mitochondria. *Biochemistry,* 15**,** 3834-42.

PUTNEY, J. W., JR. 1978. Stimulus-permeability coupling: role of calcium in the receptor regulation of membrane permeability. *Pharmacol Rev,* 30**,** 209-45.

PUTNEY, J. W., JR. 1986. A model for receptor-regulated calcium entry. *Cell Calcium,* 7**,** 1-12.

PUTNEY, J. W., JR. 1990a. The integration of receptor-regulated intracellular calcium release and calcium entry across the plasma membrane. *Curr Top Cell Regul,* 31**,** 111-27.

PUTNEY, J. W., JR. 1990b. Receptor-regulated calcium entry. *Pharmacol Ther,* 48**,** 427-34.

QUINTANA, A., PASCHE, M., JUNKER, C., AL-ANSARY, D., RIEGER, H., KUMMEROW, C., NUNEZ, L., VILLALOBOS, C., MERANER, P., BECHERER, U., RETTIG, J., NIEMEYER, B. A. & HOTH, M. 2011. Calcium microdomains at the immunological synapse: how ORAI channels, mitochondria and calcium pumps generate local calcium signals for efficient T-cell activation. *EMBO J,* 30**,** 3895-912.

RIZZUTO, R., BERNARDI, P. & POZZAN, T. 2000. Mitochondria as all-round players of the calcium game. *J Physiol,* 529 Pt 1**,** 37-47.

ROSENZWEIG, S. A., MILLER, L. J. & JAMIESON, J. D. 1983. Identification and localization of cholecystokinin-binding sites on rat pancreatic plasma membranes and acinar cells: a biochemical and autoradiographic study. *J Cell Biol,* 96**,** 1288-97.

RUAS, M., RIETDORF, K., ARREDOUANI, A., DAVIS, L. C., LLOYD-EVANS, E., KOEGEL, H., FUNNELL, T. M., MORGAN, A. J., WARD, J. A., WATANABE, K., CHENG, X., CHURCHILL, G. C., ZHU, M. X., PLATT, F. M., WESSEL, G. M., PARRINGTON, J. & GALIONE, A. 2010. Purified TPC Isoforms Form NAADP Receptors with Distinct Roles for Ca(2+) Signaling and Endolysosomal Trafficking. *Curr Biol*.

SAILLAN-BARREAU, C., CLERC, P., ADATO, M., ESCRIEUT, C., VAYSSE, N., FOURMY, D. & DUFRESNE, M. 1998. Transgenic CCK-B/gastrin receptor mediates murine exocrine pancreatic secretion. *Gastroenterology,* 115**,** 988-96.

SALUJA, A. K., LERCH, M. M., PHILLIPS, P. A. & DUDEJA, V. 2007. Why does pancreatic overstimulation cause pancreatitis? *Annu Rev Physiol,* 69**,** 249-69.

SANCHO, V., NUCHE-BERENGUER, B. & JENSEN, R. T. 2012. The Src kinase Yes is activated in pancreatic acinar cells by gastrointestinal hormones/neurotransmitters, but not pancreatic growth factors, which stimulate its association with numerous other signaling molecules. *Biochim Biophys Acta,* 1823**,** 1285-94.

SAXTON, W. M. & HOLLENBECK, P. J. 2012. The axonal transport of mitochondria. *J Cell Sci,* 125**,** 2095-104.

SCHAPIRA, A. H. 2006. Mitochondrial disease. *Lancet,* 368**,** 70-82.

SCHNEKENBURGER, J., WEBER, I. A., HAHN, D., BUCHWALOW, I., KRUGER, B., ALBRECHT, E., DOMSCHKE, W. & LERCH, M. M. 2009. The role of kinesin, dynein and microtubules in pancreatic secretion. *Cell Mol Life Sci,* 66**,** 2525-37.

SCHULTE, G. & FREDHOLM, B. B. 2003. Signalling from adenosine receptors to mitogen-activated protein kinases. *Cell Signal,* 15**,** 813-27.

SCHWINDLING, C., QUINTANA, A., KRAUSE, E. & HOTH, M. 2010. Mitochondria positioning controls local calcium influx in T cells. *J Immunol,* 184**,** 184-90.

SEO, M. D., VELAMAKANNI, S., ISHIYAMA, N., STATHOPULOS, P. B., ROSSI, A. M., KHAN, S. A., DALE, P., LI, C., AMES, J. B., IKURA, M. & TAYLOR, C. W. 2012. Structural and functional conservation of key domains in InsP3 and ryanodine receptors. *Nature,* 483**,** 108-12.

SHERWOOD, M. W., PRIOR, I. A., VORONINA, S. G., BARROW, S. L., WOODSMITH, J. D., GERASIMENKO, O. V., PETERSEN, O. H. & TEPIKIN, A. V. 2007. Activation of trypsinogen in large endocytic vacuoles of pancreatic acinar cells. *Proc Natl Acad Sci U S A,* 104**,** 5674-9.

SILVERTHORN, D. U. 1998. *Human Physiology: An Integrated Approach,* New Jersey, Prentice Hall.

SIMON, V. R., SWAYNE, T. C. & PON, L. A. 1995. Actin-dependent mitochondrial motility in mitotic yeast and cell-free systems: identification of a motor activity on the mitochondrial surface. *J Cell Biol,* 130**,** 345-54.

SINGH, V. P. & MCNIVEN, M. A. 2008. Src-mediated cortactin phosphorylation regulates actin localization and injurious blebbing in acinar cells. *Mol Biol Cell,* 19**,** 2339-47.

SJODIN, L. & GYLFE, E. 2000. Caffeine inhibits a low affinity but not a high affinity mechanism for cholecystokinin-evoked Ca2+ signalling and amylase release from guinea pig pancreatic acini. *Naunyn Schmiedebergs Arch Pharmacol,* 361**,** 113-9.

SOBOLEWSKI, P., KANDEL, J., KLINGER, A. L. & ECKMANN, D. M. 2011. Air bubble contact with endothelial cells in vitro induces calcium influx and IP3-dependent release of calcium stores. *Am J Physiol Cell Physiol,* 301**,** C679-86.

SOUBANNIER, V. & MCBRIDE, H. M. 2009. Positioning mitochondrial plasticity within cellular signaling cascades. *Biochim Biophys Acta,* 1793**,** 154-70.

STRAIGHT, A. F., CHEUNG, A., LIMOUZE, J., CHEN, I., WESTWOOD, N. J., SELLERS, J. R. & MITCHISON, T. J. 2003. Dissecting temporal and spatial control of cytokinesis with a myosin II Inhibitor. *Science,* 299**,** 1743-7.

STRAUB, S. V., GIOVANNUCCI, D. R. & YULE, D. I. 2000. Calcium wave propagation in pancreatic acinar cells: functional interaction of inositol 1,4,5-trisphosphate receptors, ryanodine receptors, and mitochondria. *J Gen Physiol,* 116**,** 547-60.

STREB, H., BAYERDORFFER, E., HAASE, W., IRVINE, R. F. & SCHULZ, I. 1984. Effect of inositol-1,4,5-trisphosphate on isolated subcellular fractions of rat pancreas. *J Membr Biol,* 81**,** 241-53.

STREB, H., IRVINE, R. F., BERRIDGE, M. J. & SCHULZ, I. 1983. Release of Ca2+ from a nonmitochondrial intracellular store in pancreatic acinar cells by inositol-1,4,5-trisphosphate. *Nature,* 306**,** 67-9.

SUPATTAPONE, S., WORLEY, P. F., BARABAN, J. M. & SNYDER, S. H. 1988. Solubilization, purification, and characterization of an inositol trisphosphate receptor. *J Biol Chem,* 263**,** 1530-4.

SWAROOP, V. S., CHARI, S. T. & CLAIN, J. E. 2004. Severe acute pancreatitis. *JAMA,* 291**,** 2865-8.

TAUFIQ UR, R., SKUPIN, A., FALCKE, M. & TAYLOR, C. W. 2009. Clustering of InsP3 receptors by InsP3 retunes their regulation by InsP3 and Ca2+. *Nature,* 458**,** 655-9.

TAYLOR, C. W., GENAZZANI, A. A. & MORRIS, S. A. 1999. Expression of inositol trisphosphate receptors. *Cell Calcium,* 26**,** 237-51.

TERRITO, P. R., MOOTHA, V. K., FRENCH, S. A. & BALABAN, R. S. 2000. Ca(2+) activation of heart mitochondrial oxidative phosphorylation: role of the F(0)/F(1)-ATPase. *Am J Physiol Cell Physiol,* 278**,** C423-35.

THORN, P., LAWRIE, A. M., SMITH, P. M., GALLACHER, D. V. & PETERSEN, O. H. 1993. Local and global cytosolic Ca2+ oscillations in exocrine cells evoked by agonists and inositol trisphosphate. *Cell,* 74**,** 661-8.

TINEL, H., CANCELA, J. M., MOGAMI, H., GERASIMENKO, J. V., GERASIMENKO, O. V., TEPIKIN, A. V. & PETERSEN, O. H. 1999. Active mitochondria surrounding the pancreatic acinar granule region prevent spreading of inositol trisphosphate-evoked local cytosolic Ca(2+) signals. *EMBO J,* 18**,** 4999-5008.

TOESCU, E. C., O'NEILL, S. C., PETERSEN, O. H. & EISNER, D. A. 1992. Caffeine inhibits the agonist-evoked cytosolic Ca2+ signal in mouse pancreatic acinar cells by blocking inositol trisphosphate production. *J Biol Chem,* 267**,** 23467-70.

TORGERSON, R. R. & MCNIVEN, M. A. 1998. The actin-myosin cytoskeleton mediates reversible agonist-induced membrane blebbing. *J Cell Sci,* 111 (Pt 19)**,** 2911-22.

TUGBA DURLU-KANDILCI, N., RUAS, M., CHUANG, K. T., BRADING, A., PARRINGTON, J. & GALIONE, A. 2010. TPC2 proteins mediate nicotinic acid adenine dinucleotide phosphate (NAADP)- and agonist-evoked contractions of smooth muscle. *J Biol Chem,* 285**,** 24925-32.

UEDA, T., TAKEYAMA, Y., ADACHI, M., TOYOKAWA, A., KISHIDA, S., YAMAMOTO, M. & SAITOH, Y. 1995. Effect of the microtubule-disrupting drug colchicine on rat cerulein-induced pancreatitis in comparison with the microtubule stabilizer taxol. *Pancreas,* 11**,** 294-302.

UEDA, T., TAKEYAMA, Y., KANEDA, K., ADACHI, M., OHYANAGI, H. & SAITOH, Y. 1992. Protective effect of a microtubule stabilizer taxol on caerulein-induced acute pancreatitis in rat. *J Clin Invest,* 89**,** 234-43.

VASINGTON, F. D. & MURPHY, J. V. 1962. Ca ion uptake by rat kidney mitochondria and its dependence on respiration and phosphorylation. *J Biol Chem,* 237**,** 2670-7.

VORONINA, S., LONGBOTTOM, R., SUTTON, R., PETERSEN, O. H. & TEPIKIN, A. 2002. Bile acids induce calcium signals in mouse pancreatic acinar cells: implications for bile-induced pancreatic pathology. *J Physiol,* 540**,** 49-55.

VORONINA, S. & TEPIKIN, A. 2012. Mitochondrial calcium in the life and death of exocrine secretory cells. *Cell Calcium,* 52**,** 86-92.

VORONINA, S. G., BARROW, S. L., GERASIMENKO, O. V., PETERSEN, O. H. & TEPIKIN, A. V. 2004. Effects of secretagogues and bile acids on mitochondrial membrane potential of pancreatic acinar cells: comparison of different modes of evaluating DeltaPsim. *J Biol Chem,* 279**,** 27327-38.

VORONINA, S. G., BARROW, S. L., SIMPSON, A. W., GERASIMENKO, O. V., DA SILVA XAVIER, G., RUTTER, G. A., PETERSEN, O. H. & TEPIKIN, A. V. 2010. Dynamic changes in cytosolic and mitochondrial ATP levels in pancreatic acinar cells. *Gastroenterology,* 138**,** 1976-87.

WAKUI, M., KASE, H. & PETERSEN, O. H. 1991. Cytoplasmic Ca2+ signals evoked by activation of cholecystokinin receptors: Ca(2+)-dependent current recording in internally perfused pancreatic acinar cells. *J Membr Biol,* 124**,** 179-87.

WAKUI, M., OSIPCHUK, Y. V. & PETERSEN, O. H. 1990. Receptor-activated cytoplasmic Ca2+ spiking mediated by inositol trisphosphate is due to Ca2(+)-induced Ca2+ release. *Cell,* 63**,** 1025-32.

WALSH, C. M., CHVANOV, M., HAYNES, L. P., PETERSEN, O. H., TEPIKIN, A. V. & BURGOYNE, R. D. 2010. Role of phosphoinositides in STIM1 dynamics and store-operated calcium entry. *Biochem J,* 425**,** 159-68.

WANG, X. & SCHWARZ, T. L. 2009. The mechanism of Ca2+ -dependent regulation of kinesin-mediated mitochondrial motility. *Cell,* 136**,** 163-74.

WANG, X., ZHANG, X., DONG, X. P., SAMIE, M., LI, X., CHENG, X., GOSCHKA, A., SHEN, D., ZHOU, Y., HARLOW, J., ZHU, M. X., CLAPHAM, D. E., REN, D. & XU, H. 2012. TPC Proteins Are Phosphoinositide- Activated Sodium-Selective Ion Channels in Endosomes and Lysosomes. *Cell,* 151**,** 372-83.

WARD, J. B., PETERSEN, O. H., JENKINS, S. A. & SUTTON, R. 1995. Is an elevated concentration of acinar cytosolic free ionised calcium the trigger for acute pancreatitis? *Lancet,* 346**,** 1016-9.

WARD, J. B., SUTTON, R., JENKINS, S. A. & PETERSEN, O. H. 1996. Progressive disruption of acinar cell calcium signaling is an early feature of cerulein-induced pancreatitis in mice. *Gastroenterology,* 111**,** 481-91.

WEBER, H., HUEHNS, S., LUETHEN, F. & JONAS, L. 2009. Calpain-mediated breakdown of cytoskeletal proteins contributes to cholecystokinin-induced damage of rat pancreatic acini. *International Journal of Experimental Pathology,* 90**,** 387-399.

WEHRENS, X. H., LEHNART, S. E. & MARKS, A. R. 2005. Intracellular calcium release and cardiac disease. *Annu Rev Physiol,* 67**,** 69-98.

WOJCIKIEWICZ, R. J., ERNST, S. A. & YULE, D. I. 1999. Secretagogues cause ubiquitination and down-regulation of inositol 1, 4,5-trisphosphate receptors in rat pancreatic acinar cells. *Gastroenterology,* 116**,** 1194-201.

WU, M. M., BUCHANAN, J., LUIK, R. M. & LEWIS, R. S. 2006. Ca2+ store depletion causes STIM1 to accumulate in ER regions closely associated with the plasma membrane. *J Cell Biol,* 174**,** 803-13.

YAMASAKI-MANN, M., DEMURO, A. & PARKER, I. 2009. cADPR stimulates SERCA activity in Xenopus oocytes. *Cell Calcium,* 45**,** 293-9.

YAMASAKI, M., THOMAS, J. M., CHURCHILL, G. C., GARNHAM, C., LEWIS, A. M., CANCELA, J. M., PATEL, S. & GALIONE, A. 2005. Role of NAADP and cADPR in the induction and maintenance of agonist-evoked Ca2+ spiking in mouse pancreatic acinar cells. *Curr Biol,* 15**,** 874-8.

YI, M., WEAVER, D. & HAJNOCZKY, G. 2004. Control of mitochondrial motility and distribution by the calcium signal: a homeostatic circuit. *J Cell Biol,* 167**,** 661-72.

YUAN, J. P., KIM, M. S., ZENG, W., SHIN, D. M., HUANG, G., WORLEY, P. F. & MUALLEM, S. 2009. TRPC channels as STIM1-regulated SOCs. *Channels (Austin),* 3**,** 221-5.

YULE, D. I. & GALLACHER, D. V. 1988. Oscillations of cytosolic calcium in single pancreatic acinar cells stimulated by acetylcholine. *FEBS Lett,* 239**,** 358-62.

ZIMMERMAN, P. M., PULLIAM, J., SCHWENGELS, J. & MACDONALD, S. E. 1985. Caffeine intoxication: a near fatality. *Ann Emerg Med,* 14**,** 1227-9.

FIGURES

Figure 1.1

Schematic of the pancreatic acinar cell. (A) The structure of the pancreatic acinus, made up of a number of pancreatic acinar cells, showing the orientation of the granular regions towards a central lumen from which the duct drains secretions. **(B)** Cellular structure of the pancreatic acinar cell, showing the location of the apical granular region; the nucleus in the basal region; the mitochondrial network in a perigranular, perinuclear, and subplasmalemmal distribution; the ER richly decorating the cytosol and extending towards the apex of the apical region; and the location of the basal, lateral and apical regions of this polarised cell type.

Figure 1.1

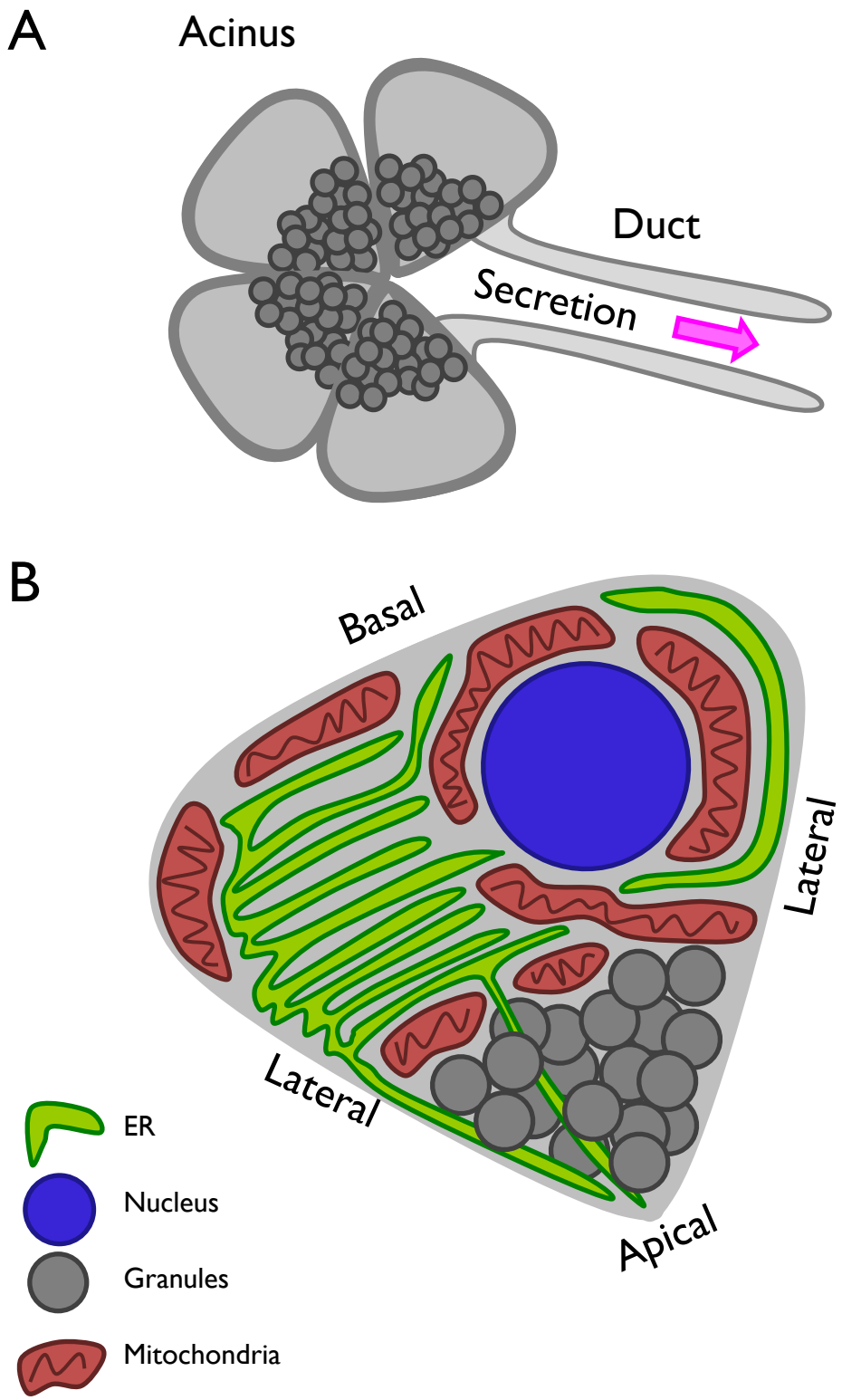
A
Acinus
Duct
Secretion
B
Basal
Lateral
Lateral
Apical
ER
Nucleus
Granules
Mitochondria

Figure 1.2

Schematic of the pancreatic acinar cell Ca^{2+} signalling machinery. The major Ca^{2+} channels and second messenger-generating machinery responsible for the generation and maintenance of Ca^{2+} signals in pancreatic acinar cells. Activation of G-protein coupled receptors stimulates the activity of CD38, ADP ribosyl cyclase and PLC to generate second messengers within acinar cells. cADPr activates RyRs whilst NAADP is thought to act directly on the acidic store, activating release via TPCs. IP_3 activates the IP_3R which recruits RyRs to generate global Ca^{2+} rises. As the Ca^{2+} store depletes, STIM senses low store Ca^{2+} and activates the ORAI channel responsible for Ca^{2+} import.

Figure 1.2

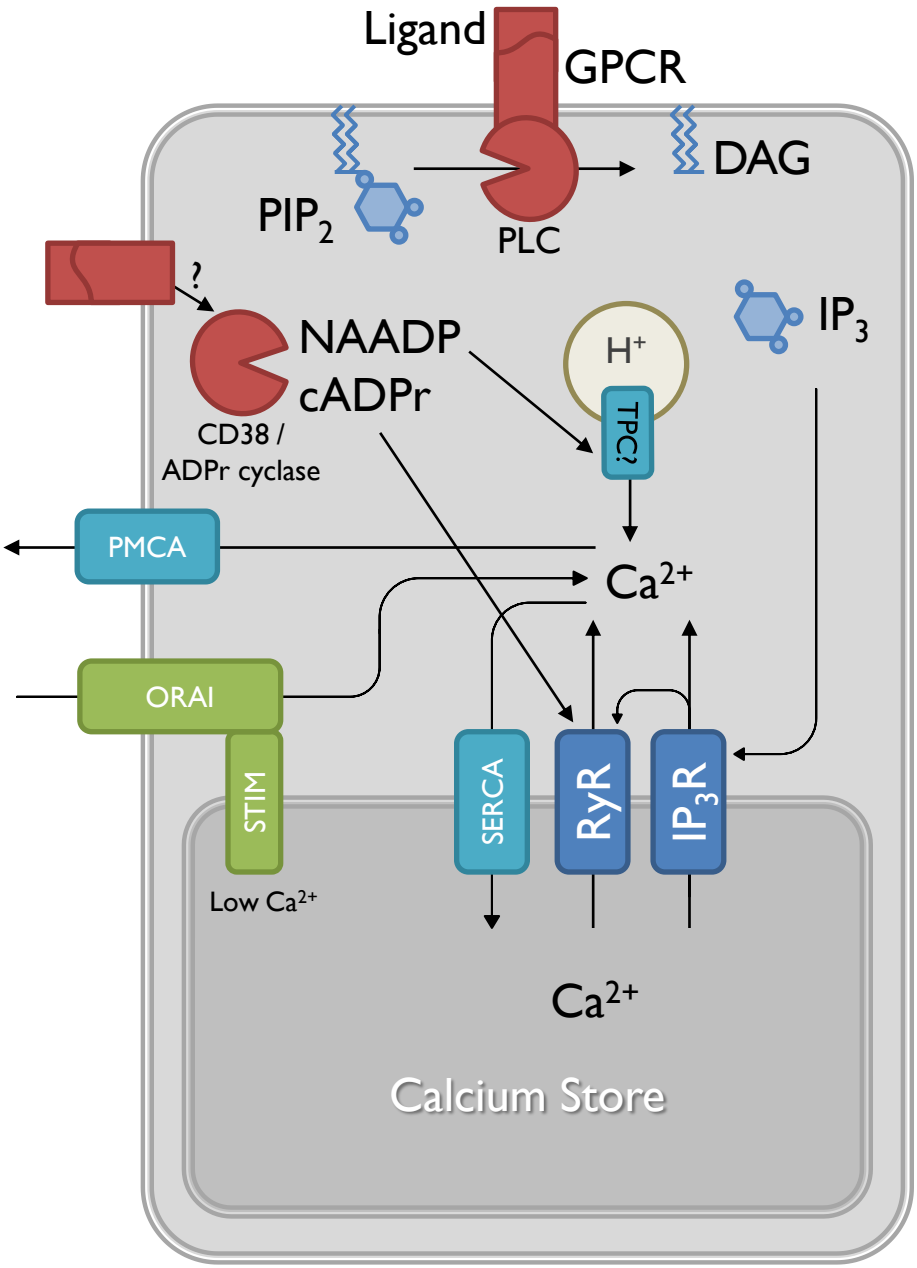
Ligand
GPCR
DAG
PIP2
PLC
?
NAADP
cADPr
CD38 /
ADPr cyclase
H+
TPC?
IP3
PMCA
Ca2+
ORAI
STIM
Low Ca2+
SERCA
RyR
IP3R
Ca2+
Calcium Store

Figure 1.3

Schematic of the mitochondrial Ca^{2+} signalling machinery. The major Ca^{2+} channels responsible for import and export of Ca^{2+} into and out of the mitochondria are shown. VDAC is responsible for permeabilisation of the outer mitochondrial membrane. The MCU is responsible for Ca^{2+} import. The hydrogen and sodium Ca^{2+} exchangers are responsible for Ca^{2+} export. Mitochondrial contents including ions, can also freely diffuse through the open mPTP.

Figure 1.3

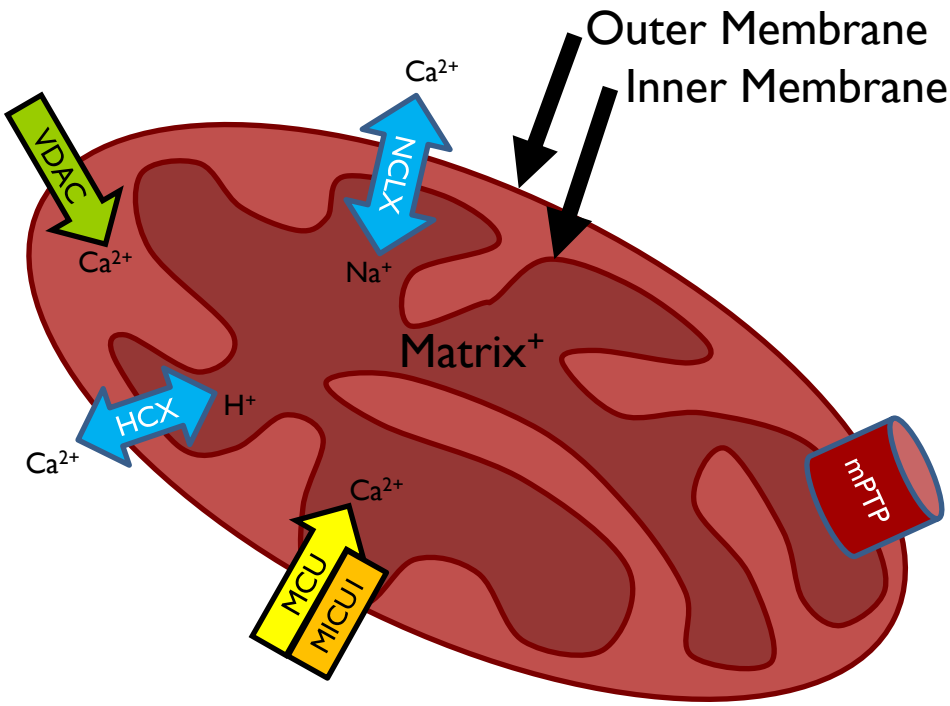
Outer Membrane
Inner Membrane
Ca2+
VDAC
NCLX
Ca2+
Na+
Matrix+
HCX
H+
Ca2+
Ca2+
MCU
MICUI
mPTP

Figure 1.4

Schematic of the mitochondrial motility machinery. The mitochondria move along microtubules by employing the cellular motors, kinesin and dynein. It is thought that mitochondria link to these motors via accessory proteins on the mitochondrial surface, for example, the Ca^{2+} sensitive miro / milton complex.

Figure 1.4

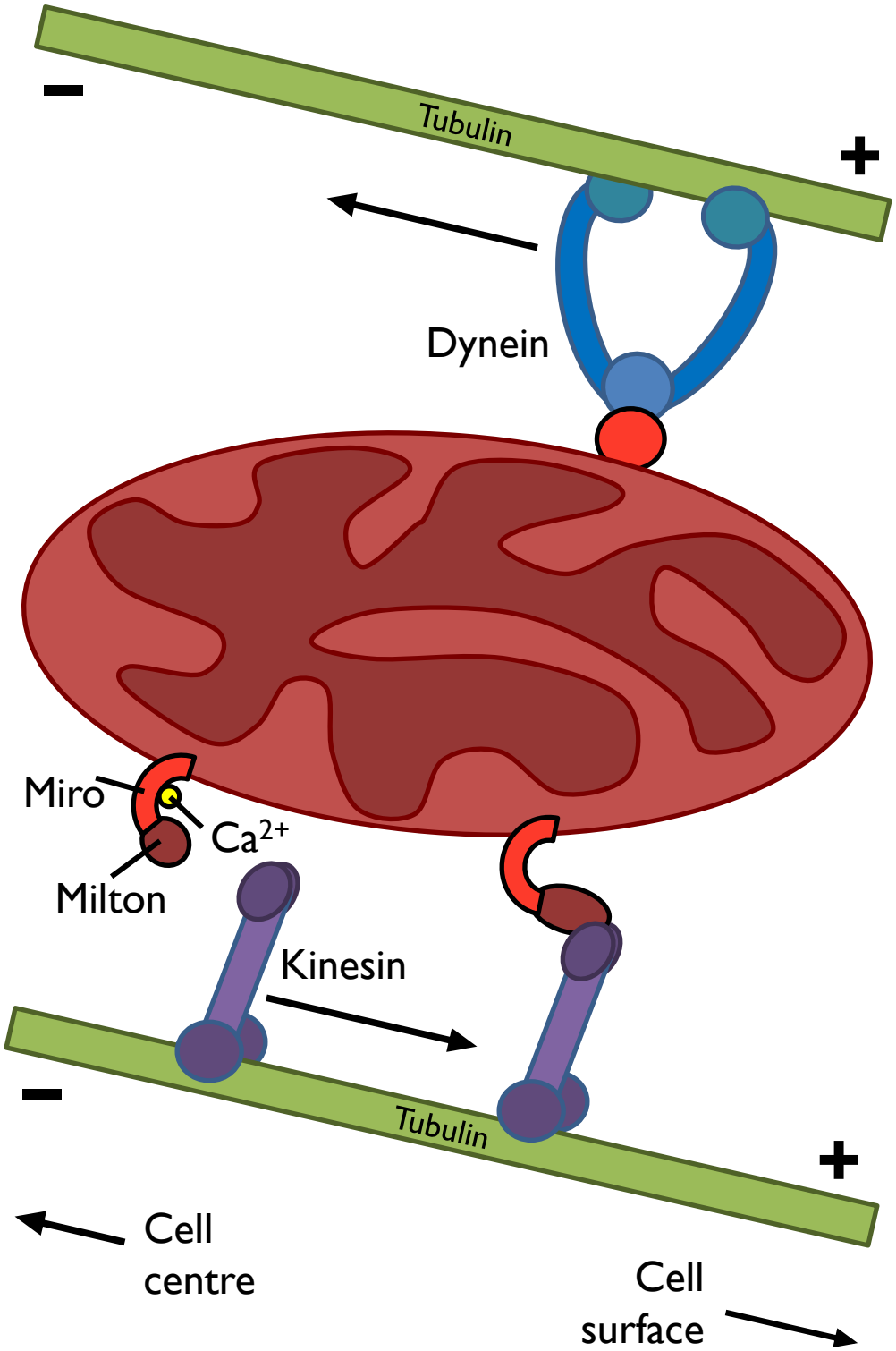
Tubulin
−
+
Dynein
Miro
Ca2+
Milton
Kinesin
Tubulin
−
+
Cell centre
Cell surface

Table 2.1

Table to show the complete list of chemical inhibitors and drugs used throughout this thesis. The name, concentration, target or specific function, and the practical use of each of the pharmacological compounds used within this thesis is listed in the table opposite. In the case of thapsigargin, 2 μM was used in most scenarios but in some specific cases pre-treatment with 2 μM was performed first, enabling 0.5 μM to be used during superfusion to reduce costs (0.5 μM was never used without at least 10 minutes treatment with 2 μM).

Table 2.1

Compound	Conc.	Target / Function	Use
BAPTA-AM	(loaded) 25 μM	Ca^{2+} chelator	Used to inhibit cytosolic Ca^{2+} signals
Blebbistatin	50 μM	Myosin IIA	Used to inhibit myosin-based actin contraction
CCCP	10 μM	Protonophore	Used to collapse $\Delta\Psi_m$
Cyclosporine	10 μM	Cyclophilin D inhibitor	Used to prevent mPTP opening
Colchicine	50 μM	Tubulin	Used to inhibit tubulin polymerisation
Cytochalasin D	10 μM	G-actin	Used to inhibit actin polymerisation
IBMX	20μM	Phosphodiesterase inhibitor	Used as positive control in phosphodiesterase assay kit
LY294002	300 μM	PI3K inhibitor	Used to deplete PIP_2
Menadione	30 μM	Oxidant: redox cycler	Used to generate ROS
NAC	10 mM	γ-glutamylcysteine synthetase substrate	Used as an antioxidant
Paclitaxel	10 μM	β-Tubulin	Used to stabilise the microtubule network
Thapsigargin	0.5 μM - 2 μM	SERCA inhibitor	Used to deplete the intracellular Ca^{2+} store
Wortmannin	30 μM	PI3K inhibitor	Used to deplete PIP_2

Figure 2.1

Schematic of the superfusion system, illustrating the method of pancreatic tissue stabilisation. (A) The top view of the chamber, showing the location of the solution input. The dashed line indicates the orientation of the cross section in (B). **(B)** Cross section view through the middle of the chamber showing the major components used to gently clamp the pancreatic tissue in place during superfusion. *Nota bene*: the same chamber was used for isolated cells but the Whatman paper was omitted.

Figure 2.1

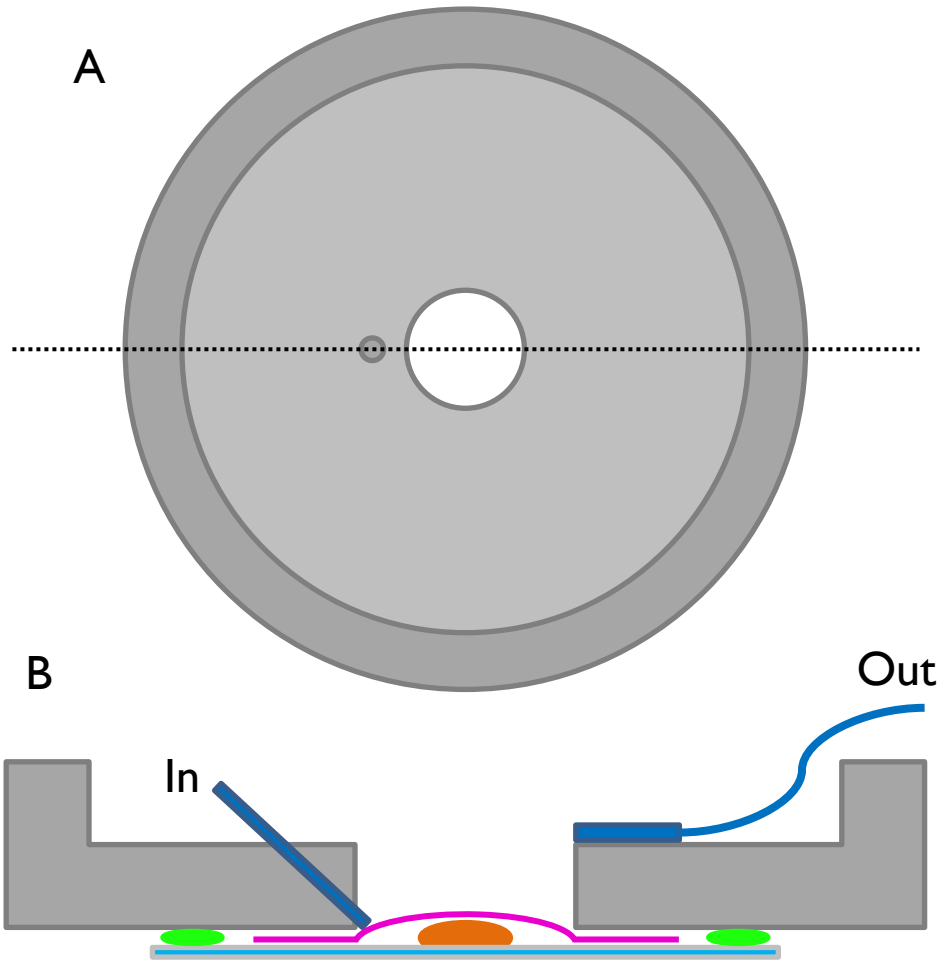
A
B
Out
In
Chamber
Tubing
High Vacuum Grease
Whatman 105
Pancreatic Tissue
Coverslip

Figure 3.1

Caffeine inhibited pathological CCK-induced Ca^{2+} overload in a dose-dependent manner in isolated pancreatic acinar cells. (A) $[Ca^{2+}]c$ was measured in primary isolated murine pancreatic acinar cells loaded with Fluo-4. 10 nM CCK was superfused over the cells on the microscope stage and $[Ca^{2+}]c$ was recorded. A partial and complete inhibition of the Ca^{2+} plateau was observed with 1 and 10 mM caffeine respectively. Traces are averages of >20 cells from at least three animals. **(B)** Average plateau height from data in (A) showing significant inhibition by 1 and 10 mM caffeine. Error bars indicate SEM; * indicates $p < 0.05$. Data has been normalised to the initial fluorescence expressed as F/F_0.

Figure 3.1

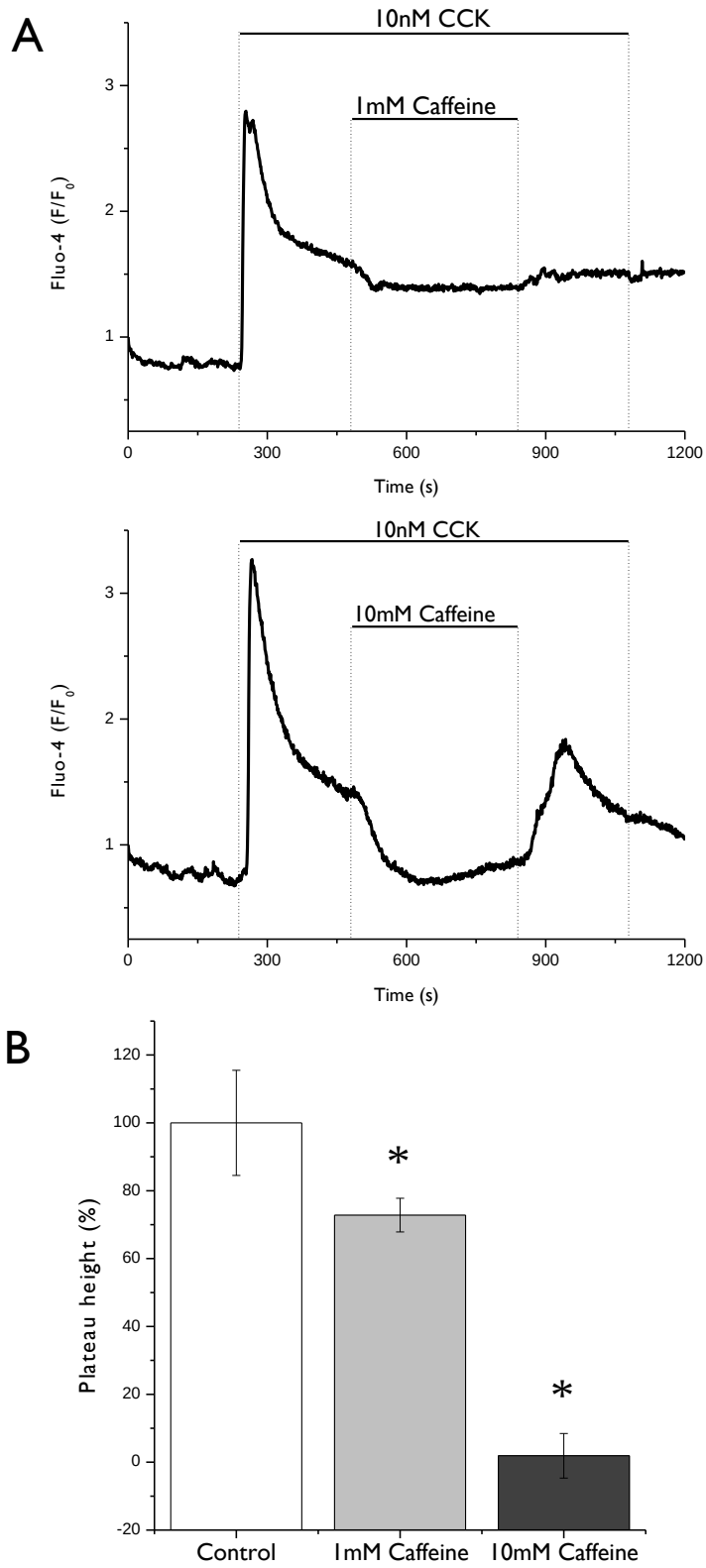
A
10nM CCK
1mM Caffeine
Fluo-4 (F/F0)
Time (s)
10nM CCK
10mM Caffeine
Fluo-4 (F/F0)
Time (s)
B
Plateau height (%)
Control
1mM Caffeine
10mM Caffeine

Figure 3.2

Caffeine inhibits the frequency but not the amplitude of physiological CCK-induced Ca^{2+} oscillations in isolated pancreatic acinar cells. (A) Average peak height of 10 pM CCK-induced Ca^{2+} oscillations in Fluo-4 loaded cells in the presence or absence of caffeine shows no significant difference (n= 16). **(B)** A significant decrease in the frequency of 10 pM CCK-induced Ca^{2+} oscillations was seen with 10 mM caffeine treatment (n= 16) * indicates $p < 0.05$. Data has been normalised to the initial fluorescence expressed as F/F_0.

Figure 3.2

A

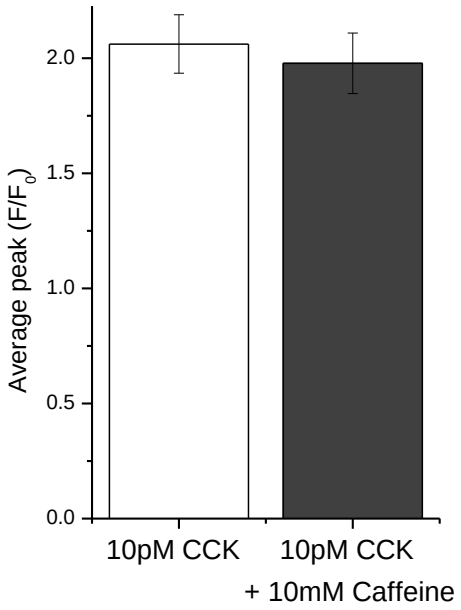
Average peak (F/F0)
2.0
1.5
1.0
0.5
0.0
10pM CCK
10pM CCK
+ 10mM Caffeine

B

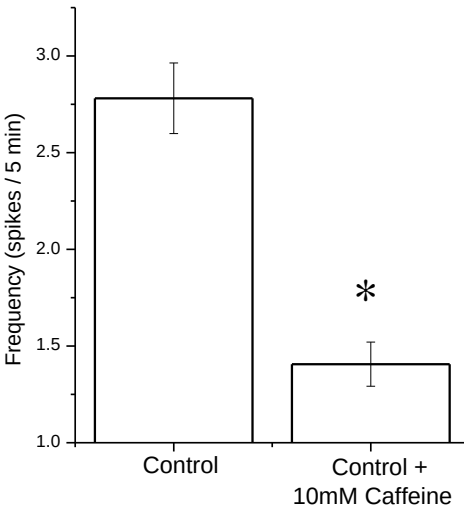
Frequency (spikes / 5 min)
3.0
2.5
2.0
1.5
1.0
*
Control
Control +
10mM Caffeine

Figure 3.3

Application of caffeine before the onset of the CCK-induced Ca^{2+} plateau only offers partial inhibition of the signal, converting it to an oscillatory response. Average trace of 100 nM CCK-induced cytosolic Ca^{2+} rise from Fluo-4 loaded pancreatic acinar cells. An oscillatory signal was formed during caffeine pre-treatment (red) compared to a complete block of the signal with caffeine applied after formation of the plateau (black). Traces shown are averages of >19 cells from three animals and error bars indicate SEM. Data has been normalised to the initial fluorescence expressed as F/F_0.

Figure 3.3

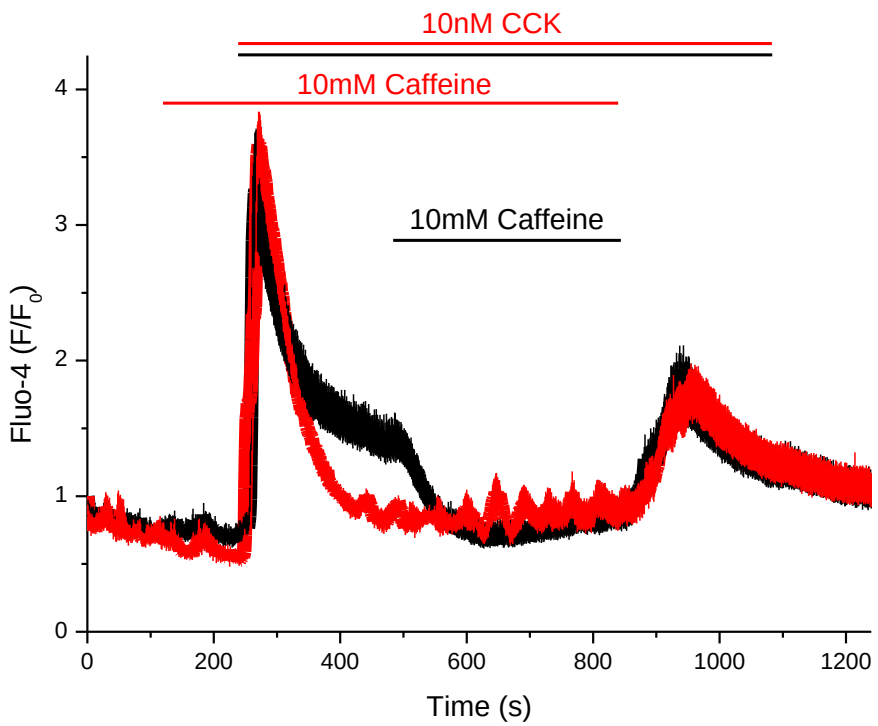
10nM CCK
10mM Caffeine
10mM Caffeine
Fluo-4 (F/F0)
0
1
2
3
4
0
200
400
600
800
1000
1200
Time (s)

Figure 3.4

Ca^{2+} traces showing dose-dependent and differential inhibition of the TLCS-induced Ca^{2+} plateau by increasing concentrations of caffeine. Caffeine inhibits TLCS-induced Ca^{2+} signals in isolated pancreatic acinar cells. No effect was observed at 1 mM caffeine (not shown). **(A)** 3 mM showed a reduction of the plateau in a reversible manner. **(B)** 5 mM caffeine showed conversion of the plateau to an oscillatory response in a reversible manner and showed a rebound of Ca^{2+} after removal of the caffeine. **(C)** complete inhibition of the TLCS-induced Ca^{2+} plateau was observed with 10 mM caffeine. Data has been normalised to the initial fluorescence expressed as F/F_0.

Figure 3.4

A

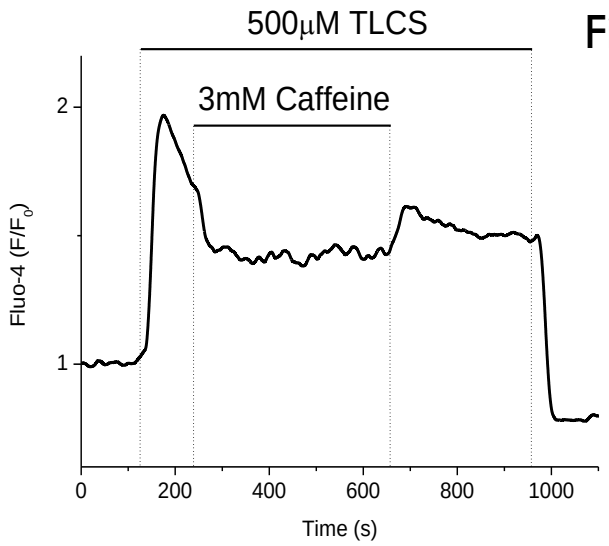

B

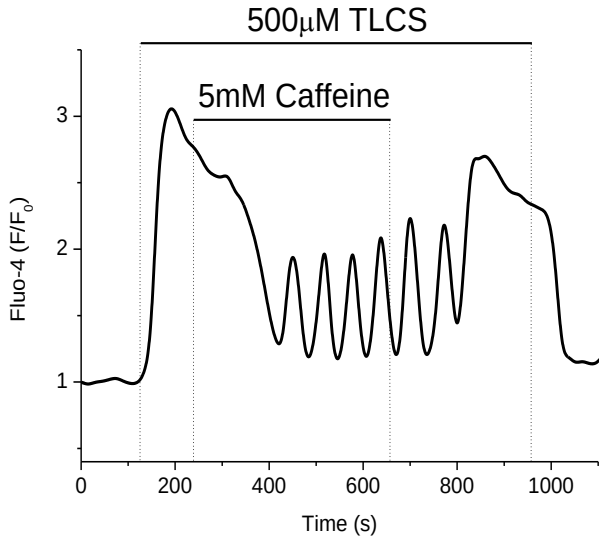

C

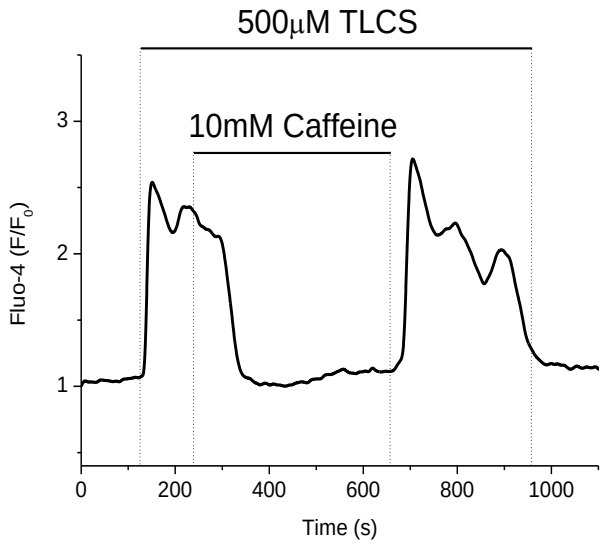

Figure 3.5

Pre-treatment with caffeine converts TLCS-induced Ca^{2+} overload to an oscillatory response. Isolated pancreatic acinar cells were exposed to 10 mM caffeine before application of TLCS. The Ca^{2+} plateau was converted to an oscillatory response, which reverted to a plateau after removal of caffeine. Data has been normalised to the initial fluorescence expressed as F/F_0.

Figure 3.5

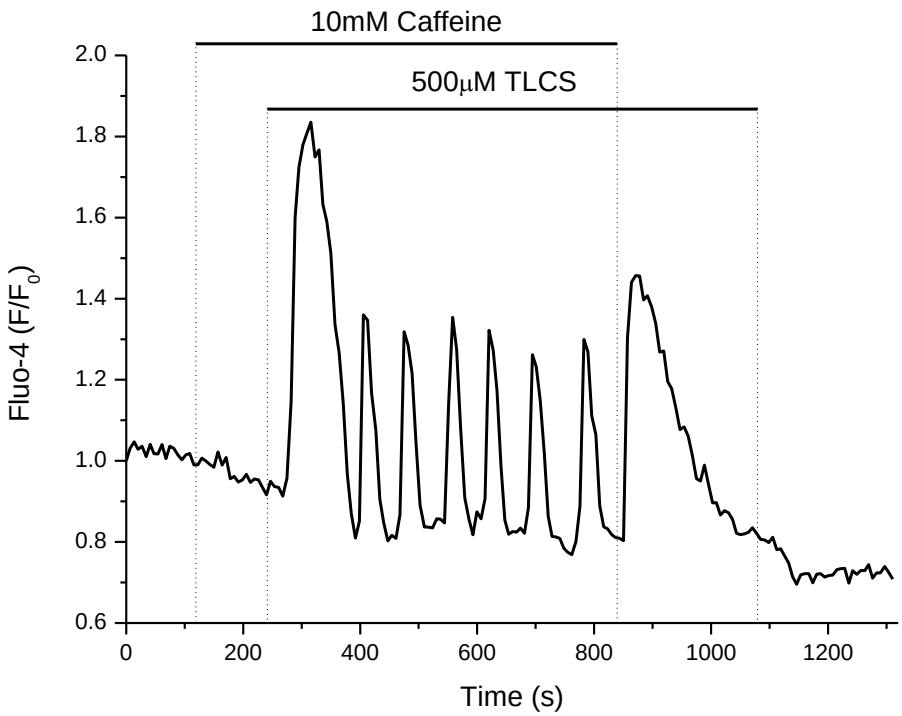
10mM Caffeine
500μM TLCS
Fluo-4 (F/F0)
2.0
1.8
1.6
1.4
1.2
1.0
0.8
0.6
0
200
400
600
800
1000
1200
Time (s)

Figure 3.6

Caffeine inhibits TLCS-induced Ca^{2+} oscillations. (A) Cytosolic Ca^{2+} signals from pancreatic acinar cells showing that 10 mM caffeine blocks Ca^{2+} oscillations induced by 200 μM TLCS in a reversible manner. Each line represents a single cell. Data has been normalised to the initial fluorescence expressed as F/F_0.

Figure 3.6

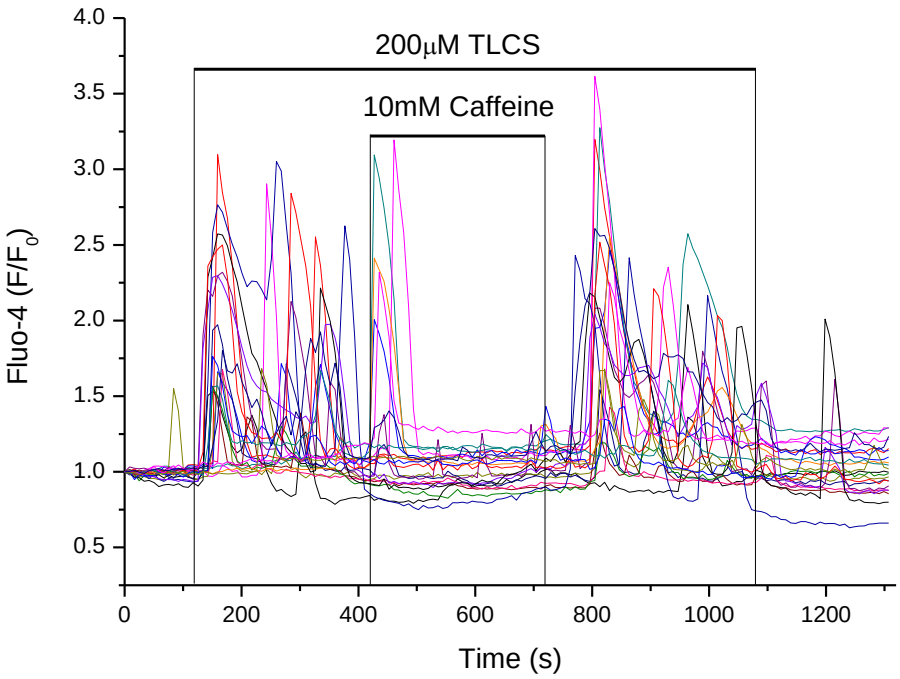
200μM TLCS
10mM Caffeine
Fluo-4 (F/F0)
Time (s)
4.0
3.5
3.0
2.5
2.0
1.5
1.0
0.5
0
200
400
600
800
1000
1200

Figure 3.7

Caffeine inhibits the store-operated Ca^{2+} plateau induced by CCK but not thapsigargin, and increases the plateau in the presence of both CCK and thapsigargin. Ca^{2+} traces were obtained by confocal microscopy of Fluo-4-loaded isolated pancreatic acinar cells. **(A)** The Ca^{2+} store was depleted by constant stimulation with CCK to ensure maintained IP_3R channel opening with zero external Ca^{2+}. After Ca^{2+} was added to the external solution a sustained Ca^{2+} plateau was induced which was sensitive to caffeine treatment (n= 19). **(B)** Counterintuitively, caffeine significantly increased the Ca^{2+} plateau in the simultaneous presence of thapsigargin and CCK (n=32). **(C)** Caffeine inhibits the cytosolic Ca^{2+} plateau induced by CCK but not thapsigargin (Tg), Traces shown are averages of at least three individual experiments and error bars indicate SEM. Data has been normalised to the initial fluorescence expressed as F/F_0 and * indicates $p < 0.05$.

Figure 3.7

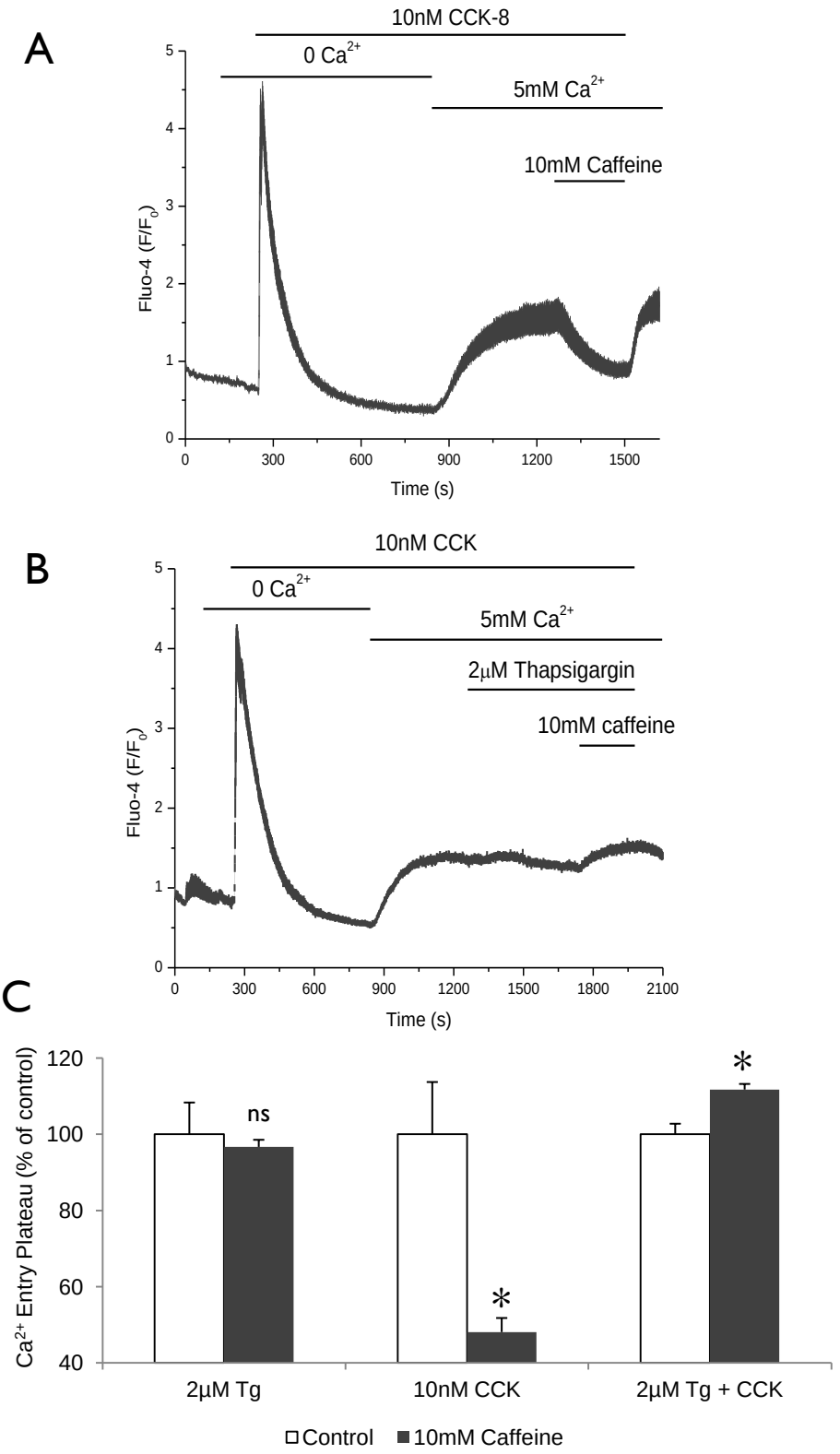
A
10nM CCK-8
0 Ca2+
5mM Ca2+
10mM Caffeine
Fluo-4 (F/F0)
Time (s)
B
10nM CCK
0 Ca2+
5mM Ca2+
2μM Thapsigargin
10mM caffeine
Fluo-4 (F/F0)
Time (s)
C
Ca2+ Entry Plateau (% of control)
ns
*
*
2μM Tg
10nM CCK
2μM Tg + CCK
Control
10mM Caffeine

Figure 3.8

Store-operated Ca^{2+} entry is faster when the store is depleted by CCK hyperstimulation, than when the store is depleted by SERCA inhibition. (A) Average Ca^{2+} traces showing only the influx segment of the traces from figure 3.4 when 5 mM extracellular Ca^{2+} was added after stimulation with either CCK (black) or thapsigargin (red) in 100 μM EGTA for 10 minutes. Traces shown are averages of at least three individual experiments and data has been normalised to the fluorescence preceding the reintroduction of Ca^{2+} expressed as F/F_{800}. **(B)** Quantification of the rate of store-operated Ca^{2+} influx with addition of 5 mM Ca^{2+} after stimulation for 10 minutes with different agonists in zero Ca^{2+}. Error bars indicate SEM and * indicates $p < 0.05$.

Figure 3.8

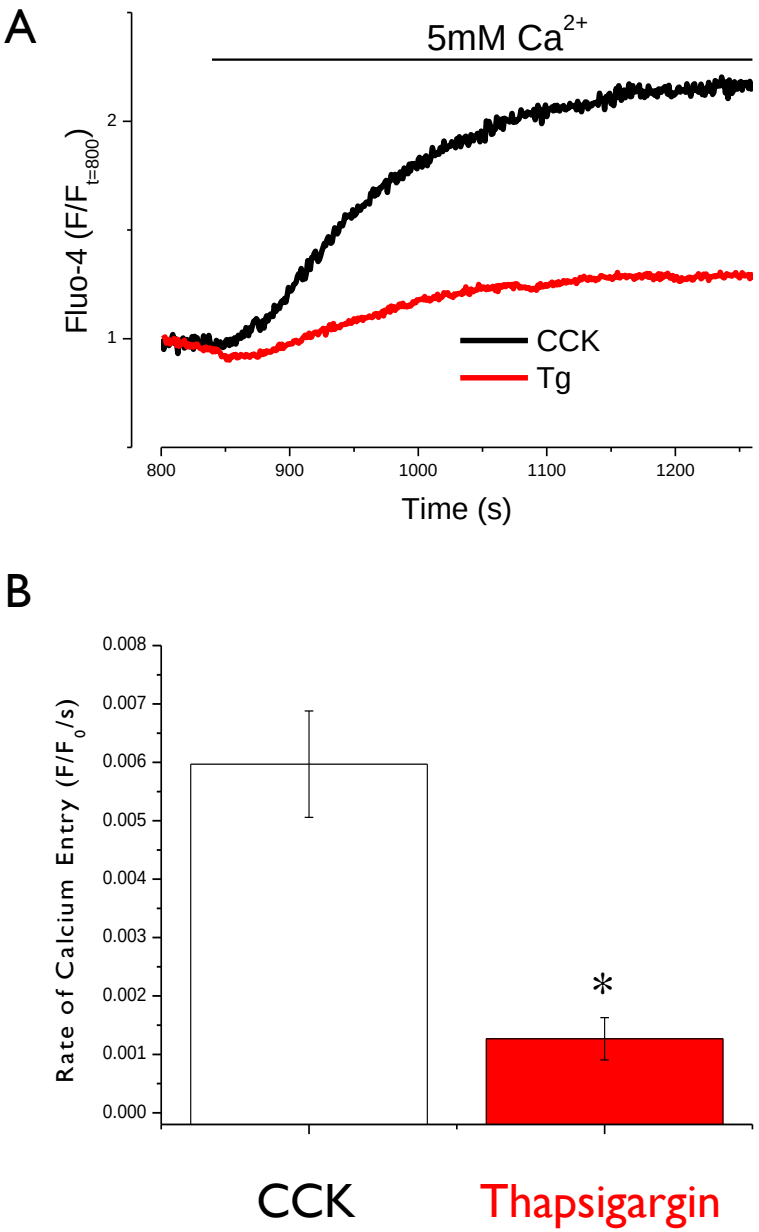
A
5mM Ca2+
Fluo-4 (F/Ft=800)
2
1
CCK
Tg
800
900
1000
1100
1200
Time (s)
B
Rate of Calcium Entry (F/F0/s)
0.008
0.007
0.006
0.005
0.004
0.003
0.002
0.001
0.000
*
CCK
Thapsigargin

Figure 3.9

Investigation of Ca^{2+} store depletion with the bile acid TLCS. **(A)** Average Ca^{2+} trace showing the effect of TLCS hyperstimulation in the presence of zero external Ca^{2+} and the result of the subsequent addition of 5 mM Ca^{2+}. Traces shown are mean ± SEM of at least three individual experiments and data has been normalised to the initial fluorescence expressed as F/F_0. **(B)** Individual traces from (A) showing varied responses and oscillations in the absence of Ca^{2+} and the sustained elevations in a peak plateau response after the addition of 5 mM Ca^{2+}.

Figure 3.9

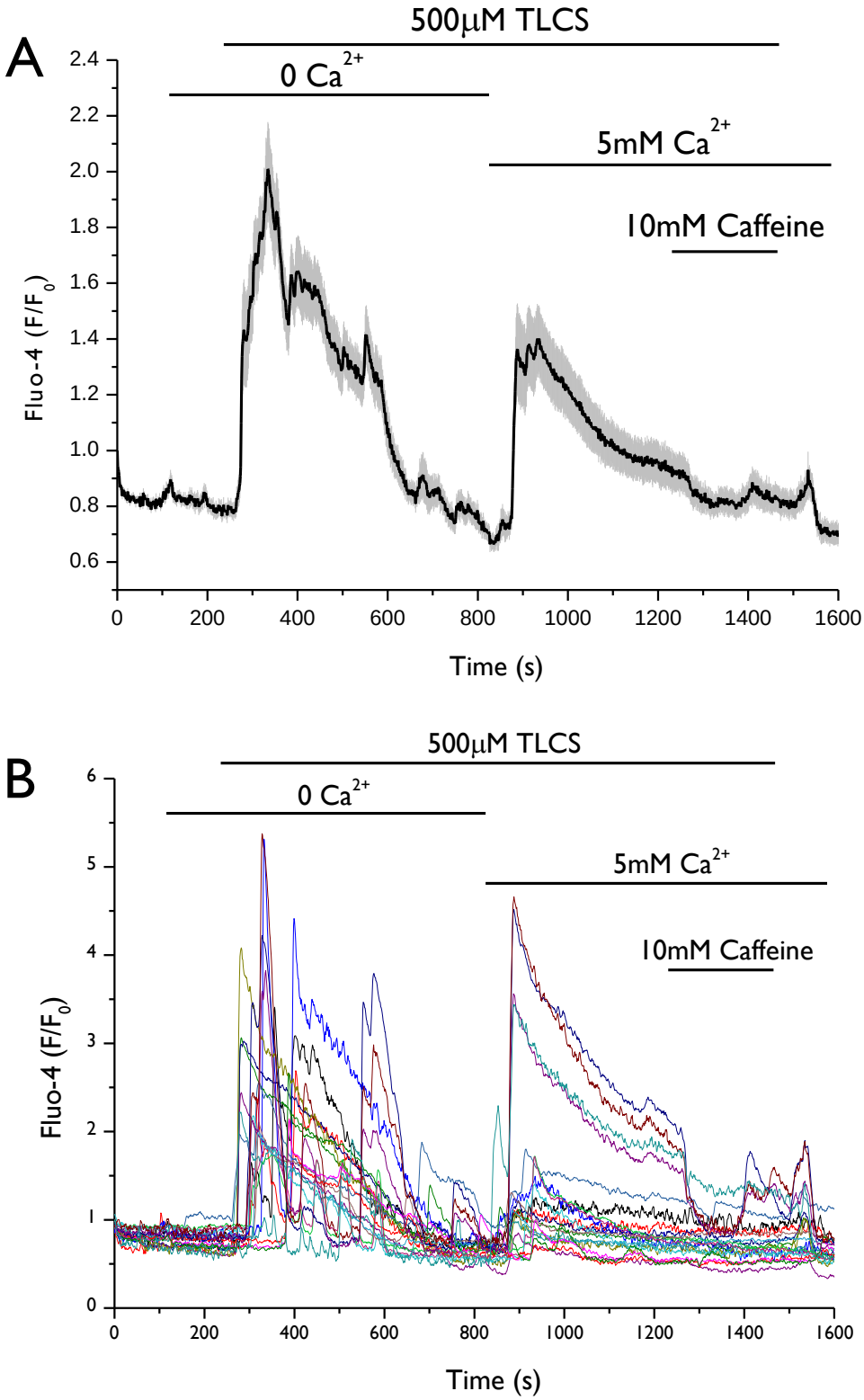
A
500μM TLCS
0 Ca2+
5mM Ca2+
10mM Caffeine
Fluo-4 (F/F0)
Time (s)
B
500μM TLCS
0 Ca2+
5mM Ca2+
10mM Caffeine
Fluo-4 (F/F0)
Time (s)

Figure 3.10

Ca^{2+} traces showing that caffeine dose-dependently inhibited ACh-elicited Ca^{2+} oscillations in a reversible manner. Fluo-4 loaded pancreatic acinar cells were stimulated with 50 nM ACh for 3 minutes to induce oscillations. **(A)** 500 μM, **(B)** 1 mM and **(C)** 2 mM caffeine were then applied along with ACh to determine inhibition of oscillations. Caffeine was then removed in order to confirm that oscillations had not stopped spontaneously. Caffeine showed increasing inhibitory activity with increased concentration. **(D)** This protocol was augmented with a further addition of 20 mM caffeine which completely blocked oscillations and also reduced the baseline fluorescence. Data has been normalised to the initial fluorescence expressed as F/F_0 and traces are representative of at least three experiments.

Figure 3.10

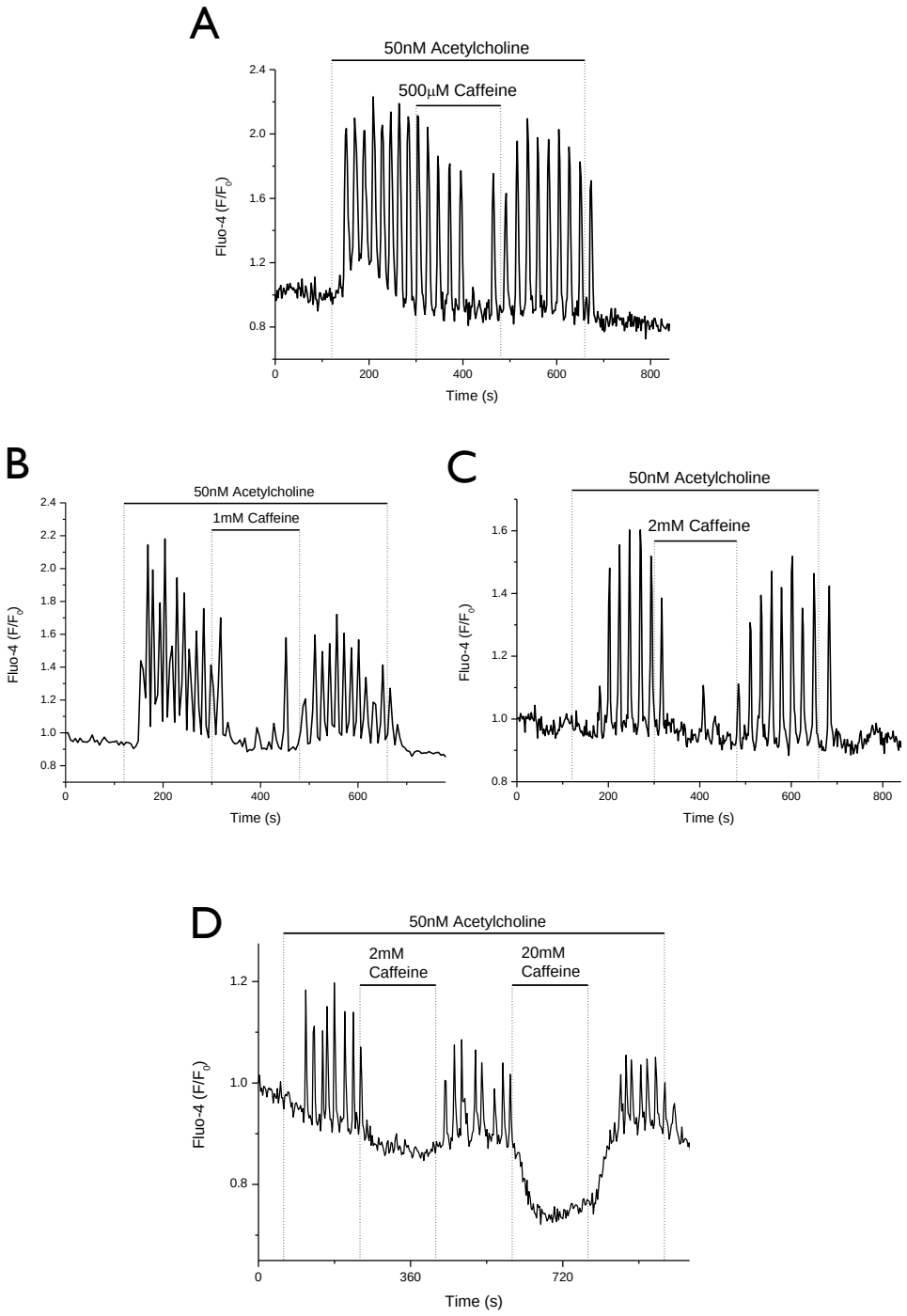
A
50nM Acetylcholine
500μM Caffeine
Fluo-4 (F/F0)
Time (s)
B
50nM Acetylcholine
1mM Caffeine
Fluo-4 (F/F0)
Time (s)
C
50nM Acetylcholine
2mM Caffeine
Fluo-4 (F/F0)
Time (s)
D
50nM Acetylcholine
2mM Caffeine
20mM Caffeine
Fluo-4 (F/F0)
Time (s)

Figure 3.11

Chemical structure of caffeine and related methylxanthines used in this study showing the positions of methylation. Compounds were classed into mono- di- and tri-methylxanthines dependent on methylation state. Positions 1,3 and 7 of the xanthine structure are shown. The names of methylxanthines respective to their different combinations of methyl groups are listed in the table.

Figure 3.11

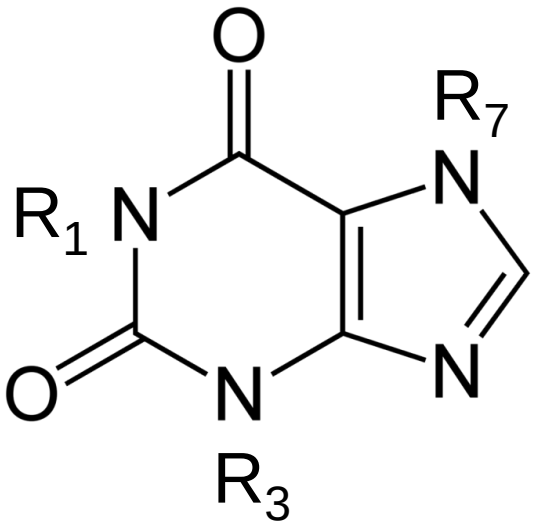

	R_1	R_3	R_7
Caffeine	$-CH_3$	$-CH_3$	$-CH_3$
Theophylline	$-CH_3$	$-CH_3$	-H
Theobromine	-H	$-CH_3$	$-CH_3$
Paraxanthine	$-CH_3$	-H	$-CH_3$
1-methylxanthine	$-CH_3$	-H	-H
7-methylxanthine	-H	-H	$-CH_3$

Figure 3.12

Di-methylxanthines theophylline, theobromine and paraxanthine inhibit ACh-induced Ca^{2+} oscillations in pancreatic acinar cells. Almost complete inhibition of oscillations was offered by 500 μM paraxanthine and theophylline (top and bottom graphs), however theobromine required a higher concentration of 2 mM to achieve inhibition (middle graph). Traces are representative of at least three repeat experiments. Data has been normalised to the initial fluorescence expressed as F/F_0.

Figure 3.12

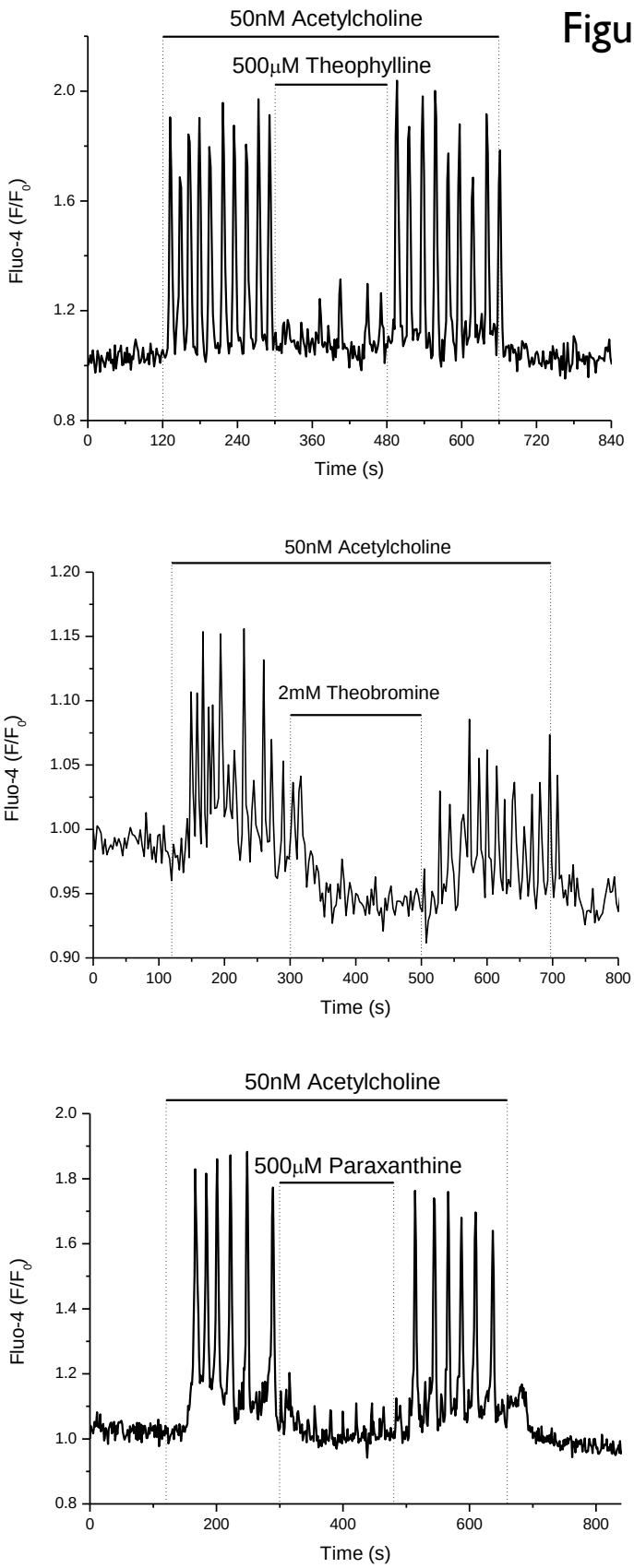
50nM Acetylcholine
500μM Theophylline
Fluo-4 (F/F0)
Time (s)
50nM Acetylcholine
2mM Theobromine
Fluo-4 (F/F0)
Time (s)
50nM Acetylcholine
500μM Paraxanthine
Fluo-4 (F/F0)
Time (s)

Figure 3.13

1-methylxanthine shows poor inhibition of ACh-induced Ca^{2+} oscillations in pancreatic acinar cells at 2 mM, with xanthine offering no inhibition at these concentrations. Ca^{2+} oscillations can be seen to continue in the presence of 2 mM 1-methylxanthine, with only minor effects on the amplitude of some of the spikes (top graph). There was no obvious effect of xanthine on Ca^{2+} oscillations (bottom graph). Traces are representative of at least three repeat experiments. Data has been normalised to the initial fluorescence expressed as F/F_0.

Figure 3.13

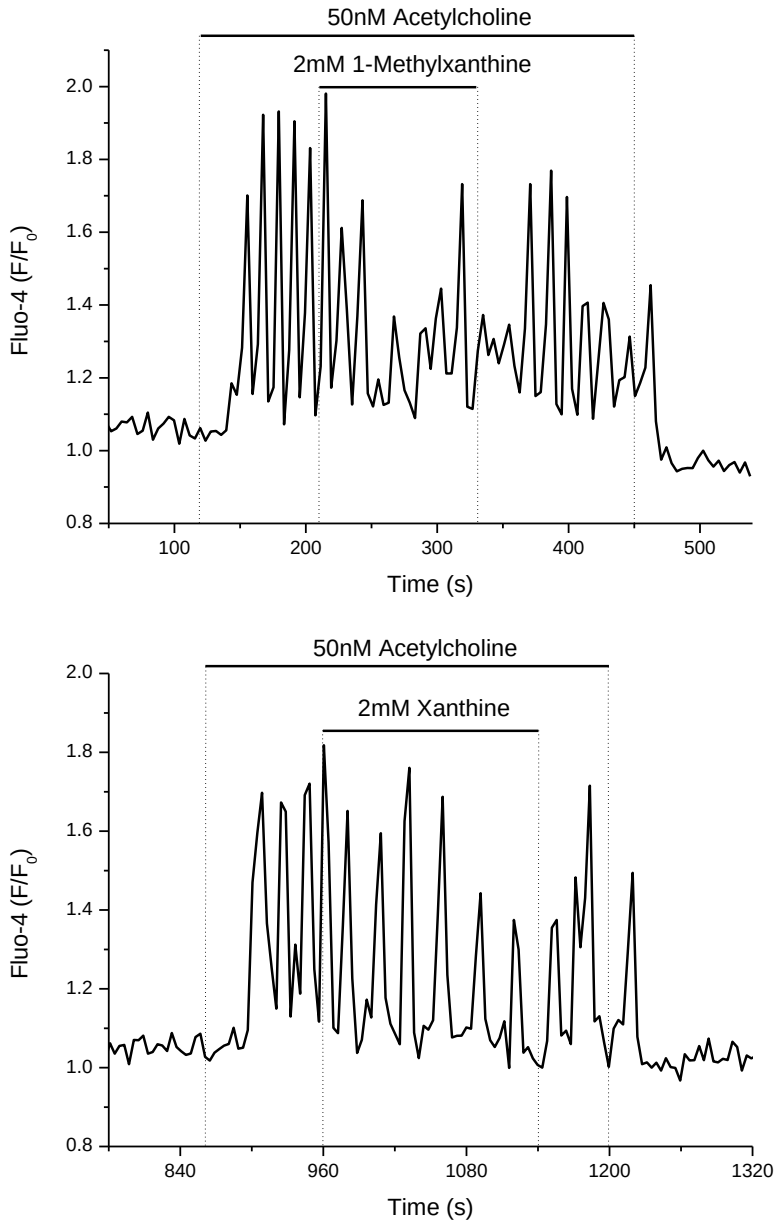
50nM Acetylcholine
2mM 1-Methylxanthine
Fluo-4 (F/F0)
2.0
1.8
1.6
1.4
1.2
1.0
0.8
100
200
300
400
500
Time (s)
50nM Acetylcholine
2mM Xanthine
Fluo-4 (F/F0)
2.0
1.8
1.6
1.4
1.2
1.0
0.8
840
960
1080
1200
1320
Time (s)

Figure 3.14

Structure activity relationships of methylxanthines on ACh-induced Ca^{2+} oscillations in pancreatic acinar cells. Quantification of cytosolic ACh-induced Ca^{2+} oscillations from pancreatic acinar cells in the presence of a range of xanthines was performed blind by an independent scientist as described in the methods section of this paper. Dose-dependent inhibition by a range of methylxanthines can be seen, with monomethylxanthines and theobromine showing the least activity. At 0.5 mM, dimethylxanthines show significantly more inhibition of ACh-induced Ca^{2+} oscillations than caffeine (* indicates $p < 0.05$). Paraxanthine shows significantly more inhibition than theobromine and theophylline. († indicates $p < 0.05$).

Figure 3.14

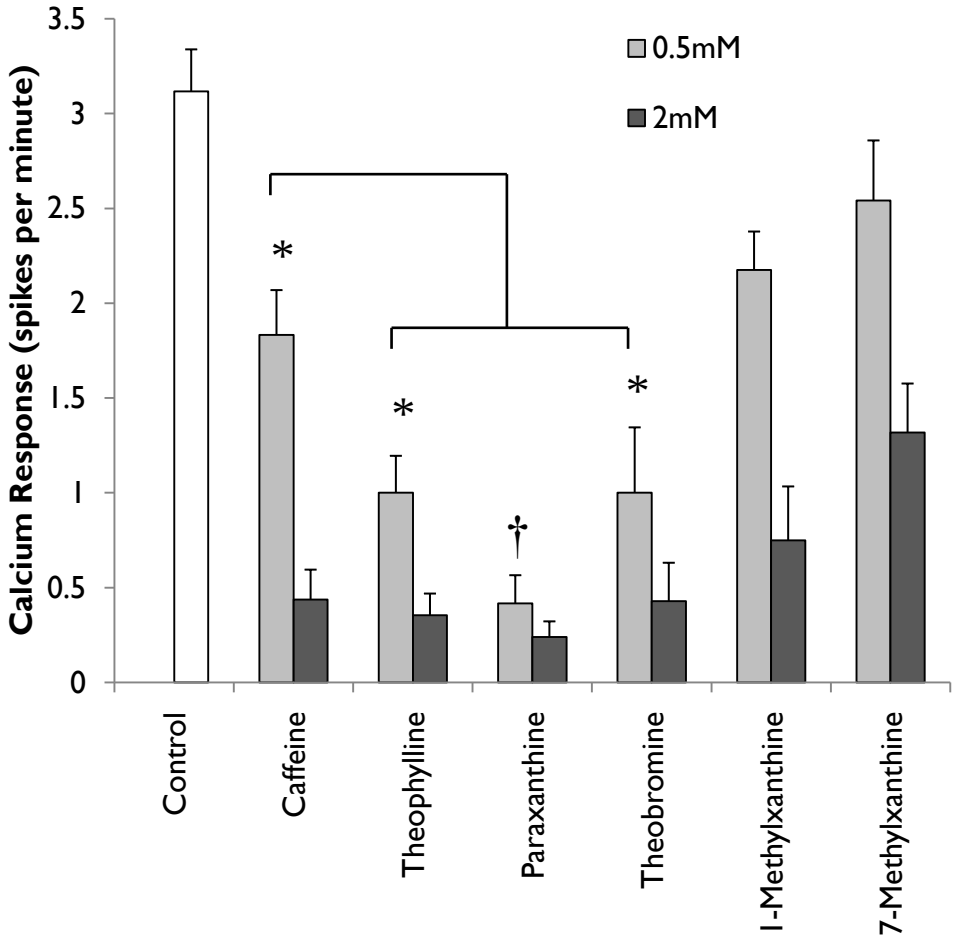
Calcium Response (spikes per minute)
3.5
3
2.5
2
1.5
1
0.5
0
0.5mM
2mM
*
*
*
†
Control
Caffeine
Theophylline
Paraxanthine
Theobromine
1-Methylxanthine
7-Methylxanthine

Figure 3.15

Methylxanthines show dose-dependent PDE inhibition in a similar profile to their inhibition of ACh-induced Ca^{2+} oscillations. This assay used a PDE assay kit to test for PDE inhibition. Methylxanthines showed significant dose-dependent inhibition with theophylline showing the greatest inhibition; similar to the IBMX positive control. († indicates $p > 0.05$ compared to IBMX). Monomethylxanthines showed the least inhibition, and no significant inhibition was detected with 500 μM 7-methylxanthine (* indicates $p < 0.05$).

Figure 3.15

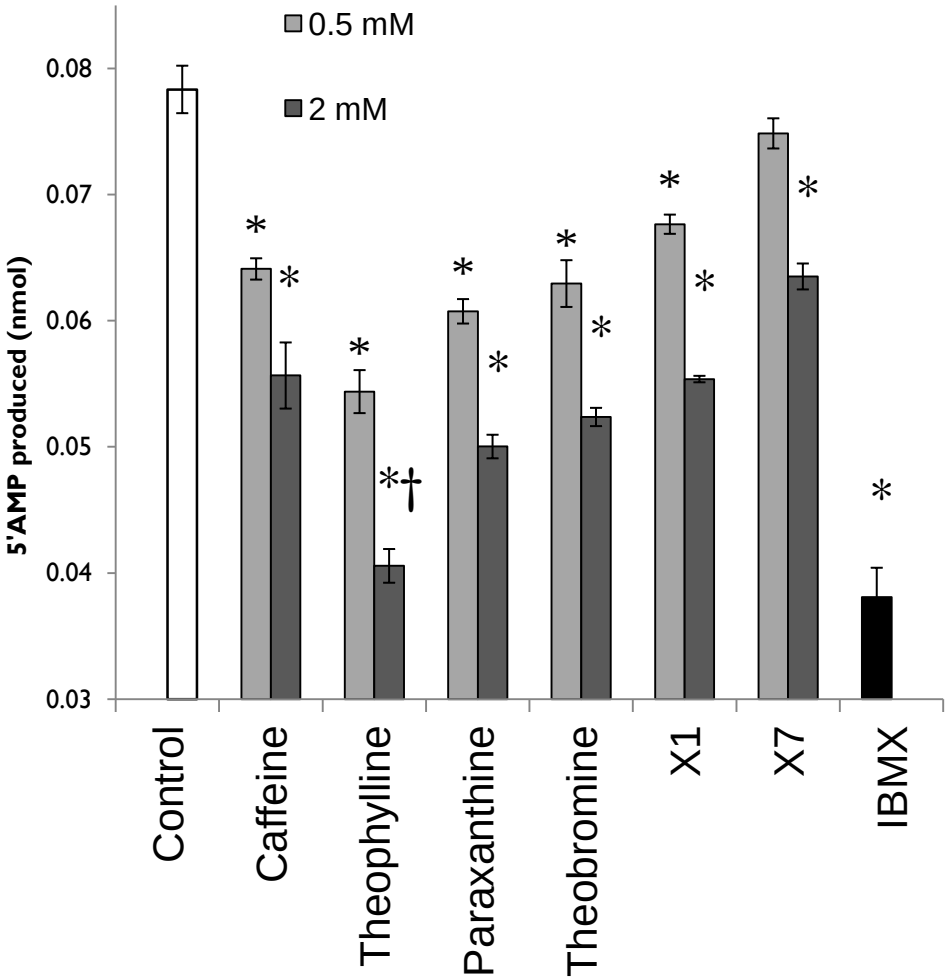
0.5 mM
2 mM
5'AMP produced (nmol)
0.08
0.07
0.06
0.05
0.04
0.03
Control
Caffeine
Theophylline
Paraxanthine
Theobromine
X1
X7
IBMX

Figure 3.16

Ca^{2+} traces showing that xanthine-based PDEIs reversibly block ACh-induced Ca^{2+} oscillations in pancreatic acinar cells. (A, B) The xanthine-based non-specific PDE inhibitors pentoxifylline and IBMX showed reversible inhibition of ACh-induced oscillations. Data has been normalised to the initial fluorescence expressed as F/F_0.

Figure 3.16

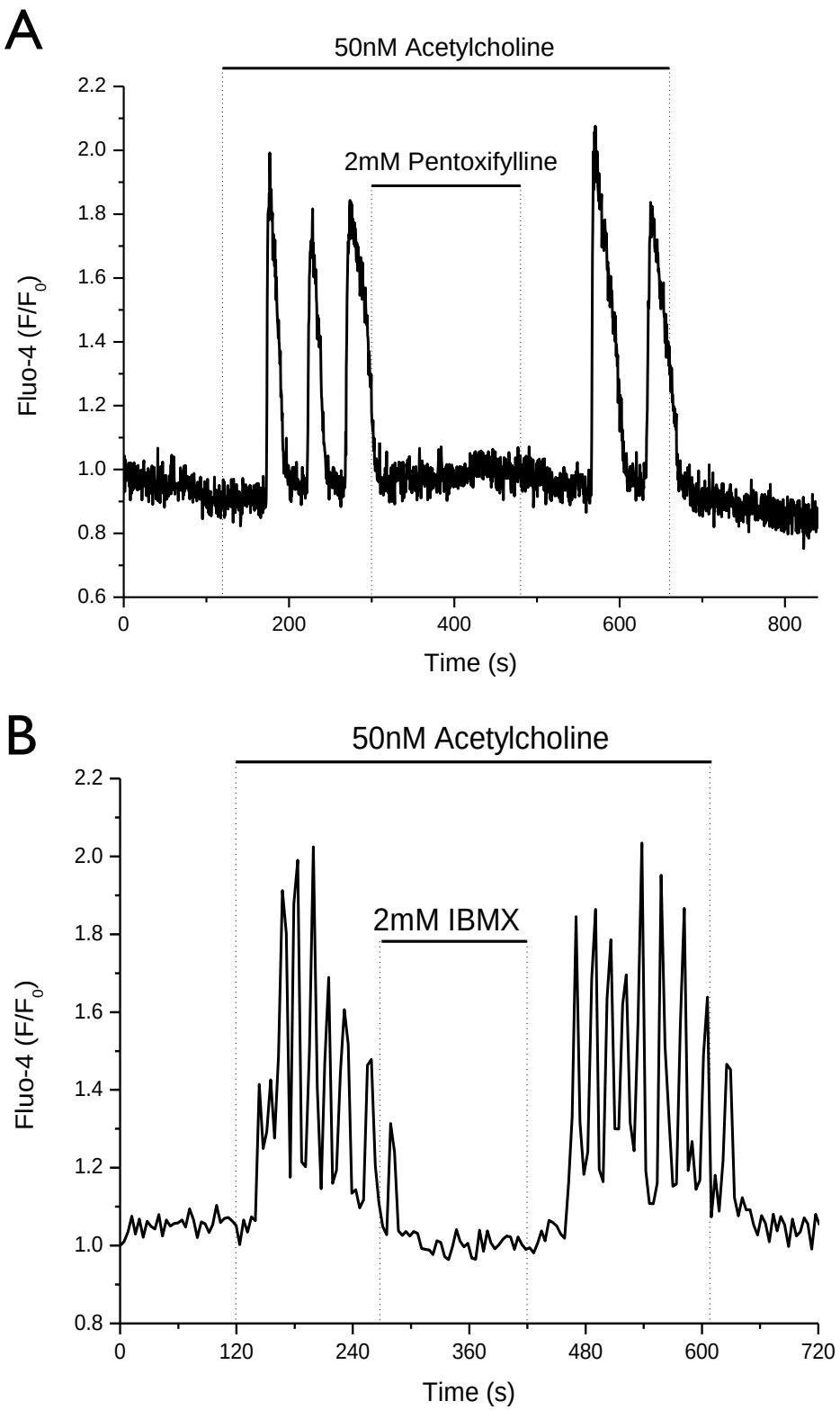
A
50nM Acetylcholine
2mM Pentoxifylline
Fluo-4 (F/F0)
2.2
2.0
1.8
1.6
1.4
1.2
1.0
0.8
0.6
0
200
400
600
800
Time (s)
B
50nM Acetylcholine
2mM IBMX
Fluo-4 (F/F0)
2.2
2.0
1.8
1.6
1.4
1.2
1.0
0.8
0
120
240
360
480
600
720
Time (s)

Figure 3.17

Non-xanthine based PDE4I, rolipram, dose-dependently inhibited ACh-induced Ca^{2+} oscillations in pancreatic acinar cells. Supramaximal doses of the non-xanthine PDE4 inhibitor rolipram showed inhibition of ACh-induced Ca^{2+} oscillations, in a reversible manner. **(A)** 100 μM rolipram showed slight inhibition of frequency and amplitude of Ca^{2+} oscillations. **(B)** 200 μM rolipram almost completely blocked ACh-induced Ca^{2+} oscillations. Data has been normalised to the initial fluorescence expressed as F/F_0.

Figure 3.17

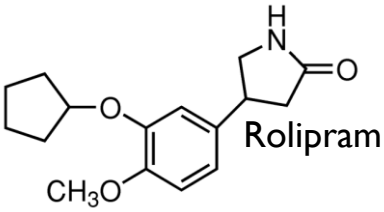

Rolipram

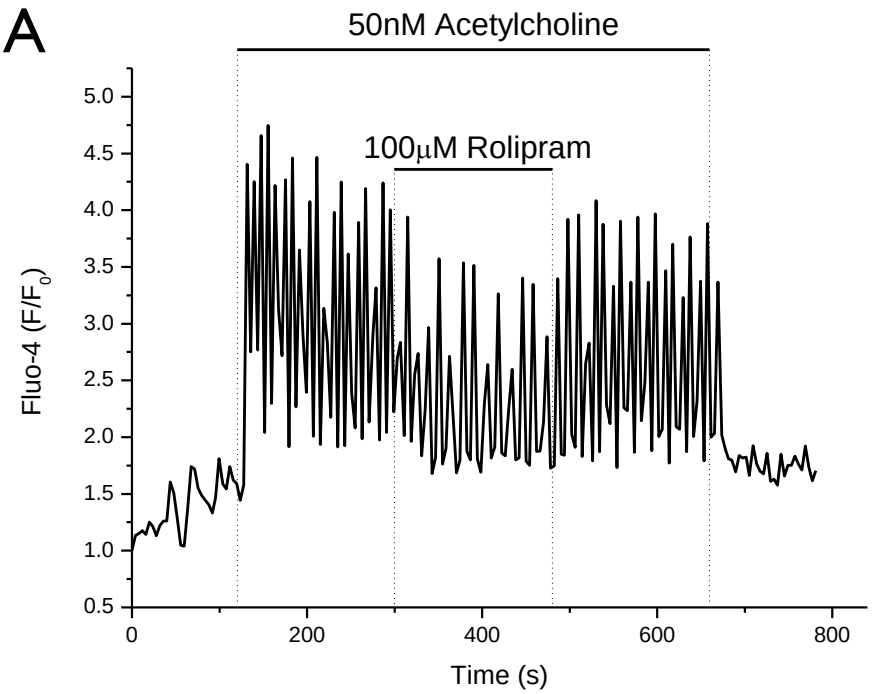

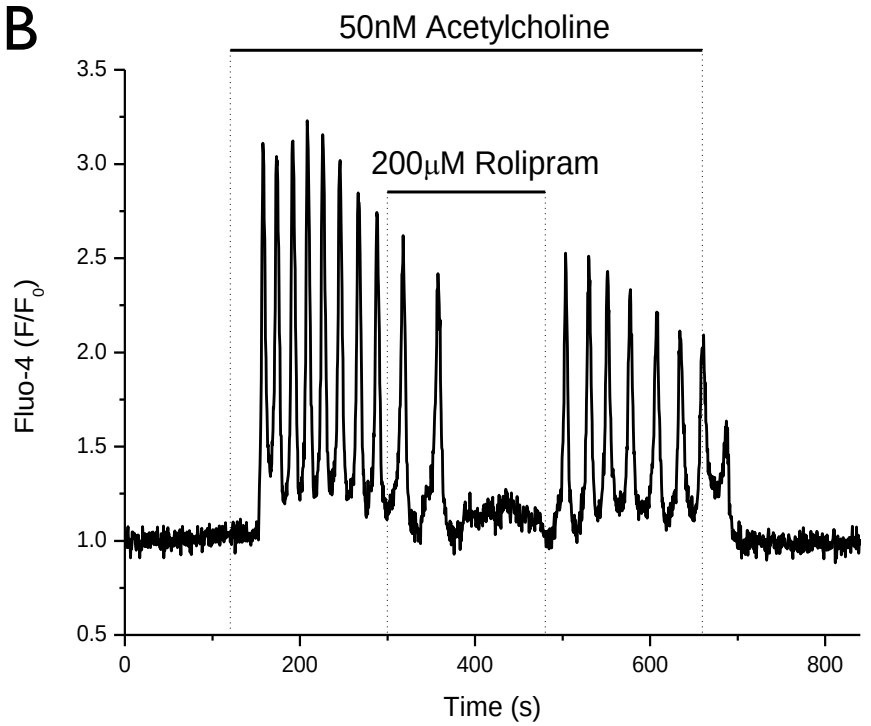

Figure 3.18

Simulation of PDE inhibition with non-hydrolysable analogues of cAMP and cGMP applied simultaneously had no effect on sustained Ca^{2+} elevation induced by 10 nM CCK. cAMP and cGMP analogues applied simultaneously to the CCK-induced Ca^{2+} plateau had no effect, indicating that inhibition of sustained Ca^{2+} rises by caffeine is not via PDE inhibition. 10 mM caffeine was used as a control to show that the Ca^{2+} plateau could be successfully inhibited and the cell was viable. Data has been normalised to the initial fluorescence expressed as F/F_0.

Figure 3.18

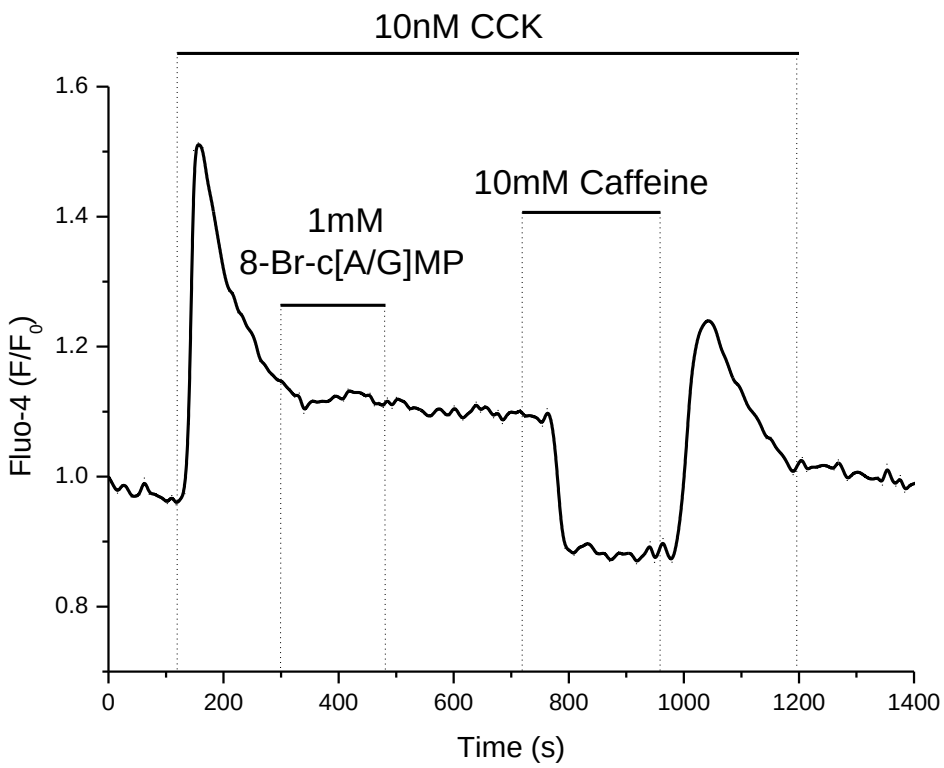
10nM CCK
10mM Caffeine
1mM
8-Br-c[A/G]MP
Fluo-4 (F/F0)
1.6
1.4
1.2
1.0
0.8
0
200
400
600
800
1000
1200
1400
Time (s)

Figure 3.19

Cytosolic Ca^{2+} signals induced by uncaging of a membrane permeable IP_3 analogue, ci-IP_3 /PM. Caged, membrane permeable IP_3 was used to elicit cytosolic Ca^{2+} elevations. UV radiation (1% 351 nm every 3.9 seconds from ~27 seconds) of ci-IP_3 /PM and Fluo-4 - loaded isolated pancreatic acinar cells induced an increase in $[Ca^{2+}]c$. **(A)** A range of Ca^{2+} responses could be seen, from oscillatory to sustained and there was significant variation between cells. The traces each represent one cell and these data are compiled from experiments from three animals. **(B)** Mean ± SEM from the data in (A) showing the average increase in Ca^{2+} responses. These data have been normalised to the initial fluorescence expressed as F/F_0.

Figure 3.19

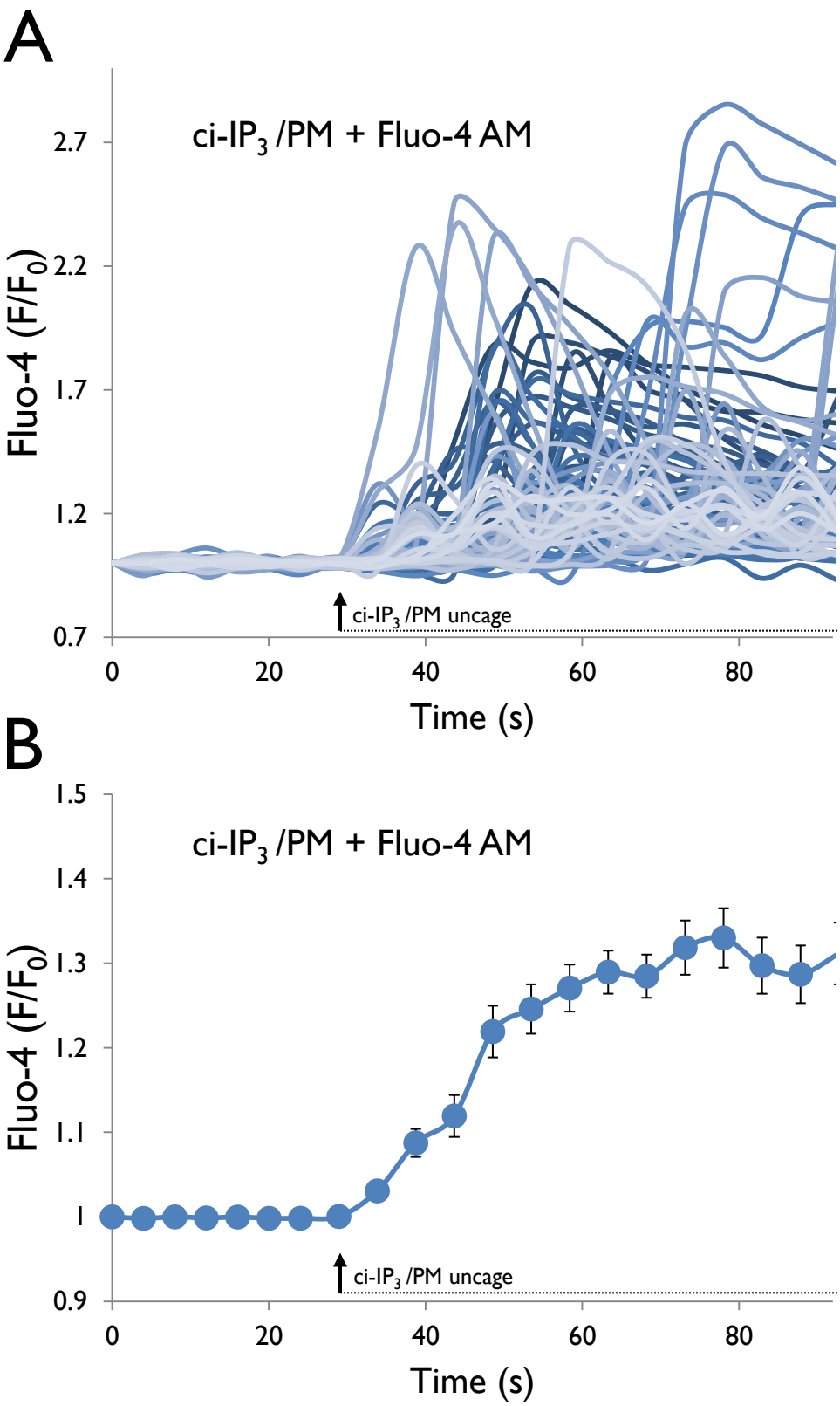
A
ci-IP3 /PM + Fluo-4 AM
Fluo-4 (F/F0)
2.7
2.2
1.7
1.2
0.7
ci-IP3 /PM uncage
0
20
40
60
80
Time (s)
B
ci-IP3 /PM + Fluo-4 AM
Fluo-4 (F/F0)
1.5
1.4
1.3
1.2
1.1
1
0.9
ci-IP3 /PM uncage
0
20
40
60
80
Time (s)

Figure 3.20

Caffeine, theophylline and paraxanthine all significantly inhibited Ca^{2+} signals induced by uncaging of the membrane permeable IP_3 analogue, ci-IP_3 /PM but no significant difference between these compounds could be detected. (A,B) Caged, membrane permeable IP_3 was used to determine the inhibition of IP_3-mediated Ca^{2+} signals. UV radiation (351 nm) of ci-IP_3 /PM and Fluo-4 -loaded isolated pancreatic acinar cells induced an increase in $[Ca^{2+}]c$ which was significantly inhibited by caffeine in a dose-dependent manner. **(C)** Quantification of $[Ca^{2+}]c$ inhibition by area under the curve analysis, normalised to the control response, shows significant dose-dependent inhibition by caffeine, theophylline and paraxanthine, but no significant difference between inhibition by the three methylxanthines (* indicates $p < 0.05$). Data has been normalised to the initial fluorescence expressed as F/F_0.

Figure 3.20

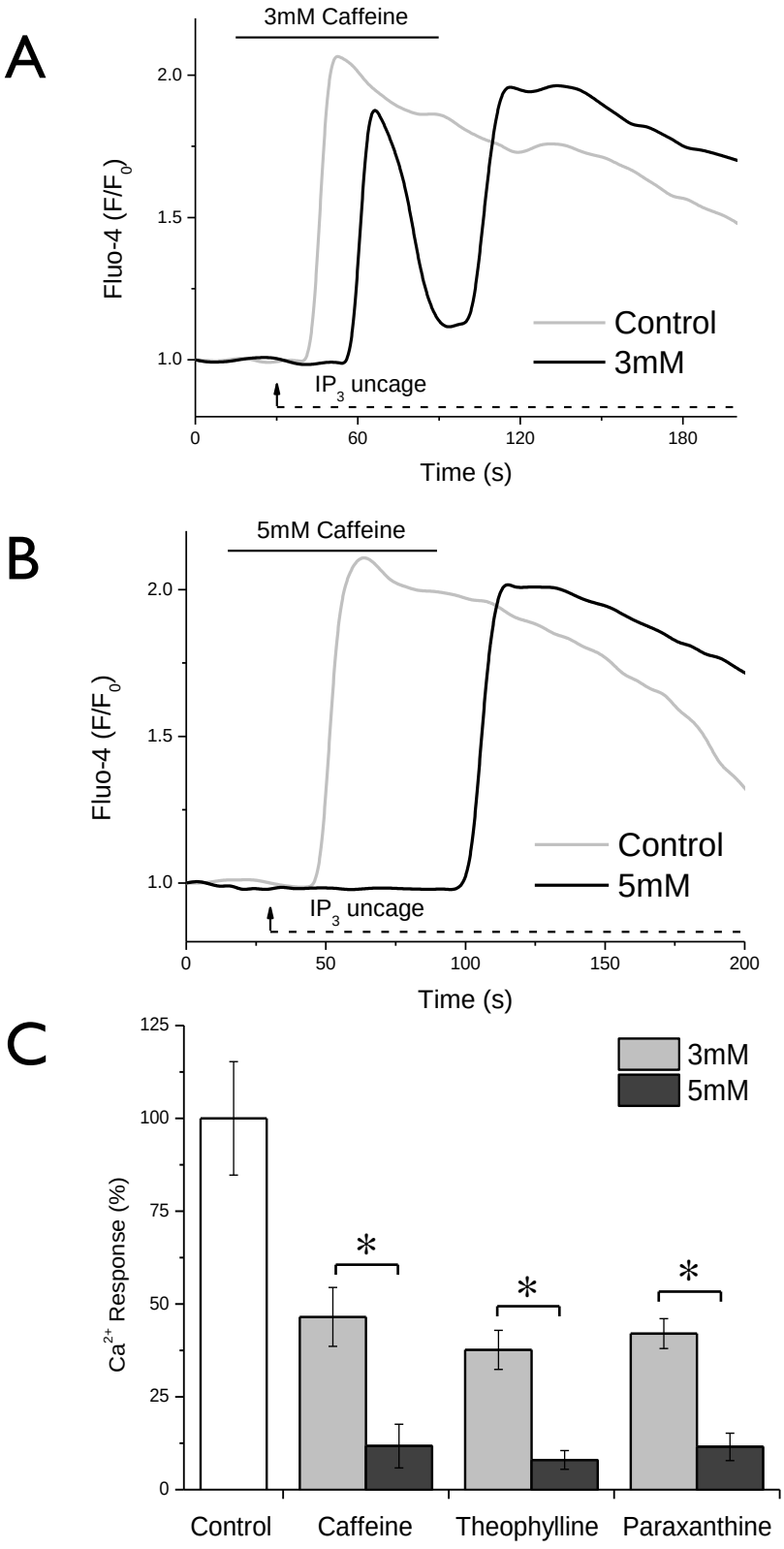
A
3mM Caffeine
Fluo-4 (F/F0)
2.0
1.5
1.0
Control
3mM
IP3 uncage
0
60
120
180
Time (s)
B
5mM Caffeine
Fluo-4 (F/F0)
2.0
1.5
1.0
Control
5mM
IP3 uncage
0
50
100
150
200
Time (s)
C
3mM
5mM
Ca2+ Response (%)
125
100
75
50
25
0
*
*
*
Control
Caffeine
Theophylline
Paraxanthine

Figure 3.21

Methylxanthines ameliorate TLCS-induced pancreatic acinar cell necrosis measured by propidium iodide fluorescence. Caffeine (A), theophylline (B) and paraxanthine (C) all show dose dependent amelioration of TLCS-induced necrosis, but no amelioration was observed at 3 mM. n = 6 repeats from 3 animals. * indicates $p < 0.05$. There is no significant difference between the xanthines; all three compounds ameliorated necrosis to the same observable extent. Data has been normalised to the maximum fluorescence and expressed as a percentage of that value.

Figure 3.21

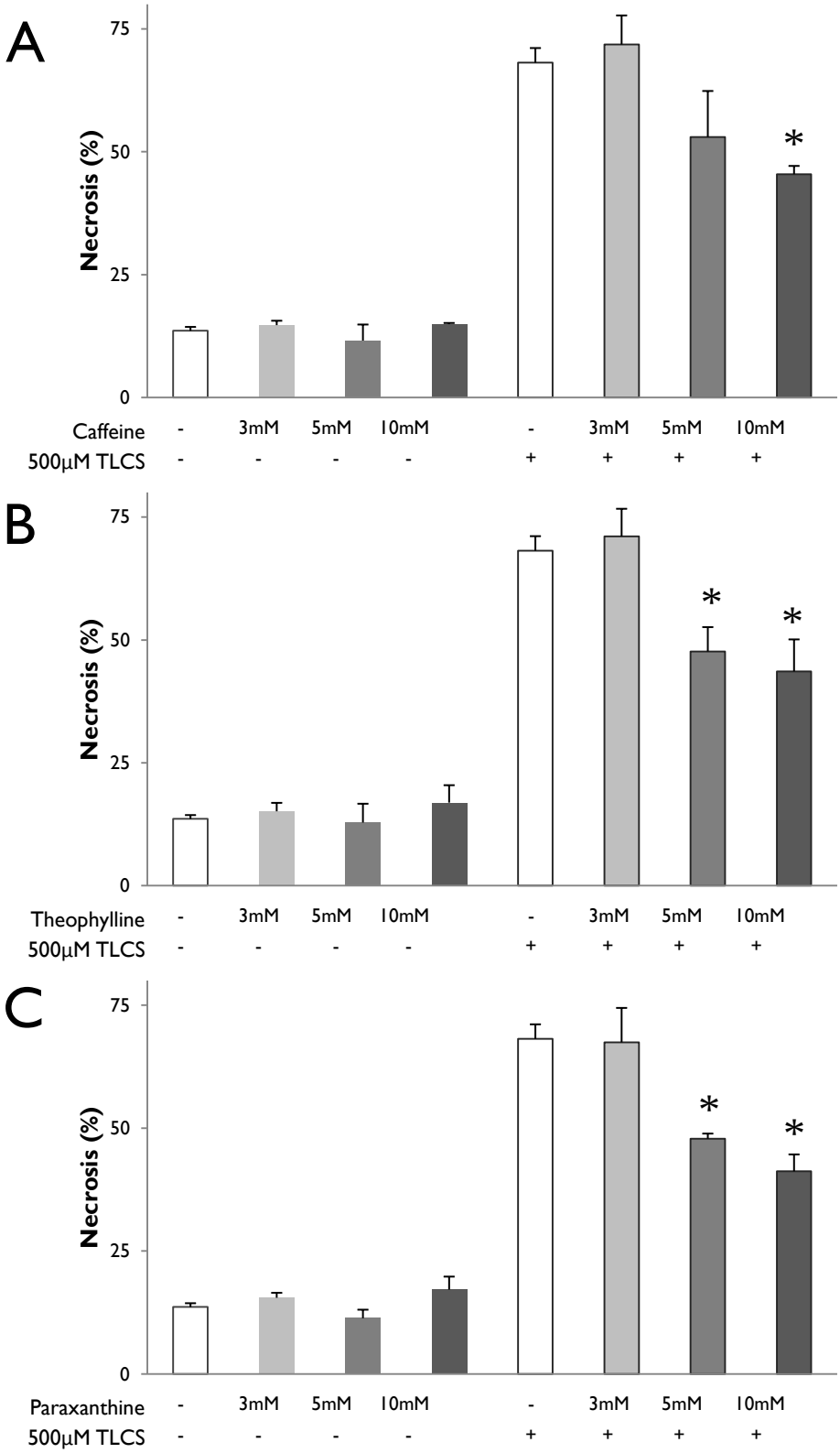
A
B
C
Necrosis (%)
75
50
25
0
Caffeine
Theophylline
Paraxanthine
500μM TLCS
-
3mM
5mM
10mM
+
*

Figure 3.22

Changes in mitochondrial redox potential and $\Delta\Psi_m$ associated with cytosolic Ca^{2+} overload are reverted after inhibition of the Ca^{2+} signal with 10 mM caffeine. (A) Hyperstimulation with 10 nM CCK reduces the $\Delta\Psi_m$ and this effect is reverted by the addition of 10 mM caffeine. After removal of the caffeine the TMRM signal drops once more, and addition of the protonophore CCCP collapses this to a minimal level. **(B)** NAD(P)H auto-fluorescence from isolated pancreatic acinar cells drops after the application of 10 nM CCK. 10 mM caffeine reverts this phenomenon. Traces are mean ± SEM from 3 experiments.

Figure 3.22

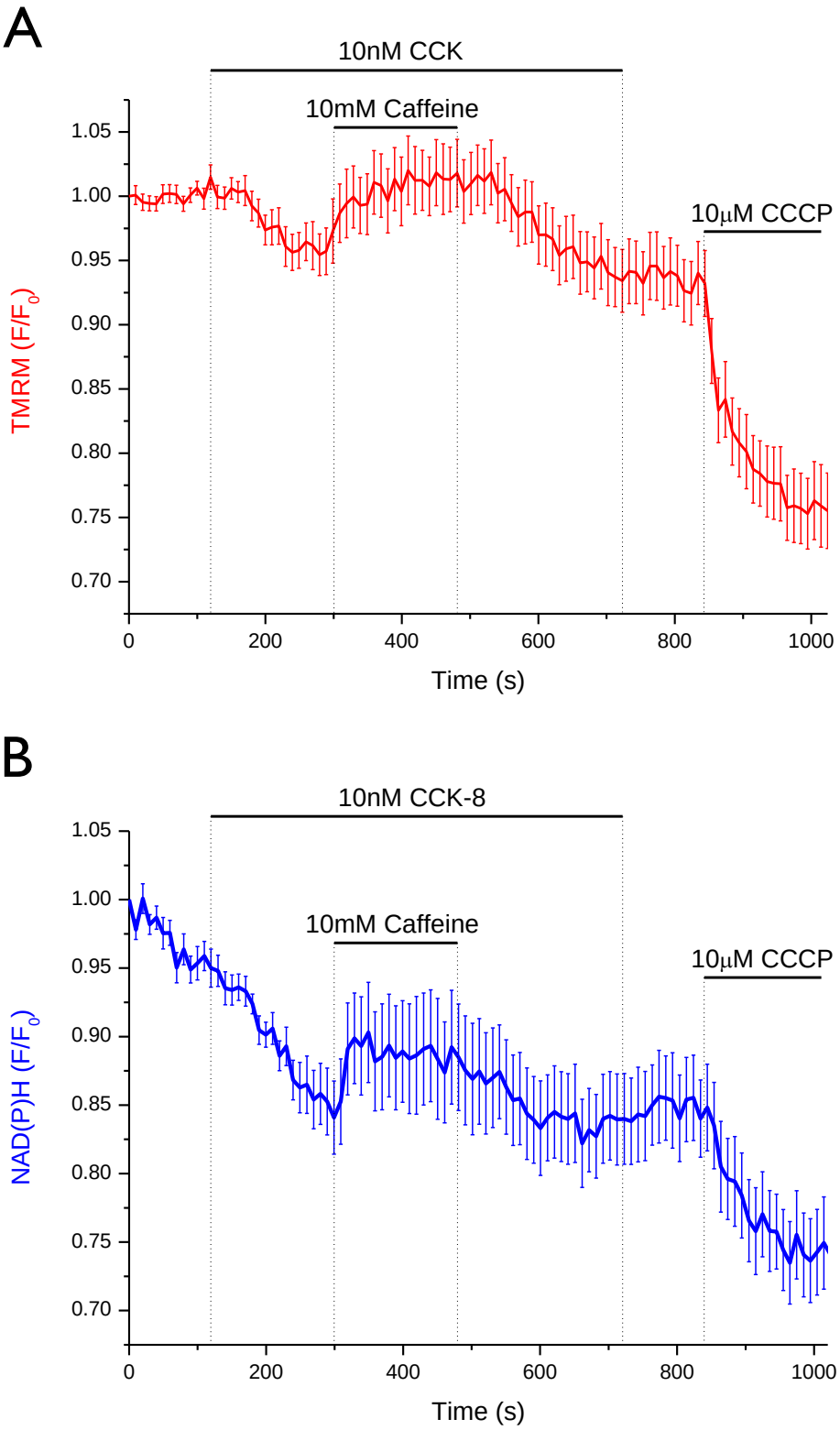
A
10nM CCK
10mM Caffeine
10μM CCCP
TMRM (F/F0)
1.05
1.00
0.95
0.90
0.85
0.80
0.75
0.70
0
200
400
600
800
1000
Time (s)
B
10nM CCK-8
10mM Caffeine
10μM CCCP
NAD(P)H (F/F0)
1.05
1.00
0.95
0.90
0.85
0.80
0.75
0.70
0
200
400
600
800
1000
Time (s)

Figure 4.1

Responses in $\Delta\Psi_M$ can be measured in a microplate format using 'dequench mode' TMRM. Low and high (normal and dequench mode) concentrations of TMRM were employed to measure $\Delta\Psi_M$ in isolated pancreatic acinar cells using a plate reader. **(A)** 50 nM TMRM loading did not enable measurement of changes in $\Delta\Psi_M$ induced by the addition of increasing concentrations of CCCP to pancreatic acinar cells. **(B)** The addition of increasing concentrations of CCCP to pancreatic acinar cells loaded with 10 μM TMRM (dequench mode) induced significant and dose-dependent changes in fluorescence. n=3 and bars indicate SEM.

Figure 4.1

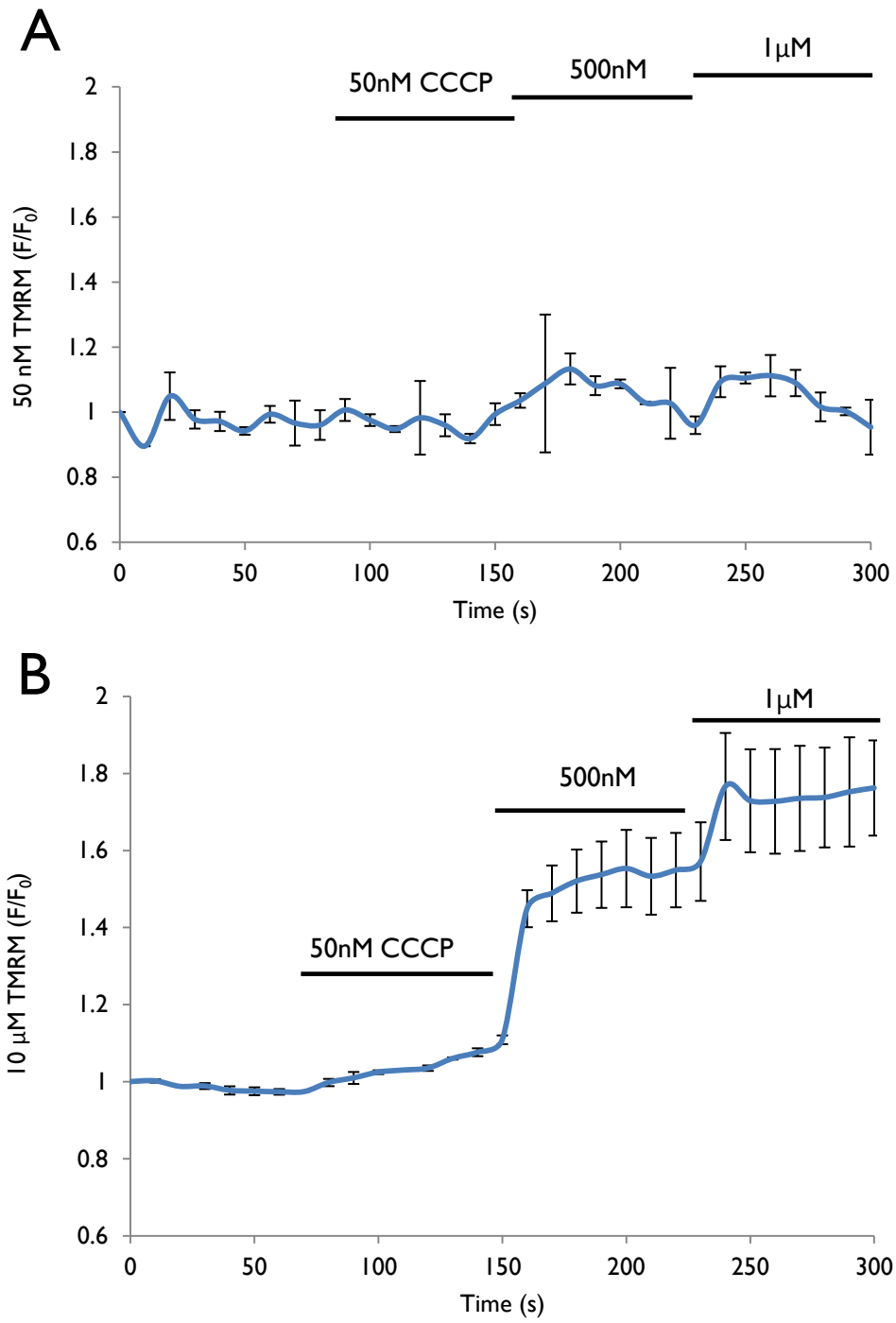
A
50nM CCCP
500nM
1μM
50 nM TMRM (F/F0)
2
1.8
1.6
1.4
1.2
1
0.8
0.6
0
50
100
150
200
250
300
Time (s)
B
50nM CCCP
500nM
1μM
10 μM TMRM (F/F0)
2
1.8
1.6
1.4
1.2
1
0.8
0.6
0
50
100
150
200
250
300
Time (s)

Figure 4.2

Changes in $\Delta\Psi_M$ were induced by hyperstimulation of pancreatic acinar cells with 500 µM TLCS and measured in a microplate format using dequench mode TMRM. (A) 500 µM TLCS caused an increase in TMRM dequench fluorescence, corresponding to a fall of $\Delta\Psi_M$. CCCP was then added as an internal control at the end of the experiment to depolarise the mitochondria. Fluorescence was therefore normalised to both the maximum and minimum values using the formula $(F - F_{max}) / (F_{max} - F_{min})$. **(B)** Zoom of the TLCS region from (A) showing the increase in fluorescence in comparison to control cells.

Figure 4.2

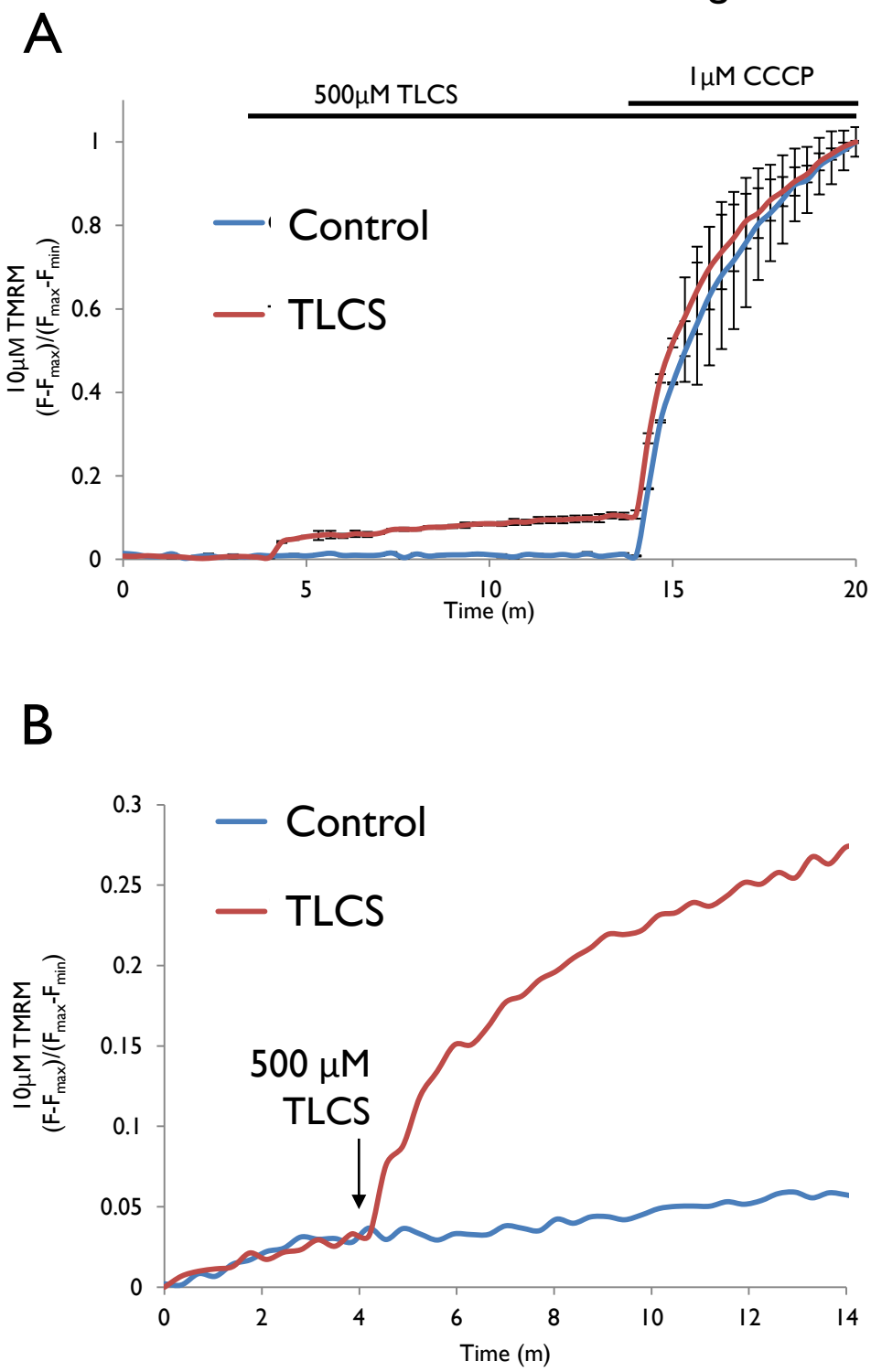
A
500μM TLCS
1μM CCCP
Control
TLCS
10μM TMRM
(F-Fmax)/(Fmax-Fmin)
Time (m)
B
Control
TLCS
500 μM
TLCS
10μM TMRM
(F-Fmax)/(Fmax-Fmin)
Time (m)

Figure 4.3

Depolarisation of $\Delta\Psi_M$ can also be determined using dequench mode TMRM-loaded human pancreatic tissue slices induced by the bile acid TLCS. Freshly isolated human pancreatic tissue slices were set in gelatine and sliced using a vibratome to 150 µm. **(A)** Transmitted light image showing the structure of the human tissue slice. **(B)** Fluorescence microplate reader data showing the change in $\Delta\Psi_M$ over time determined by dequench mode TMRM fluorescence. The injection of 500 µM TLCS showed an elevation of fluorescence corresponding to a drop in $\Delta\Psi_M$ (blue). Tissue in unstimulated conditions remained stable (red).

Figure 4.3

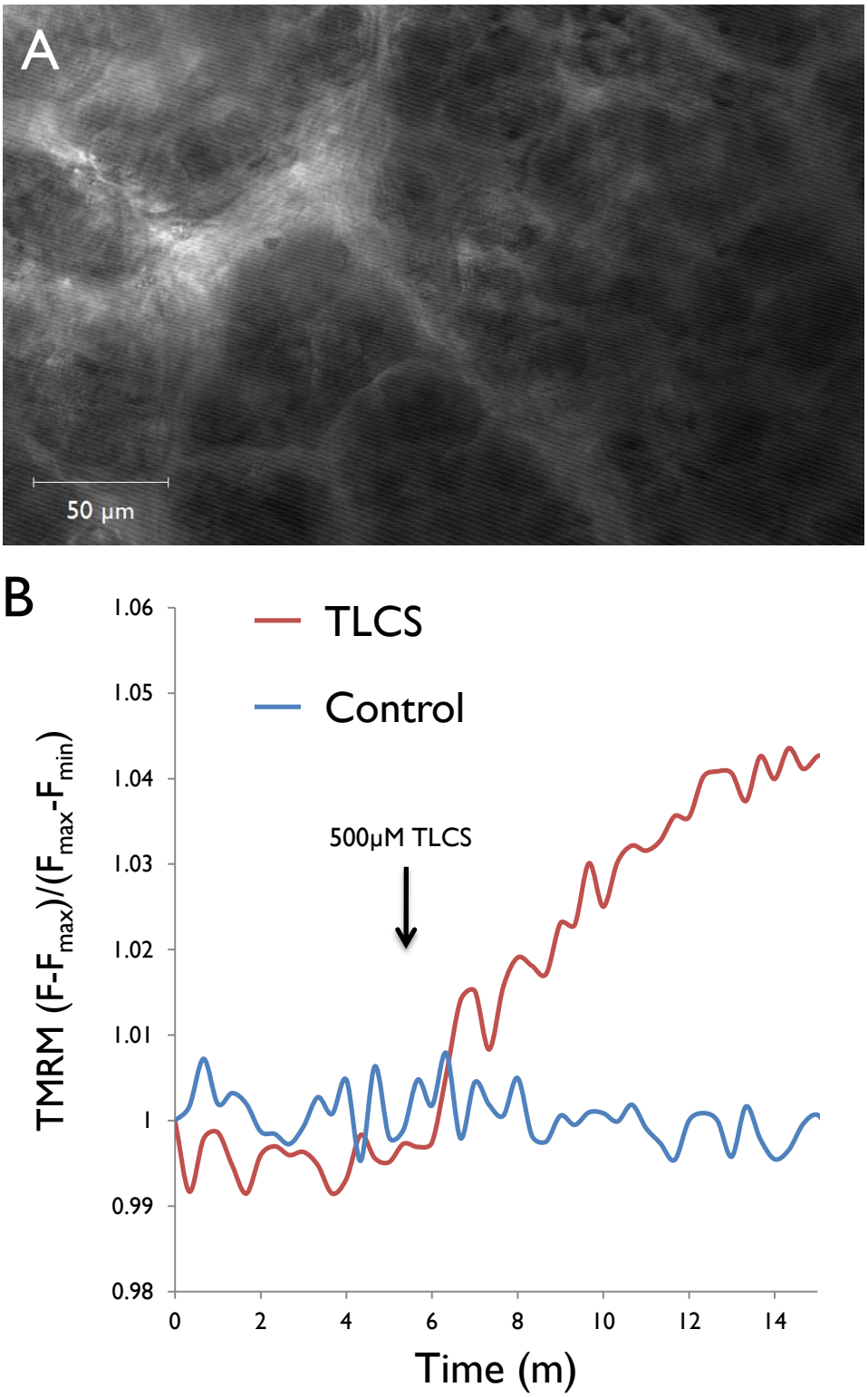
A
50 µm
B
TLCS
Control
500µM TLCS
TMRM (F-F_max)/(F_max-F_min)
1.06
1.05
1.04
1.03
1.02
1.01
1
0.99
0.98
0
2
4
6
8
10
12
14
Time (m)

Figure 4.4

Depolarisation of $\Delta\Psi_M$ induced by the bile acid TLCS is significantly attenuated by the addition of Ciclosporin (CsA), an inhibitor of CyP-D. To evaluate the effect of 50 μM CsA on the $\Delta\Psi_M$, pancreatic acinar cells were loaded with 10 μM TMRM. Traces were normalised to the minimum and maximum fluorescence using the equation $(F-F_{max})/(F_{max}-F_{min})$ as previously described. **(A)** The injection of 500 μM TLCS caused an elevation in fluorescence for both treated and non treated cells. 1 μM CCCP caused further depolarisation. **(B)** Mean ± SEM of CsA + TLCS and TLCS alone from the initial region of TLCS-induced depolarization (n=3). **(C)** Quantification of the area under the curve for the region in (B) 4-8 minutes. * indicates $p < 0.05$.

Figure 4.4

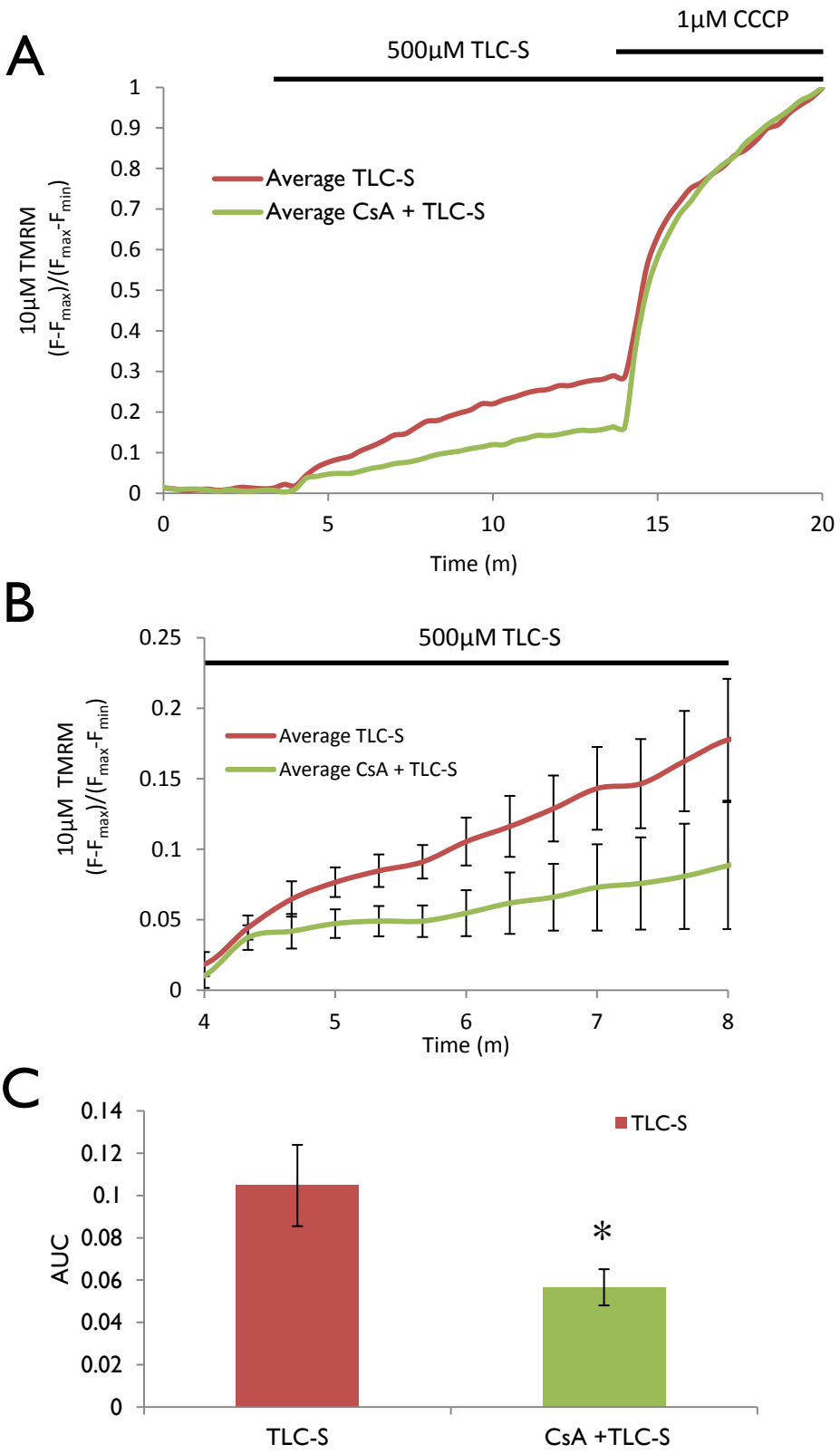
A
500µM TLC-S
1µM CCCP
Average TLC-S
Average CsA + TLC-S
10µM TMRM
(F-F_max)/(F_max-F_min)
Time (m)
B
500µM TLC-S
Average TLC-S
Average CsA + TLC-S
10µM TMRM
(F-F_max)/(F_max-F_min)
Time (m)
C
TLC-S
AUC
*
TLC-S
CsA +TLC-S

Figure 4.5

Live microplate cell death assay in multiplex format shows amelioration of CCK-induced cell death with caffeine in a dose dependent manner. Primary pancreatic acinar cells were placed in a 96 well plate in the presence of PI and in the presence or absence of a supramaximal concentration of CCK and or an incremental concentration of caffeine. CCK induced a gradual increase in cell death over a number of hours whilst control cells remained stable. **(A)** 1 mM caffeine showed no obvious amelioration of cell death. **(B, C)** 2 and 5 mM caffeine showed dose dependent inhibition of the CCK-induced necrosis. Data shown is mean ± SEM from 3 individual experiments.

Figure 4.5

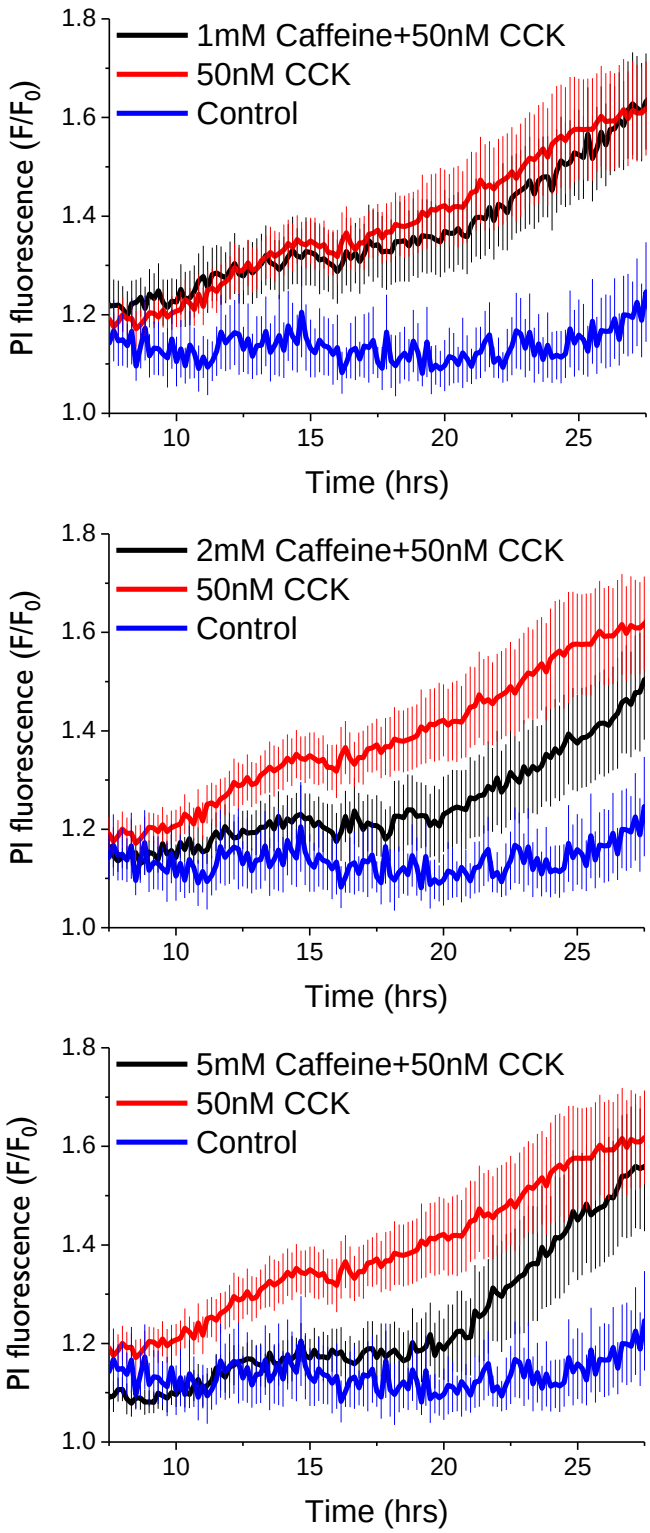
1mM Caffeine+50nM CCK
50nM CCK
Control
PI fluorescence (F/F0)
Time (hrs)
2mM Caffeine+50nM CCK
50nM CCK
Control
PI fluorescence (F/F0)
Time (hrs)
5mM Caffeine+50nM CCK
50nM CCK
Control
PI fluorescence (F/F0)
Time (hrs)

Figure 4.6

Live microplate cell death assay in multiplex format at 37°C using an internal control of triton X-100, showing the induction of cell death with 500 µM TLCS. Primary pancreatic acinar cells were placed in a 96 well plate in the presence of PI and the presence or absence of caffeine. TLCS and triton X-100 were injected automatically. Caffeine did not show any statistically significant amelioration. Data shown is mean ± SEM from 3 individual experiments. Traces were normalised to the minimum and maximum fluorescence using the equation $(F-F_{max})/(F_{max}-F_{min})$ as previously described.

Figure 4.6

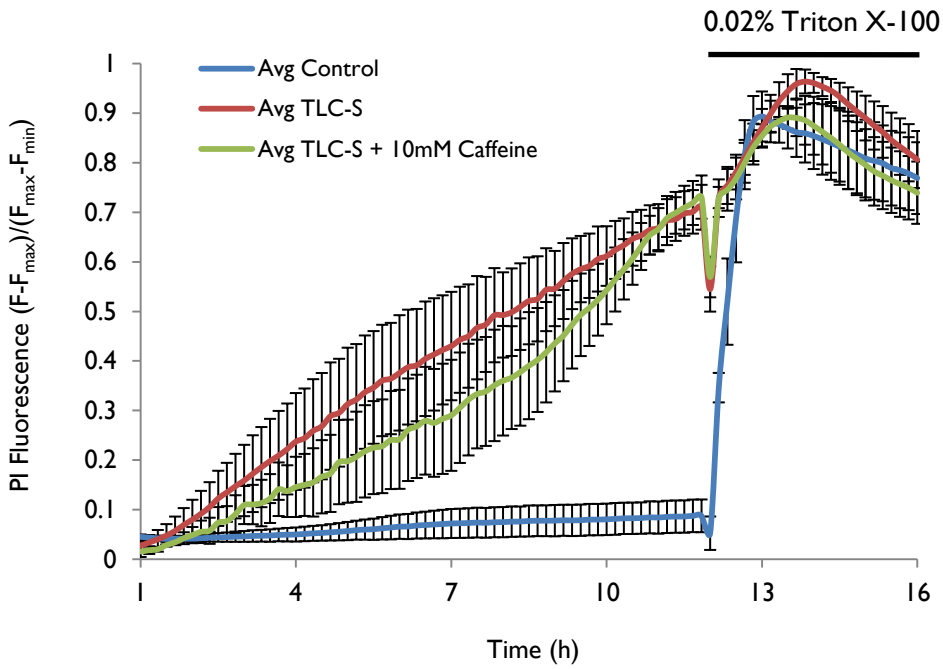
0.02% Triton X-100
Avg Control
Avg TLC-S
Avg TLC-S + 10mM Caffeine
PI Fluorescence (F-Fmax)/(Fmax-Fmin)
0
0.1
0.2
0.3
0.4
0.5
0.6
0.7
0.8
0.9
1
1
4
7
10
13
16
Time (h)

Figure 5.1

Mitochondria in pancreatic exocrine tissue redistribute into a perigranular belt and subplasmalemmal distribution after stimulation with physiological concentrations of CCK. (A) Immunofluorescence staining (Tom20) of fixed murine pancreatic tissue segments in unstimulated conditions shows mitochondria throughout the cytosol. **(B)** After stimulation for 30 minutes with 100 pM CCK the mitochondria were found in a perigranular belt formation with subplasmalemmal mitochondria also seen. Bar indicates 10 μm. Images are representative of at least three individual experiments.

Figure 5.1

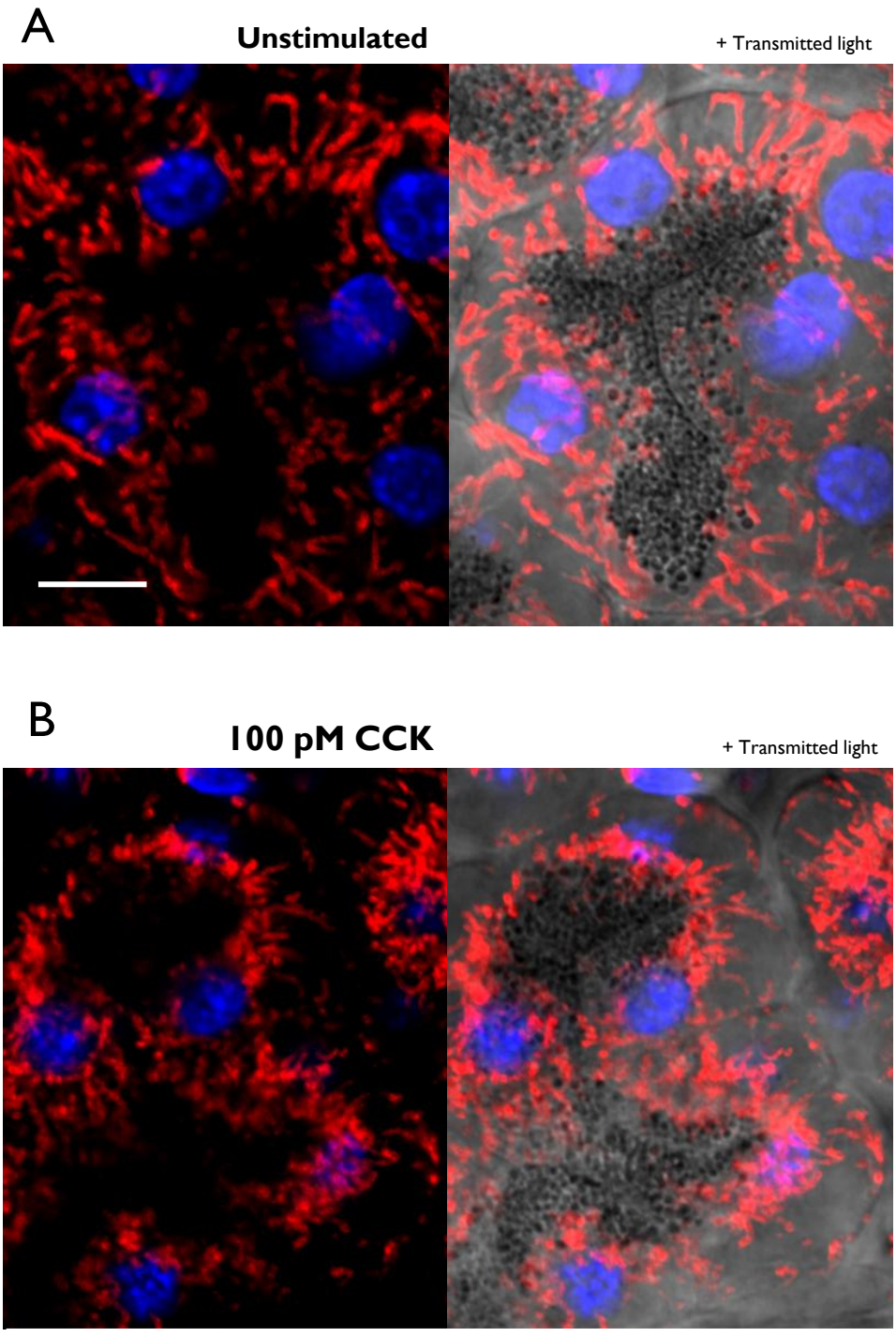
A
Unstimulated
+ Transmitted light
B
100 pM CCK
+ Transmitted light
Mitochondria
Nucleus

Figure 5.2

Quantification and further analysis of the mitochondrial distribution before and after physiological stimulation. (A) Mitochondrial distribution visualised by immunofluorescence of Tom20 within an individual acinar cell. Basal to apical profiling of mitochondrial distribution is indicated by the white rectangle, showing the mitochondria present throughout the cytosolic region in unstimulated conditions (left) and showing the perigranular and subplasmalemmal mitochondria after stimulation with 100 pM CCK (right). The arrow indicates the direction of the profiling performed in (B). **(B)** Graphical representation of mitochondrial profiling, showing the average distribution of mitochondria from the basal membrane towards the apex of the cell in unstimulated conditions (Burgundy line) and after stimulation with 100 pM CCK (Red line). The Grey region shows the inverse of the transmitted light from the profiled region, to give an impression of the location of the optically dense zymogen granules. These data are mean ± SEM from at least 9 regions from at least three individual experiments.

Figure 5.2

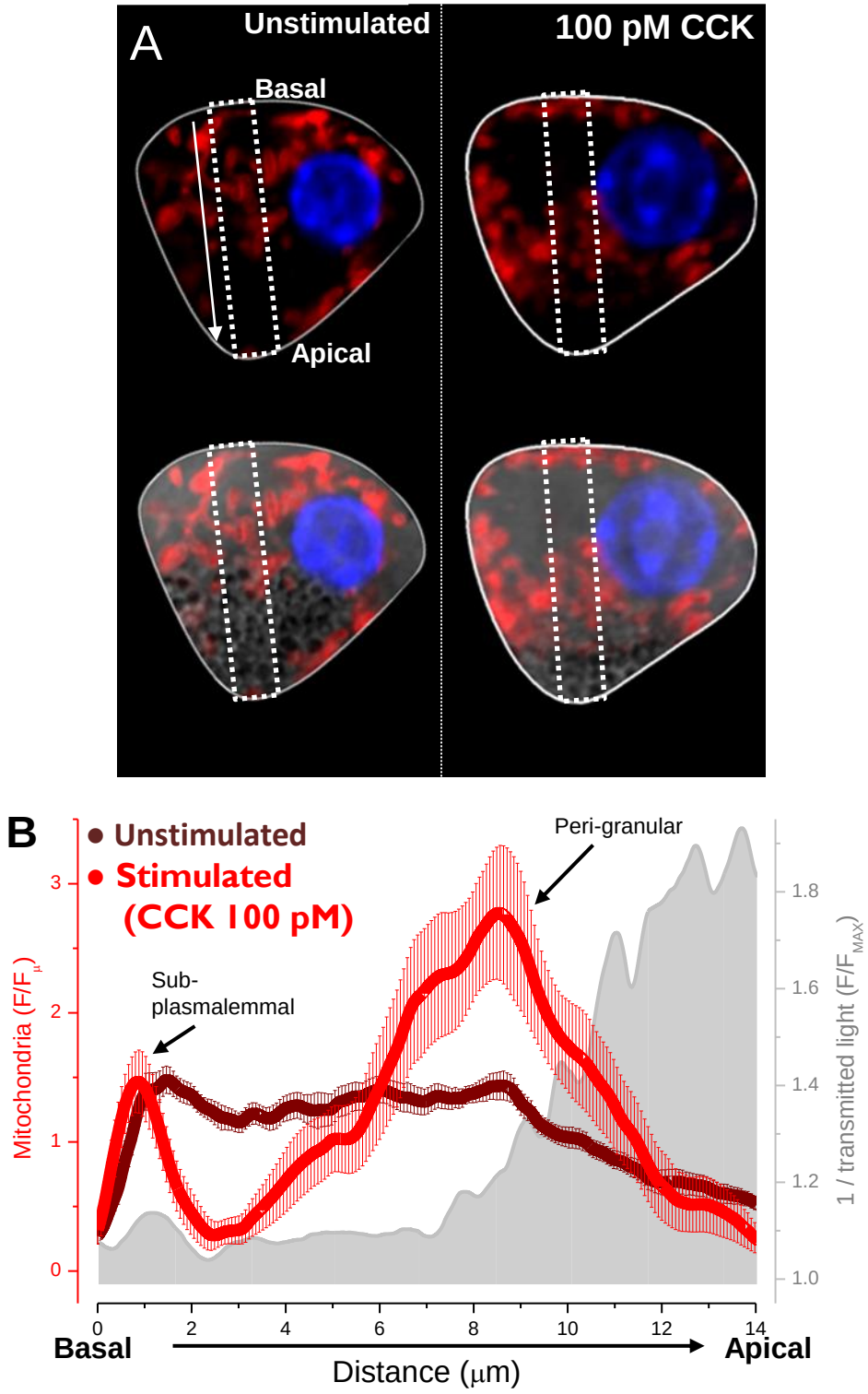
A
Unstimulated
100 pM CCK
Basal
Apical
B
Unstimulated
Stimulated
(CCK 100 pM)
Peri-granular
Sub-
plasmalemmal
Mitochondria (F/F$_\mu$)
1 / transmitted light (F/F$_{MAX}$)
0
1
2
3
1.0
1.2
1.4
1.6
1.8
0
2
4
6
8
10
12
14
Basal
Apical
Distance (μm)

Figure 5.3

Mitochondrial redistribution can be seen to occur progressively after stimulation and is reversible. (A) Mitochondrial profiling visualised by immunofluorescence of Tom20 from a series of experiments showing the formation of the mitochondrial belt over time, and the diffusion of the belt after removal of the stimulus at t=30 minutes. Glow-scale represents the density of the mitochondria in that region based upon the relative intensity of the fluorescence signal. Time points collected were 0, 10, 20, 30, 40, 50, 60 and 90 minutes. These data are the mean value from at least 9 regions from at least three individual experiments. Error is presented in (B). **(B)** Quantification of the mitochondrial profile time series presented in (A), showing mean and SEM of the intensity of the regions from 2-4 μm (trend line - polynomial, $y = 5E\text{-}06x^3 - 0.0011x^2 + 0.0552x + 1.184$, $R^2 = 0.9429$) and from 6-11 μm (trend line - polynomial, $y = -1E\text{-}07x^4 + 2E\text{-}05x^3 - 0.0004x^2 - 0.0245x + 1.1559$, $R^2 = 0.9395$) from the basal membrane.

Figure 5.3

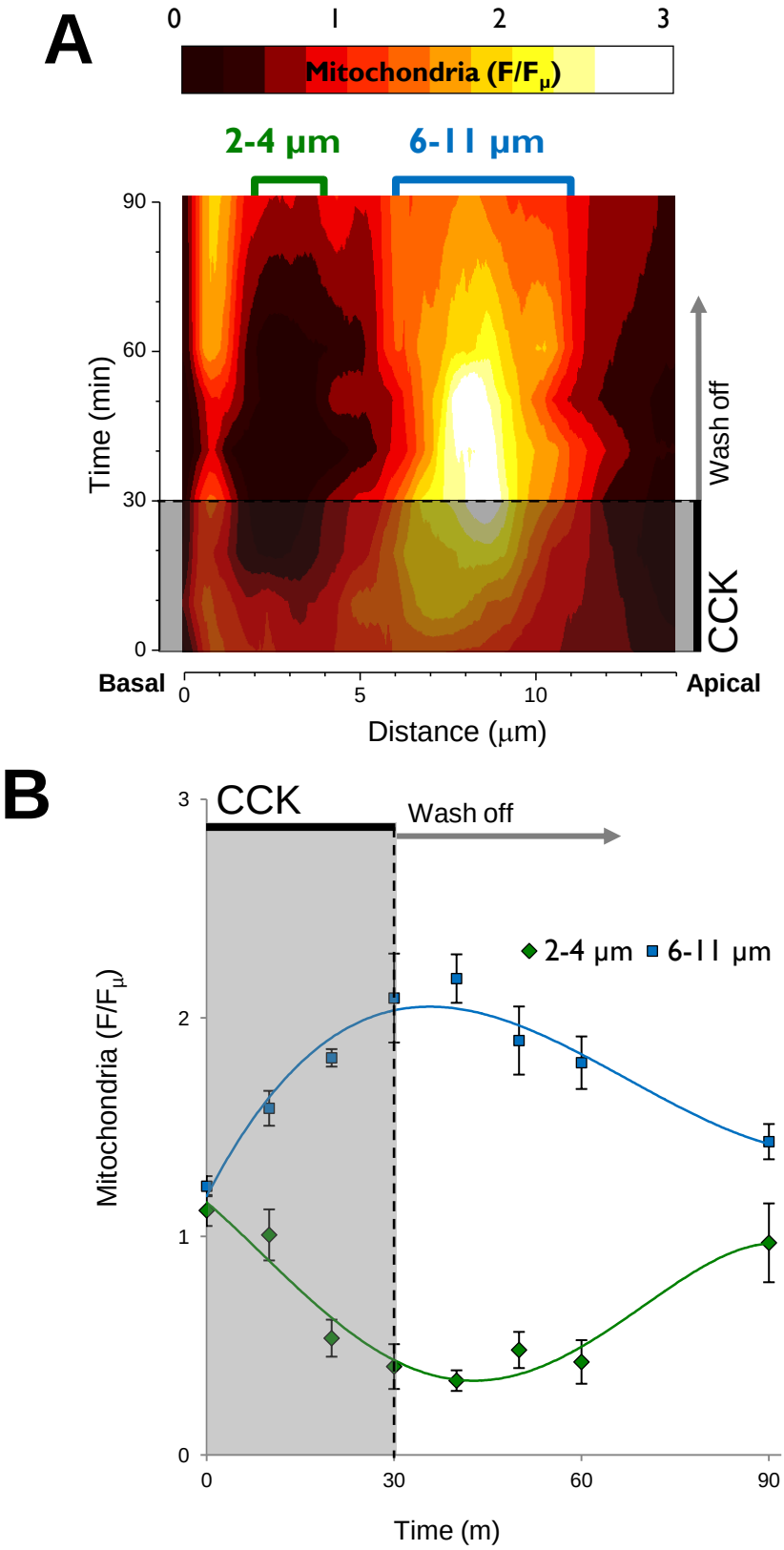
A
0
1
2
3
Mitochondria (F/Fμ)
2-4 μm
6-11 μm
90
60
30
0
Time (min)
Wash off
CCK
Basal
0
5
10
Apical
Distance (μm)
B
CCK
Wash off
3
2
1
0
2-4 μm
6-11 μm
Mitochondria (F/Fμ)
0
30
60
90
Time (m)

Figure 5.4

Redistribution of mitochondria induced by 100 pM CCK is dependent upon microtubules. (A, B) Immunofluorescence maximum intensity projection of α-tubulin staining of pancreatic tissue with or without 1 hour treatment with 50 μM colchicine to inhibit tubulin polymerisation and formation of microtubules. Bar indicates 10 μm. **(C, D)** Triple stained immunofluorescence of pancreatic tissue showing tubulin (α-tubulin, green), mitochondria (Tom20, red), and nuclei (Hoechst, blue) after depolymerisation of the microtubule network with colchicine in unstimulated conditions, and after stimulation with 100 pM CCK. **(E)** Average relative profiles of mitochondria from colchicine pre-treated tissue in stimulated (Burgundy) and unstimulated (Red) conditions, showing no significant change in the mitochondrial distribution. These data are mean ± SEM from at least 9 regions from at least three individual experiments.

Figure 5.4

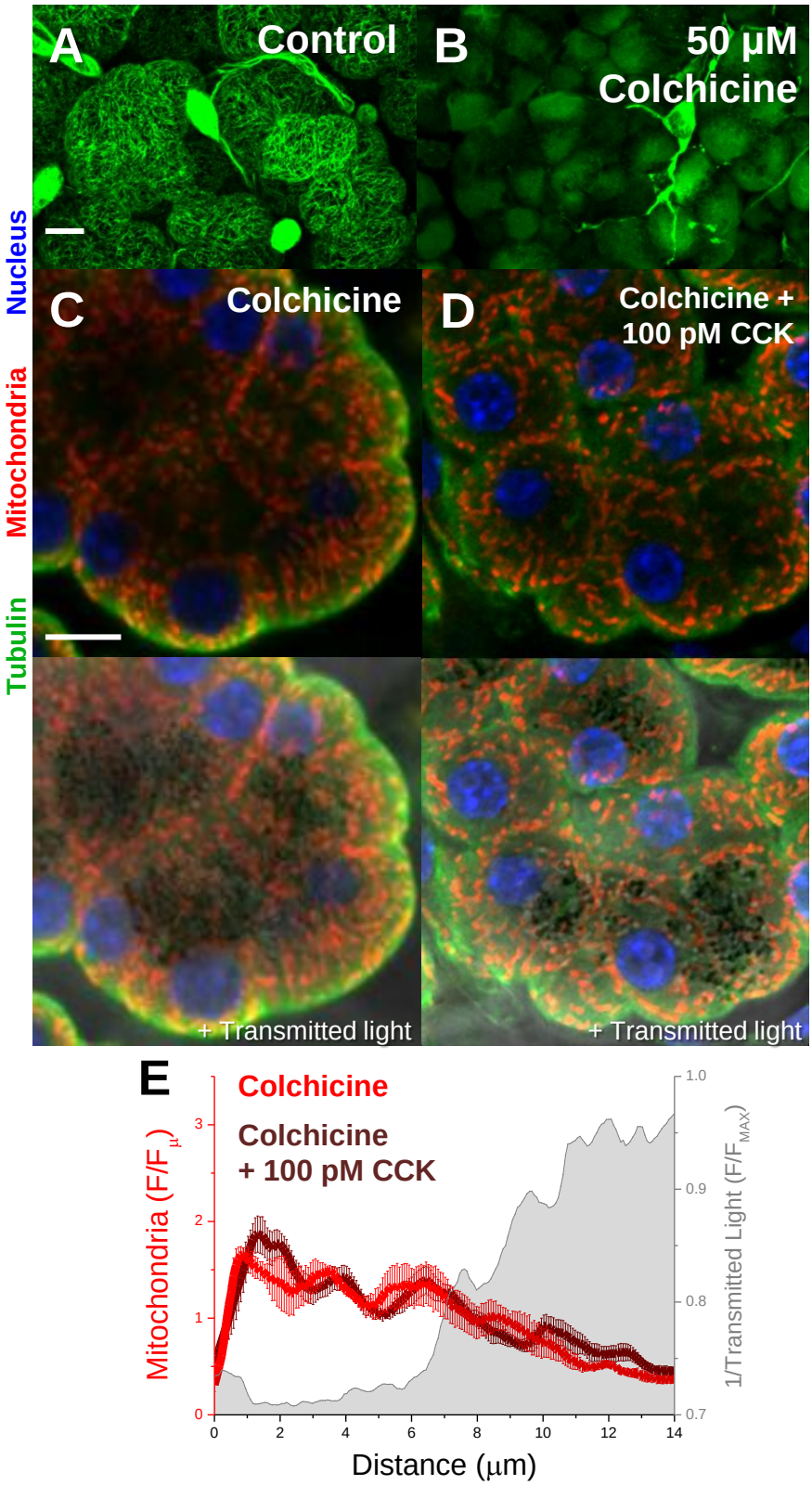
A
Control
B
50 µM
Colchicine
C
Colchicine
D
Colchicine +
100 pM CCK
Nucleus
Mitochondria
Tubulin
+ Transmitted light
+ Transmitted light
E
Colchicine
Colchicine
+ 100 pM CCK
Mitochondria (F/F$_\mu$)
1/Transmitted Light (F/F$_{MAX}$)
Distance (µm)
0
1
2
3
0.7
0.8
0.9
1.0
0
2
4
6
8
10
12
14

Figure 5.5

Mitochondrial redistribution induced by 100 pM CCK is inhibited by the Ca^{2+}-chelating agent, BAPTA-AM. (A) Representative Ca^{2+} traces showing that BAPTA-AM-loading successfully inhibited signals generated by 100 pM CCK. Traces are representative of three experiments. **(B)** Immunofluorescence of mitochondria (Tom20) after 100 pM CCK stimulation of pancreatic tissue loaded with BAPTA-AM, to chelate intracellular Ca^{2+}. Bar indicates 10 μm. **(C)** Mitochondrial profile from basal to apical region of the cell in BAPTA-AM-loaded tissue (Burgundy) and in BAPTA-AM-loaded tissue stimulated with 100 pM CCK for 30 minutes (Red). These data are mean ± SEM from at least 9 regions from at least three individual experiments.

Figure 5.5

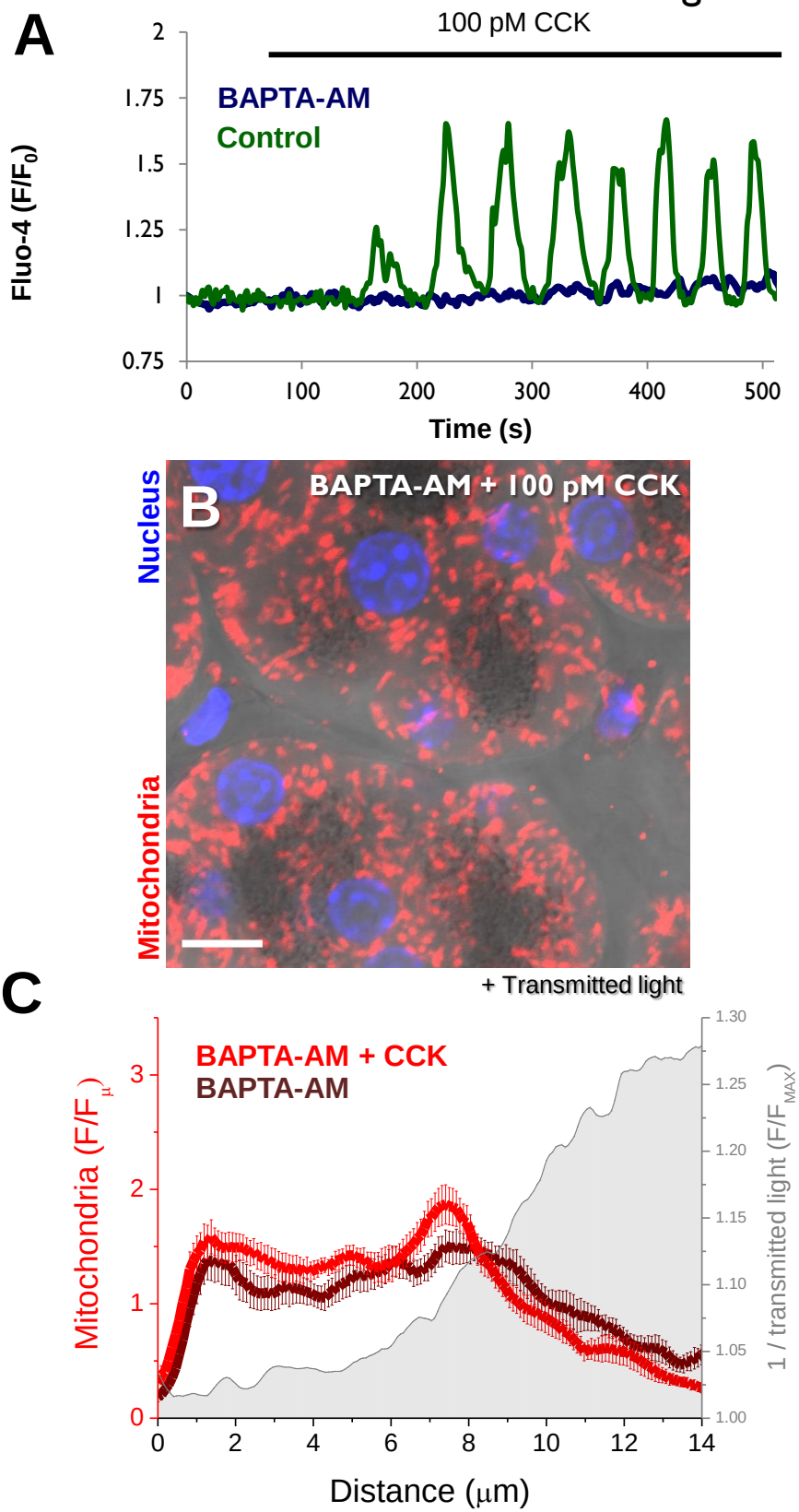
A
100 pM CCK
BAPTA-AM
Control
Fluo-4 (F/F0)
2
1.75
1.5
1.25
1
0.75
0
100
200
300
400
500
Time (s)
B
BAPTA-AM + 100 pM CCK
Nucleus
Mitochondria
+ Transmitted light
C
BAPTA-AM + CCK
BAPTA-AM
Mitochondria (F/Fμ)
1 / transmitted light (F/FMAX)
3
2
1
0
1.30
1.25
1.20
1.15
1.10
1.05
1.00
0
2
4
6
8
10
12
14
Distance (μm)

Figure 5.6

Mitochondrial redistribution can be induced by agonist independent Ca^{2+} increase. (A) Cytosolic Ca^{2+} rise in pancreatic tissue loaded with Fluo-4 by application of thapsigargin and 10 mM external Ca^{2+}. **(B)** Mitochondrial distribution after treatment with thapsigargin + 10 mM external Ca^{2+} for 30 minutes, to induce a cytosolic Ca^{2+} rise independent of CCK stimulation. **(C)** Mitochondrial basal-to-apical profile, visualised by immunofluorescence (Tom20) after thapsigargin-induced Ca^{2+} rise showing the development of subplasmalemmal and peri-granular mitochondrial populations in an agonist independent manner. These data are mean ± SEM from at least 9 regions from at least three individual experiments.

Figure 5.6

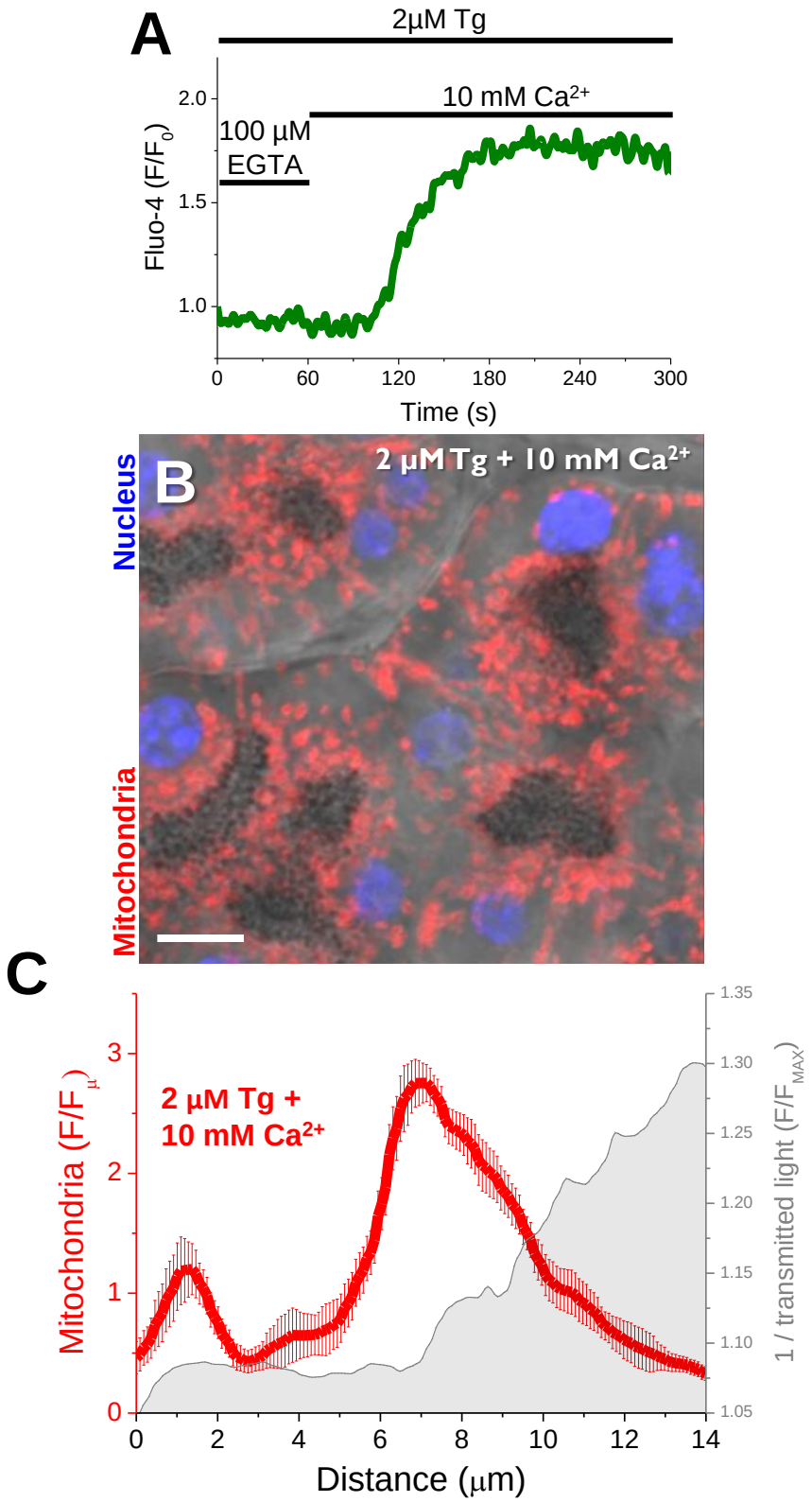
A
2µM Tg
10 mM Ca2+
100 µM
EGTA
Fluo-4 (F/F0)
2.0
1.5
1.0
0
60
120
180
240
300
Time (s)
B
2 µM Tg + 10 mM Ca2+
Nucleus
Mitochondria
C
2 µM Tg +
10 mM Ca2+
Mitochondria (F/Fµ)
1 / transmitted light (F/FMAX)
0
1
2
3
1.05
1.10
1.15
1.20
1.25
1.30
1.35
0
2
4
6
8
10
12
14
Distance (µm)

Figure 5.7

Mitochondrial redistribution to the plasma membrane induced by 100 pM CCK is dependent upon external Ca^{2+}. **(A)** Mitochondrial distribution after pre-treatment with the membrane impermeable Ca^{2+} chelator EGTA for 90 minutes prior to stimulation with 100 pM CCK, shown by immunofluorescence (Tom20). Bar indicates 10 μm. **(B)** Corresponding mitochondrial profile which compares the EGTA pre-treated sample (Red) with the distribution after stimulation in the presence of 1 mM extracellular Ca^{2+} (Grey). These data are mean ± SEM from at least 9 regions from at least three individual experiments.

Figure 5.7

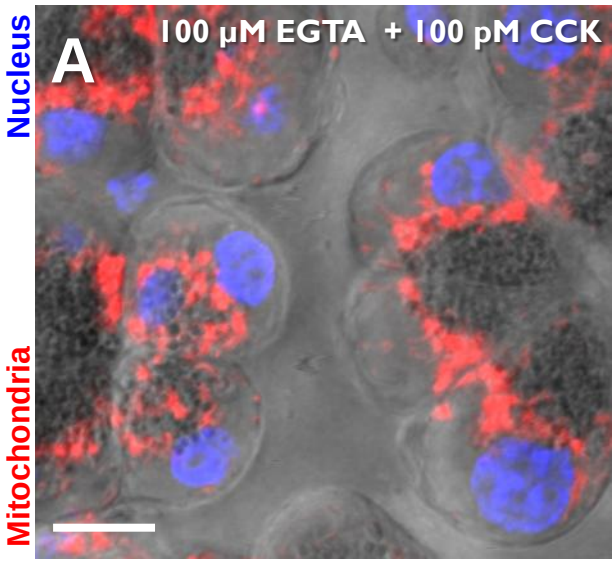
A
100 µM EGTA + 100 pM CCK
Nucleus
Mitochondria

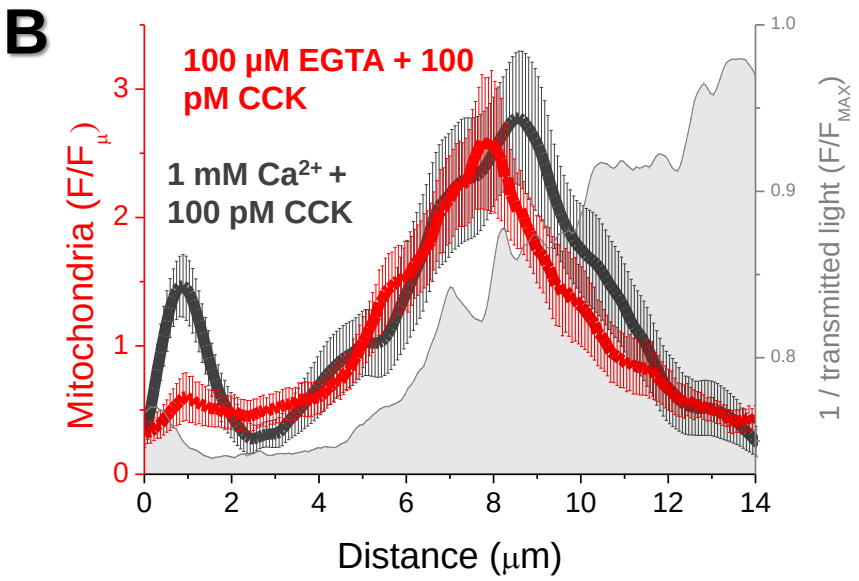
B
100 µM EGTA + 100 pM CCK
1 mM Ca2+ + 100 pM CCK
Mitochondria (F/Fμ)
1 / transmitted light (F/FMAX)
Distance (μm)
0
1
2
3
0
2
4
6
8
10
12
14
0.8
0.9
1.0

Figure 5.8

Hyperstimulation of pancreatic exocrine tissue with CCK or the bile acid TLCS induces severe apical mitochondrial redistribution. (A) Immunofluorescence (Tom20) showing the mitochondrial distribution after treatment with 100 nM CCK or 500 μM TLCS. Bar indicates 10 μm. **(B)** Corresponding average mitochondrial profile showing total dislocation of the mitochondria away from the plasma membrane towards the apical region of the cells after treatment with 100 nM CCK (Red) or 500 μM TLCS (Burgundy), contrasted with the control distribution (Grey). These data are mean ± SEM from at least 9 regions from at least three individual experiments.

Figure 5.8

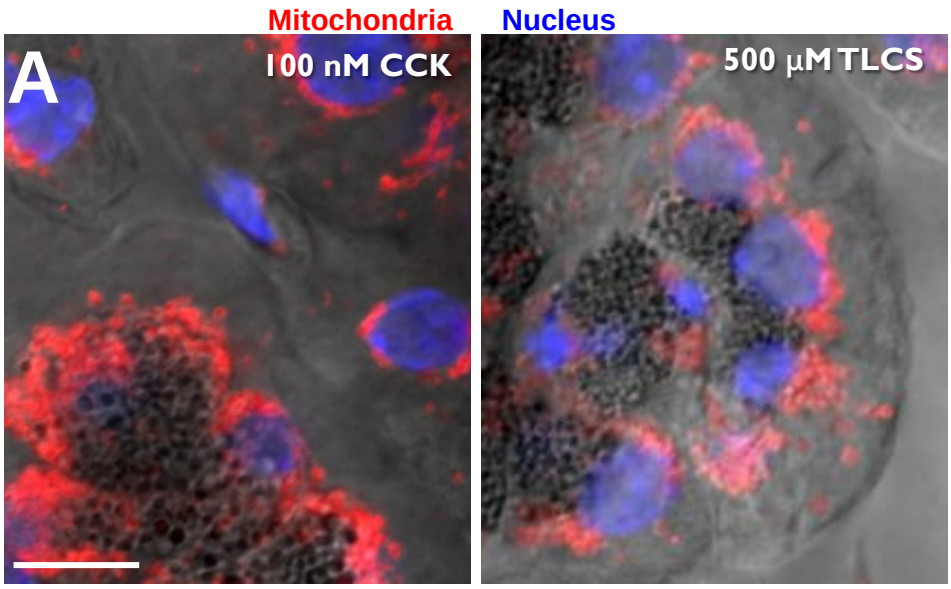
Mitochondria
Nucleus
A
100 nM CCK
500 µM TLCS

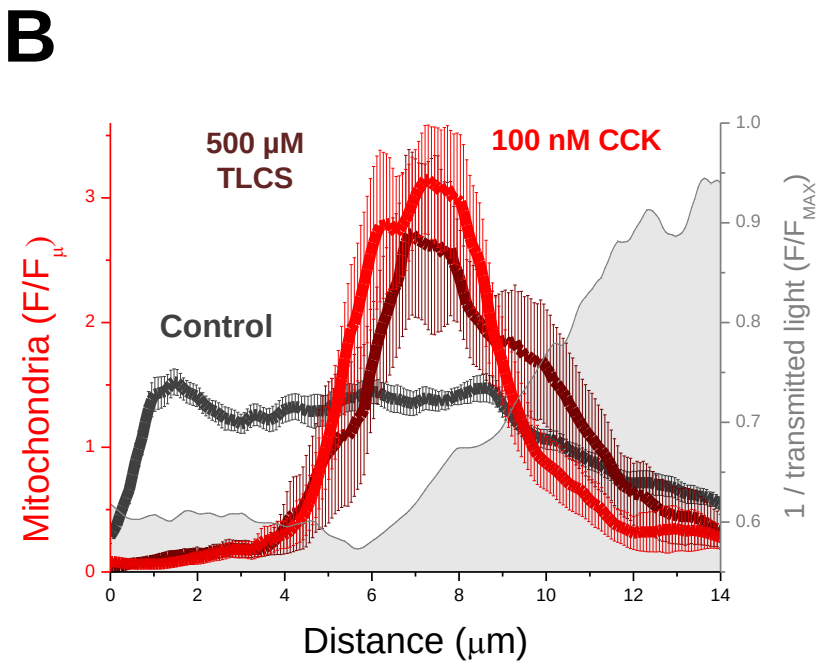
B
500 µM TLCS
100 nM CCK
Control
Mitochondria (F/F µ)
1 / transmitted light (F/F MAX)
Distance (µm)
0
1
2
3
0.6
0.7
0.8
0.9
1.0
0
2
4
6
8
10
12
14

Figure 5.9

Severe apical mitochondrial redistribution induced by hyperstimulation of pancreatic exocrine tissue with CCK or the bile acid TLCS is independent of the microtubule network (A) Immunofluorescence of tubulin (α-tubulin, green), mitochondria (Tom20, red), and nuclei (Hoechst, blue), showing the mitochondrial distribution in tissue pre-treated with 50 μM colchicine for 1 hour prior to hyperstimulation with 100 nM CCK or 500 μM TLCS. Bar indicates 10 μm. **(B)** Corresponding average mitochondrial profile showing total dislocation of the mitochondria away from the plasma membrane towards the apical region of the cells after treatment with 100 nM CCK (Red) or 500 μM TLCS (Burgundy), contrasted with the colchicine control distribution (Grey). These data are mean ± SEM from at least 9 regions from at least three individual experiments.

Figure 5.9

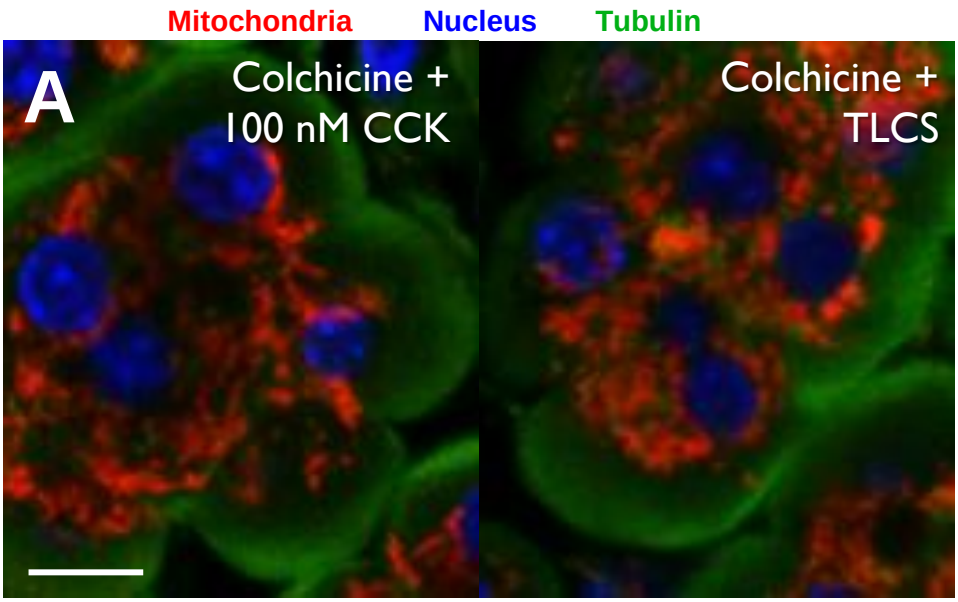
Mitochondria
Nucleus
Tubulin
A
Colchicine +
100 nM CCK
Colchicine +
TLCS

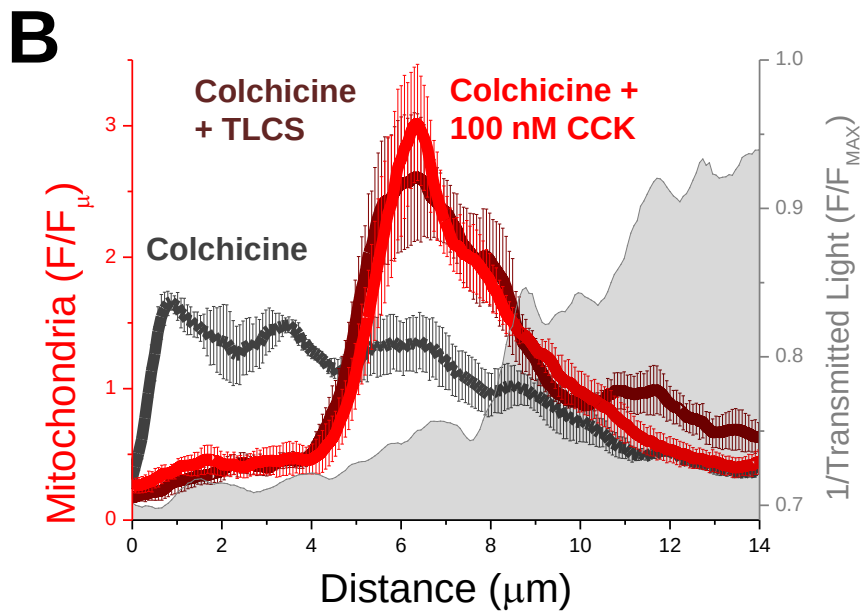
B
Colchicine
+ TLCS
Colchicine +
100 nM CCK
Colchicine
Mitochondria (F/F$_\mu$)
1/Transmitted Light (F/F$_{MAX}$)
Distance (μm)
0
1
2
3
0.7
0.8
0.9
1.0
0
2
4
6
8
10
12
14

Figure 5.10

Severe apical mitochondrial redistribution induced by hyperstimulation of pancreatic exocrine tissue with CCK or the bile acid TLCS is not inhibited by BAPTA-AM loading. Immunofluorescence images of the mitochondrial distribution (Tom20) in tissue loaded with BAPTA-AM **(A)**; and loaded with BAPTA-AM and subsequently hyperstimulated with 100 nM CCK **(B)**; indicating that the mitochondrial redistribution induced by 100 nM CCK is Ca^{2+} -independent. Bar indicates 10 μm. These data are representative of at least three individual experiments.

Figure 5.10

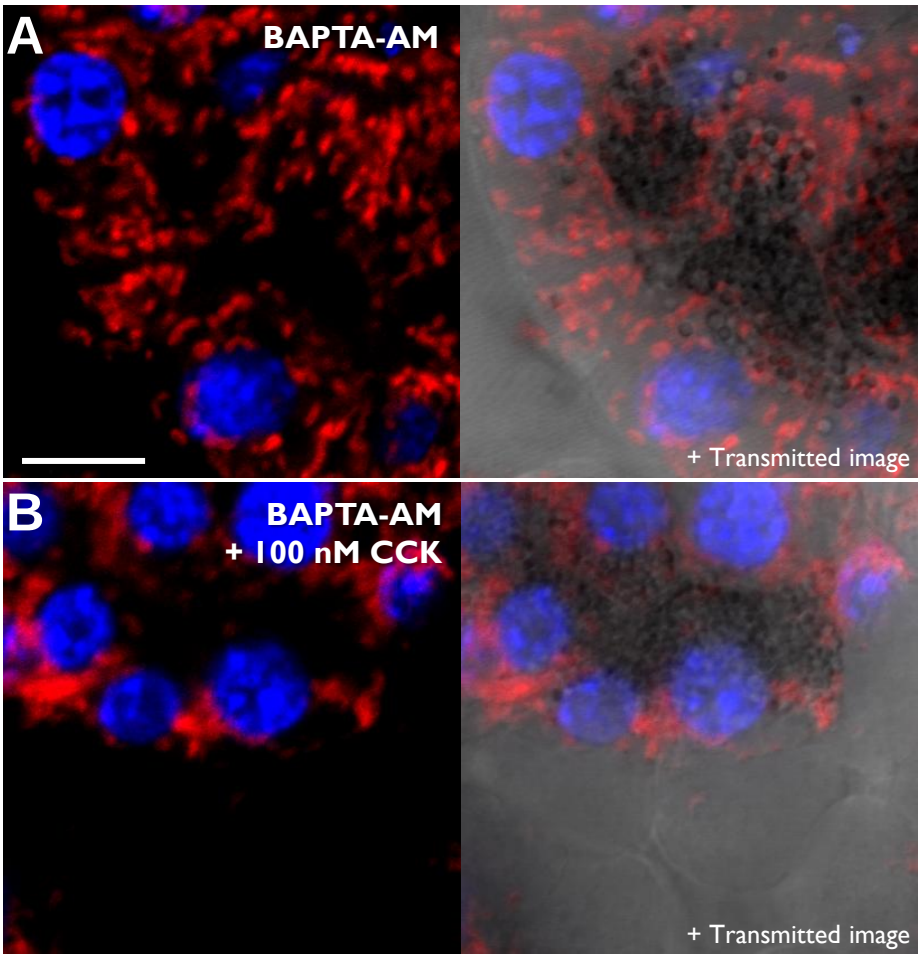
A
BAPTA-AM
+ Transmitted image
B
BAPTA-AM
+ 100 nM CCK
+ Transmitted image

Figure 5.11

Quantification of hyperstimulation induced mitochondrial distribution by area analysis. Average density of mitochondria (Tom20 immunofluorescence) in the subplasmalemmal (<2 μm from the basal membrane) and peri-granular (<5 μm from the granular region) regions in unstimulated or 100 nM CCK hyperstimulated tissue, and hyperstimulated tissue in the presence of colchicine; after BAPTA-AM loading; and after depolarisation of the mitochondria with the protonophore CCCP. These data are mean ± SEM from at least 6 regions from at least three individual experiments and * indicates $p < 0.05$ compared to the respective control (perigranular or subplasmalemmal region).

Figure 5.11

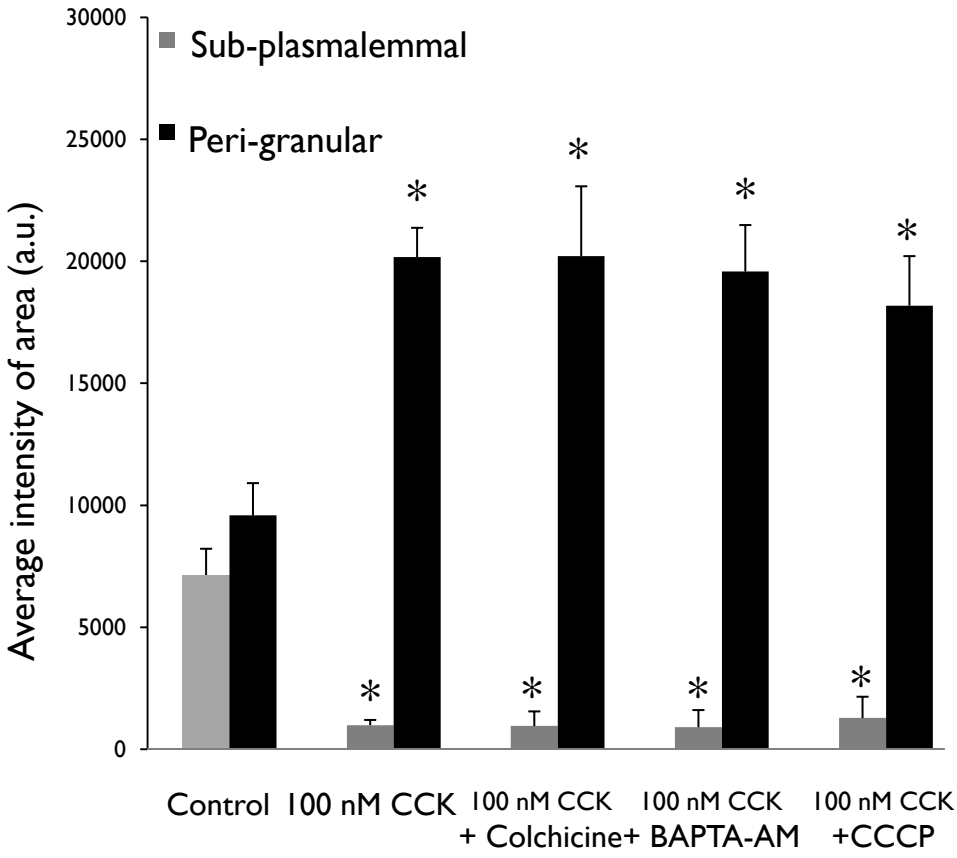
30000
25000
20000
15000
10000
5000
0
Average intensity of area (a.u.)
Sub-plasmalemmal
Peri-granular
*
Control
100 nM CCK
100 nM CCK + Colchicine
100 nM CCK + BAPTA-AM
100 nM CCK +CCCP

Figure 5.12

Pathological Ca^{2+} redistribution induced by 100 nM CCK is independent of reactive oxygen species. (A) Treatment with 30 μM menadione for 30 minutes resulted in a diffuse mitochondrial distribution (Tom20 immunofluorescence) similar to control conditions. **(B)** Treatment of the tissue with 10 mM NAC for 10 minutes prior to stimulation with 100 nM CCK for 30 minutes, did not prevent severe apical redistribution of mitochondria (red). Bar indicates 10 μm. These data are representative of at least three individual experiments.

Figure 5.12

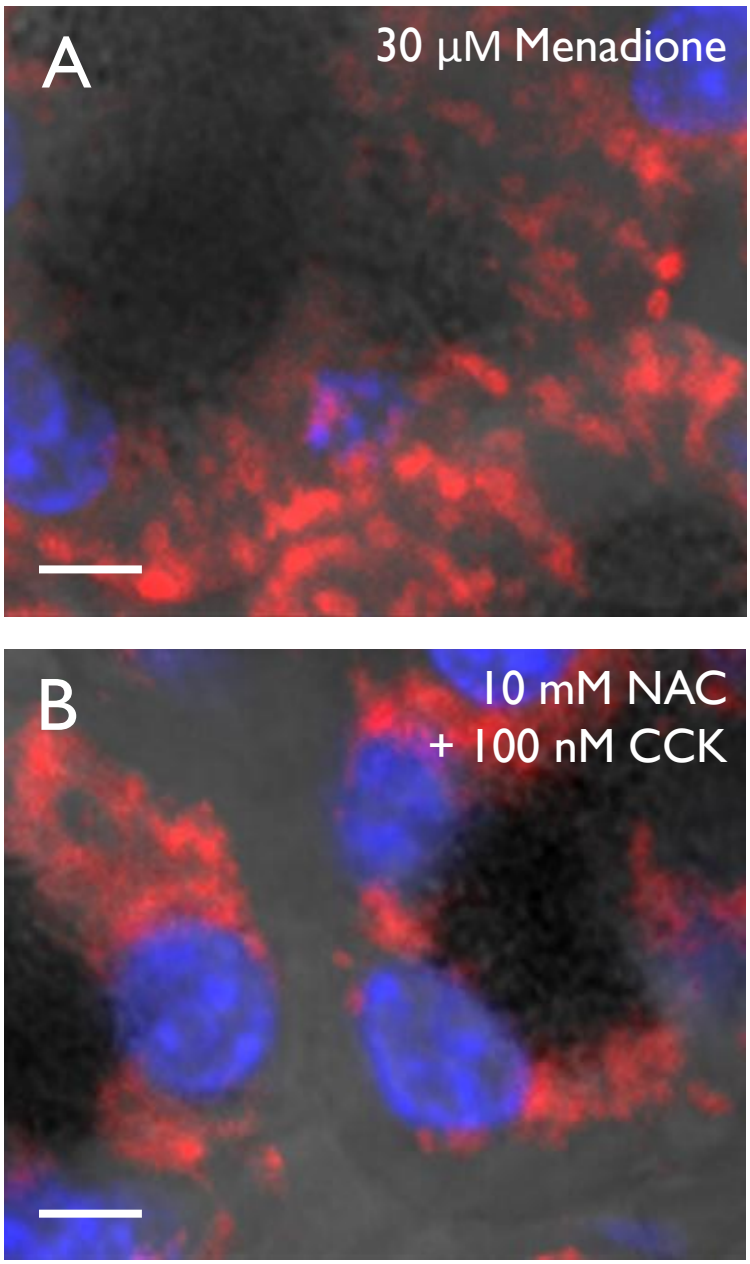

Figure 5.13

3D projection of cytoskeletal redistribution induced by hyperstimulation of pancreatic tissue with 100 nM CCK for 30 minutes. (A) Immunofluorescence, maximum intensity projections of low magnification regions of pancreatic tissue showing the actin alone (pink, top) or tubulin and actin (green and pink respectively, bottom) distribution in unstimulated conditions (left) and after hyperstimulation with 100 nM CCK for 30 minutes (right). Bar indicates 20 μm. **(B)** 3D projection of the actin (pink) and tubulin (green) distribution in unstimulated murine pancreatic tissue (left) and after hyperstimulation with 100 nM CCK (right) visualised by immunofluorescence showing the thinner tubulin distribution and the lack of actin patches on the plasma membrane after hyperstimulation. These data are representative of at least three individual experiments.

Figure 5.13

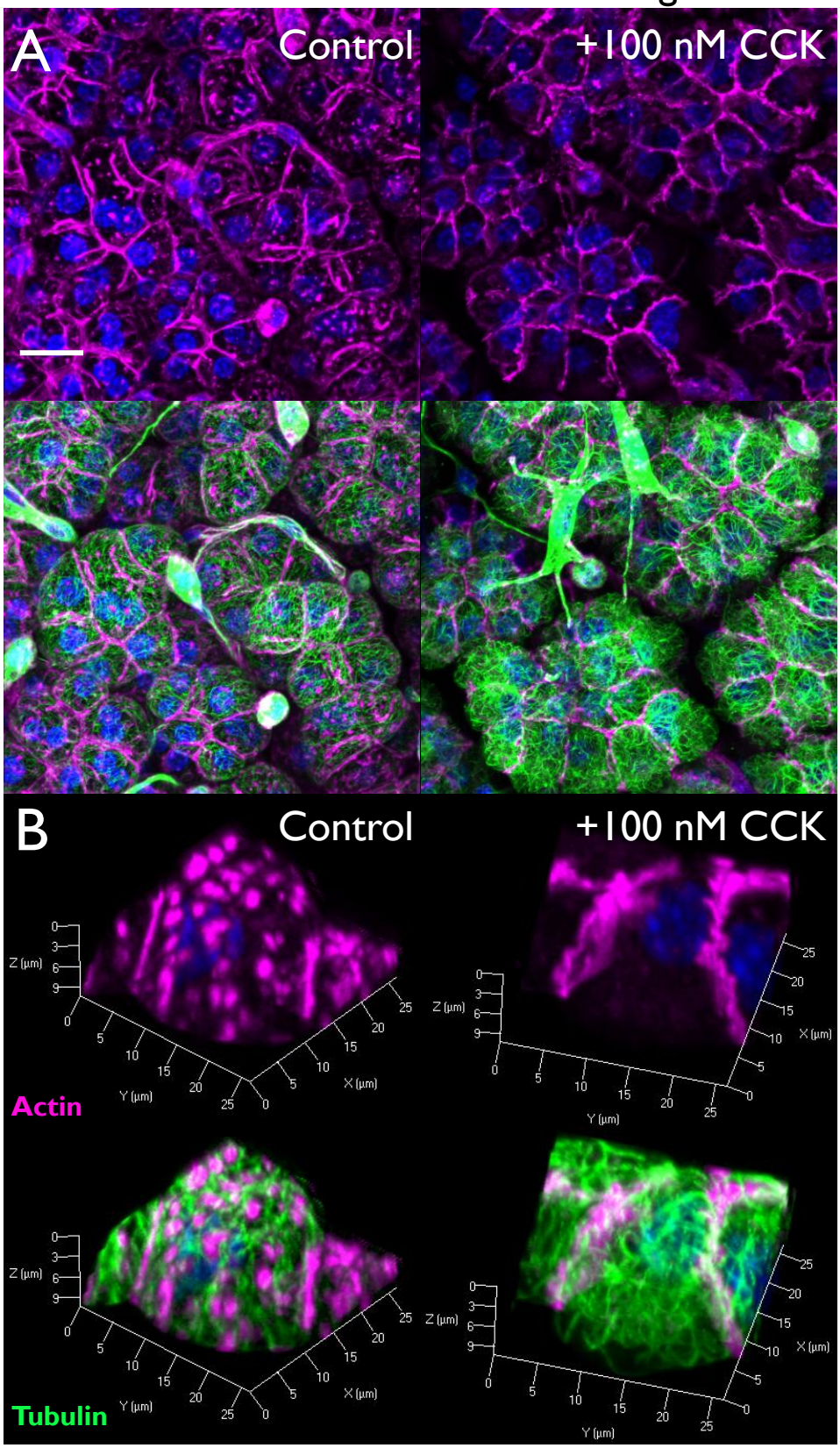
A
Control
+100 nM CCK
B
Control
+100 nM CCK
Actin
Tubulin
Z (µm)
Y (µm)
X (µm)

Figure 5.14

Confocal cytoskeletal redistribution induced by hyperstimulation of pancreatic tissue with 100 nM CCK for 30 minutes. Immunofluorescence showing the cytoskeletal distribution in unstimulated tissue (left) and after hyperstimulation (right). Yellow arrows in the control images indicate the location of actin patches on the basal membrane and the microtubule decoration extending all the way to the basal membrane. The basal membrane is more easily identified on the transmitted light images (bottom). Red arrows in the hyperstimulated images indicate the formation of actin cables within the cytosol, and the microtubule build up, distal to the actin cables. Bar indicates 20 μm. These data are representative of at least three individual experiments.

Figure 5.14

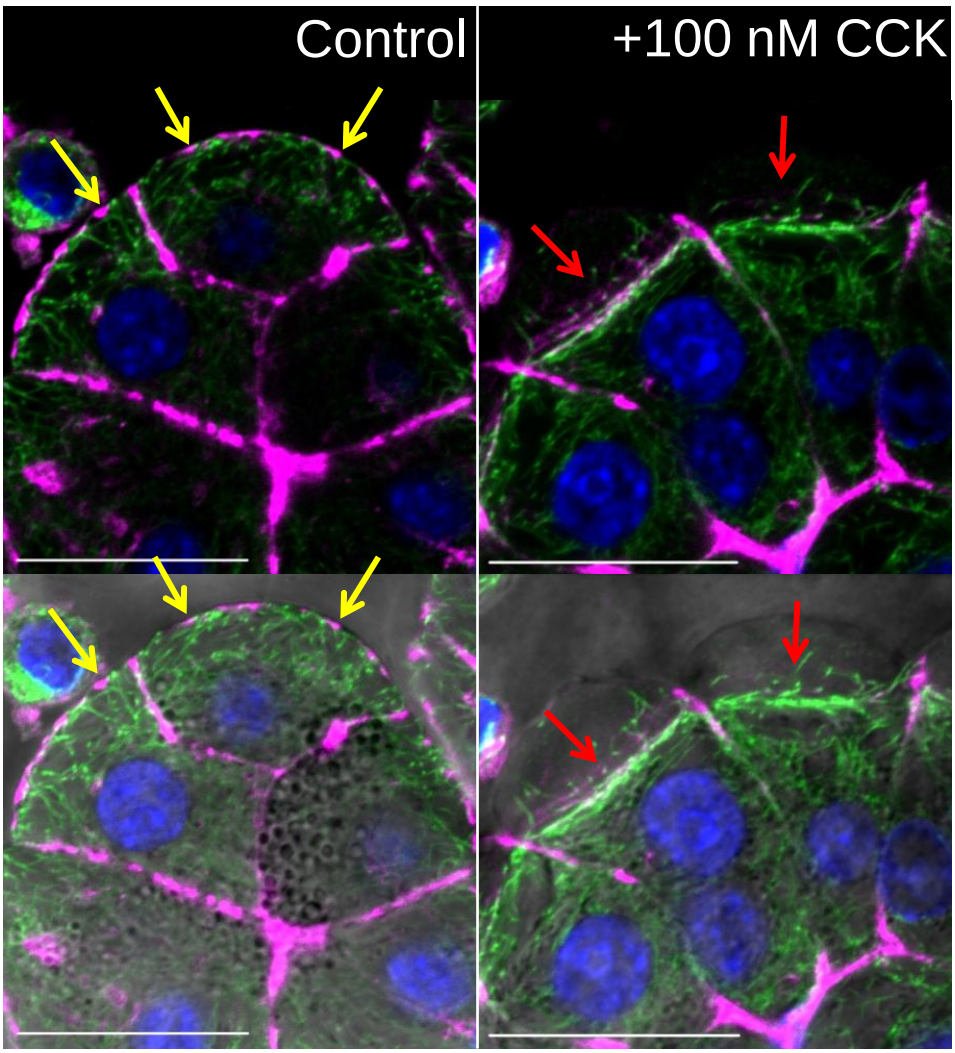

Figure 5.15

Cytoskeleton and mitochondrial distribution after stimulation with 100 pM CCK showing propinquity of mitochondria and actin patches after physiological stimulation. (A) Confocal slice close to the cover slip, showing the subplasmalemmal actin and mitochondrial distribution. White hashed box indicated region of interest for images in (C). **(B)** Schematic to show the confocal slice and orientation of these images. **(C)** Actin, (phalloidin, pink) tubulin (green) and mitochondrial (Tom20, red) distributions in the subplasmalemmal region, showing close proximity but lack of overlap. Bar indicates 10 μm. These data are representative of at least three individual experiments.

Figure 5.15

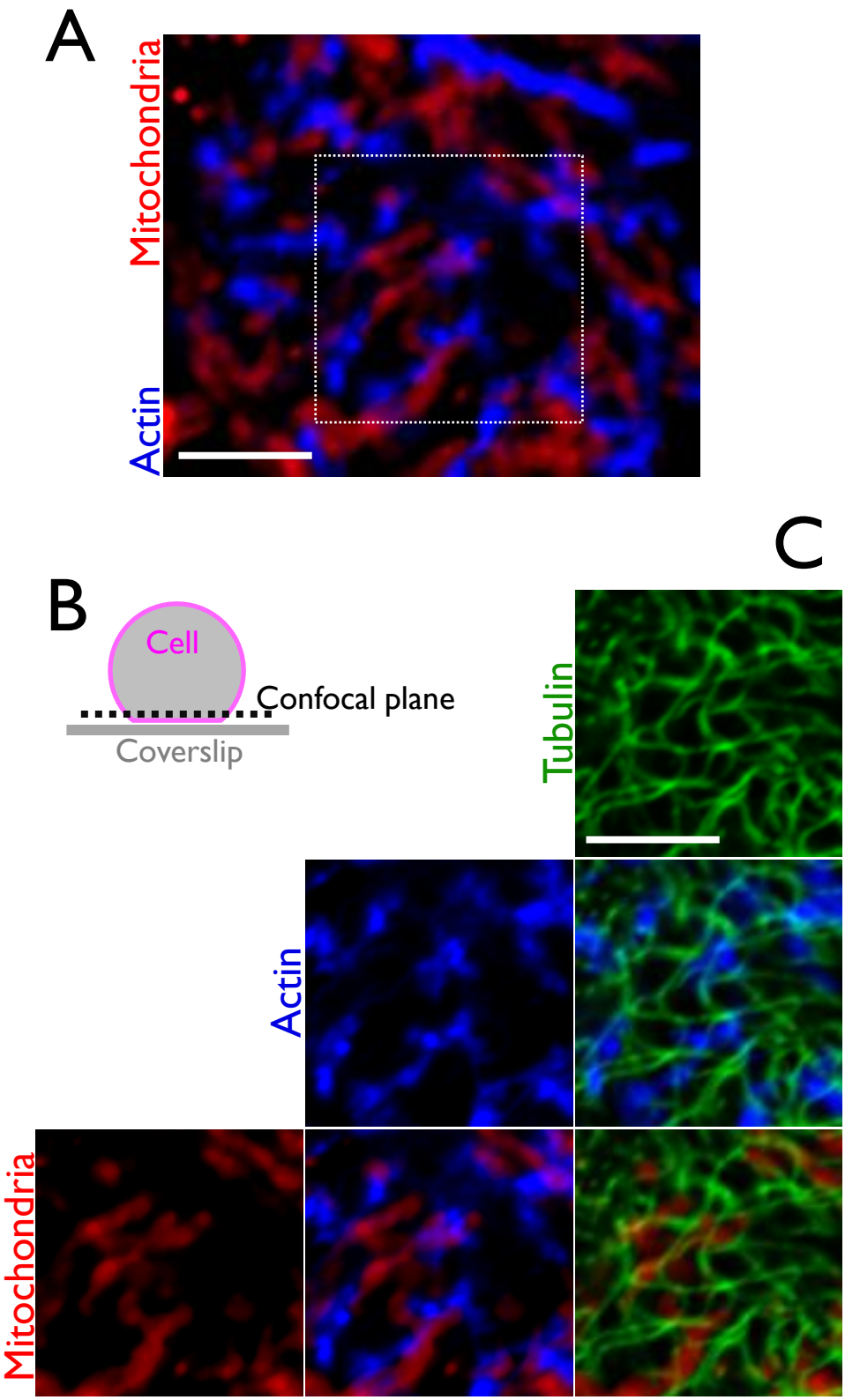
A
Mitochondria
Actin
B
Cell
Confocal plane
Coverslip
C
Tubulin
Actin
Mitochondria

Figure 5.16

Cytoskeletal and mitochondrial redistribution induced by hyperstimulation with 100 nM CCK is not inhibited by BAPTA-AM loading. Immunofluorescence showing the cytoskeletal (Phalloidin, pink; tubulin, green) and mitochondrial (Tom20, red) distribution in pancreatic tissue hyperstimulated with 100 nM CCK after BAPTA-AM loading. The yellow arrow indicates the presence of actin cables and the red arrow highlights the location of microtubule bundles beneath these actin cables. Bar indicates 5μm. These data are representative of at least three individual experiments.

Figure 5.16

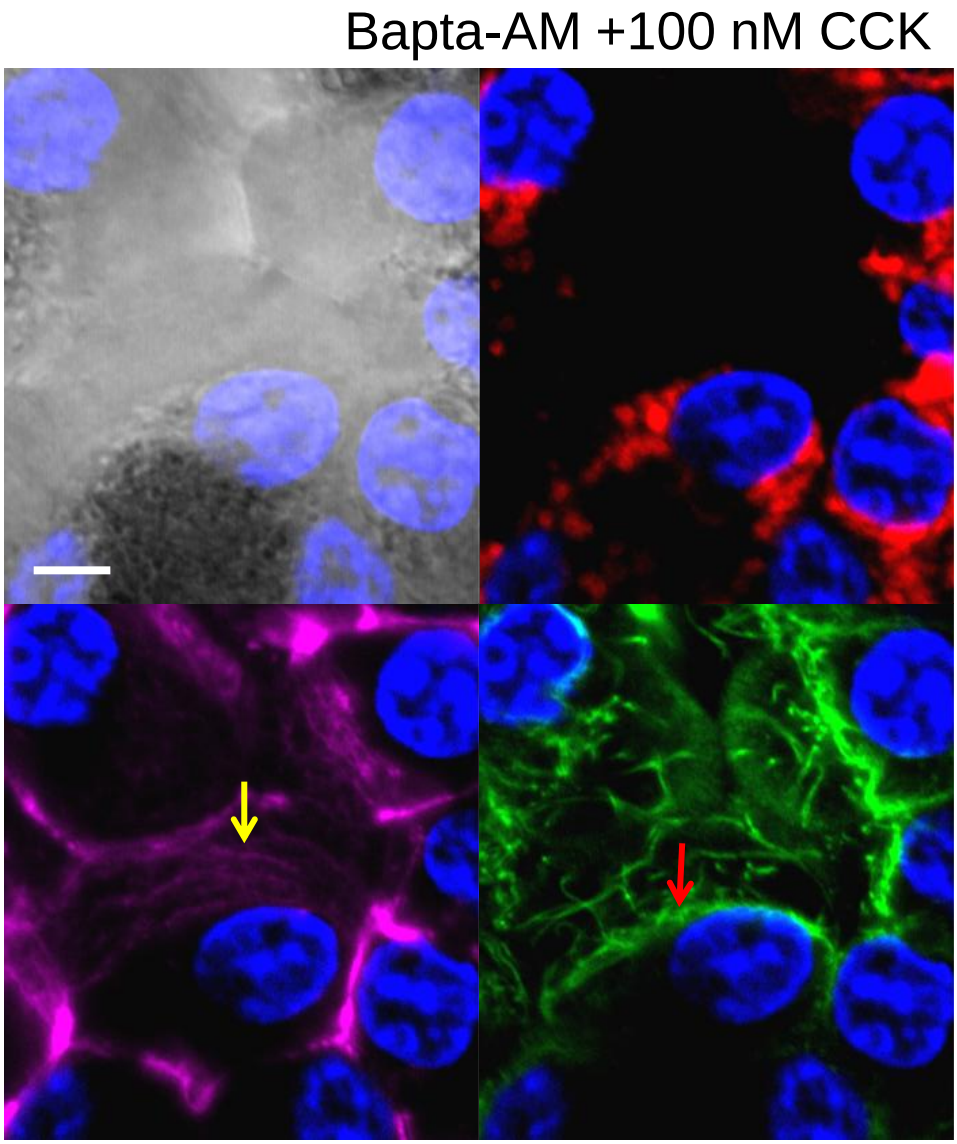

Figure 5.17

Redistribution of tubulin, actin and mitochondria by hyperstimulation with 500 μM TLCS is not inhibited by BAPTA-AM -loading. (A) Immunofluorescence of BAPTA-AM -loaded tissue showing that 500 μM TLCS induced severe apical redistribution of mitochondria (Tom20, red) and the formation of a belt of microtubules (green) and actin cables (phalloidin, pink) which are on the basal side of the mitochondria. Microtubules extend beyond this belt into the basal region of the cells even reaching the basal membrane, but are distinctly sparser in the basal region than the perigranular region. Yellow boxes indicate region of zoom in **(B - please turn over).** Bar indicates 20 μm. These data are representative of at least three individual experiments.

Figure 5.17

Bapta-AM + TLCS

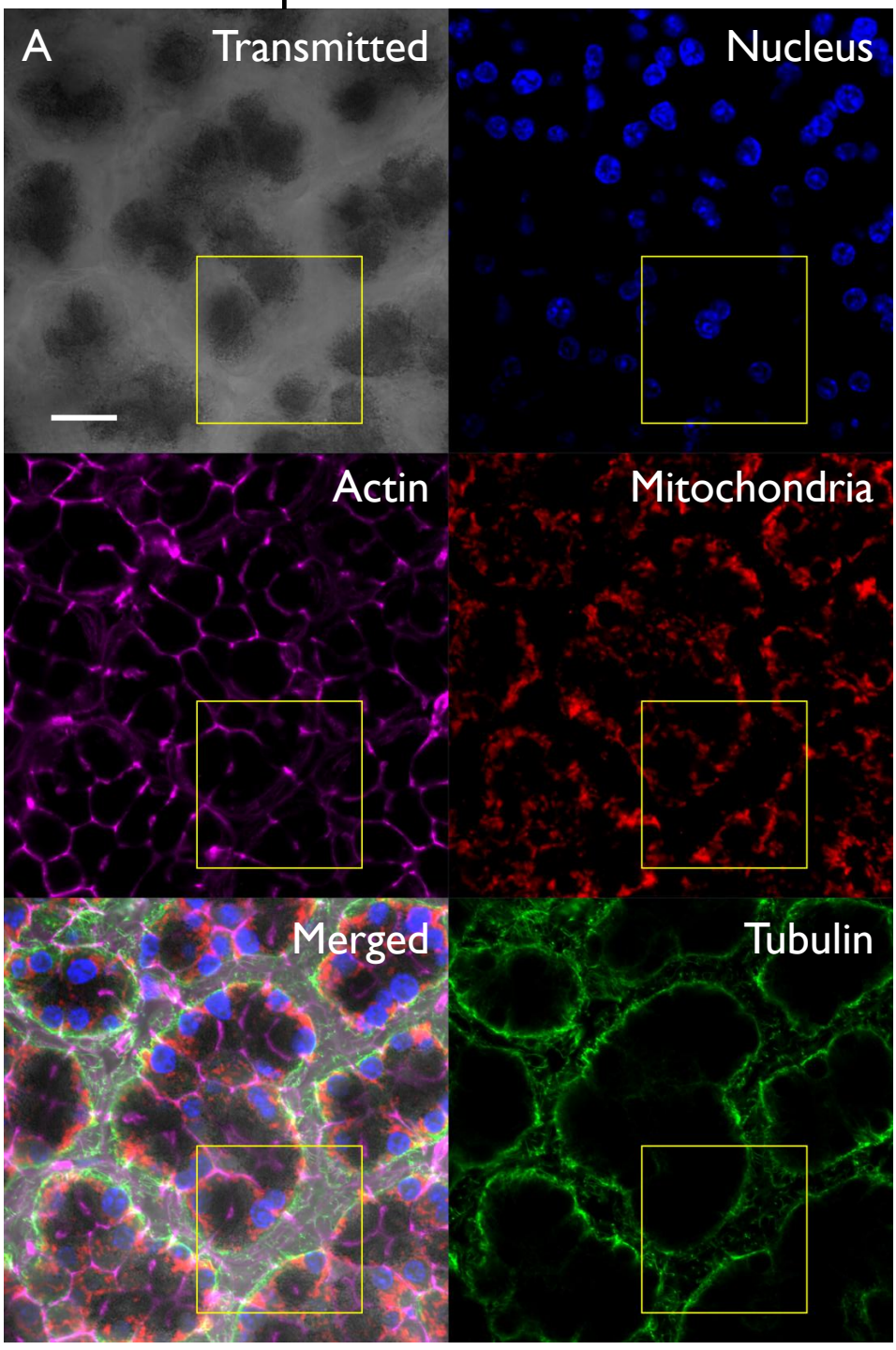

Mitochondria Nucleus Tubulin Actin

Figure 5.17B

Redistribution of tubulin, actin and mitochondria by bile acid is not inhibited by BAPTA-AM –loading. Zoom of previous images, showing severe apical redistribution of mitochondria (Tom20 red) and the formation of a belt of microtubules (green) and actin cables (phalloidin, pink) which are on the basal side of the mitochondria. Bar indicates 10 μm. These data are representative of at least three individual experiments.

Figure 5.17B

Bapta-AM + TLCS

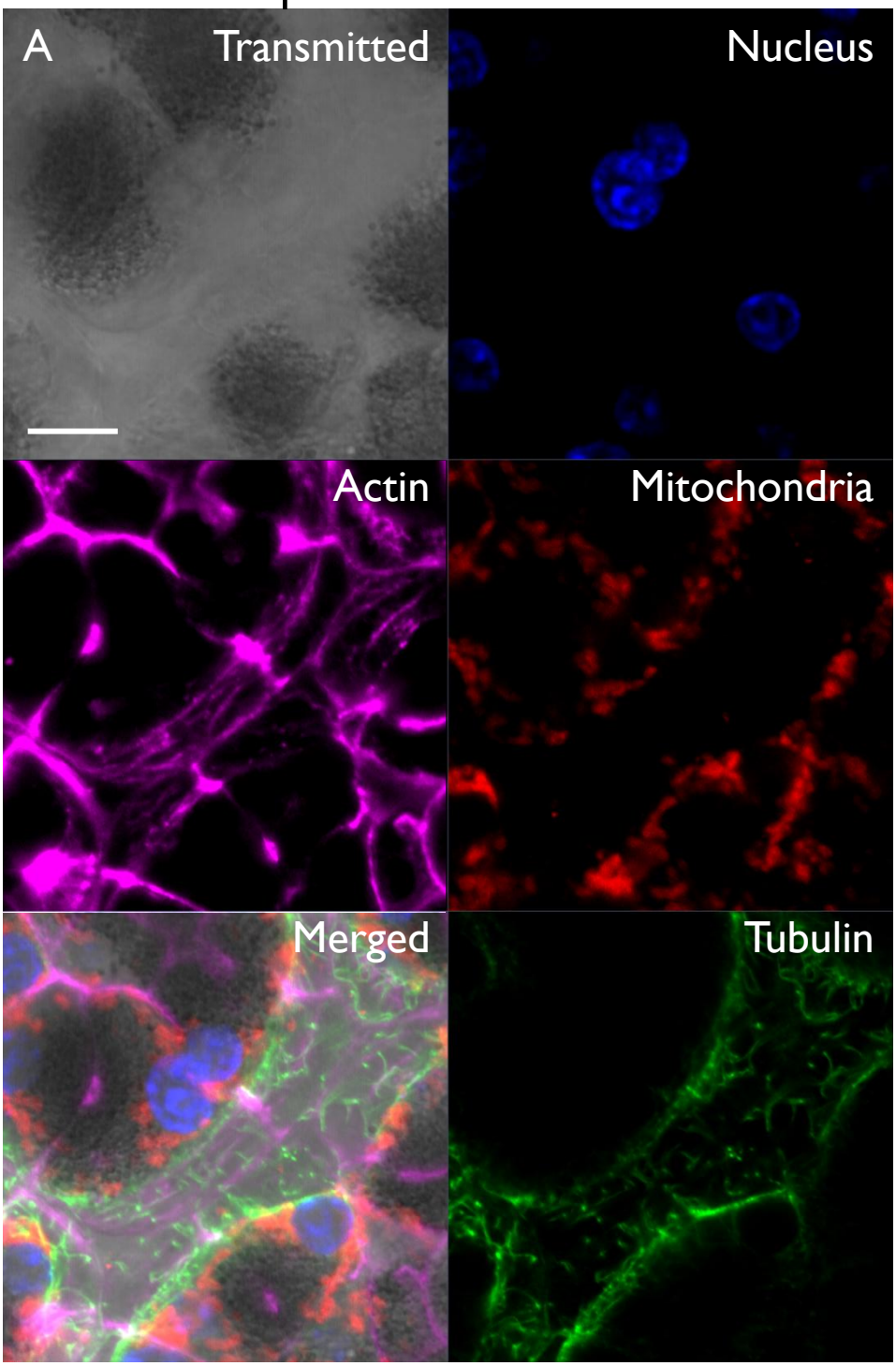

Mitochondria Nucleus Tubulin Actin

Figure 5.18

Cytoskeletal and mitochondrial redistribution induced by hyperstimulation with 100 nM CCK is not inhibited by prior depletion of the intracellular Ca^{2+} store. (A) Cytosolic Ca^{2+} trace from Fluo-4 loaded pancreatic tissue hyperstimulated with 100 nM CCK after depletion of the intracellular Ca^{2+} store. Tissue was pre-treated with 2 μM thapsigargin for 10 minutes and then superfused. CCK did not induce a Ca^{2+} rise when the store is depleted but a Ca^{2+} rise was induced by the addition of external Ca^{2+}. **(B)** Immunofluorescence showing actin, (phalloidin, pink) tubulin (green) and mitochondrial (Tom20, red) distributions in tissue after depletion of the Ca^{2+} store with thapsigargin for 30 minutes (top panel) and in tissue hyperstimulated with 100 nM CCK for 30 minutes after thapsigargin depletion of the Ca^{2+} store for 30 minutes (Bottom panel). Bars indicate 10 μm. These data are representative of at least three individual experiments.

Figure 5.18

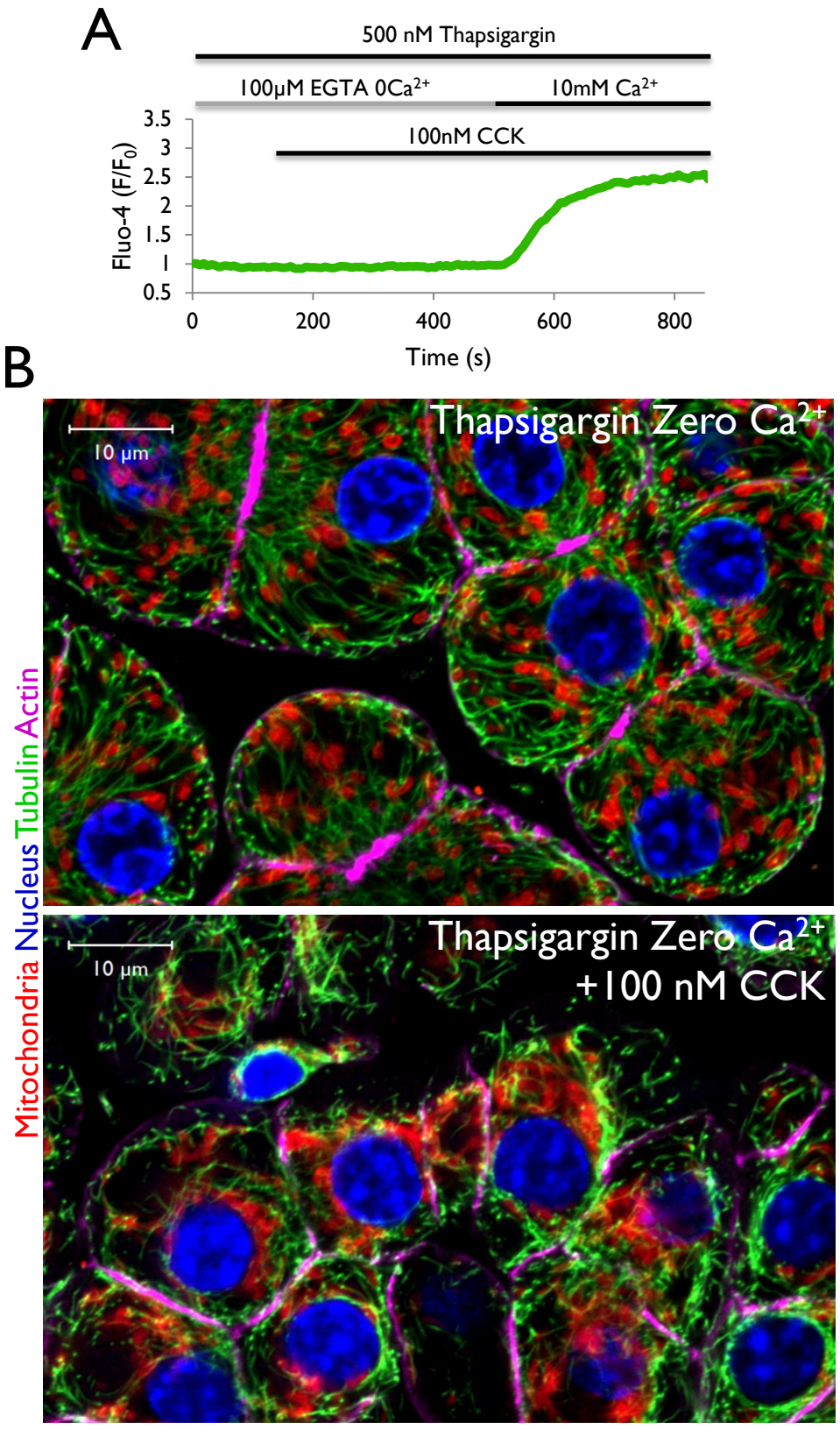
A
500 nM Thapsigargin
100μM EGTA 0Ca2+
10mM Ca2+
100nM CCK
Fluo-4 (F/F0)
3.5
3
2.5
2
1.5
1
0.5
0
200
400
600
800
Time (s)
B
Thapsigargin Zero Ca2+
10 μm
Thapsigargin Zero Ca2+
+100 nM CCK
10 μm
Mitochondria Nucleus Tubulin Actin

Figure 5.19

Effect of cytochalasin D and blebbistatin on actin distribution in basal conditions. Immunofluorescence of the actin distribution after 1 hour pre-treatment with cytochalasin D (left) or blebbistatin (right). Actin patches were visible in a punctate state after depolymerisation of actin by cytochalasin D, and apical decoration similar to control conditions was visible after inhibition of myosin IIA by blebbistatin. Bar indicates 10 μm. These data are representative of at least three individual experiments.

Figure 5.19

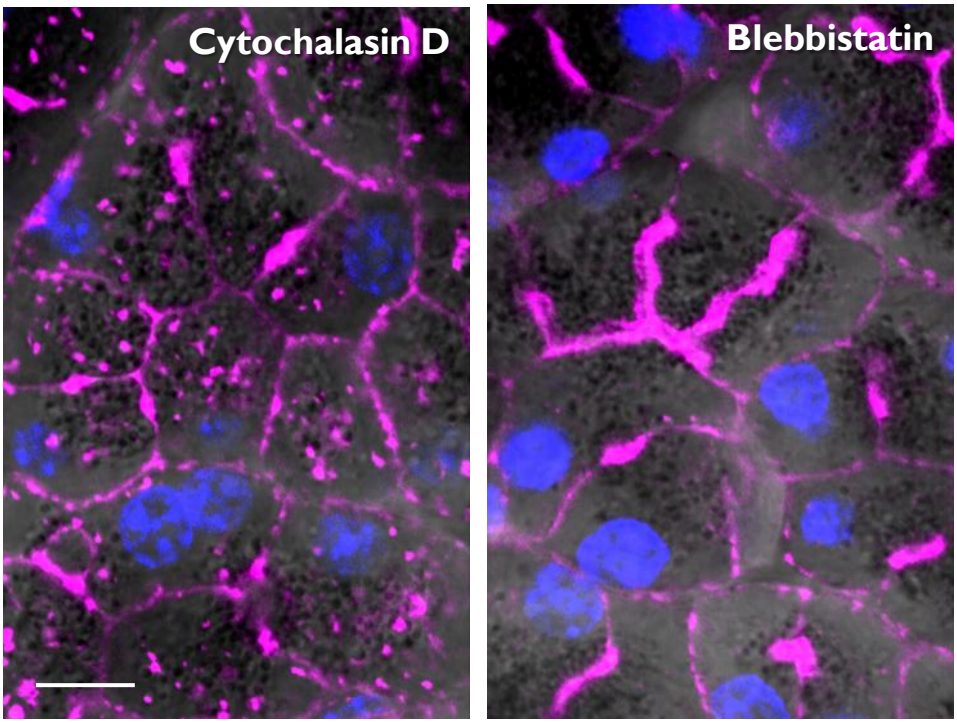

Figure 5.20

Subplasmalemmal dislocation induced by hyperstimulation is dependent upon polymerised actin. Immunofluorescence after depolymerisation of actin by cytochalasin D in unstimulated tissue, showing a diffuse mitochondrial distribution (Tom20, red) (A); after hyperstimulation with 100 nM CCK showing mitochondria in a perigranular belt (B); and stimulation with 100 nM CCK after depolymerisation of tubulin with colchicine (C). Bar indicates 10 μm. These data are representative of at least three individual experiments.

Figure 5.20

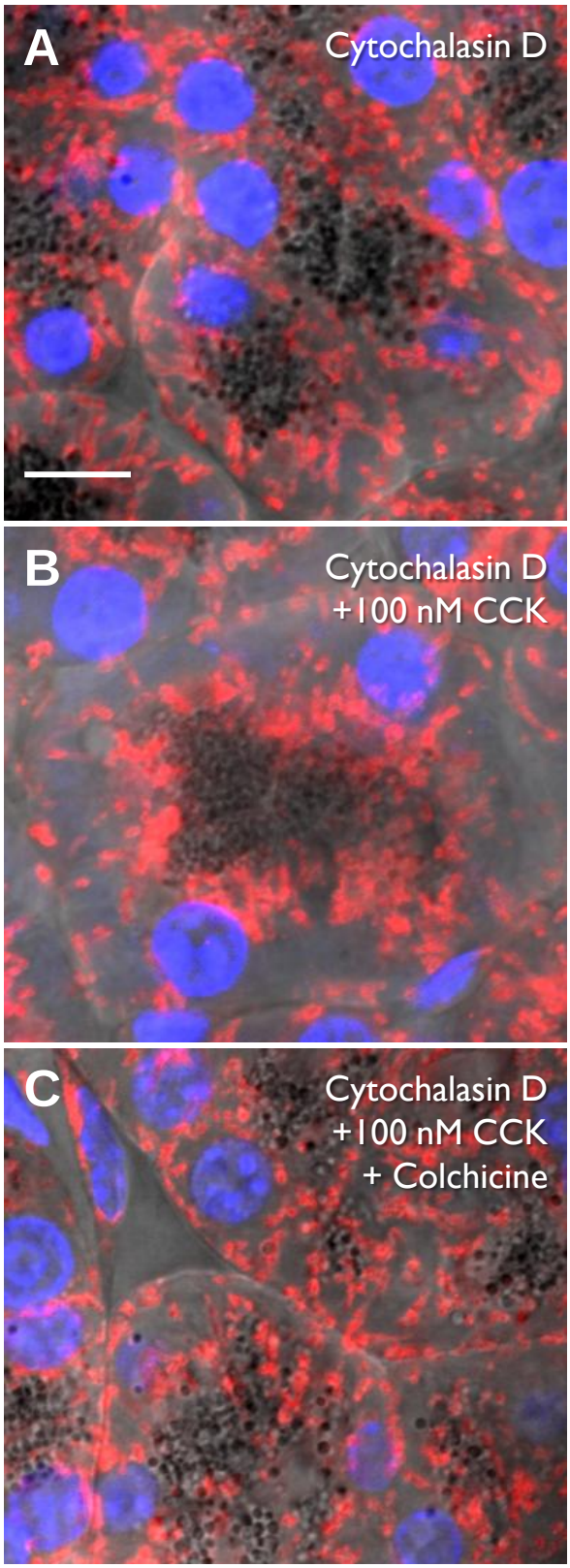
A
Cytochalasin D
B
Cytochalasin D
+100 nM CCK
C
Cytochalasin D
+100 nM CCK
+ Colchicine

Figure 5.21

Subplasmalemmal dislocation induced by hyperstimulation is dependent upon myosin IIA-dependent actin dynamics. Immunofluorescence after 1 hour pre-treatment of blebbistatin to inhibit myosin IIA in unstimulated tissue, showing a diffuse mitochondrial distribution (Tom20, red) (A); after hyperstimulation with 100 nM CCK showing mitochondria in a perigranular belt (B); and stimulation with 100 nM CCK after depolymerisation of tubulin with colchicine (C). Bar indicates 10 μm. These data are representative of at least three individual experiments.

Figure 5.21

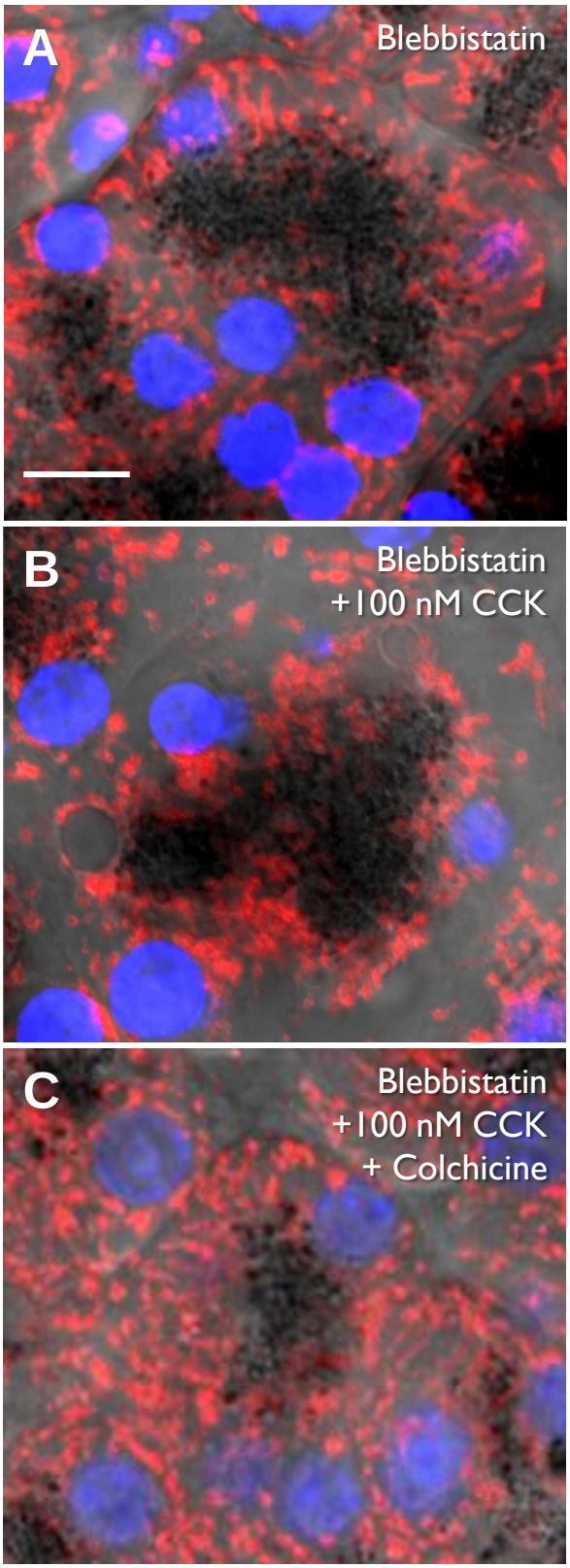
A
Blebbistatin
B
Blebbistatin
+100 nM CCK
C
Blebbistatin
+100 nM CCK
+ Colchicine

Figure 5.22

Quantification of mitochondrial distribution after actin and tubulin modulation. (D) Quantification of mitochondrial perigranular belt (<5 μm from the granular region) and subplasmalemmal (<2 μm from the basal membrane) populations after treatment with blebbistatin or cytochalasin D in the presence or absence of hyperstimulation and tubulin depolymerisation by colchicine. These data are mean ± SEM from at least 6 regions from at least three individual experiments. * indicates $p < 0.05$ compared to the respective control (perigranular or subplasmalemmal region).

Figure 5.22

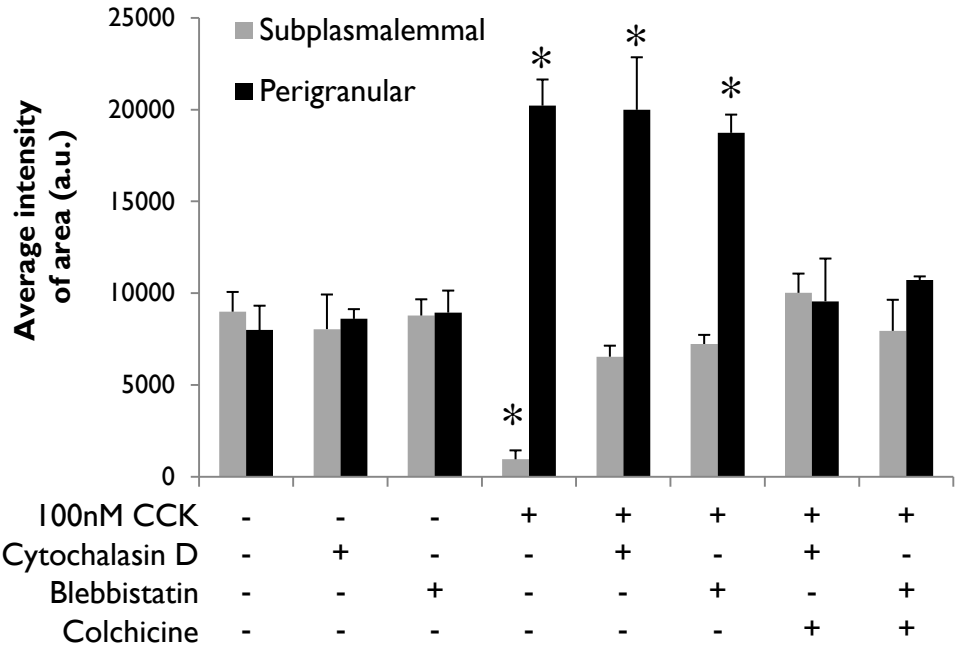
Subplasmalemmal
Perigranular
Average intensity of area (a.u.)
25000
20000
15000
10000
5000
0
*
*
*
*
100nM CCK - - - + + + + +
Cytochalasin D - + - - + - + -
Blebbistatin - - + - - + - +
Colchicine - - - - - - + +

Figure 5.23

Actin cable formation does not require polymerised tubulin. Tissue was treated with 50 μM colchicine for 1 hour prior to hyperstimulation with 100 nM CCK for 30 minutes. Tissue showed diffuse cytosolic depolymerised tubulin (green), confirming that colchicine treatment was effective. Actin staining (phalloidin, pink) showed the formation of actin cables (white arrows) which appeared to push the mitochondria (Tom20, red) into the apical region of the cell. The nucleus (blue) was also found beneath these actin cables. These data are representative of at least three individual experiments.

Figure 5.23

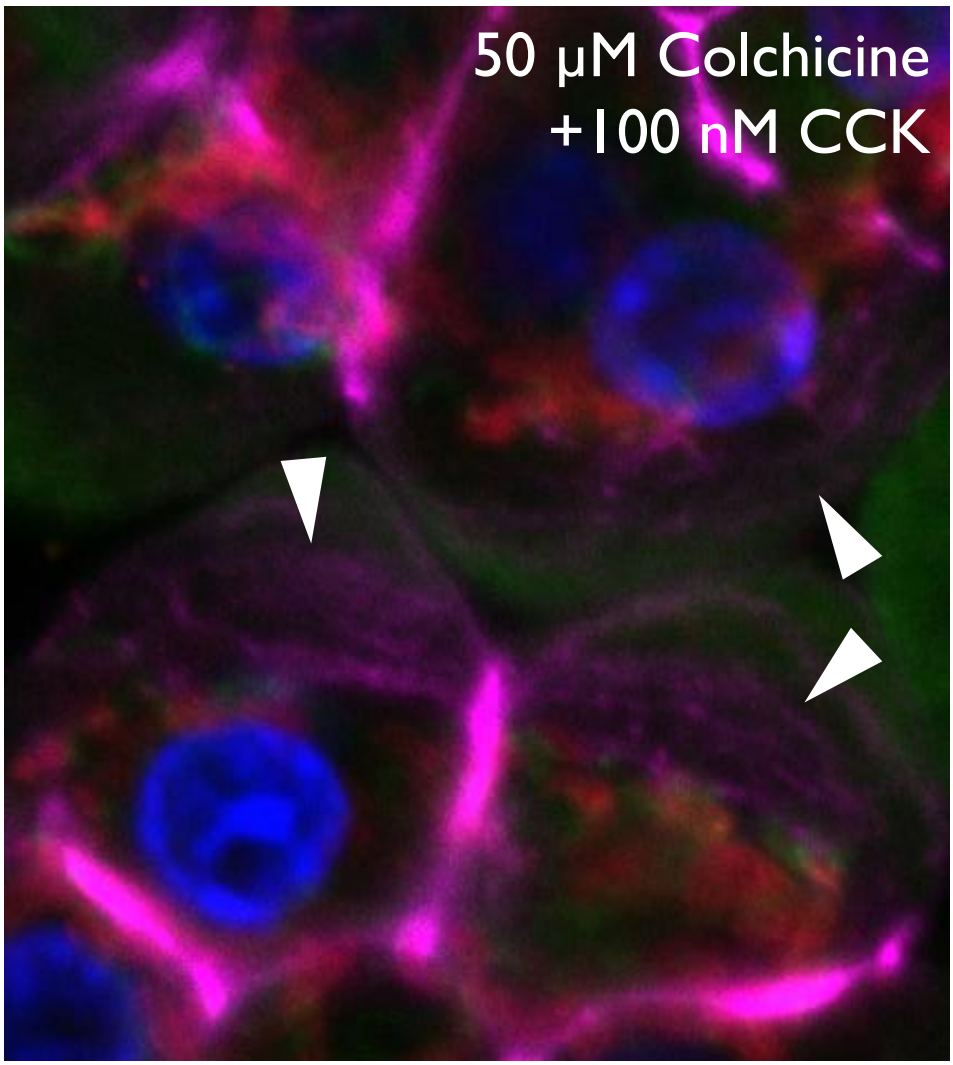

Mitochondria Nucleus Tubulin Actin

Figure 5.24

Inhibition of CCK-induced Ca^{2+} signals by depletion of PIP_2 through the inhibition of PI3K with wortmannin and LY294002. (A) Tissue segments incubated in 30 μM wortmannin and 300 μM LY-294002 for 1 hour showed no inhibition of CCK-induced Ca^{2+} signal. **(B)** Tissue segments incubated for 2 hours showed partial inhibition of the CCK-induced Ca^{2+} signal. **(C)** 3.5 hours of wortmannin & LY-294002 treatment was required to completely block the CCK-induced Ca^{2+} signal. However this elevated the basal Ca^{2+} level.

Figure 5.24

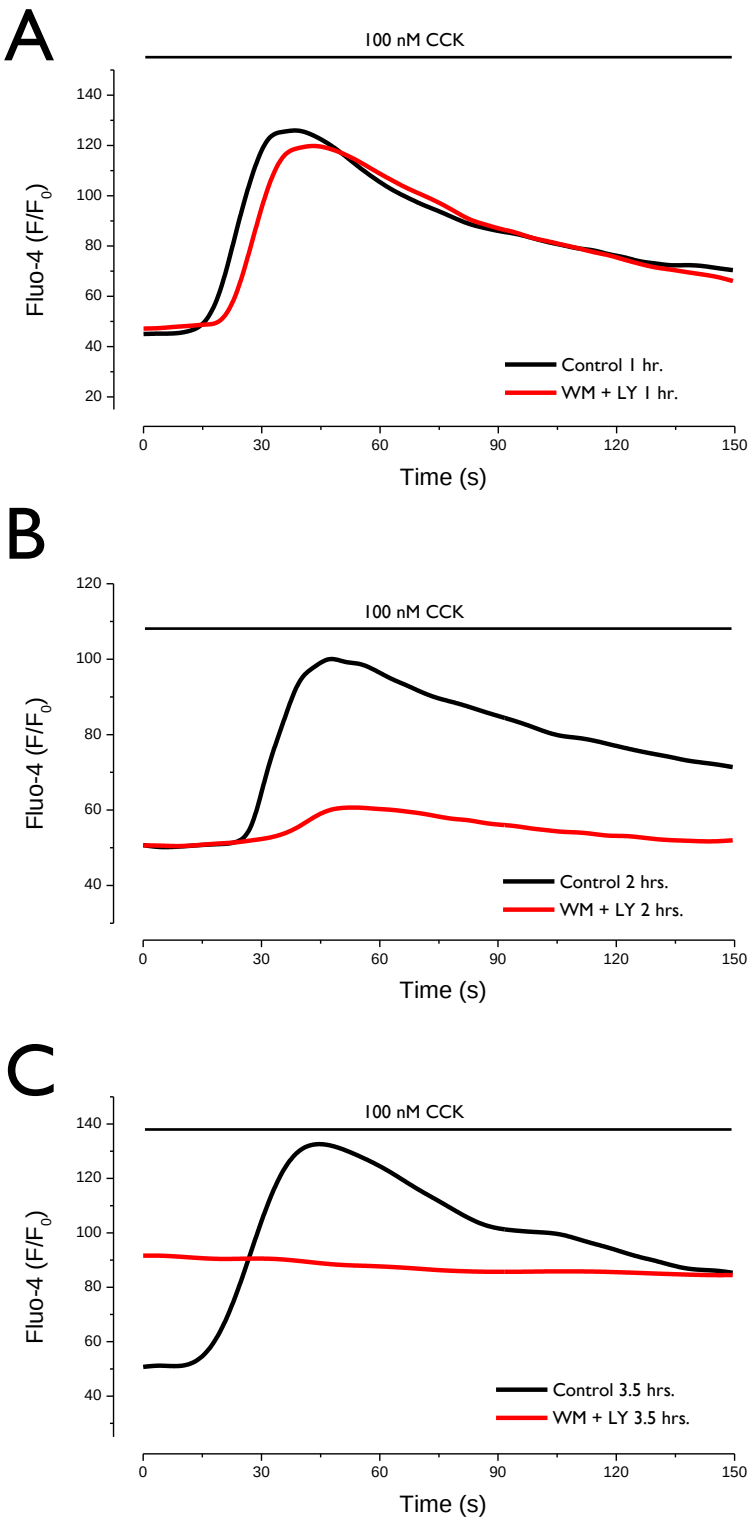
A
100 nM CCK
Fluo-4 (F/F0)
140
120
100
80
60
40
20
Control 1 hr.
WM + LY 1 hr.
0
30
60
90
120
150
Time (s)
B
100 nM CCK
Fluo-4 (F/F0)
120
100
80
60
40
Control 2 hrs.
WM + LY 2 hrs.
0
30
60
90
120
150
Time (s)
C
100 nM CCK
Fluo-4 (F/F0)
140
120
100
80
60
40
Control 3.5 hrs.
WM + LY 3.5 hrs.
0
30
60
90
120
150
Time (s)

Figure 5.25

Depletion of PIP_2 by inhibition of PI3K with Wortmannin and LY-294002 did not induce pathological mitochondrial redistribution. (A) Tissue segments incubated in 30 μM Wortmannin and 300 μM LY-294002 displayed rich basal staining of mitochondria (Tom20, red) and there were no visible signs of actin (phalloidin, pink) cable formation in the cytosol. Bar indicates 10 μm. These data are representative of at least three individual experiments.

Figure 5.25

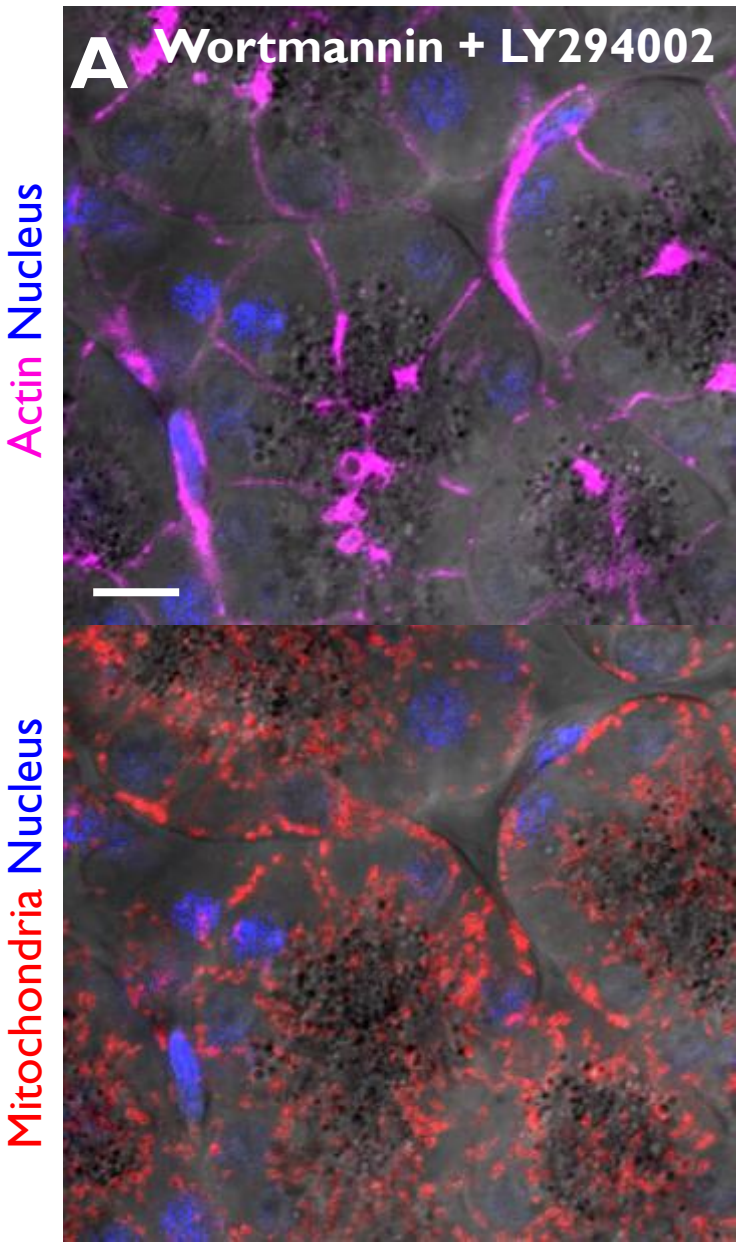
A
Wortmannin + LY294002
Actin Nucleus
Mitochondria Nucleus

Figure 5.26

Effects of hyperstimulation with 100 nM CCK or the protonophore CCCP on thapsigargin-induced store-operated Ca^{2+} entry and corresponding mitochondrial distribution. (A) Cytosolic Ca^{2+} was measured using Fluo-4 in tissue pre-treated with 2 μM thapsigargin for 10 minutes, after the re-addition of 1 mM external Ca^{2+} . Top panels show the mitochondrial distribution in red (TMRM) at times 0 and 900 showing a diffuse distribution, with mitochondria decorating the basal membranes. **(B)** The graph shows Ca^{2+} influx in tissue stimulated for 30 minutes with 100 nM CCK and subsequently pre-treated with 2 μM thapsigargin for 10 minutes. The second re-addition of 1 mM external Ca^{2+} was accompanied by 10 μM CCCP to compare the effect of depolarising mitochondria to the effect of redistributing the mitochondria away from the basal membrane. The top panels show the mitochondrial distribution (red, TMRM) at times 0 and 900, showing a severe perigranular belt distribution, with the basal membranes devoid of mitochondria at time 0, and a cytosolic staining of TMRM after depolarisation of the mitochondria with CCCP. Bars indicate 5 μm. These data are representative of at least three individual experiments. Data has been normalised to the initial fluorescence expressed as F/F_0.

Figure 5.26

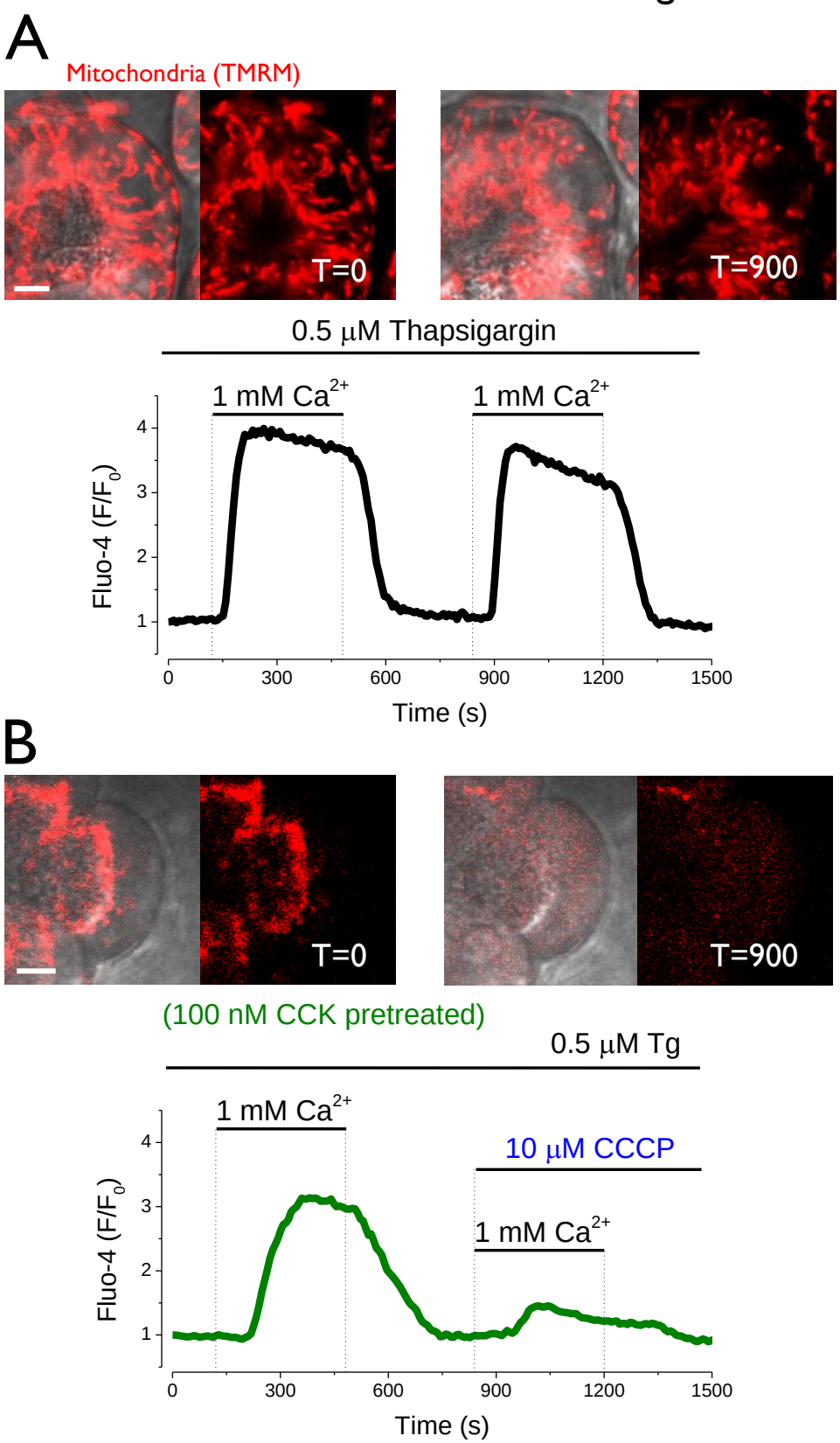
A
Mitochondria (TMRM)
T=0
T=900
0.5 μM Thapsigargin
1 mM Ca2+
1 mM Ca2+
Fluo-4 (F/F0)
Time (s)
B
T=0
T=900
(100 nM CCK pretreated)
0.5 μM Tg
1 mM Ca2+
10 μM CCCP
1 mM Ca2+
Fluo-4 (F/F0)
Time (s)

Figure 5.27

Store-operated Ca^{2+} entry is significantly reduced after redistribution of mitochondria away from the basal membrane (induced by 100 nM CCK). Depolarisation of the mitochondrial membrane potential greatly reduces the influx rate to a much larger extent. (A) Quantification of thapsigargin-induced store-operated Ca^{2+} entry under control conditions (black) and after pre-treatment with either 100 nM CCK for 30 minutes (green) or 10 μM CCCP for 10 minutes (blue). **(B)** Average times at which the store entry curve reaches 20, 50, and 80% of the maximum fluorescence (calculated by sigmoid lines of best fit of which the average $R^2 = 0.99$) for control (black) and 100 nM CCK pre-treated (green). *indicates $p<0.05$.

Figure 5.27

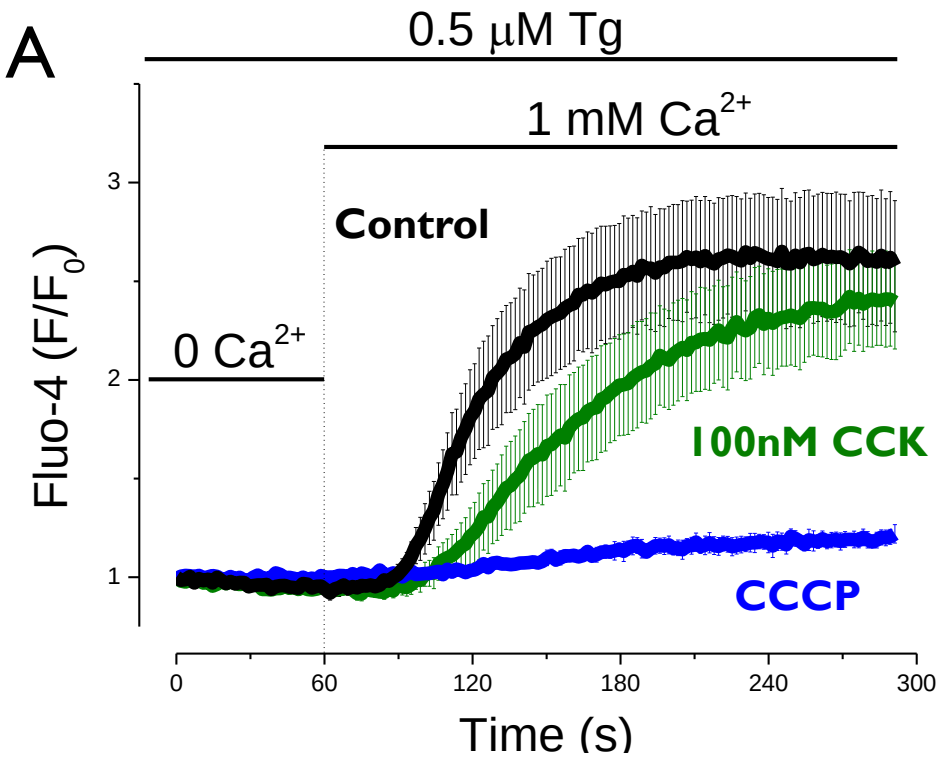
A
0.5 μM Tg
1 mM Ca2+
Control
0 Ca2+
100nM CCK
CCCP
Fluo-4 (F/F0)
Time (s)
0
60
120
180
240
300
1
2
3

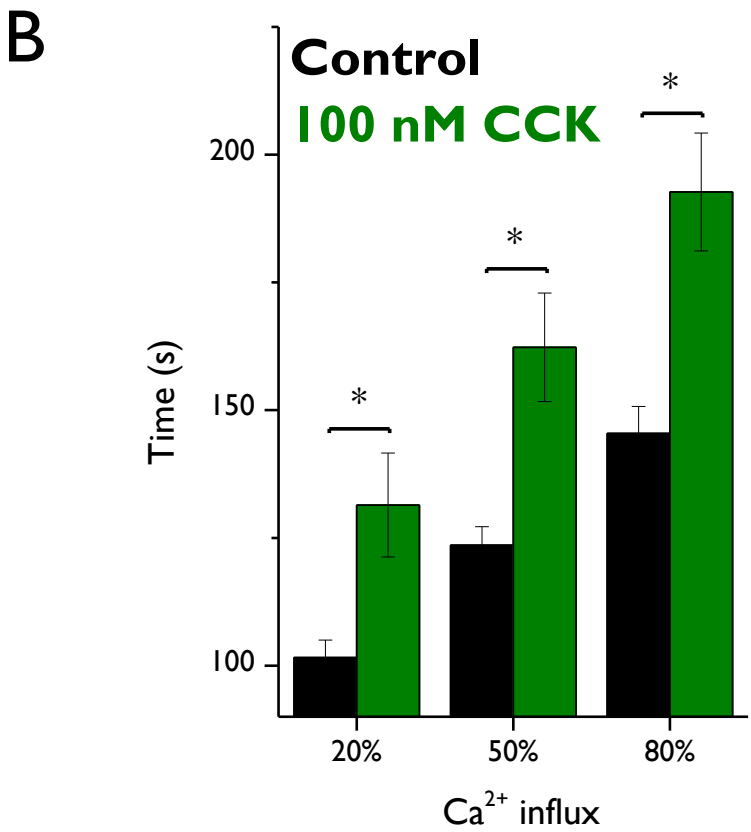
B
Control
100 nM CCK
Time (s)
100
150
200
20%
50%
80%
Ca2+ influx
*
*
*

Figure 5.28

3¾ examples of nuclear vacuolisation induced by hyperstimulation. Staining of fixed pancreatic tissue after treatment with 500 μM TLCS for 30 minutes showing the formation of nuclear vacuoles. Vacuoles can be seen in the transmitted images and also by the absence of the DNA Hoechst staining (white arrows). An incompletely invaginated vacuole which is slightly indented into the nucleus can also be seen (white *). A common feature of the nuclear vacuoles is the presence of a 'fountain' of actin at the transition with the cytosol (yellow arrows). Bars indicate 10 μm.

Nota bene - nuclear vacuoles were never seen in unstimulated conditions.

Figure 5.28

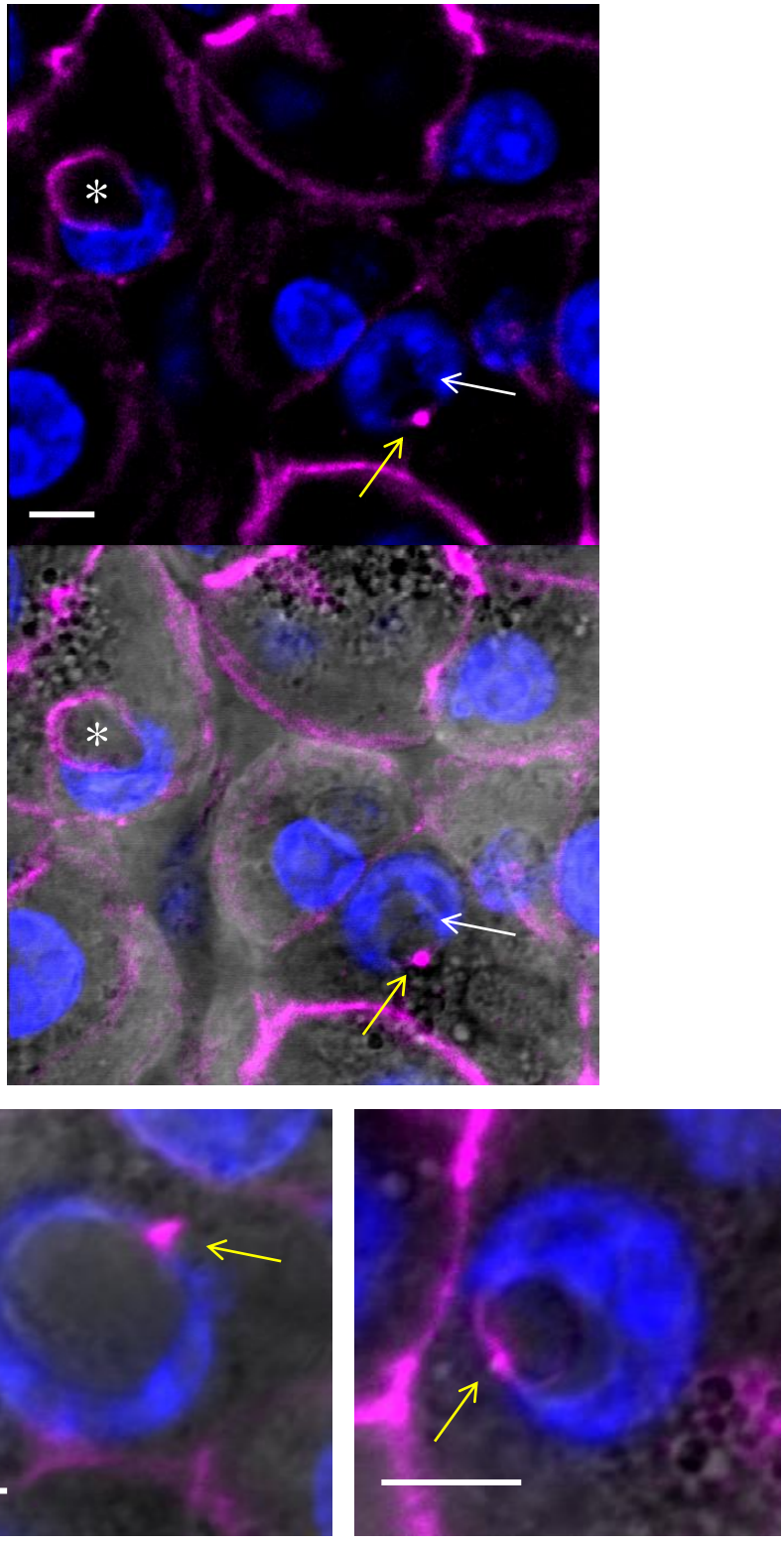

Figure 5.29

Nuclear vacuoles also form after TLCS treatment in the presence of NAC. Three images at differing z dimension distances from the cover slip of fixed pancreatic tissue showing nuclear vacuolisation. Tissue was treated with 10 mM NAC for 10 minutes and 500 μM TLCS for 30 minutes and the formation of nuclear vacuoles was still seen (bisected in the z=14.76 micron section, centre panels). The vacuole can clearly be seen in the transmitted image (top panels) and the crescent of the DNA Hoechst staining (white arrow). Also apparent is the presence of actin staining at the transition between the nuclear vacuole and the apically derived endocytic vacuole (white star*) which also spreads into the nuclear vacuole on the bottom side (yellow arrows)

Figure 5.29

Nucleus Actin Mitochondria

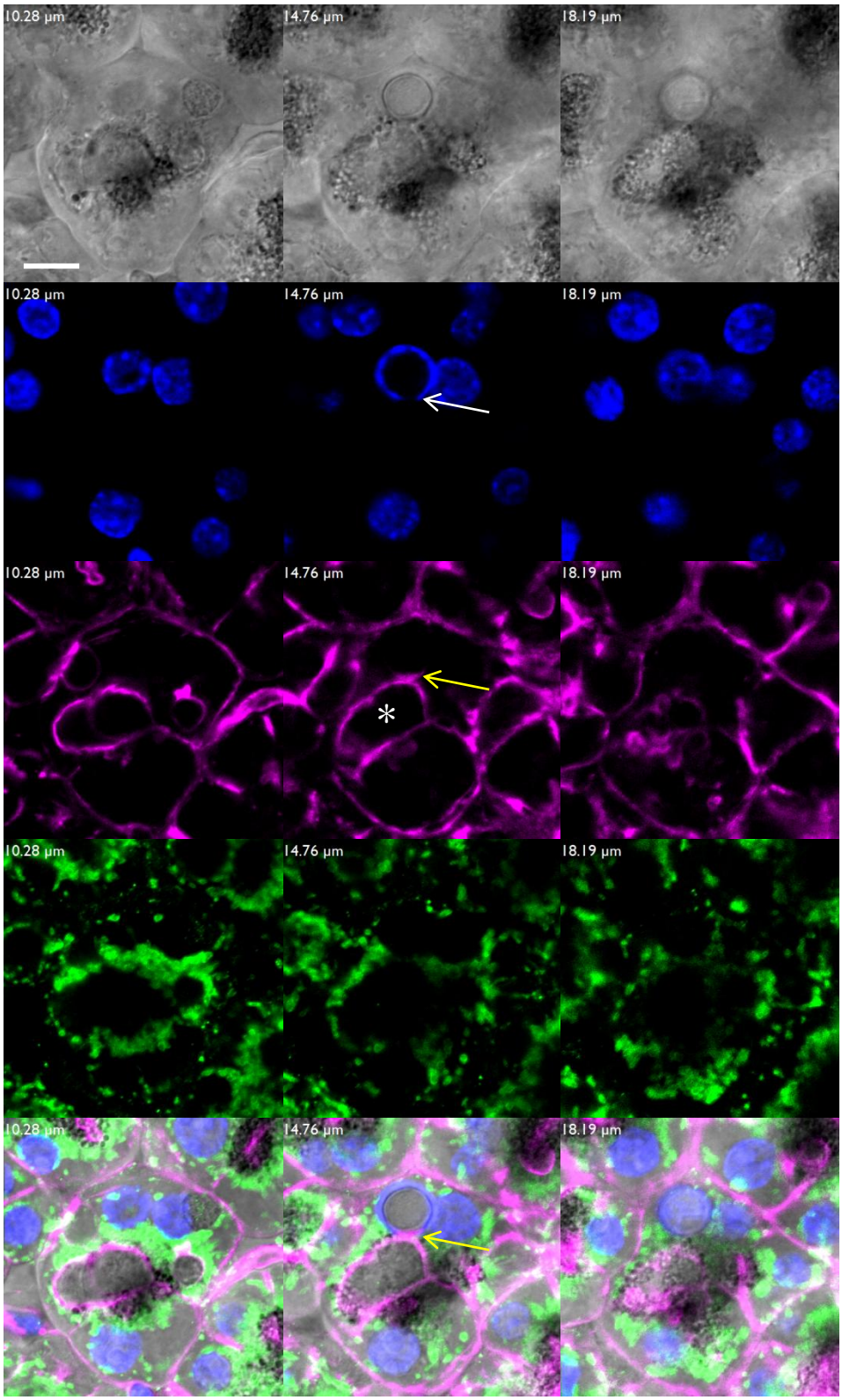

Figure 5.30

Lucifer yellow staining of the pancreatic ductal tree. Transmitted image (top) and 3D confocal projection of Lucifer yellow fluorescence (bottom) from live pancreatic tissue after injection of the membrane impermeable fluorescent indicator, Lucifer yellow, prior to hyperstimulation with 500 μM TLCS for 30 minutes. The duct is clearly seen along with endocytic vacuoles and invaginations of the luminal membrane. A necrotic cell is also visible (pink *).

Figure 5.30

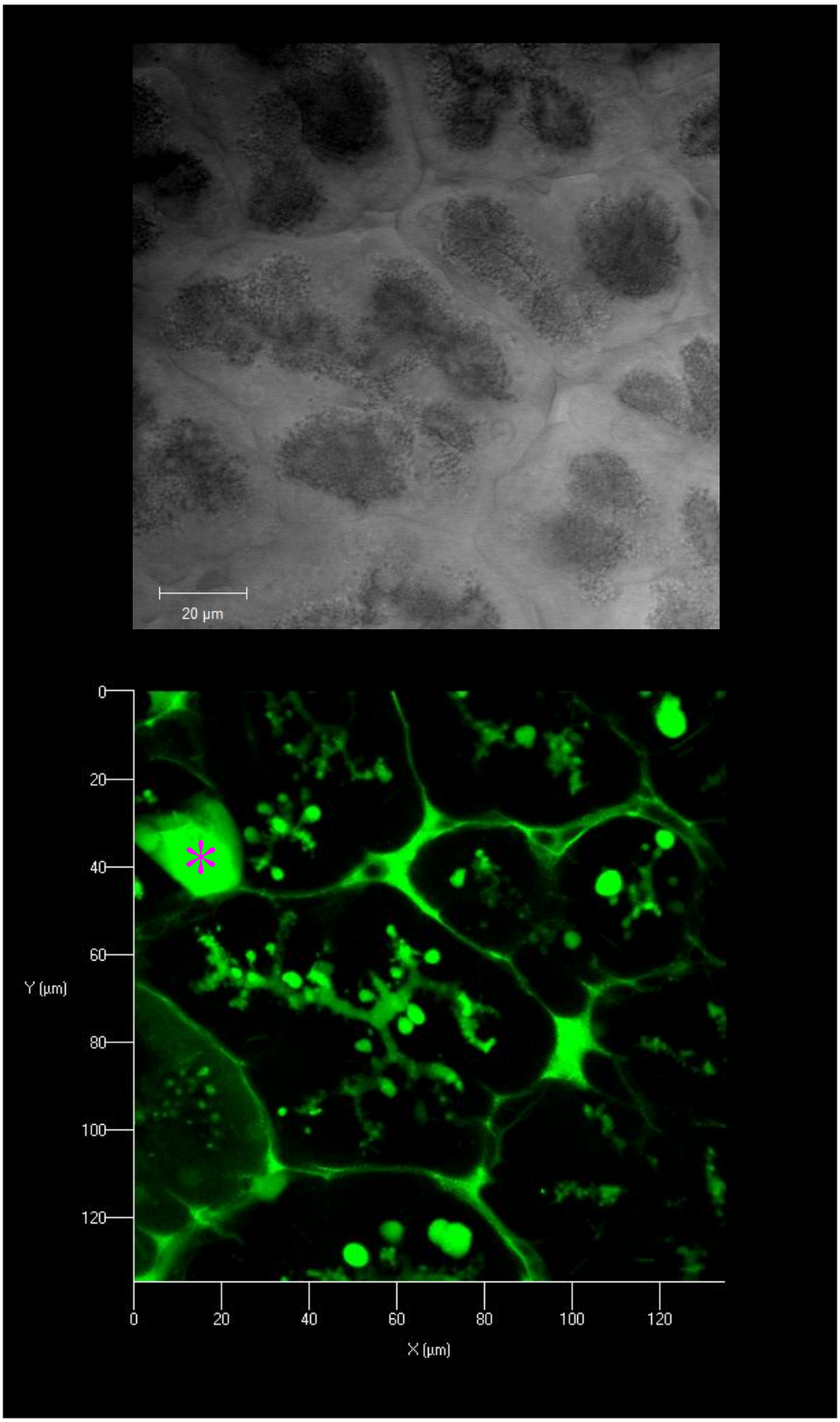

Figure 5.31

Peri-nuclear and nuclear vacuoles are derived from endocytic structures. Confocal fluorescence imaging of live pancreatic tissue after injection of the membrane impermeable fluorescent indicator, Lucifer yellow, prior to hyperstimulation with 500 μM TLCS for 30 minutes. Nuclear vacuoles in various stages of development can be seen stained with Lucifer yellow indicating that they have been formed by endocytosis of the extracellular membrane-impermeable stain. A nuclear vacuole is visible (pink *) as well as vacuoles in close proximity to the nuclei (white arrows). Red arrows show a heavily distorted nucleus in close proximity to a vacuole.

Figure 5.31

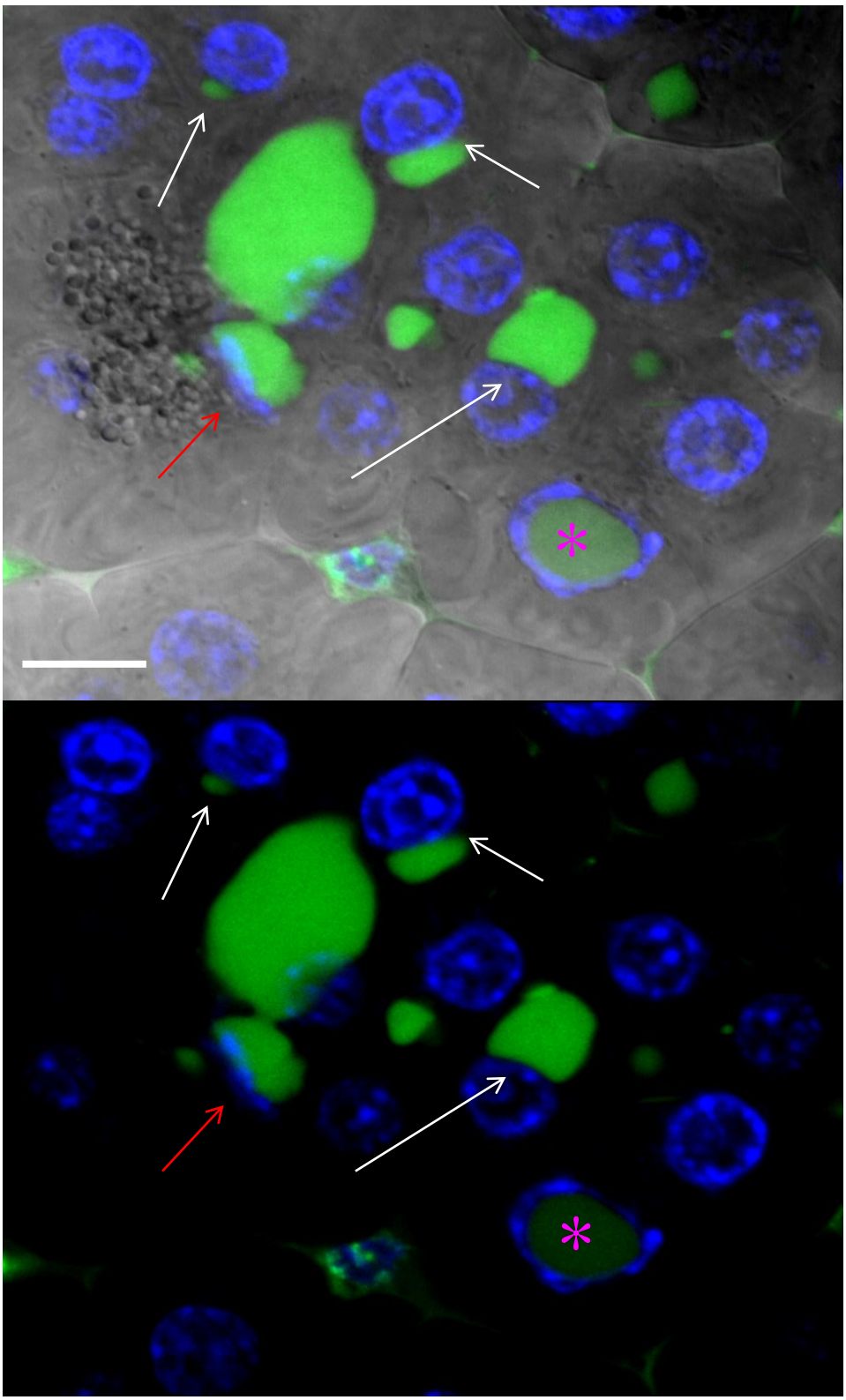

Figure 5.32

Nuclear vacuoles stain positive for bile salt-activated lipase, a component of the secretion pathway. Immunofluorescence of pancreatic tissue after hyperstimulation with 100 nM CCK for 30 minutes. Nuclear vacuoles from two z-sections of neighbouring cells can be seen containing carboxyl ester lipase (green). Mitochondria can be seen in red (Tom20).

Figure 5.32